

Structure-function relationships of E-type endonuclease colicins

Structure-function relationships of E-type endonuclease colicins

**Structuur-functie relaties van E-type
endonuclease colicins**

(met een samenvatting in het Nederlands)

Proefschrift

ter verkrijging van de graad van doctor aan de Universiteit Utrecht
op gezag van de Rector Magnificus, Prof. Dr. W.H. Gispen,
ingevolge het besluit van het College voor Promoties
in het openbaar te verdedigen op donderdag 13 mei 2004
des middags te 12.45 uur.

door

Ewald Theodorus Johannes van den Bremer

geboren op 17 september 1973,
te Leusden

Promotor: Prof. Dr. A.J.R. Heck
Faculteit Scheikunde, Universiteit Utrecht

Copromotor: Dr. W. Jiskoot
Faculteit Farmaceutische Wetenschappen, Universiteit Utrecht

ISBN: 90-393-3678-4

Printed by Ponsen & Looijen B.V., Wageningen

Cover: Rob Lamper

Het in dit proefschrift beschreven onderzoek werd gefinancierd door de Nederlandse Organisatie voor Wetenschappelijk Onderzoek (NWO).

Table of Contents

Chapter 1	Introduction colicin biology	7
Chapter 2	Mass spectrometry in protein conformational analysis and molecular recognition	25
Chapter 3	Probing metal ion binding and conformational properties of the colicin E9 endonuclease by electrospray ionization time-of-flight mass spectrometry	53
Chapter 4	Distinct conformational stability and functional activity of four highly homologous endonuclease colicins	79
Chapter 5	Ligand induced changes in the conformational dynamics of a bacterial cytotoxic endonuclease	99
Chapter 6	Metal induced selectivity in phosphate ion binding in colicin E9 DNase	119
Chapter 7	Probing the H-N-H active site in colicin E9 for metal and phosphate-ligand binding	127
Chapter 8	Summarizing discussion	141
	List of abbreviations	149
	Nederlandse samenvatting	150
	Dankwoord	156
	Curriculum vitae	159
	List of publications	160

Chapter 1

Introduction
colicin biology

Colicin biology

Environmental stress, like intense competition for limited nutrients, resulted in the evolution of mechanisms that provide bacterial strains with competitive advantage, with the aim to rescue their own population. One such mechanism, which is often found in Eubacteria and Archaeobacteria, is the secretion of bacteriocins; toxins that kill closely related bacteria. Prominent amongst these are the protein toxins, a group that includes pyocins (*Pseudomonas aeruginosa*) (1), klebicins (*Klebsiella pneumoniae*) (2), and colicins (*Escherichia coli*) (3) of which the colicins DNases E2, E7, E8 and E9 are the focus of this thesis. It has been estimated that up to 30% of clinical isolates of *E.coli* produce colicins, which emphasizes their importance in bacterial survival mechanisms (4).

Structurally each colicin shows the same type of organization that comprises three domains, 1) a domain involved in the recognition of a specific outer-membrane receptor, 2) a domain involved in translocation, and 3) a domain for the lethal activity. Since a full length three domain structure is not yet available for colicins E2, E7, E8 or E9, an extended version of the related colicin E3 X-ray structure is given in Figure 1, showing all three domains responsible for each of the three aforementioned functions needed in the uptake process. Colicin E3 belongs to the same family (based on translocation system and cell surface receptor) as the DNase colicins (E2, E7, E8 and E9). The first 450 residues of all these proteins are almost identical (domain 1 and 2; >90%) (5, 6).

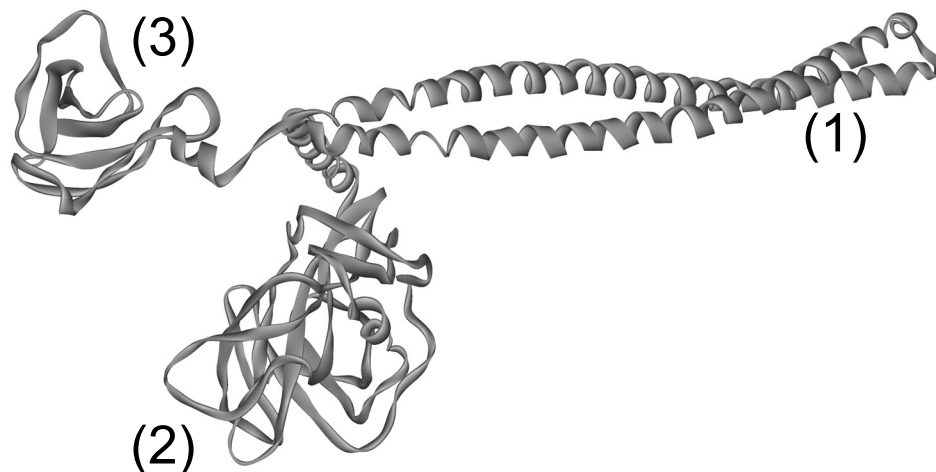


Figure 1. Extended X-ray crystal structure showing the three domain organization of colicin E3 (PDB: 1JCH, 1UJW) with 1) an R-domain involved in the recognition of a specific outer-membrane receptor, 2) a T-domain involved in translocation, and 3) a C-domain for the lethal activity [Adapted from (7, 8)].

Colicin synthesis and immunity

Colicins are 50-70 kDa proteins produced by *E.coli* that carry the Col plasmid. The Col plasmid contains an operon of three genes that are essential for colicin cytotoxicity. The first of these genes encodes the colicin (*ceaI* in case of the ColE9-J plasmid) and is under the transcriptional control of the DNA damage-inducible SOS promoter (9). The second gene (*imm*) encodes a ~9.5 kDa immunity protein that prevent the cell to commit suicide when producing the cytotoxic protein. The final lysis gene (*lys*) encodes the bacteriocin release protein (BRP), and is believed to trigger dimerization of the membrane anchored phospholipase A₂ leading to permeabilization of the membrane allowing colicin release (10, 11). Enzymatic colicins are released in the form of a heterodimeric complex with their immunity proteins (11, 12). An additional, weaker, promoter found within in the colicin structural gene results in constitutive immunity protein expression. Therefore, a colicin-producing cell makes an excess of immunity protein that ensures inhibition of incoming colicin. A common feature of colicin encoding plasmids is the presence of genes for immunity proteins that act against colicins other than that encoded by the host plasmid (13), and hence allows the cell to be resistant to more than one type of colicin.

Colicin Classification

One methodology for colicins classification is to group them according to which sets of periplasmic proteins are used in their uptake. The Tol system of periplasmic proteins is used for group A colicins, and the Ton system for group B colicins. However, some proteins such as TolC are used by members of both groups (5). The various different receptors and periplasmic proteins involved in uptake of different colicins are summarized in Table 1. The Tol proteins were originally identified during selection for proteins that contain spontaneous mutations allowing the cell to become *tolerant* to colicins (14). TonB and its associated proteins, ExbB and ExbD, are involved in the transduction of metabolic energy, represented by the proton-motive force present across the inner-membrane to the iron-siderophore receptors (e.g. FhuA, FebA) allowing regulated uptake of these nutrients (15).

Table 1. Classification of colicin family of proteins: their activities, receptors and translocation proteins involved in uptake [Adapted from Lazdunski et al. (5)].

Colicin	Activity	Receptor	Translocation system
Group A			
A	Pore formation	BtuB	OmF, Tol ABQR
Cloacin DF13	rRNase	IutA	TolAQR
E1	Pore formation	BtuB	TolCAQ
E2, E7, E8, E9	DNase	BtuB	OmpF, Tol ABQR
E3,E4, E6	rRNase	BtuB	OmpF, Tol ABQR
E5	tRNase	BtuB	OmpF, Tol ABQR
N	Pore formation	OmpF	OmpF, Tol AQ
K	Pore formation	Tsx	OmpF, Tol ABQR
Group B			
B	Pore formation	FebA	TonB, ExbBD
Col5	Pore formation	Tsx	TolC, TonB, ExbBD
Col10	Pore formation	Tsx	TolC, TonB, ExbBD
D	tRNase	FebA	TolC, ExbBD
Ia,Ib	Poreformation	CirA	TolC, ExbBD
M	Mureine synthesis inhibition	FhuA	TolC, ExbBD

Mechanism of enzymatic colicin uptake

Export of proteins from cells occurs through specialized machineries such as the *sec* dependent translocation pathways (16). There are no specific proteins present for colicin uptake. Instead, colicins use outer membrane receptors that are normally involved in nutrient uptake. Enzymatic colicin mediated cell killing is schematically illustrated in Figure 2 and can be dissected in a number of stages. Firstly, the R-domain binds to the outer-membrane BtuB receptor bringing the T-domain close to the membrane surface, in a position where it can interact with other membrane proteins such as OmpF allowing the T-domain to pass across the outer-membrane (7). Secondly, the T-domain binds to its periplasmic protein binding partner(s) and dissociation of immunity protein from the cytotoxic domain occurs. Finally, the cytotoxic domain enters the periplasm through a pore-forming ability allowing them to cross the inner-membrane spontaneously (17). Recent evidence suggests that nuclease colicins are proteolytically processed from this point (18, 19), releasing the cytotoxic domain from the rest of the colicin protein.

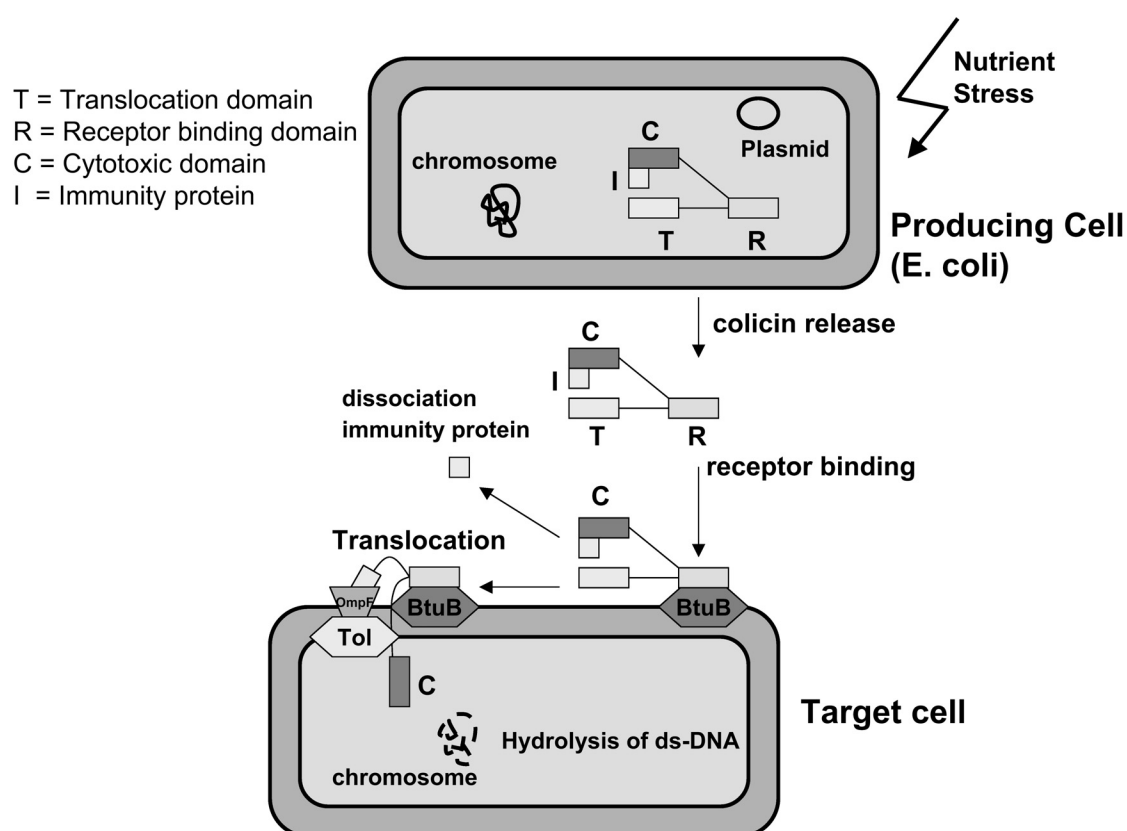


Figure 2. Mechanism of cell killing by E-type endonuclease colicins.

Colicin uptake receptors

The *E. coli* outer membrane receptor(s) used by the E-group colicins, colicin A and phage BF23 is the 594-residue *E. coli* outer membrane cobalamin (Vitamin B12) translocator BtuB (20, 21). Recently, crystal structures have been obtained for (i) apo-BtuB (ii) Ca^{2+} -BtuB and Ca^{2+} -cobalamin BtuB (22) and, in conjunction with the colicin E3 R-domain (7). The 22-strand antiparallel β -barrel motif found for BtuB has been described for the iron siderophore-binding FepA (23) and FhuA (15), which are receptors for colicins B and M, respectively, and ferric citrate-binding FecA (24). All of these outer-membrane proteins contain an N-terminal globular domain of 130-150 residues, 132 residues in BtuB, which folds into the lumen of the β -barrel like a channel 'cork'. This 'cork' occludes the lumen of the β -barrel and shares an extending binding surface with the inside of the barrel (15, 23) so that it is difficult to envisage how these receptors translocate substrates without some displacement of the 'cork' (see Figure 3). The problem of bypassing the cork domain is even more remarkable for translocation of a colicin polypeptide (e.g. DNase domain). The co-crystal structure as well as recent spin-labelling results (25, 26) show that the TonB box (a highly conserved region in the TonB inner membrane

protein) does not move away from the BtuB plug domain (as would required if uptake passed through the barrel) – instead it moves closer into the protein, which is in contrast to the binding of vit. B12 (a ligand that cause movements of the plug) where the TonB box moves away from the rest of the BtuB. Next the function of the three colicin domains will be described in more detail.

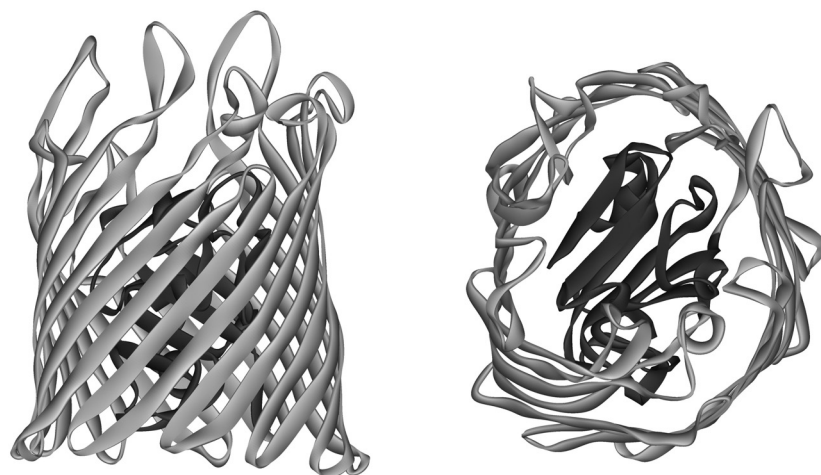


Figure 3. Showing the BtuB colicin uptake receptor. The N-terminal 132 residues in BtuB shown in dark grey, folds into the lumen of the β -barrel like a channel ‘cork’. [Adapted from Chimento et al. (22)]

Colicin R-domains: Receptor recognition

The R-domain, which is involved in the first stage of colicin uptake, binds to the outer-membrane receptor, and hence governs the specificity of binding by the colicins. Penfold et al. identified the E colicin R-domain through mutagenesis (6). The structures of three R-domains are known – that from the nuclease colicins E2-E9 (8), colicin Ia (27) and colicin N (28). The amino acid sequences of the R-domain of colicins E2-E9 are almost identical (> 90%) (6) and, as such, they are all likely to share the same structure as those of colicin E3 (Figure 1). Both colicins Ia and E3 R-domains are highly elongated molecules and both bind to receptors that are likely to possess the same structural fold since the receptor for colicin Ia (CirA) is also a TonB dependent receptor (27). In contrast, the R-domain for colicin N has mainly β -sheet character and binds to a different type of outer-membrane protein – OmpF (28). Hence, it is possible that the different structures of the R-domain are related to the type of uptake receptor they use. For instance, cloacin DF13 is a related toxin to colicin E3 (the RNase domains show strong sequence conservation) but the R-domain sequences are different and, hence, cloacin DF13 operate via a different uptake receptor (IutA) (6). The role of the R-domain in conferring receptor specificity was demonstrated by making chimeric proteins; colicin E9 with the R-domain of cloacin DF13 kills cell expressing only IutA but not those only expressing BtuB (6).

Colicin T-domains: Translocation

The T-domain is involved in the second stage of colicin uptake (translocation) and shares high sequence identities (> 90 %) with other E colicin T-domains, as such, they are all likely to share the same structure as those of colicin E3 (Figure 1).

The periplasm and inner membrane of *E. coli* contain a number of proteins involved in nutrient uptake. The two groups of colicins (A and B) bind to different members of these using their translocation domains. Group A colicins interact with different members of the Tol proteins (proposed to be involved in outer membrane stability or communication of the proton motive force to control porin function), whilst group B colicins interact with the Ton group proteins (5, 29-31). The T-domain of E colicin nuclease binds to the β -propeller domain of TonB, through a region of the T-domain (residues 35-DGSGW-39) called the TolB box (32) that is conserved in all colicins that interact with TolB (33, 34).

After translocation, it is possible that the R-domain of nuclease colicins remains bound to BtuB as has been proposed to occur for colicin Ia uptake (27). However, the linker distance between the minimal R-domain and cytotoxic C-domain (~30 residues or 105 Å) for nuclease colicins is too short to span the outer-membrane, periplasm, and inner-membrane (a distance of ~200 Å). Mosbahi et al. showed for colicin E9 a pore-forming ability allowing it to cross the inner membrane spontaneously (17). An inner-membrane protease called LepB (18) has been shown to cleave colicin D between its R- and cytotoxic C-domains. Although colicin D is a group B colicin with nuclease activity, a similar processing event is proposed to occur with group A nuclease E colicins (18, 19) in case of DNase colicins (E2, E7, E8 and E9).

Colicin C-domains: cytotoxicity and immunity

Nuclease colicins target essential components of the bacterial cell. The first sub-class is comprised of colicins E5 and D that cleave transfer RNAs. Colicin E5 cleaves tRNAs for Tyr, His, Asn, and Asp (35) whilst colicin D cleaves at the four tRNAs for arginine (36). The second subclass is comprised of colicins E3, E4 and E6 that target a single phosphodiester bond in 16S ribosomal RNA, which result in the inhibition of translation. The lethal effect induced by colicin DNases (E2, E7, E8 and E9) is through non-specific degradation of chromosomal DNA.

Each colicin-producing cell protects itself by co-synthesizing an immunity protein. The crystal structure for colicin E3 rRNase-Im3 complex was solved by Carr et al. (37). The structures of both the E3 rRNase domain and Im3 are mainly β -sheet, which is in marked contrast to the mainly α -helical structures of the cytotoxic domains of DNase colicins and their immunity proteins (Figure 4).

The E9 DNase-Im9 complex shows no sequence or structural similarity with the E3 rRNase-Im3 complex, which is probably also related to their different modes of action. However,

one feature they share is that the active site is C-terminal and the immunity protein is making no interactions to catalytic residues (not shown). Hence colicin immunity proteins are exosite enzyme inhibitors (38). This mode of inhibition is in contrast to most other protein inhibitors of enzymes that bind directly to the active site, such as barstar inhibition of the RNase barnase (39). The mechanism of colicin inhibition relies on the fact that the substrate for nuclease colicins is a large anionic polymer (DNA and 16S rRNA for DNase and rRNase colicins, respectively). Modeling studies using B-form dsDNA and the E9 DNase-Im9 complex have demonstrated that oligonucleotides longer than 10 bp would extend out from the active site and result in steric and electrostatic conflict with the Im9 protein (40).

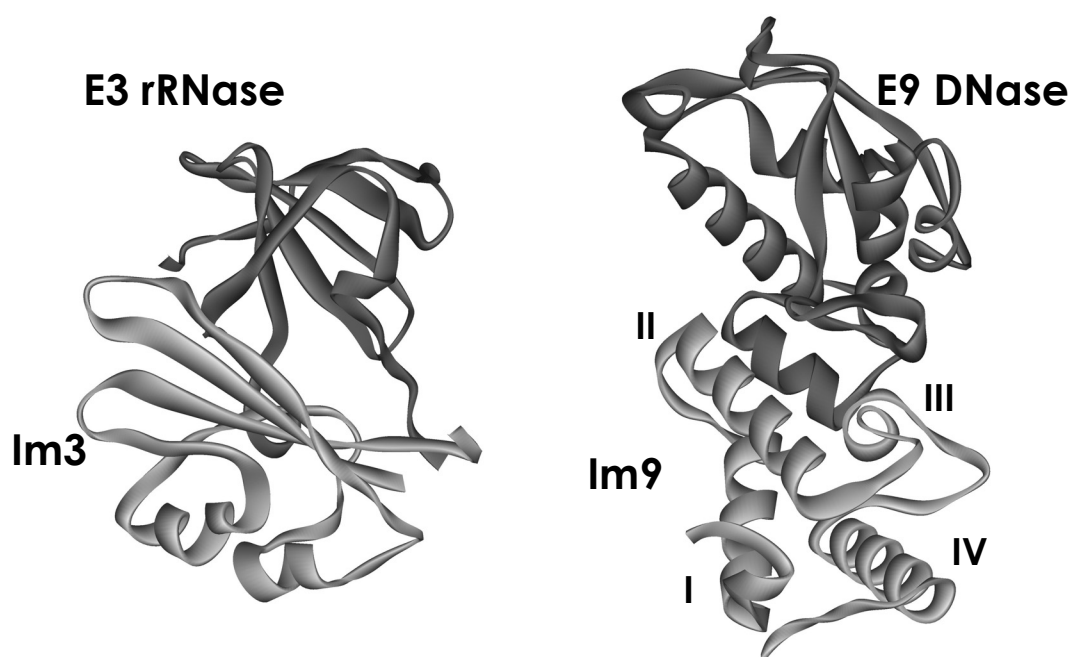


Figure 4. X-ray structures of the cytotoxic domain of colicins E3 and E9 bound to their natural inhibitors Im3 and Im9, respectively. The structures of both the E3 rRNase domain and Im3 are mainly β -sheet, which is in marked contrast to the mainly α -helical structures of the cytotoxic domains of DNase colicins and their immunity proteins (37, 40). Im9 α -helices are numbered.

Binding studies of E9 DNase to its cognate (Im9) and non-cognate immunity proteins (Im2, Im7 and Im8) demonstrated three main features of these complexes that is: 1) Diffusion controlled association ($10^9 \text{ M}^{-1}\text{s}^{-1}$ in buffers with low salt); 2) Very slow dissociation rates constants (10^7 s^{-1}) that result in very tight binding (10^{-16} M^{-1}) and; 3) Cognate complexes show 10^5 - 10^{10} fold tighter binding than non-cognate complexes. (41-43) In addition, the helix rich immunity proteins are very fast folding proteins ($\sim 2200 \text{ s}^{-1}$) (40) making immunity proteins efficient inhibitors. This is necessary since as soon as nuclease colicins are translated by the ribosome the nuclease folds to the active form and can induce cytotoxic activities.

The structure of the E9 cytotoxic domain bound to its cognate immunity protein Im9 is shown in Figure 4. The Im9 protein is a distorted four α -helix bundle with two helices (II and III) constituting the major E9 DNase binding site, with only minor changes in its structure occurring upon binding to the enzyme (40, 44-46). The structures of free Im7 (47, 48) and Im8 (49, 50) have also been determined, all of which have essentially the same structure as Im9. Although residues from helices II and III of the immunity protein make contacts with the exosite of the DNase (Figure 4), alanine scanning mutagenesis across both Im9 and Im2 (41, 51, 52) has demonstrated that the two helices do not contribute equally to the energetics of binding. Residues on the conserved helix III provide the bulk of binding energy with helix II (a variable helix) being a relatively minor contributor. Nevertheless, Li et al. (51) demonstrated via helix swapping experiments that helix II is responsible almost entirely for the specificity of the inhibitor protein. These observations led Kleanthous et al. (53) to propose a “dual recognition” model to explain immunity binding specificity whereby stability is conferred by conserved residues in helix III with residues from helix II defining specificity by affecting the overall binding free energy.

DNase colicins

Both the DNase domain of E2, E7, E8 and E9 (~15 kDa) and the immunity proteins Im2, Im7, Im8 and Im9 (~9.5 kDa) show strong sequence identity (65-80% and 55-65%, respectively). The DNase domains also share strong sequence homology to cytotoxic domains of toxins from other species e.g. klebicin B from *Klebsiella pneumoniae* (2) and pyocins AP41, S1 and S2 from *Pseudomonas aeruginosa* (4, 54). DNase colicins kill cells by degrading chromosomal DNA and it is believed that DNase activity eventually results in double strand breaks that overwhelm the DNA repair machinery of the cell (55-57).

The structure of the E7 DNase-Im7 complex has also been determined (with Zn^{2+} bound in the active site) (58) and revealed essentially a similar structure as the E9 DNase-Im9 complex (59). The active site of the DNase domains comprises the last ~30 amino acids of the protein (38), defined by site directed mutagenesis (60, 61). These last 30 amino acids comprise a $\beta\beta\alpha$ -fold that was found to bind a tetrahedrally coordinated metal ion – Ni^{2+} in E9 (40) or Zn^{2+} in E7 (58). This structure is reminiscent of a zinc-finger fold. These residues also contain the consensus sequence for a group of intron/intein encoded homing endonucleases called H-N-H endonucleases. The H-N-H motif is found in a range of endonucleases (62) as well as mismatch repair enzymes (63), recombinases such as T4 endonuclease VII (T4 DNase in Table 2) (64), and in some type II restriction endonucleases (65). H-N-H enzymes share even limited active site sequence similarities with CAD (Caspase Activated DNase) enzymes, DNases involved in the degradation of chromatin during the terminal stages of apoptosis. Sequence alignments of general H-N-H homing enzymes are shown in Table 2.

Table 2. H-N-H motif consensus sequence of several H-N-H homing enzymes.

Protein	Sequence		
	103	118	127
Colicin E9	YELH H DKPISQGGEVYDMD N IRVTTPKR H IDIH		
Colicin E2	FELH H DKPISQDGGVYDMD N IRVTTPKR H IDIH		
Colicin E8	FELH H DKPISQDGGVYDMD N LRITTPKR H IDIH		
Colicin E7	FELH H EKPISQNGGVYDMI N LSVVTTPKR H IDIH		
Klebicin B	VELH H KVEISKGGDVYNVD N LNALTPKR H IEIH		
Pyocin AP41	FEIH H VKPLESGGALYNID N LVIIVTPKR H SEIH		
Pyocin S2	IEIH H KVRIADGGGVYNMD N LVAVTPKR H IEIH		
Pyocin S1	IEIH H KVRVADGGGVYNMD N LVAVTPKR H IEIH		
Usp	FQIH H VVAIEHGGGVYDID N FRIVTPRL H DEIH		
T4 DNase	TETH H IIPRCMGG-TDDKT N LVLTPPE H FTAH		
McrA	LEVH H VIPLSSGG-ADTTD N CVALCPNC H RELH		
PsbA Orf	MEKH H IIPRHAGG-PDEKW N LISLTPED H IEAH		
RTase P0157	WQVH H IIRVDGG-SNCL S NLIMLHPM C HTLVH		
Consensus	ELHH	G	NL P H IH

Alignment of sequences containing the H-N-H motif from a PSI-Blast search using residues 96-131 of E9 DNase as the search sequence. Spaces are included in the sequences to optimize the alignment. The consensus sequence of the majority of the sequences is shown at the bottom of the figure. The H-N-H motif residues are shown in bold. The numbers refer to the residues of the colicin E9 DNase. [Adapted from Walker et al. (61)].

Homing endonucleases promote the homing of open reading frames coding for intronless/inteinless allelic sites. They are grouped according to the active site consensus sequence; H-N-H endonucleases have an absolutely conserved histidine- X_{14-32} -asparagine- X_{8-42} -histidine motif (66, 67). Three other groups of homing endonucleases are known, called the LAGLIDADG, GIY-YIG, and His-Cys box enzymes (68). Currently, the crystal structures of the E9 (40) and E7 (58) DNase domains are the only ones available. Homing endonucleases generally have very long recognition sequences in dsDNA (14-40bp), are usually dimeric and hence, cleave both DNA strands. This in contrast to the low specificity of monomeric colicin DNases (55). Additionally, most homing endonucleases are bilobal, containing a DNA recognition domain as well as a catalytic domain, whereas the 15 kDa colicin DNases are single domain proteins (68).

Kühlmann et al. (69) showed through structural alignments that H-N-H enzymes are in fact related to the active sites of the His-Cys box family homing endonucleases I-*PpoI* and the extracellular non-specific nuclease from *Serratia marcescens* (*Serratia* nuclease). Structural homology between *Serratia* nuclease and I-*PpoI* has previously been noted by Friedhoff et al. (70). Kühlmann et al. (69) also proposed that colicin DNases, I-*PpoI* and the *Serratia* nuclease can be classified as a single super family called the $\beta\beta\alpha$ -Me endonucleases. Independently, structural

similarities of T4 endonuclease VII to the colicin DNases were reported by Aravind et al. (64) who called this group the His-Me endonucleases.

One difference between the colicin DNases and the other $\beta\beta\alpha$ -Me endonucleases is the identity of the metal ion bound in the active site; transition metals in the colicin DNases (Ni^{2+} in the E9 DNase) but $\text{Mg}^{2+}/\text{Ca}^{2+}$ in all other cases. This likely represents the use of histidines as the metal ligating residues compared with asparagines in other cases (68, 69). Previous studies by Pommer et al. (55-57) have demonstrated that Ni^{2+} and Mg^{2+} are co-factors for colicin DNases, although they induce DNA cleavage via distinct mechanisms. Walker et al. (61) mutated many of the active site residues and assayed their endonuclease activity using Mg^{2+} or Ni^{2+} . They demonstrated that considerably more H-N-H residues are essential for the Mg^{2+} based activity than for the Ni^{2+} activity.

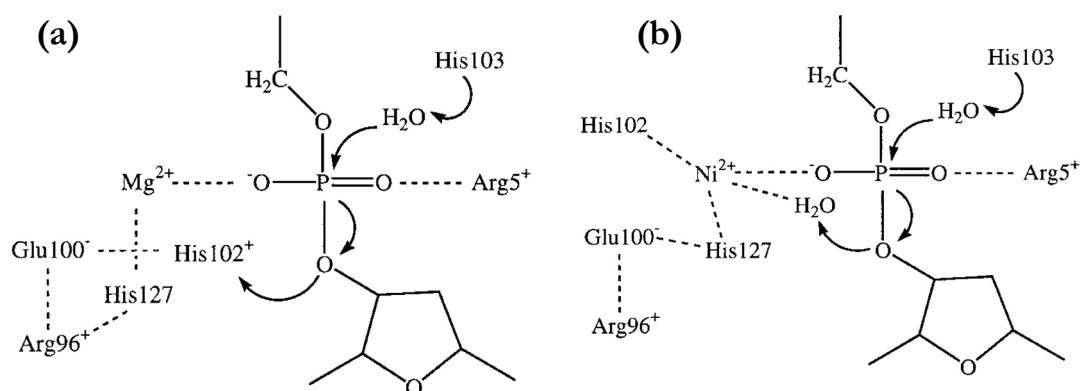


Figure 5. Putative mechanisms for the hydrolysis of DNA catalyzed by the H-N-H motif bound to (a) Mg^{2+} and (b) Ni^{2+} based on the X-ray structures of the E9 DNase in the apo and Ni^{2+} -ligated forms (40, 59). [Adapted from Pommer et al. (55)]

Pommer et al. (55) have proposed a catalytic mechanism for the Mg^{2+} supported activity involving a catalytic tetrad within the H-N-H motif (Figure 5). In this mechanism, His103 (which has a structural equivalent in I-*Ppo*I) activates a water molecule allowing it to make a nucleophilic attack on the scissile phosphate. Controversially, they postulated that a His127 coordinated Mg^{2+} ion stabilizes the developing negative charge on the phosphate oxygens, with His102 acting as a general acid to protonate the 3'-OH leaving group. This maybe assisted by a hydrogen bond from Arg96 to H127 (likely decreasing its pKa), and a Gly100 hydrogen bond to His102 (likely raising its pKa)(55). The role of His131 is still controversial (55, 61).

Aims and outline of this thesis

Proteins have evolved to carry out very specific functions within the cell by interacting with a diverse set of biomolecules. Understanding how a protein's higher order structure relates to its function is important for defining the molecular basis of these interactions. Proteins do not have rigid static structures. Instead, they display complex conformational dynamics, such as vibrational and rotational movements of side-chains and movements of whole domains relative to one another. Characterization of protein dynamics remains one of the major targets for structural biology. Established methods for studying proteins suffer from some limitations. Determination of protein structures by X-ray crystallography (solid phase) has produced huge strides forward in understanding the biophysical chemistry of proteins. However, the very nature of the crystallization process often selects for a single, uniform conformation (the one that crystallizes well) out of the population of structures that may be present in solution. Whilst analysis of crystal structures and diffraction techniques have improved the understanding of conformational dynamics of proteins trapped within crystal lattices, a true reflection of the dynamics within a protein requires studying it in solution. Nuclear Magnetic Resonance (NMR) spectroscopy, which is a solution-based technique, can give unique insights in protein complex formation as well as dynamics but has a limited protein mass range and requires large amounts of protein sample.

In recent years, mass spectrometry has become an important tool for studying protein structure and function. The primary goal of the work described in this thesis is to investigate structure-function relationships of E-type endonuclease colicins by mass spectrometry. Electrospray ionization mass spectrometry (ESI-MS) is used as the principal technique within this thesis for a) identifying structural changes and b) identifying the formation of non-covalent complexes. Since ESI-MS is a gas phase based technique we used a number of other biophysical techniques (in solution) to validate our MS based findings. Therefore, we used isothermal titration calorimetry (ITC), differential scanning calorimetry (DSC) circular dichroism (CD), steady state tryptophan fluorescence and time-resolved tryptophan fluorescence and anisotropy measurements. The latter two provide useful information about the molecular structure as well as the dynamics of proteins in solution (71) on the fluorescence time scale (i.e. nanoseconds), which allows for example to probe rotation of the entire protein or segments thereof.

In **Chapter 2** I will provide theory surrounding concepts and examples of how mass spectrometry can be implemented in the analysis of proteins higher-order structures (i.e. conformational analysis and non-covalent interactions). These concepts will be further used in the work described in this thesis to elucidate the role of the cytotoxic DNase domain in the colicin system.

The work described in **Chapter 3** is focused on the conformational dynamics of colicin E9 DNase by taking the unique capability of ESI-MS to allow simultaneous assessment of

conformational heterogeneity and metal ion binding. Alterations in charge state distributions on metal ion binding/release were validated with spectral changes observed in far- and near-UV CD and intrinsic tryptophan fluorescence. In addition, hydrogen/deuterium exchange experiments were used to probe structural integrity.

Chapter 4 extends the work described in chapter 3. The conformational stabilities of the four (E2, E7, E8 and E9), highly homologous, colicin DNases were compared side-by-side. These showed that the thermal stabilities of the apo-proteins differ by up to 20 °C. The observed differences correlate with the observed conformational behavior, i.e., the tendency of the protein to form either an open, less stable, or closed, more stable, conformation in solution, as deduced by both tryptophan accessibility measurements and ESI-MS studies. Kunitz DNase activity assays were performed for all four colicins to monitor the kinetics of DNA hydrolysis at different temperatures.

The work described in **Chapter 5** is a time-resolved fluorescence and anisotropy study of colicin E9 DNase to further investigate the conformational dynamics on the nanosecond timescale in combination with steady state acrylamide quenching experiments. The dynamic properties of the apo-enzyme were compared to those of the E9 DNase ligated to the transition metal ion Zn^{2+} and the natural inhibitor Im9. Further I investigated the contributions of each of the two tryptophans within the E9 DNase (Trp22 and Trp58), using two single-tryptophan mutants (E9 W22F and E9 W58F).

In **Chapter 6** I describe the measurement of the ligation of a single phosphate ion to the enzyme colicin E9 DNase via electrospray ionization mass spectrometry (ESI-MS). In contrast to what was expected from extensive X-ray structural data this single phosphate ion ligation turned out to be specifically regulated by preceding Zn^{2+} ligation to the enzyme. The ESI-MS data presented here were validated by isothermal titration calorimetry (ITC). As DNA is the natural substrate of the enzyme I have hypothesized that the findings reported here have impact on the detailed functional mechanism of the enzyme and the role of the metal ion co-factors therein.

Chapter 7 extends the work described in chapter 6 to elucidate further the biological impact of the specifically regulated ligation of the single phosphate ion. To find the origin for this inhibition alanine mutants were constructed for the metal ligating (H102, H127 and for H131 that possibly ligates the metal ion) and phosphate ion ligating residues (H103 and Arg5). ESI-MS was used to study the Ni^{2+} , Zn^{2+} and single nucleotide (rAMP and dAMP) binding capabilities. Moreover, ITC experiments were performed to complement the ESI-MS findings.

The final chapter of this thesis, **Chapter 8**, offers a summarizing discussion.

References

1. Riley, M. A., and Wertz, J. E. (2002) Bacteriocins: evolution, ecology, and application *Annu. Rev. Microbiol.* 56, 117-137.
2. Riley, M. A., Pinou, T., Wertz, J. E., Tan, Y., and Valletta, C. M. (2001) Molecular characterization of the klebicin B plasmid of *Klebsiella pneumoniae* *Plasmid* 45, 209-221.
3. James, R., Penfold, C. N., Moore, G. R., and Kleanthous, C. (2002) Killing of *E. coli* cells by E group nuclease colicins *Biochimie* 84, 381-389.
4. Riley, M. A. (1998) Molecular mechanisms of bacteriocin evolution *Annu. Rev. Genet.* 32, 255-278.
5. Lazdunski, C. J., Bouveret, E., Rigal, A., Journet, L., Llobes, R., and Benedetti, H. (1998) Colicin import into *Escherichia coli* cells *J. Bacteriol.* 180, 4993-5002.
6. Penfold, C. N., Garinot-Schneider, C., Hemmings, A. M., Moore, G. R., Kleanthous, C., and James, R. (2000) A 76-residue polypeptide of colicin E9 confers receptor specificity and inhibits the growth of vitamin B12-dependent *Escherichia coli* 113/3 cells. PG - 639-49 *Mol. Microbiol.* 38, 639-649.
7. Kurisu, G., Zakharov, S. D., Zhalnina, M. V., Bano, S., Eroukova, V. Y., Rokitskaya, T. I., Antonenko, Y. N., Wiener, M. C., and Cramer, W. A. (2003) The structure of BtuB with bound colicin E3 R-domain implies a translocon *Nat. Struct. Biol.* 10, 948-954.
8. Soelaiman, S., Jakes, K., Wu, N., Li, C., and Shoham, M. (2001) Crystal structure of colicin E3: implications for cell entry and ribosome inactivation *Mol. Cell* 8, 1053-1062.
9. Chak, K. F., and James, R. (1986) Characterization of the ColE9-J plasmid and analysis of its genetic organization *J Gen Microbiol* 132 (Pt 1), 61-70.
10. Dekker, N., Tommassen, J., and Verheij, H. M. (1999) Bacteriocin release protein triggers dimerization of outer membrane phospholipase A in vivo *J. Bacteriol.* 181, 3281-3283.
11. James, R., Kleanthous, C., and Moore, G. R. (1996) The biology of *E. coli* colicins: paradigms and paradoxes *Microbiology* 142, 1569-1580.
12. Jakes, K. S., and Zinder, N. D. (1974) Highly purified colicin E3 contains immunity protein *Proc. Natl. Acad. Sci. U.S.A.* 71, 3380-3384.
13. Riley, M. A., and Gordon, D. M. (1999) The ecological role of bacteriocins in bacterial competition *Trends Microbiol.* 7, 129-133.
14. Webster, R. E. (1991) The tol gene products and the import of macromolecules into *Escherichia coli* *Mol. Microbiol.* 5, 1005-1011.
15. Ferguson, A. D., Hofmann, E., Coulton, J. W., Diederichs, K., and Welte, W. (1998) Siderophore-mediated iron transport: crystal structure of FhuA with bound lipopolysaccharide *Science* 282, 2215-2220.
16. Thanassi, D. G., and Hultgren, S. J. (2000) Multiple pathways allow protein secretion across the bacterial outer membrane *Curr. Opin. Cell. Biol.* 12, 420-430.
17. Mosbahi, K., Lemaitre, C., Keeble, A. H., Mobasheri, H., Morel, B., James, R., Moore, G. R., Lea, E. J., and Kleanthous, C. (2002) The cytotoxic domain of colicin E9 is a channel-forming endonuclease *Nat. Struct. Biol.* 9, 476-484.
18. de Zamaroczy, M., Mora, L., Lecuyer, A., Geli, V., and Buckingham, R. H. (2001) Cleavage of colicin D is necessary for cell killing and requires the inner membrane peptidase LepB *Mol. Cell.* 8, 159-168.
19. Liao, C. C., Hsiao, K. C., Liu, Y. W., Leng, P. H., Yuen, H. S., and Chak, K. F. (2001) Processing of DNase domain during translocation of colicin E7 across the membrane of *Escherichia coli* *Biochem. Biophys. Res. Commun.* 284, 556-562.
20. Bradbeer, C., Woodrow, M. L., and Khalifah, L. I. (1976) Transport of vitamin B12 in *Escherichia coli*: common receptor system for vitamin B12 and bacteriophage BF23 on the outer membrane of the cell envelope *J. Bacteriol.* 125, 1032-1039.
21. Di Masi, D. R., White, J. C., Schnaitman, C. A., and Bradbeer, C. (1973) Transport of vitamin B12 in *Escherichia coli*: common receptor sites for vitamin B12 and the E colicins on the outer membrane of the cell envelope *J. Bacteriol.* 115, 506-513.

22. Chimento, D. P., Mohanty, A. K., Kadner, R. J., and Wiener, M. C. (2003) Substrate-induced transmembrane signaling in the cobalamin transporter BtuB *Nat. Struct. Biol.* 10, 394-401.
23. Buchanan, S. K., Smith, B. S., Venkatramani, L., Xia, D., Esser, L., Palnitkar, M., Chakraborty, R., van der Helm, D., and Deisenhofer, J. (1999) Crystal structure of the outer membrane active transporter FepA from *Escherichia coli* *Nat. Struct. Biol.* 6, 56-63.
24. Ferguson, A. D., Chakraborty, R., Smith, B. S., Esser, L., van der Helm, D., and Deisenhofer, J. (2002) Structural basis of gating by the outer membrane transporter FecA *Science* 295, 1715-1719.
25. Fanucci, G. E., Cadieux, N., Kadner, R. J., and Cafiso, D. S. (2003) Competing ligands stabilize alternate conformations of the energy coupling motif of a TonB-dependent outer membrane transporter *Proc Natl Acad Sci U S A* 100, 11382-11387.
26. Fanucci, G. E., Lee, J. Y., and Cafiso, D. S. (2003) Membrane mimetic environments alter the conformation of the outer membrane protein BtuB *J Am Chem Soc* 125, 13932-13933.
27. Wiener, M., Freymann, D., Ghosh, P., and Stroud, R. M. (1997) Crystal structure of colicin Ia *Nature* 385, 461-464.
28. Vetter, I. R., Parker, M. W., Tucker, A. D., Lakey, J. H., Pattus, F., and Tsernoglou, D. (1998) Crystal structure of a colicin N fragment suggests a model for toxicity *Structure* 6, 863-874.
29. Derouiche, R., Gavioli, M., Benedetti, H., Prilipov, A., Lazdunski, C., and Lloubes, R. (1996) TolA central domain interacts with *Escherichia coli* porins *Embo J.* 15, 6408-6415.
30. Lazzaroni, J. C., Germon, P., Ray, M.-C., and Vianney, A. (1999) The Tol proteins of *Escherichia coli* and their involvement in the uptake of biomolecules and outer membrane stability *FEMS Microbiol. Lett.* 177, 191-197.
31. Germon, P., Ray, M. C., Vianney, A., and Lazzaroni, J. C. (2001) Energy-dependent conformational change in the TolA protein of *Escherichia coli* involves its N-terminal domain, TolQ, and TolR *J. Bacteriol.* 183, 4110-4114.
32. Carr, S., Penfold, C. N., Bamford, V., James, R., and Hemmings, A. M. (2000) The structure of TolB, an essential component of the tol-dependent translocation system, and its protein-protein interaction with the translocation domain of colicin E9 *Structure Fold. Des.* 8, 57-66.
33. Bouveret, E., Rigal, A., Lazdunski, C., and Benedetti, H. (1997) The N-terminal domain of colicin E3 interacts with TolB which is involved in the colicin translocation step *Mol. Microbiol.* 23, 909-920.
34. Garinot-Schneider, C., Penfold, C. N., Moore, G. R., Kleanthous, C., and James, R. (1997) Identification of residues in the putative TolA box which are essential for the toxicity of the endonuclease toxin colicin E9 *Microbiology* 143, 2931-2938.
35. Ogawa, T., Tomita, K., Ueda, T., Watanabe, K., Uozumi, T., and Masaki, H. (1999) A cytotoxic ribonuclease targeting specific transfer RNA anticodons *Science* 283, 2097-2100.
36. Tomita, K., Ogawa, T., Uozumi, T., Watanabe, K., and Masaki, H. (2000) A cytotoxic ribonuclease which specifically cleaves four isoaccepting arginine tRNAs at their anticodon loops *Proc. Natl. Acad. Sci. U S A* 97, 8278-8283.
37. Carr, S., Walker, D., James, R., Kleanthous, C., and Hemmings, A. M. (2000) Inhibition of a ribosome-inactivating ribonuclease: the crystal structure of the cytotoxic domain of colicin E3 in complex with its immunity protein *Structure Fold. Des.* 8, 949-960.
38. Kleanthous, C., and Walker, D. (2001) Immunity proteins: enzyme inhibitors that avoid the active site *Trends Biochem. Sci.* 26, 624-631.
39. Buckle, A. M., and Fersht, A. R. (1994) Subsite binding in an RNase: structure of a barnase-tetranucleotide complex at 1.76-Å resolution *Biochemistry* 33, 1644-1653.
40. Kleanthous, C., Kuhlmann, U. C., Pommer, A. J., Ferguson, N., Radford, S. E., Moore, G. R., James, R., and Hemmings, A. M. (1999) Structural and mechanistic basis of immunity toward endonuclease colicins *Nat. Struct. Biol.* 6, 243-252.
41. Li, W., Hamill, S. J., Hemmings, A. M., Moore, G. R., James, R., and Kleanthous, C. (1998) Dual recognition and the role of specificity-determining residues in colicin E9 DNase-immunity protein interactions *Biochemistry* 37, 11771-9.
42. Wallis, R., Leung, K. Y., Pommer, A. J., Videler, H., Moore, G. R., James, R., and Kleanthous, C. (1995b) Protein-protein interactions in colicin E9 DNase-immunity protein complexes. 2.

- Cognate and noncognate interactions that span the millimolar to femtomolar affinity range *Biochemistry* 34, 13751-13759.
43. Wallis, R., Moore, G. R., James, R., and Kleanthous, C. (1995a) Protein-protein interactions in colicin E9 DNase-immunity protein complexes. 1. Diffusion-controlled association and femtomolar binding for the cognate complex *Biochemistry* 34, 13743-13750.
 44. Osborne, M. J., Lian, L. Y., Wallis, R., Reilly, A., James, R., Kleanthous, C., and Moore, G. R. (1994) Sequential assignments and identification of secondary structure elements of the colicin E9 immunity protein in solution by homonuclear and heteronuclear NMR *Biochemistry* 33, 12347-12355.
 45. Osborne, M. J., Breeze, A. L., Lian, L. Y., Reilly, A., James, R., Kleanthous, C., and Moore, G. R. (1996) Three-dimensional solution structure and ¹³C nuclear magnetic resonance assignments of the colicin E9 immunity protein Im9 *Biochemistry* 35, 9505-9512.
 46. Boetzel, R., Czisch, M., Kaptein, R., Hemmings, A. M., James, R., Kleanthous, C., and Moore, G. R. (2000) NMR investigation of the interaction of the inhibitor protein Im9 with its partner DNase *Protein Sci.* 9, 1709-1718.
 47. Chak, K. F., Safo, M. K., Ku, W. Y., Hsieh, S. Y., and Yuan, H. S. (1996) The crystal structure of the immunity protein of colicin E7 suggests a possible colicin-interacting surface *Proc. Natl. Acad. Sci. U.S.A.* 93, 6437-6442.
 48. Dennis, C. A., Videler, H., Pauptit, R. A., Wallis, R., James, R., Moore, G. R., and Kleanthous, C. (1998) A structural comparison of the colicin immunity proteins Im7 and Im9 gives new insights into the molecular determinants of immunity-protein specificity *Biochem. J.* 333, 183-191.
 49. Videler, H. (1998) Colicin E8 immunity protein: structure and interaction *PhD thesis, University of East Anglia*.
 50. Le Duff, C. S. (2001) Probing fold and function of immunity proteins Im7 and Im8 using NMR spectroscopy *PhD thesis, University of East Anglia*.
 51. Li, W., Dennis, C. A., Moore, G. R., James, R., and Kleanthous, C. (1997) Protein-protein interaction specificity of Im9 for the endonuclease toxin colicin E9 defined by homologue-scanning mutagenesis *J. Biol. Chem.* 272, 22253-22258.
 52. Wallis, R., Leung, K. Y., Osborne, M. J., James, R., Moore, G. R., and Kleanthous, C. (1998) Specificity in protein-protein recognition: conserved Im9 residues are the major determinants of stability in the colicin E9 DNase-Im9 complex *Biochemistry* 37, 476-485.
 53. Kleanthous, C., Hemmings, A. M., Moore, G. R., and James, R. (1998) Immunity proteins and their specificity for endonuclease colicins: telling right from wrong in protein-protein recognition *Mol. Microbiol.* 28, 227-233.
 54. Parret, A. H., and De Mot, R. (2002) Bacteria killing their own kind: novel bacteriocins of *Pseudomonas* and other gamma-proteobacteria *Trends Microbiol.* 10, 107-112.
 55. Pommer, A. J., Cal, S., Keeble, A. H., Walker, D., Evens, S. J., Kuhlman, U. C., Cooper, A., Connolly, B. A., Hemmings, A. M., Moore, G. R., James, R., and Kleanthous, C. (2001) Mechanisms and cleavage specificity of the H-N-H endonuclease colicin E9 *J.Mol.Biol.* 314, 735-749.
 56. Pommer, A. J., Kuhlmann, U. C., Cooper, A., Hemmings, A. M., Moore, G. R., James, R., and Kleanthous, C. (1999) Homing in on the role of transition metals in the HNH motif of colicin endonucleases *J. Biol. Chem.* 274, 27153-27160.
 57. Pommer, A. J., Wallis, R., Moore, G. R., James, R., and Kleanthous, C. (1998) Enzymological characterization of the nuclease domain from the bacterial toxin colicin E9 from *Escherichia coli* *Biochem. J.* 334, 387-392.
 58. Ko, T. P., Liao, C. C., Ku, W. Y., Chak, K. F., and Yuan, H. S. (1999) The crystal structure of the DNase domain of colicin E7 in complex with its inhibitor Im7 protein *Structure Fold. Des.* 7, 91-102.
 59. Kuhlmann, U. C., Pommer, A. J., Moore, G. R., James, R., and Kleanthous, C. (2000) Specificity in protein-protein interactions: the structural basis for dual recognition in endonuclease colicin-immunity protein complexes *J. Mol. Biol.* 301, 1163-1178.

60. Garinot-Schneider, C., Pommer, A. J., Moore, G. R., Kleanthous, C., and James, R. (1996) Identification of putative active-site residues in the DNase domain of colicin E9 by random mutagenesis *J. Mol. Biol.* **260**, 731-742.
61. Walker, D. C., Georgiou, T., Pommer, A. J., Walker, D., Moore, G. R., Kleanthous, C., and James, R. (2002) Mutagenic scan of the H-N-H motif of colicin E9: implications for the mechanistic enzymology of colicins, homing enzymes and apoptotic endonucleases *Nucleic Acids Res.* **30**, 3225-3234.
62. Dalgaard, J. Z., Klar, A. J., Moser, M. J., Holley, W. R., Chatterjee, A., and Mian, I. S. (1997) Statistical modeling and analysis of the LAGLIDADG family of site-specific endonucleases and identification of an intein that encodes a site-specific endonuclease of the HNH family *Nucleic Acids Res.* **25**, 4626-4638.
63. Malik, H. S., and Henikoff, S. (2000) Dual recognition-incision enzymes might be involved in mismatch repair and meiosis *Trends Biochem. Sci.* **25**, 414-418.
64. Aravind, L., Makarova, K. S., and Koonin, E. V. (2000) Survey and Summary: holliday junction resolvases and related nucleases: identification of new families, phyletic distribution and evolutionary trajectories *Nucleic Acids Res.* **28**, 3417-3432.
65. Bujnicki, J. M., Radlinska, M., and Rychlewski, L. (2001) Polyphyletic evolution of type II restriction enzymes revisited: two independent sources of second-hand folds revealed *Trends Biochem. Sci.* **26**, 9-11.
66. Belfort, M., and Roberts, R. J. (1997) Homing endonucleases: keeping the house in order *Nucleic Acids Res.* **25**, 3379-3388.
67. Shub, D. A., Goodrich-Blair, H., and Eddy, S. R. (1994) Amino acid sequence motif of group I intron endonucleases is conserved in open reading frames of group II introns *Trends Biochem. Sci.* **19**, 402-404.
68. Chevalier, B. S., and Stoddard, B. L. (2001) Homing endonucleases: structural and functional insight into the catalysts of intron/intein mobility *Nucleic Acids Res.* **29**, 3757-3774.
69. Kuhlmann, U. C., Moore, G. R., James, R., Kleanthous, C., and Hemmings, A. M. (1999) Structural parsimony in endonuclease active sites: should the number of homing endonuclease families be redefined? *FEBS Lett.* **463**, 1-2.
70. Friedhoff, P., Franke, I., Meiss, G., Wende, W., Krause, K. L., and Pingoud, A. (1999) A similar active site for non-specific and specific endonucleases *Nat. Struct. Biol.* **6**, 112-113.
71. Lakowicz, J. R. (1999) *Principles of Fluorescence Spectroscopy*, Second ed., Kluwer Academic / Plenum Publishers, New York, Dordrecht, London, Moscow.

Chapter 2

Mass spectrometry in protein conformational analysis and molecular recognition

Ewald T.J. van den Bremer, Albert J. R. Heck¹

Adapted from: Biotechnology: pharmaceutical aspects;
Vol.3 Methods for structural analysis of protein pharmaceuticals;
AAPS Press (2004), *in press*

¹Dept. of Biomolecular mass spectrometry, Utrecht University, Utrecht

Introduction to mass spectrometry

Mass spectrometry is a technique that has already been around for more than 100 years. However, over the last decade mass spectrometry (MS) has developed into a mature tool to study larger biomolecules in general and proteins in particular. MS has proven to be extremely useful in determining the primary structure of proteins including possible post-translational modifications. Therefore, currently MS is a key technology in proteome research. MS-based proteomics is a discipline made possible by the availability of gene and genome sequence databases and technical and conceptual advances in many areas but most notably by the discovery of ionization methods for larger biomolecules. Today, MS-based proteomics is a multifaceted, rapidly developing open-ended endeavor. Also recently, MS has been utilized in the analysis of secondary and tertiary protein structures, for instance in combination with hydrogen/deuterium exchange (e.g. (1, 2)). Additionally, MS has been applied to study quaternary structures of proteins and protein complexes and their interactions with enzymes, cofactors, substrates or other ligands. The use of MS in the analysis of protein higher-order structures are the main focus of this chapter. In mass spectrometry we can in general separate the methodology in three different stages; 1) sample introduction and ionization, 2) separation of ions according to their mass-to-charge ratios in time or space and, 3) ion detection and recording of the mass spectrum.

For many years electron impact (EI) and chemical ionization (CI) were the only ionization methods available for analyzing molecules by MS, although these methods were limited to volatile compounds. In the early 1980's a new ionization technique was introduced termed plasma desorption MS (3, 4). In PDMS secondary gaseous ions are generated in a sputtering process by bombardment with high-energy primary ions (MeV). PDMS was one of the first ionization techniques that allowed the analysis of peptides. A real breakthrough for this application in protein chemistry at that time came after the observation in mass spectra of molecular ions of larger peptides such as insulin (5). Subsequently, Barber and co-workers developed around 1980 an ionization technique based on bombardment with neutral atoms (e.g. Xe, Ar) (6) termed fast atom bombardment (FAB) MS. FABMS was a useful ionization method that, like PDMS, allowed observation of molecular ions of larger peptides (7, 8). FAB involves the bombardment of a solid mixture of a matrix (small organic species, e.g. glycerol or thioglycerol) and analyte by a fast particle beam of neutral Ar or Xe atoms. When this high-energy atom beam strikes the matrix, kinetic energy is transferred to the surface molecules and is dissipated in various ways, some of which result in evaporation and ionization of both matrix and analyte molecules. These two techniques, PDMS and FAB, opened the development of new strategies in protein analysis and made it possible to analyze compounds of higher mass up to several tens of kDa. Disadvantages were still the low upper mass limit, the low ionization efficiency (9) and the high background due to matrix ion signals. Although PDMS and FAB were important developments, the current prominent role of mass spectrometry in the analysis of

biological macromolecules is particularly due to two major technical breakthroughs in the late 1980's: the development of matrix-assisted laser desorption/ionization (MALDI)-MS and electrospray ionization (ESI)-MS. The inventors of these novel ionization methods, John Fenn and Koichi Tanaka, were awarded by the 2002 Nobel prize in chemistry indicating the importance of these developments. The development of the 'soft' ionization techniques MALDI and ESI was revolutionary since it permits analysis of biomolecules in a mass range of up to and over 100 kDa. These techniques require less energy and thereby introduce the biomolecules intact into the gas-phase. Nowadays, these two techniques are routinely used on a wide variety of biomolecules, especially for peptide and protein analysis. The sensitivity of these two techniques is considered to be extremely good, reaching down to the femtomole level. In the following sections the principles of MALDI and ESI will be discussed in more detail.

Electrospray ionization mass spectrometry

The principle of ESI found its origin in molecular beamwork at the end of the 1960's and was first described by Dole et al. (10). The potential of ESI as a mass spectrometric technique was for the first time demonstrated by Fenn and co-workers in the late 1980's. They described that molecular ions (i.e. proteins) with a high charge-state could be obtained (11). The ESI process is shown schematically in Figure 1. Electrospray is basically based on two processes: 1) the generation of a fine spray of charged droplets and, 2) the removal of the solvent to produce molecular ions (e.g. proteins). As described in detail by Kobarle (12) in electrospray initially small charged droplets are formed at the tip of the capillary and are electrostatically attracted to the mass spectrometer inlet. Due to the action of the applied electric field on the solution at the capillary tip (1-4 kV) the liquid is enriched for positive ions (in positive ion mode).

Two mechanisms have been proposed to explain the final gas-phase ion formation named (a) the charge residue model and (b) the ion evaporation model. The first mechanism proposes that ions detected in the mass spectrometer are the charged species that remain after all of the solvent has evaporated from a droplet (13). Continuous evaporation and fission events would eventually leads to the formation of "droplets" containing a single highly charged ion. In the evaporation model, ions are emitted from the small, highly charged droplets when the repulsion between the charged ion and other charges of the droplet cause expulsion of the ions (14) In ESI the formation of ions take place at atmospheric pressure and is very gentle (15, 16).

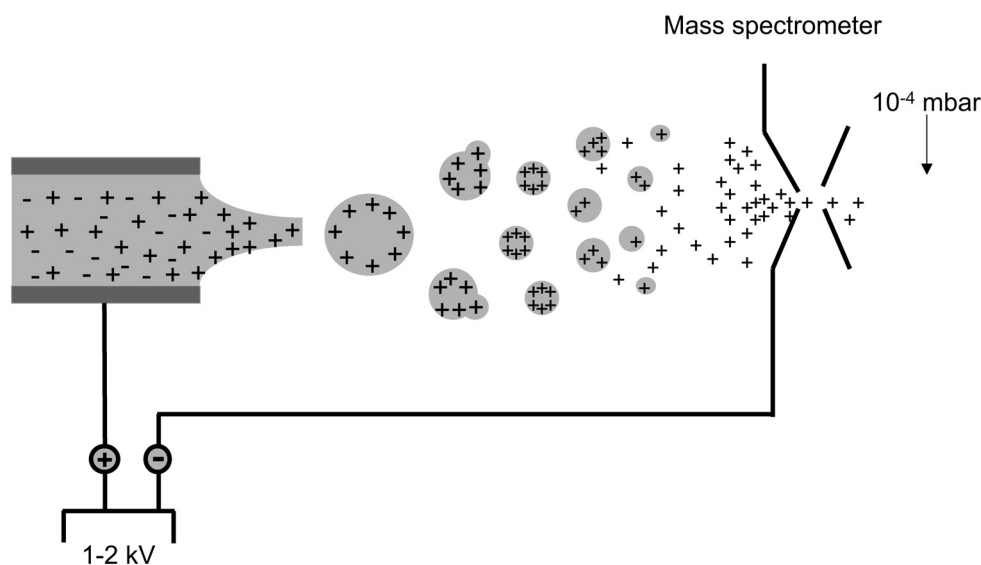


Figure 1. Illustrating the nano-flow ESI process in the positive ion mode. The nano-ESI source disperses the liquid analyte purely by electrostatic means. Continuous evaporation and fission events would eventually lead to the formation of “droplets” containing a single highly charged ion [Adapted from Ganem et al. (17)].

The introduction of nano-flow ESI, which is a low-flow variant, has played an important role in the analysis of proteins. This allowed the analysis of very small amounts of analyte due to an introduction rate of nanoliters per minute (15). Using nano-ESI MS, typically less than $1 \mu\text{l}$ is introduced into the ion source through a gold-coated glass capillary with an orifice of $1\text{-}3 \mu\text{m}$. The nano-ESI source disperses the liquid analyte purely by electrostatic means and no assistance such as nebulising gas is needed. It improves desolvation, ionization, and transfer efficiencies into the mass analyzer. The initial droplets have a diameter of less than 200 nm , thus, their volume is about $100\text{-}1000$ times smaller than that of the droplets generated using conventional ESI sources. In this way nano-ESI enables analysis of proteins at concentrations of less than $1 \text{ pmole}/\mu\text{l}$. A small drawback is that the evaporation process favors solvents and buffers that are volatile. This puts certain restrictions on its compatibility with wet biochemical procedures; ESI-MS is most suited for analysis of samples that are highly purified in terms of salts and low-molecular-weight contaminants.

On the other hand, a great advantage of ESI-MS is that it is very well suited to study protein-protein, protein-ligand and protein-metal interactions since in the ESI process weak non-covalent interactions may be preserved. The use of ESI-MS for such applications is rapidly expanding and is even not solely restricted to investigate protein interactions on the inter- but also on the intramolecular level, e.g. in protein folding as further discussed in this chapter.

Matrix-assisted laser desorption ionization mass spectrometry

The first results of laser/desorption ionization of high weight molecules were presented in 1987 at the 2nd Japan-China Joint Symposium on Mass spectrometry and published in 1988 (18). In the original work, Tanaka and co-workers used a sample preparation where the analyte is mixed with ultrafine cobalt powder and glycerol as vacuum-stable binding medium. When irradiated with a laserpulse glycerol and intact analyte molecules could be desorbed into the gas phase. Nowadays, the original method is hardly used. Instead a closely related method, matrix-assisted laser desorption/ionization (MALDI) developed by Karas and Hillenkamp has become the method of choice (19). This technique requires a solid matrix with which the sample is co-crystallized. The three most frequently used matrices for the analysis of proteins and peptides are α -cyano-4-hydroxycinnamic acid, 2,5-dihydroxybenzoic acid, and sinapinic acid. The matrix α -cyano-4-hydroxycinnamic acid is mostly used for the analysis of peptides and small proteins and peptides. Sinapinic acid, in contrast, is mostly used for larger proteins. 2,5-dihydroxybenzoic acid is a more generally applicable matrix for both peptides and proteins. The matrix absorbs most of the incident energy and is believed to facilitate the ionization process. The charged molecules are directed by electrostatic lenses from the ionization source into the mass analyzer. Subsequently, time-of-flight analysis is often used to separate the ions according to their mass-to-charge ratio. In contrast to ESI, the ionization process in MALDI, mainly yields singly charged proteins or peptides (20) which makes analysis of mixtures of proteins or peptides relatively simple. MALDI has many attractive features. First, the sensitivity is remarkably high, with spectra of as little as 1 fmole of lysozyme being reported (21). Very little suppression is observed in mixture analysis (22). The tolerance to the presence of salts and impurities of various kinds is high, which allows analysis of crude samples of biological origin (23). This high tolerance has been explained by co-crystallization of the protein with matrix molecule with concomitant exclusion of impurities from the crystals (24). A drawback of MALDI is that protein complexes are often not preserved.

Ion separation and detection

Once the ions have been produced, they need to be separated according to their mass-to-charge ratios (m/z), which must be determined. There are many different mass analyzers, just as there are a great variety of ion sources. In recent years the development of hybrid mass analyzers brought together several advantages from different MS analyzers. Hybrid systems combine two different mass analyzers. Presently, the most frequently used hybrid mass analyzer is the quadrupole time-of-flight system.

A quadrupole (Q) is a device that uses the stability of the trajectories in oscillating electric fields to separate ions according to their mass-to-charge ratios. In case of a positive ion entering the space between the rods the ion will be drawn towards a negative rod. If the potential changes sign before it discharges itself on this rod, the ion will change direction. By applying an

alternating radio frequency (RF) on top of a direct current (DC) voltage, ions traveling at relatively low velocity with different (m/z) values follow different trajectories through the rods. At a particular voltage, ions with a certain m/z value traverse the quadrupole, while others collide with the rods and are lost. By scanning the voltages keeping the ratios between the DC and the RF voltages constant, ions with different m/z values pass successively through the mass analyzer. A quadrupole analyzer is very well suitable for coupling with ESI, since it can operate at relatively high pressure and does not require high accelerating fields. Drawbacks of a quadrupole instruments include their relatively low resolution and their limited mass range (typically up to m/z 3000-4000)

In the quadrupole time-of-flight hybrid mass analyzer, a quadrupole is coupled to a time-of-flight (ToF) analyzer, resulting in a Q-ToF mass spectrometer. The ToF analyzer is one of the simplest mass analyzing devices and is commonly used with MALDI and ESI. ToF is based on accelerating a set of ions to a detector with the same amount kinetic energy (E_k). Since $E_k = \frac{1}{2} m v^2$, where m stands for the mass of the ion and v for the velocity of the ion, ions will fly a certain distance d (which is given by the length of ToF tube) within a time t , where t is dependent on the m/z of the ion. The most important drawback of linear ToF analyzers is their poor mass resolution. An electrostatic reflector, also called a reflectron, may be incorporated into the flight tube to reduce the spread in initial kinetic energies of the ions produced and so improve the resolution. For an extensive review on the fundamentals of Q-ToF analysis, see ref. (25)

Most commonly a hybrid tandem mass spectrometer is constructed from a quadrupole and an orthogonal ToF mass analyzer (see Figure 2). In order to record mass spectra using this instrument, the quadrupole operates in the RF-only mode and acts as a wide band-pass filter transmitting ions across the entire m/z range. The ions are in a pulsed mode extracted orthogonally into the flight tube to correct for spatial or velocity spread of the ions in the direction of the ion source and so improve resolution (25). In the MS/MS mode, the quadrupole serves as a mass filter for selection of precursor ions up to m/z 4000 for collision induced dissociation (CID). For the work described in this thesis mostly an orthogonal ESI-ToF instrument was used (Figure 2). In this instrument ions generated in the ESI source are focused and transferred through two stages of differentially pumped vacuum chambers using hexapole ion bridges before they are orthogonally accelerated into the reflectron ToF analyzer. The reason for the use of this instrument is that the work presented here focuses on intact protein molecules and thus MS/MS is not really required.

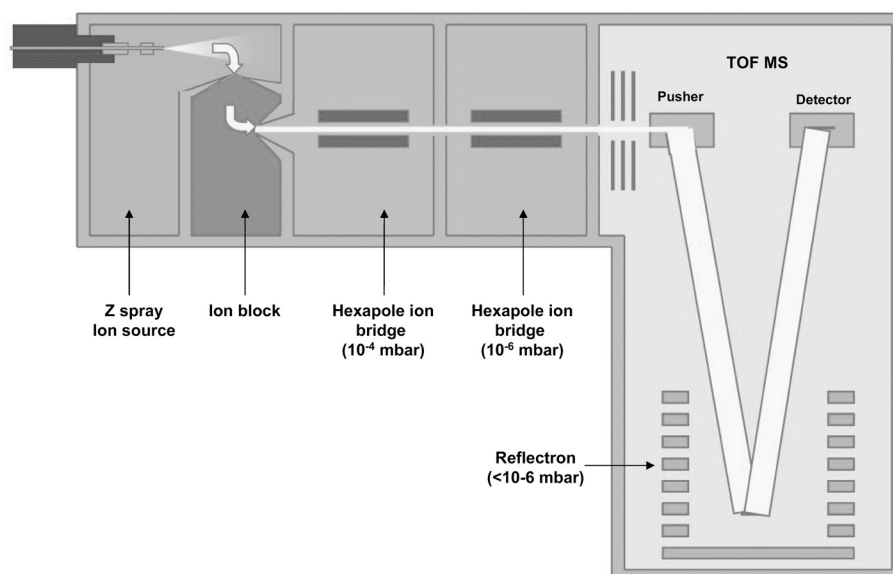


Figure 2. Schematic representation of a Micromass ESI ToF mass spectrometer.

Structural analysis of proteins

Conformational changes based on charge-state distribution

It was not long after the introduction of ESI-MS that the potential of this technique to probe higher-order structure of proteins was realized. Much of the early work with ESI was focused on the mechanistic aspects of desorption and ionization events. Solutions of pH 3-4 were commonly used for basic peptides and proteins because of their optimal ionization efficiency. The effect of higher pH toward the neutral, physiological regime and to the more basic end of the pH scale was studied for their effects on biological molecules (26-28). Early studies (29, 30) demonstrated that folded and unfolded proteins produced a different distribution of charge-states in their electrospray mass spectra. One obvious difference observed from high pH solutions was that the charge distribution typically shifted towards lower charging or higher mass-to-charge. Fenn et al. have explained this phenomenon within the “ion-evaporation” model (31). According to that theory, tightly folded protein molecules are expected to have significantly smaller projected areas compared to less-structured protein molecules, and would, therefore, accommodate fewer charges on the surface during the ion evaporation stage. As a result, two protein molecules whose geometries are very different from each other (e.g. compact folded states versus less-folded states) will produce ions with significant differences in charge density. If both states are populated simultaneously in solution under certain conditions, then the resultant charge-state distribution in the ESI spectrum could exhibit a bimodal character. This effect has been utilized extensively over the past several years to investigate protein-unfolding reactions.

Konermann and Douglas pioneered this approach to study acid induced unfolding of several proteins (32-34). For instance in Figure 3 ESI-MS spectra are shown of cytochrome *c* sprayed from solutions at different pH. Between pH 8.5 and 3.2 cytochrome *c* is folded and displays a “low” charge distribution. When the pH is further reduced ESI-MS spectra reveal a “high” charge distribution indicative for a more unfolded protein. Related to this Mohimen et al. reported a chemometric approach for the analysis of multiple overlapping charge-state distributions to resolve protein conformers in solution (35).

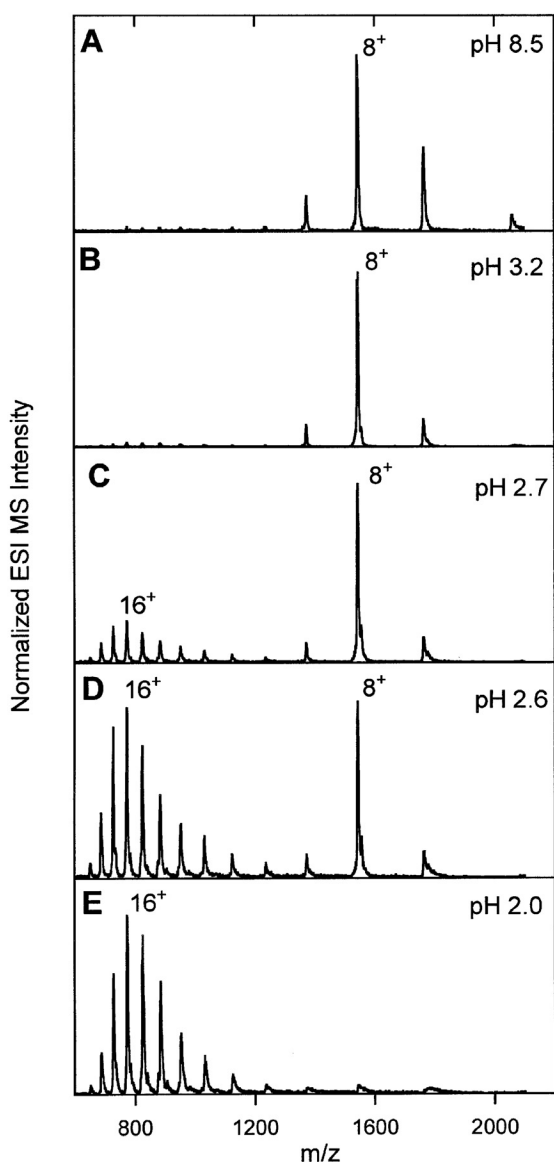


Figure 3. ESI mass spectra of cytochrome *c* recorded at different pH: (a) pH 8.5, (b) pH 3.2 (c) pH 2.7, (d) pH 2.6 and (e) pH 2.0. The pH was adjusted by addition of ammonium hydroxide and/or acetic acid. [Adapted from Konermann et al. (33)]

More recently, Konermann and coworkers developed an approach for studying protein folding termed “time-resolved ESI”. This interesting approach has been used to study the folding of cytochrome *c* (36) and myoglobin (32). In the first of these studies, acid denatured cytochrome *c* and a buffer (pH 3.0) were rapidly mixed using a continuous-flow mixing

apparatus connected directly to the mass spectrometer. ESI was used to monitor changes in charge-state distributions with a time resolution of about 0.1 seconds. In this case, no conformational intermediate between folded and unfolded protein was detected. In contrast to these results with cytochrome *c* a similar time-resolved ESI experiment with holo-myoglobin revealed the presence of an intermediate partly unfolded holo-myoglobin species during its acid-induced denaturation into apo-myoglobin (Figure 4). The decay of the peak intensity of the charge-state distribution of the partly unfolded holo-myoglobin revealed that the lifetime of this intermediate was on the order of 0.4 seconds, which correlated well with lifetime measurements obtained in a related stopped-flow solution phase experiments.

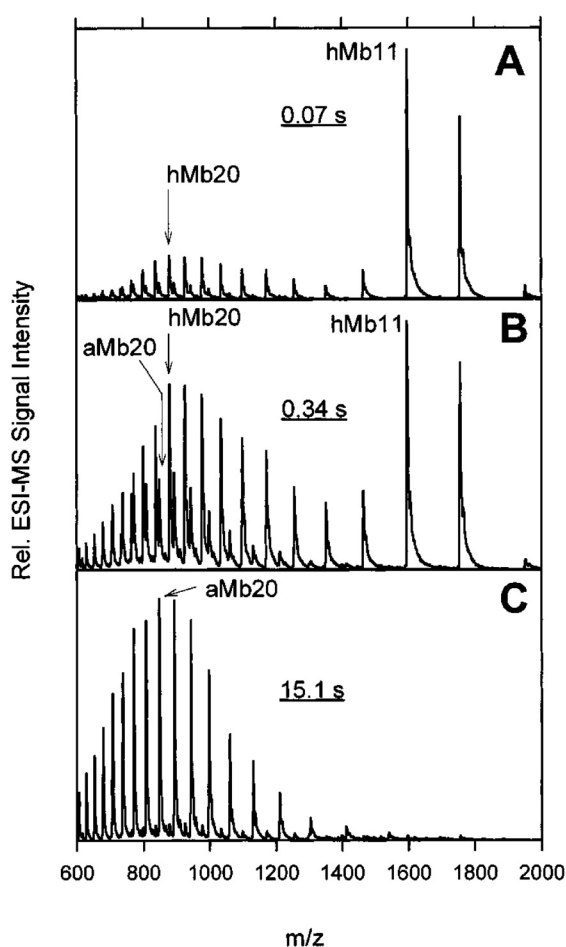


Figure 4. ESI mass spectra of Mb at different times after a pH-jump from 6.5 to 3.2; the spectra were recorded after 0.07 s (A), 0.34 s (B), and 15.1 s (C). Notation: hMb20 = holo-myoglobin + 20 H⁺; aMb20 = apo-myoglobin + 20 H⁺, etc. The decay of the peak intensity of the charge-state distribution of the partly unfolded holo-myoglobin revealed that the lifetime of this intermediate was on the order of 0.4 seconds. [Adapted from Konermann et al. (32)]

The “time-resolved ESI” experiments illustrated here show that ESI mass spectrometry can be used to detect intermediates in protein-folding processes. Furthermore, ESI-MS has the advantage over other techniques such as circular dichroism (CD) and steady state fluorescence in that sub-populations of protein conformers can be analyzed individually instead of the properties of the ensemble of the different sub-populations.

Protein structural analysis by hydrogen deuterium exchange

In the previous section I described applications of the use of charge-state distributions in protein conformational analysis and how this may be used to distinguish between folded and unfolded forms of a protein. Although charge-state distributions are highly informative about conformational states of a protein, an even more detailed view can be achieved by hydrogen/deuterium (H/D) exchange experiments. H/D exchange has long been used to obtain structural and dynamic information (37, 38) and mass spectrometry has simply extended these capabilities. The principle of H/D exchange is that some of the solvent exposed hydrogens in proteins are capable to exchange with hydrogens from the solvent molecules surrounding the protein. If an isotope of hydrogen is used as the solvent, such as deuterium oxide (D_2O), incorporation into the protein leads to a mass increase that can be monitored. There are several different kinds of hydrogens in proteins. Hydrogens covalently bound to carbon essentially do not exchange, whereas the free amine hydrogens located at the side chains may exchange very rapidly. Backbone amide hydrogens exchange relatively slow partly because these can be involved in the formation of hydrogen bonds in secondary structural elements (e.g., α -helices or β -sheets). The rate of exchange for these amide hydrogens is typically dependent on solvent accessibility (protein conformation), temperature and pH. Amide hydrogens buried within the hydrophobic core of a protein, or those involved in intramolecular hydrogen bonding can have exchange rates up to eight orders of magnitude slower than solvent-exposed amide hydrogens (39). The general assumption is that proteins with open structures have more hydrogens that are accessible to the solvent (D_2O), and therefore H/D exchange will proceed to a greater extent. One of the first applications of ESI-MS to monitor H/D exchange was reported by Katta and Chait (40, 41). They detected the exchange of labile hydrogens with deuterium by monitoring the mass increase of the intact protein. In case of ubiquitin they showed that only 62% of the exchangeable hydrogens in “native” ubiquitin exchanged with solvent deuterons, compared to 91% exchange for the unfolded molecule. Exchange rates can be highly informative about the state of a protein and this has been used in a number of different systems over the last decade including: α -helical or β -sheet peptides (42), lysozyme (41, 43) GroEL-bound human dihydrofolate reductase (DHFR) (44), GroEL-bound α -lactalbumin (45), myoglobin (46), cytochrome *c* (47), and calmodulin (48).

In one interesting case, the role of a single amino acid mutation in the stability of cytochrome c_{553} was investigated (49). Four mutant proteins were constructed in which Tyr 64 was replaced with either Phe, Leu, Val or Ala. Subsequently the rates of H/D exchange were determined for each mutant (Figure 5) and were used to evaluate the relative stability of these four analogs in comparison to the wild-type: wild-type > Y64F = Y64L > Y64V > Y64A. Data obtained with the Phe, Leu and Val mutants using spectrophotometric methods (50) indicated

that only the Val mutation destabilized the protein, whereas the Phe and Leu mutations had no effect on protein's stability.

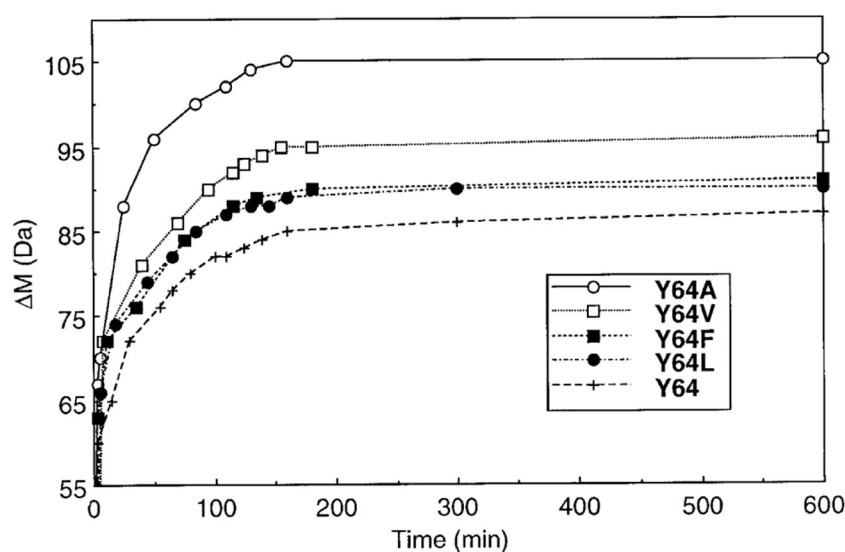


Figure 5. The time-course of H/D exchange in wild-type cytochrome c_{553} and four analogs. Based on the isotopic exchange rates, the relative stabilities of the mutants were found to be: wild-type > Y64F = Y64L > Y64V > Y64A. [Adapted from Guy et al. (49)]

An interesting strategy to further monitor protein conformational dynamics was demonstrated by Simmons and Konermann by combining time-resolved electrospray ionization (see previous section) in conjunction with H/D exchange (1). In Figure 6 the experimental set-up of this approach is shown schematically and involves both the rapid mixing of first native heme with unfolded apo-myoglobin followed by mixing with D_2O . The reaction time for reconstitution of holo-myoglobin can be varied by the length of the mixing capillary (51). This approach combines structural information from the ESI charge-state distribution and from the H/D exchange levels of individual protein states, while at the same time different ligand binding states can be monitored. This technique was used to study the reconstitution of holo-myoglobin (hMb) from unfolded apomyoglobin (aMb) and free heme. In this way they observed a short-lived folding intermediate with two heme groups attached representing a protein-bound heme dimer. This state appeared to have a compactness close to that of native hMb; however, H/D exchange results indicated a significantly perturbed structure.

A complication in on-line H/D exchange MS is that the final reaction mixture must be compatible with MS. Thus, the use of urea, guanidine salts, or other non-volatile solvent additives can be difficult. Folding experiments triggered by a pH jump are relatively easy.

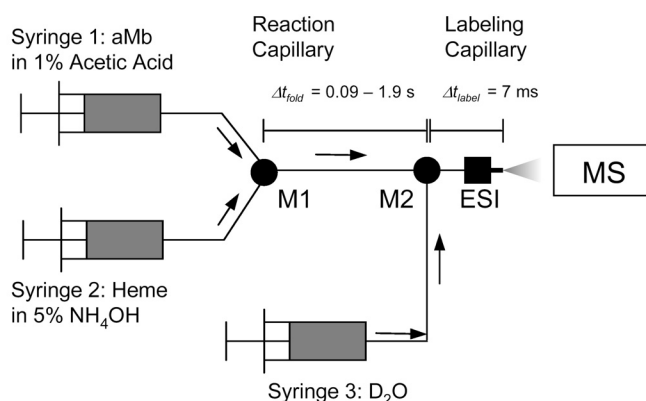


Figure 6. Scheme of the continuous-flow apparatus used to monitor the reconstitution of holo-myoglobin by isotopic pulse-labeling with on-line ESI-MS detection. Heme in basic solution and acid denatured aMb are mixed at mixer M1, where reconstitution is initiated at pH 10.4. After various reaction time (90 msec to 1.9 sec), the mixture is diluted with D₂O in a 4:1 ratio (v:v) for isotopic pulse-labeling at mixer M2. On-line analysis by ESI-MS occurs 7 ms after initiation of H/D exchange [Adapted from Simmons and Konermann (*1*)]

Most of the H/D exchange work in the examples given above characterized the global behavior of proteins and polypeptides. Smith et al, introduced an elegant method by adapting a technique originally developed to probe 1H/3H exchange in a more site specific fashion (52-54). This methodology uses an enzymatic digestion of the protein under slow-back-exchange conditions, followed by measurement of the isotope incorporation in the proteolytic fragments. In the mass spectrometry-based strategy developed by Smith et al., protein amide exchange is quenched by reducing the solution pH to 2-3, and the temperature to 0 °C, followed by rapid proteolytic fragmentation of the protein with pepsin. The number of amide deuterons present in each peptic fragment can then be deduced directly from mass measurements, following the separation of peptic fragments with fast HPLC (55). A general scheme of this methodology is presented in Figure 7.

Following several modifications (56) this approach to produce site-specific H/D exchange data has become very popular. One important modification of this procedure utilizes immobilized pepsin, so that the entire protein sample can be passed through a series of columns to digest separate peptides prior to MS analysis. Back exchange that occurs during the proteolysis and peptide separation steps does not appear to exceed 10%, and may be accounted for by introducing a “back-exchange” correction factor (57, 58). Importantly, these “local” H/D exchange measurements can be carried out in parallel with “global” dynamics studies.

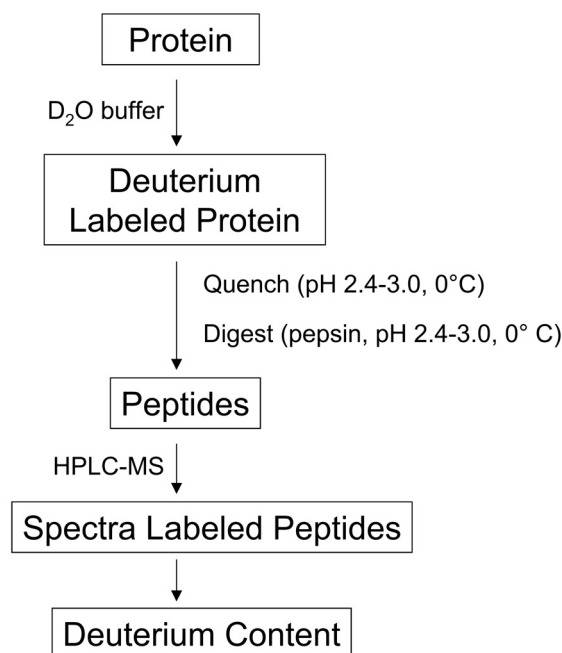


Figure 7. Procedure used to determine deuterium levels in short peptide segments of intact proteins incubated in D₂O.

Although ESI has thus far been the most popular technique in combination with exchange measurements, MALDI is now also gaining acceptance in the field. Early studies were carried out by Mandell et al. using the standard protocol (H/D exchange-quench-proteolysis) implemented with MALDI-MS to monitor deuterium incorporation in a site specific fashion (59). Only minor modifications of established MALDI sample preparation protocols are required to carry out such experiments. For instance, quenching of amide and peptic digests after exchange are followed by chilled and rapid drying of samples on the MALDI target to ensure minimal loss of deuterons from peptide amide groups. It was found, however, that when the sample remains completely dry and is kept under high vacuum during the analysis, the deuterium content decreases gradually over time. Therefore, a correction for the back exchange prior to mass analysis had to be made (59).

Non-covalent protein complexes

Non-covalent interactions of proteins are important in many biological processes, such as in signaling cascades, enzyme-substrate or enzyme-drug interactions and multi-protein machineries including for instance viruses and proteasomes/ribosomes. ESI-MS with its unique ability to preserve weaker non-covalent bonds when transferring species from solution into the gas phase,

has recently proven to be extremely useful for studying protein conformations and to characterize non-covalent protein complexes, including their dynamic behavior.

Although it is evident that the conformations and structures of multiple charged, desolvated proteins in the gas-phase are not identical to the corresponding structures in solution (60), there are pieces of indirect evidence which suggest that data obtained by mass spectrometry may sometimes be used to extract information about that species relevant to its behavior in solution. The most clear evidence lies in the specificity of the non-covalent interactions observed with ESI-MS in many well-documented cases, whereby the by MS detected non-covalent interactions are consistent with those measured using solution-phase based methods. Starting from the early reports showing the ability to observe intact non-covalent complexes using ESI-MS, (40, 61) numerous studies have now been described using this technique (60). Quite a range of different types of interactions have been reported including protein-metal, protein-ligand, protein-oligonucleotide/DNA/RNA and protein-protein interactions. In the following section I will describe several illustrative recent studies, relevant to the work described in this thesis, without giving a comprehensive review of the vast literature on the application of mass spectrometry to investigate noncovalent protein interactions studies (see for reviews (62-65)).

Protein-metal interactions

ESI-MS has become very useful in the study of non-covalent protein-metal interactions. ESI-MS can provide a direct and accurate measure of the metal-binding stoichiometry of a protein, based on an observed shift in the mass of the protein arising from the non-covalent binding of the metal ions (66-68). Here just two such examples have been described. First, ESI-MS has been used to evaluate the metal-binding stoichiometry of the Ca^{2+} -binding protein, calbindin $\text{D}_{28\text{K}}$ (69). Calbindin is composed of six EF-hand Ca^{2+} -binding domains. Traditional methods suggested a stoichiometry anywhere from three to six Ca^{2+} -binding sites (70-72). ESI-MS conclusively showed that one calbindin $\text{D}_{28\text{K}}$ molecule binds 4 Ca^{2+} ions (69). This conclusion was based on a mass difference of 151 Da between the metal-free protein and the protein saturated with Ca^{2+} ($4 \times 38 = 152$). The mass of Ca^{2+} ion is 40 Da, however a mass increase of 38 Da is observed for each Ca^{2+} . This result is observed since Ca^{2+} ions, and divalent metal ions in general, replaces two protons (2 Da) upon binding.

The second example shows how ESI-MS was used to measure conformational changes within the DNA-binding domain of the vitamin D receptor (VDR DBD) upon binding zinc (Zn^{2+}) (68). As increasing concentrations of Zn^{2+} were added to the VDR DBD, a gradual shift in the mass envelope to lower charge states was observed in the multiply charged spectrum. The shift in the charge states was correlated to changes observed in the far-ultraviolet circular dichroic (far-UV CD) spectrum of the protein as it was titrated with Zn^{2+} . Both the multiply charged ESI and far-UV CD spectra of the Zn^{2+} -titrated protein show that the binding of the

first Zn^{2+} ion to the protein results in very little conformational change in the protein. The binding of a second Zn^{2+} ion resulted in a significant alteration in the structure of the protein as indicated by changes in both the multiply charged ESI and far-UV CD spectra. The results presented indicate that ESI-MS is a powerful method to measure conformational changes induced by the binding of metals to metalloproteins.

Protein-ligand interactions

Some of the earliest studies showing non-covalent interactions by mass spectrometry between ligands and proteins were the observation of the intact heme-myoglobin complex (40) and an intact complex FK binding protein (FLBP) (61), the latter being an immunosuppressive binding protein, bound to the immunosuppressive agents FK506 and rapamycin. Since non-covalent ESI-MS is able to measure the molecular mass of protein-ligand complexes it is able to accurately distinguish two closely related ligands that bind to a common site. An illustrative example is the study of the *ras* protein that may be bound by GDP and GTP (73, 74). The *ras* protein is involved in the regulation of cell growth and differentiation; however, the protein is inactive when bound to GDP. Therefore, when investigating uncontrolled cell growth it is important to be able to differentiate between GDP-bound *ras* protein and GTP-bound *ras* protein. GDP bound and GTP-bound *ras* proteins are easily distinguished using ESI-MS due to the differing molecular mass between the two non-covalent complexes (Mw GDP-*ras* = 19295 Da; GTP-*ras* = 19375 Da). The direct measurement provided by ESI-MS left no ambiguity to the identity of the ligand bound within the active site of the *ras* protein.

ESI-MS is not only useful to determine the mass of the ligand and its binding stoichiometry, it can also be used to evaluate the relative strength of different protein-ligand complexes in solution (75-77). Loo et al. applied this to the SH2 domain on a tyrosine kinase protein from the Src family (75). The SH2 domain mediates critical protein-protein interactions in many signal transduction pathways (78). Therefore, it makes this a potential drug target for intervention in a wide variety of biological processes. The binding of tyrosyl phosphopeptides can mimic these interactions. The relative abundances of the multiple charged ions for the complex between Src SH2 protein and several nonphosphorylated and phosphorylated peptides were compared. The mass spectrometry data correlated well to the measured binding constants derived from solution-based methods, indicating that the mass spectrometry-based method can be used to assess the affinity of such interactions. ESI-MS of a solution containing Src SH2 with a mixture of phosphopeptides showed the expected protein-phosphopeptide complex as the dominant species in the mass spectrum, demonstrating the method's potential for screening mixtures from peptide libraries. Still, however, care must be taken when relating gas phase findings with solution phase binding properties because there also reports that showed less correlation (e.g. (79)).

Another illustrative example by Rostom et al. (80) dealt with the 58 kDa periplasmic peptide receptor protein OppA that was allowed to interact with 11 peptides with diverse properties. Peptides with two, three and five amino acid residues were added to OppA. ESI-MS showed that the highest-affinity complexes were observed for OppA with tripeptide ligands. Lower-affinity complexes were observed for OppA with dipeptide ligands and no complex formation was detected with pentapeptides or a tripeptide in which the N-terminal amino acid group was acetylated. Tripeptides containing a single D amino acid residue were found not to bind to native OppA. Analysis of the proportions of peptide-bound and free proteins under low-energy MS conditions showed a reasonable correlation with solution-phase K_d measurements. Increasing the internal energy of the gas-phase complex led to dissociation of the complex. The ease of dissociation highlighted the stability of the complex. The results from this study correlate very well with the physiological role of this protein in allowing into the cell di- and tripeptides containing naturally occurring amino acids, regardless of their sequence.

Protein-DNA interactions

One of the first ESI-MS studies in which ds-DNA was complexed with a natural binding partner involved the DNA-binding domain of the eukaryotic transcription factor, PU.1 (81). Mixtures of PU.1-DNA Binding Domain (DBD) protein and wild-type target DNA sequence yielded ESI-MS spectra showing only protein-ds-DNA complex ions of 1:1 stoichiometry and free ds-DNA. When PU.1-DBD protein, wild-type target DNA, and mutant target DNA lacking the consensus sequence were mixed, only the 1:1 complex with the wild-type DNA was observed, consistent with gel electrophoresis mobility shift assay results. These results provided strong evidence that the detected PU.1 protein DNA complex was not merely the result of a basic peptide interaction nonspecifically with the negative phosphate DNA backbone. Furthermore, the data highlighted the sequence-specific interactions between the protein and as observed in solution.

In another report Potier and co-workers used a similar approach to detect protein-DNA complexes (82). ESI-MS was used to study interactions among the *trp* apo-repressor (TrpR), tryptophan, and its specific operator DNA sequence. The *trp* operator/repressor is one of the most studied transcription systems in biochemistry (83). Binding of tryptophan to the repressor protein changes its conformational shape and allows it to bind to its operator DNA sequence, preventing transcription of genes by RNA polymerase. In 5 mM ammonium acetate, TrpR was detected as partially unfolded monomer. In the presence of a 21-base-pair DNA possessing the two symmetrically arranged CTAG consensus required for specific TrpR binding, a homodimer-dsDNA complex with a 1:1 stoichiometry was observed. Furthermore, to check the binding specificity of the TrpR for its target DNA they performed a competition experiment. In here, the protein was mixed with an equimolar amount of three different DNA's in which the two CTAG sequences were separated by 2, 4, and 6 bp, respectively. Only the DNA with the correct

consensus spacing of 4 bp was able to form stable interactions with TrpR. This experiment demonstrates the potential of ESI-MS to test the sequence-specificity of protein-DNA complexes.

Although the application of ESI to protein-DNA complexes is relatively new these two reports show that mass spectrometry can provide precise binding stoichiometries and can characterize relative affinities of a protein for a particular DNA sequence. However, one disadvantage in the analysis of protein-DNA complexes is the high polarity of the DNA phosphate backbone. Alkali metal cations have a tendency to bind very tightly to oligonucleotides, which may lead to broader peaks and to erroneous mass measurements. However, nowadays, the resolution of mass spectrometers is often sufficient to separate the sodium adducts so that a very precise assignment of the complex may be measured.

Protein-protein interactions

Many proteins interact *in vivo* strongly and/or weakly with similar proteins to form oligomers or with other proteins to establish functional protein complexes and/or signaling pathways. ESI-MS may provide direct, unambiguous data showing the formation of a protein-protein complex based on the mass of the formed complex. This technique has a significant advantage compared to other spectroscopic techniques, for instance, when examining cofactor dependent protein-protein interactions (84, 85). The protein-protein and cofactor stoichiometry is readily determined within a single experiment since the observed mass of the non-covalent complex should be the sum of the masses of all these identities.

ESI-MS on the quaternary structure of 4-oxalocrotonate tautomerase was one of the first studies in which the oligomeric state of a protein was probed by MS (86). 4-oxalocrotonate tautomerase was estimated to be a pentamer on the basis of size-exclusion chromatography and ultracentrifugation (87). X-ray crystallography and mass spectrometry clearly showed that the protein forms a hexamer of 41 kDa (86, 88). Four single point-mutated 4-oxalocrotonate tautomerase, on the other hand, only formed monomeric proteins ions. Thus these data provide information about the oligomerization behavior of wild-type protein and residues important in maintaining the hexameric structure.

Following the pioneering work of the research group of Standing et al. several other groups have used ESI-MS for the analysis of the stoichiometry of oligomeric protein complexes of known and unknown composition. Interesting studies are reported on complexes of proteasome activator proteins (89, 90), the chaperone complex GroEL (91), and many different variants of hemoglobin (92-96). ESI-MS experiments have confirmed that GroEL is composed of 14 non-covalently bound subunits arranged in two heptameric rings with a total molecular mass of 800kDa (91). For its functional activity, GroEL requires the presence of a co-chaperone GroES. The association of the mobile loop of GroES and the model substrate helix D from

rhodandese to GroEL was also probed by mass spectrometry (97). Together, with the results from fluorescence binding studies it was concluded that chaperone GroES and substrate proteins have, at least partially, distinct binding sites even in the intact GroEL tetradecamer.

Hemoglobin is in most mammalian systems present as a tetrameric complex of approximately 60 kDa possibly in equilibrium with dimers in lower abundance, as also revealed by mass spectrometry. Mass spectrometry has been used extensively to study forms of hemoglobin. For example, the study of hemoglobin S and fetal hemoglobin in blood from patient material of patients with homozygous sickle cell disease (98). This study concentrated on the quantitative distribution of asymmetric hemoglobin hybrid and other tetrameric species in blood of patients with sickle cell disease. Therefore, the non-covalent association of hemoglobin subunits was studied by ESI mass spectrometry. Mass spectra of both patient and fetal blood revealed intact hetero-hemoglobin tetramers of both $\alpha_2\beta_2$ and hybrid $\alpha_2\gamma\beta$. A unique tetrameric marker protein of average mass 64.6 kDa was identified in hemolysates from patients with sickle cell disease in accordance with the calculated mass of the asymmetric hemoglobin hybrid.

Another elegant study revealing the ability of mass spectrometry is in the investigation of protein oligomerization on the transthyretin system (99). The tetrameric human protein transthyretin transfers the hormone thyroxine and, through its non-covalent interactions with the retinol binding protein, retinol. Transthyretin is thought to be one of the human proteins involved in the formation of amyloid fibrils, which is associated with diseases such as Alzheimer's, type II diabetes and the transmissible spongiform encephalopathies. Under normal conditions, transthyretin transports thyroxine and retinol, but misfolding of wild-type and single point mutations lead to senile systemic amyloidosis and familial amyloid polyneuropathy, respectively. Dissociation of the tetrameric transthyretin complex is thought to be the first step in the formation of transthyretin amyloid fibrils (100). McCammon et al. examined a series of 18 possible inhibitors of this process by mass spectrometry (99). The ligands were evaluated for their ability to bind to and stabilize the tetrameric structure, their cooperativity in binding to the transthyretin complex and their ability to compete with the natural ligand thyroxine. The observation of the multifaceted ten-component complex containing six protein subunits (four transthyretin and two retinol binding protein), two retinol molecules and two synthetic ligands allowed them to conclude that ligand binding does not inhibit association of transthyretin with retinol bound retinol binding protein. Thyroxine and the probed synthetic ligands showed different cooperativity characteristics. Negative, positive and non-cooperativity mechanisms could be observed; amongst them the well established negative cooperativity for thyroxine binding.

Another interesting example of the use of mass spectrometry on very large protein complexes is the work of Pinkse et al. on the supramolecular assembly of *Helicobacter Pylori* urease (101). *H. Pylori* is a gram-negative spiral bacterium infecting approximately half of the world's

population and an important etiologic agent in a variety of diseases (102). The abundant protein complex urease is essential for survival in the acidic environment of the stomach. Urease catalyses the hydrolysis of urea, present in the gastric juice, to ammonium and carbamate. It has been suggested that the acid resistance *H. pylori* urease is probably dependent on its supramolecular architecture and contributes to its ability to resist and survive in the harsh conditions in the stomach. Therefore, urease is considered as a potentially useful target for developing new therapeutic avenues for eradicating *H. Pylori* infections. *H. Pylori* urease consists of two subunits, a 25.5 kDa α -subunit and a 61.7 kDa β -subunit (103, 104). Nano-flow ESI mass spectrometry established that the urease complex has a molecular weight of $1,063,900 \pm 600$ Da, corresponding to a dodecameric $(\alpha\beta)_{12}$ assembly of α - and β -subunits (Figure 8). The observation that the dodecamer readily disassembles into $(\alpha\beta)_3$ subunits is in strong support for a $((\alpha\beta)_3)_4$ architecture. This structural design was consistent with the recently published X-ray structure, revealing a spherical assembly of twelve catalytic $(\alpha\beta)$ units (105).

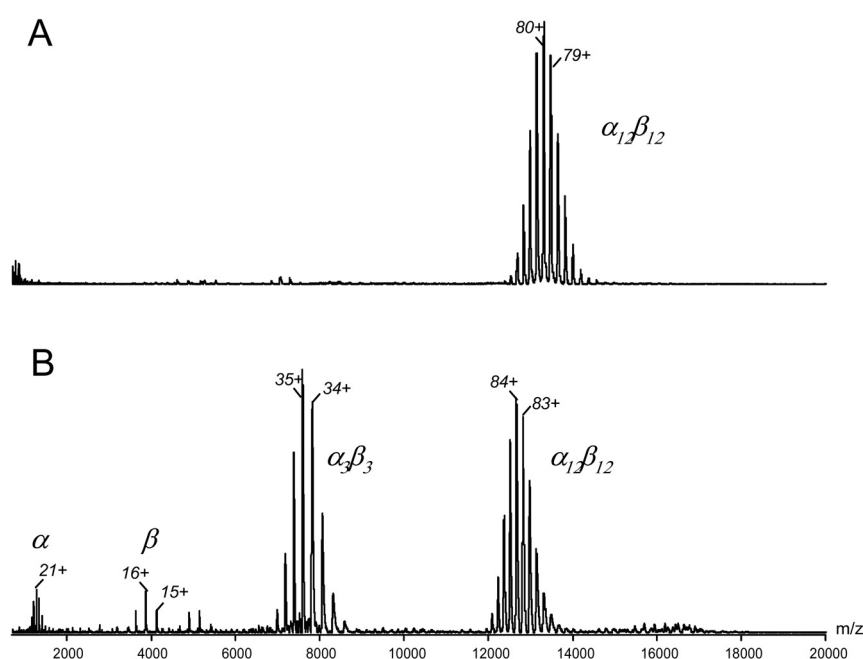


Figure 8. ESI mass spectra of *H. Pylori* urease, electrosprayed from an aqueous 200 mM ammonium acetate solution, pH 6.4, at an estimated $[\alpha\beta]$ concentration of $\sim 20 \mu\text{M}$, acquired in (A) positive ion mode with a source temperature of 40°C ; (B) with a source temperature of 70°C . [Adapted with permission from Pinkse et al. (101).]

Conclusions

In this chapter I have described some of the prospectives of MS-based techniques for the investigation of protein folding and protein non-covalent interactions related to the work

described in this thesis. The examples presented in this chapter indicate that in recent years mass spectrometry has become an alternative tool in structural biology that may complement more established methods. Although mass spectrometry has its limitations, as it is still a gas-phase based method, it also has its unique strengths. Mass spectrometry is highly sensitive, requiring very little sample, is very selective and has nearly no limitations in size of the species under investigation. As ESI-MS allows the simultaneous monitoring of multi-component species (differentiating by mass) or even conformations (differentiating by charge) present in solution, it allows the investigation of dynamic features, such as assembly of disassembly, and equilibria, and therefore opens up the possibility to study particular biological problems that cannot easily be addressed by alternative methods. The application of ESI-MS in structural biology is still in its infancy, but I believe that it will grow quite extensively in the near future in the direction from the more fundamental applications described in this chapter towards more pharmaceutical applications.

References

1. Simmons, D. A., and Konermann, L. (2002) Characterization of transient protein folding intermediates during myoglobin reconstitution by time-resolved electrospray mass spectrometry with on-line isotopic pulse labeling *Biochemistry* 41, 1906-1914.
2. Miranker, A., Robinson, C. V., Radford, S. E., Aplin, R. T., and Dobson, C. M. (1993) Detection of transient protein folding populations by mass spectrometry *Science* 262, 896-900.
3. Sundqvist, B., and Macfarlane, R. D. (1985) *Mass. Spectrom. Rev.* 4, 421-460.
4. Macfarlane, R. D., and Torgerson, D. F. (1976) *Int. J. Mass spectrom. Ion Phys.* 21, 81-92.
5. Håkansson, P., Kamensky, I., Sundqvist, B., Fohlman, J., Peterson, P., McNeal, C. J., and Macfarlane, R. D. (1982) 127-I Plasma desorption mass spectrometry of insulin *J. Am. Chem. Soc.* 104, 2948-2949.
6. Barber, M., Bordoli, R. S., Sedwick, R. D., and Tyler, A. N. (1981) Fast atom bombardment of solids (F.A.B.): "A new ion source for mass spectrometry *J. Chem. Soc. Chem. Commun.* 1981, 325-327.
7. Dell, A., and Morris, H. R. (1982) Fast atom bombardment-high field magnetic mass spectrometry of 6000 Da polypeptides *Biochem. Biophys. Res. Commun.* 106, 1456-1461.
8. Barber, M., Bordoli, R. S., Elliot, G. J., Sedgwick, R. D., and Tyler, A. N. (1982) Fast atom bombardment mass spectrometry of bovine insulin and other large peptides *J. Chem. Soc. Chem. Commun.* 1982, 936-938.
9. Williams, D. H., Bradley, C. V., Santikarn, S., and Bojesen, G. (1982) Fast-atom-bombardment mass spectrometry. A new technique for the determination of molecular weights and amino acid sequences of peptides *Biochem. J.* 201, 105-117.
10. Dole, M., Mack, L. L., Hines, R. L., Mobley, R. C., Ferguson, L. O., and Alice, M. B. (1968) Molecular beams of macroions *J. Chem. Phys.* 49, 2240-2249.
11. Fenn, J. B., Mann, M., Meng, C. K., Wong, S. F., and Whitehouse, C. M. (1989) Electrospray ionization for mass spectrometry of large biomolecules *Science* 246, 64-71.
12. Kebarle, P. (2000) A brief overview of the present status of the mechanisms involved in electrospray mass spectrometry *J. Mass. Spectrom.* 35, 804-817.

13. Kebarle, P., and Tang, L. (1993) From Ions in Solution to Ions in the Gas-Phase - the Mechanism of Electrospray Mass-Spectrometry *Anal. Chem.* *65*, A972-A986.
14. Iribarne, J. V., and Thomson, B. A. (1976) On the evaporation of small ions from charged droplets *J. Chem. Phys.* *64*, 2287-2294.
15. Wilm, M. S., and Mann, M. (1994) Electrospray and Taylor-Cone Theory, Doles Beam of Macromolecules at Last *Int. J. Mass Spectrom. Ion Process.* *136*, 167-180.
16. Gaskell, S. J. (1997) Electrospray: Principles and practice *J. Mass Spectrom.* *32*, 677-688.
17. Ganem, B., and Henion, J. D. (2003) Going gently into flight: analyzing noncovalent interactions by mass spectrometry *Bioorg. Med. Chem.* *11*, 311-314.
18. Tanaka, K. (1988) Protein and polymer analysis up to m/z 100,000 by laser ionization time-of-flight mass spectrometry *Rapid Commun. Mass Spectrom.* *2*, 151-153.
19. Karas, M., and Hillenkamp, F. (1988) Laser desorption ionization of proteins with molecular masses exceeding 10,000 daltons *Anal. Chem.* *60*, 2299-2301.
20. Karas, M., Gluckmann, M., and Schafer, J. (2000) Ionization in matrix-assisted laser desorption/ionization: singly charged molecular ions are the lucky survivors *J. Mass Spectrom.* *35*, 1-12.
21. Karas, M., Ingendoh, A., Bahr, U., and Hillenkamp, F. (1989) Ultraviolet-Laser Desorption Ionization Mass-Spectrometry of Femtomolar Amounts of Large Proteins *Biomed. Environ. Mass Spectrom.* *18*, 841-843.
22. Beavis, R. C., and Chait, B. T. (1990) Rapid, sensitive analysis of protein mixtures by mass spectrometry *Proc. Natl. Acad. Sci. U S A* *87*, 6873-6877.
23. Goldberg, D. E., Slater, A. F., Beavis, R., Chait, B., Cerami, A., and Henderson, G. B. (1991) Hemoglobin degradation in the human malaria pathogen *Plasmodium falciparum*: a catabolic pathway initiated by a specific aspartic protease *J. Exp. Med.* *173*, 961-969.
24. Karas, M., Bahr, U., Ingendoh, A., Nordhoff, E., Stahl, B., Strupat, K., and Hillenkamp, F. (1990) Principles and applications of matrix-assisted UV-laser desorption/ionization mass spectrometry *Anal. Chim. Acta* *1990*, 175-185.
25. Chernushevich, I. V., Loboda, A. V., and Thomson, B. A. (2001) An introduction to quadrupole-time-of-flight mass spectrometry *J Mass Spectrom* *36*, 849-65.
26. Guevremont, R., Siu, K. W. M., Leblanc, J. C. Y., and Berman, S. S. (1992) Are the Electrospray Mass-Spectra of Proteins Related to Their Aqueous-Solution Chemistry *J. Am. Soc. Mass Spectrom.* *3*, 216-224.
27. Le Blanc, J. C. Y., Guevremont, R., and Siu, K. W. M. (1993) Electrospray Mass-Spectrometry of Some Proteins and the Aqueous-Solution Acid-Base-Equilibrium Model in the Negative-Ion Detection Mode *Int. J. Mass Spectrom. Ion Process.* *125*, 145-153.
28. Kelly, M. A., Vestling, M. M., Fenselau, C. C., and Smith, P. B. (1992) Electrospray Analysis of Proteins - a Comparison of Positive-Ion and Negative-Ion Mass-Spectra at High and Low pH *Org. Mass Spectrom.* *27*, 1143-1147.
29. Loo, J. A., Edmonds, C. G., Udseth, H. R., and Smith, R. D. (1990) Effect of reducing disulfide-containing proteins on electrospray ionization mass spectra *Anal. Chem.* *62*, 693-698.
30. Chowdhury, S. K., Katta, V., and Chait, B. T. (1990) Probing conformational changes in proteins by mass spectrometry *J. Am. Chem. Soc.* *112*, 9012-9013.
31. Fenn, J. B. (1993) Ion formation from charged droplets: Roles of geometry, energy, and time *J. Am. Soc. Mass Spectrom.* *4*, 524-535.
32. Konermann, L., Rosell, F. I., Mauk, A. G., and Douglas, D. J. (1997) Acid-induced denaturation of myoglobin studied by time-resolved electrospray ionization mass spectrometry *Biochemistry* *36*, 6448-6454.

33. Konermann, L., and Douglas, D. J. (1998) Equilibrium unfolding of proteins monitored by electrospray ionization mass spectrometry: distinguishing two-state from multi-state transitions *Rapid Commun. Mass Spectrom.* *12*, 435-442.
34. Konermann, L., and Douglas, D. J. (1998) Unfolding of proteins monitored by electrospray ionization mass spectrometry: a comparison of positive and negative ion modes *J. Am. Soc. Mass. Spectrom.* *9*, 1248-1254.
35. Mohimen, A., Dobo, A., Hoerner, J. K., and Kaltashov, I. A. (2003) A chemometric approach to detection and characterization of multiple protein conformers in solution using electrospray ionization mass spectrometry *Anal. Chem.* *75*, 4139-4147.
36. Konermann, L., Collings, B. A., and Douglas, D. J. (1997) Cytochrome c folding kinetics studied by time-resolved electrospray ionization mass spectrometry *Biochemistry* *36*, 5554-5559.
37. Hvidt, A., and Nielsen, S. O. (1966) Hydrogen exchange in proteins *Adv. Protein Chem.* *21*, 287-386.
38. Englander, S. W., and Kallenbach, N. R. (1983) Hydrogen exchange and structural dynamics of proteins and nucleic acids *Q. Rev. Biophys.* *16*, 521-655.
39. Smith, D. L. (1998) Local structure and dynamics in proteins characterized by hydrogen exchange and mass spectrometry *Biochemistry* *63*, 338-348.
40. Katta, V., and Chait, B. T. (1991) Conformational changes in proteins probed by hydrogen-exchange electrospray-ionization mass spectrometry *Rapid Commun. Mass Spectrom.* *5*, 214-217.
41. Katta, V., and Chait, B. T. (1993) Hydrogen-Deuterium Exchange Electrospray-Ionization Mass-Spectrometry - a Method for Probing Protein Conformational- Changes in Solution *J. Am. Chem. Soc.* *115*, 6317-6321.
42. Wagner, D. S., Melton, L. G., Yan, Y., Erickson, B. W., and Anderegg, R. J. (1994) Deuterium exchange of alpha-helices and beta-sheets as monitored by electrospray ionization mass spectrometry *Protein Sci.* *3*, 1305-1314.
43. Mao, D., Babu, K. R., Chen, Y. L., and Douglas, D. J. (2003) Conformations of gas-phase lysozyme ions produced from two different solution conformations *Anal. Chem.* *75*, 1325-1330.
44. Gross, M., Robinson, C. V., Mayhew, M., Hartl, F. U., and Radford, S. E. (1996) Significant hydrogen exchange protection in GroEL-bound DHFR is maintained during iterative rounds of substrate cycling *Protein Sci.* *5*, 2506-2513.
45. Robinson, C. V., Gross, M., Eyles, S. J., Ewbank, J. J., Mayhew, M., Hartl, F. U., Dobson, C. M., and Radford, S. E. (1994) Conformation of Groel-Bound Alpha-Lactalbumin Probed by Mass-Spectrometry *Nature* *372*, 646-651.
46. Wang, F., and Tang, X. (1996) Conformational heterogeneity of stability of apomyoglobin studied by hydrogen/deuterium exchange and electrospray ionization mass spectrometry *Biochemistry* *35*, 4069-4078.
47. Wagner, D. S., and Anderegg, R. J. (1994) Conformation of cytochrome c studied by deuterium exchange-electrospray ionization mass spectrometry *Anal. Chem.* *66*, 706-711.
48. Nemirovskiy, O., Giblin, D. E., and Gross, M. L. (1999) Electrospray ionization mass spectrometry and hydrogen/deuterium exchange for probing the interaction of calmodulin with calcium *J. Am. Soc. Mass. Spectrom.* *10*, 711-718.
49. Guy, P., Remigy, H., Jaquinod, M., Bersch, B., Blanchard, L., Dolla, A., and Forest, E. (1996) Study of the new stability properties induced by amino acid replacement of tyrosine 64 in cytochrome C553 from *Desulfovibrio vulgaris* Hildenborough using electrospray ionization mass spectrometry *Biochem. Biophys. Res. Commun.* *218*, 97-103.
50. Blanchard, L., Dolla, A., Bersch, B., Forest, E., Bianco, P., Wall, J., Marion, D., and Guerlesquin, F. (1994) Effects of the Tyr64 substitution on the stability of cytochrome c553, a low

- oxidoreduction-potential cytochrome from *Desulfovibrio vulgaris* Hildenborough *Eur. J. Biochem.* 226, 423-432.
51. Wilson, D. J., and Konermann, L. (2003) A capillary mixer with adjustable reaction chamber volume for millisecond time-resolved studies by electrospray mass spectrometry *Anal. Chem.* 75, 6408-6414.
 52. Smith, R. D., Bruce, J. E., Wu, Q. Y., and Lei, Q. P. (1997) New mass spectrometric methods for the study of noncovalent associations of biopolymers *Chem. Soc. Rev.* 26, 191-202.
 53. Rosa, J. J., and Richards, F. M. (1979) An experimental procedure for increasing the structural resolution of chemical hydrogen-exchange measurements on proteins: application to ribonuclease S peptide *J. Mol. Biol.* 133, 399-416.
 54. Englander, J. J., Rogero, J. R., and Englander, S. W. (1985) Protein hydrogen exchange studied by the fragment separation method *Anal. Biochem.* 147, 234-244.
 55. Zhang, Z. Q., and Smith, D. L. (1993) Determination of Amide Hydrogen-Exchange by Mass-Spectrometry - a New Tool for Protein-Structure Elucidation *Protein Sci.* 2, 522-531.
 56. Wang, L., and Smith, D. L. (2003) Downsizing improves sensitivity 100-fold for hydrogen exchange-mass spectrometry *Anal. Biochem.* 314, 46-53.
 57. Engen, J. R., and Smith, D. L. (2001) Investigating protein structure and dynamics by hydrogen exchange MS *Anal. Chem.* 73, 256A-265A.
 58. Smith, D. L., Deng, Y., and Zhang, Z. (1997) Probing the non-covalent structure of proteins by amide hydrogen exchange and mass spectrometry *J. Mass Spectrom.* 32, 135-146.
 59. Mandell, J. G., Falick, A. M., and Komives, E. A. (1998) Measurement of amide hydrogen exchange by MALDI-TOF mass spectrometry *Anal. Chem.* 70, 3987-3995.
 60. Loo, J. A. (1997) Studying noncovalent protein complexes by electrospray ionization mass spectrometry *Mass Spectrom. Rev.* 16, 1-23.
 61. Ganem, B., Li, Y. T., and Henion, J. D. (1991) Detection of Noncovalent Receptor Ligand Complexes by Mass-Spectrometry *J. Am. Chem. Soc.* 113, 6294-6296.
 62. Heck, A. J. R., and Van den Heuvel, R. H. H. Investigation of Intact Protein Complexes by Mass Spectrometry *Mass Spectrom. Rev.*, *in press*.
 63. Hernandez, H., and Robinson, C. V. (2001) Dynamic protein complexes: insights from mass spectrometry *J. Biol. Chem.* 276, 46685-46688.
 64. Daniel, J. M., Friess, S. D., Rajagopalan, S., Wendt, S., and Zenobi, R. (2002) Quantitative determination of noncovalent binding interactions using soft ionization mass spectrometry *Int. J. Mass Spectrom.* 216, 1-27.
 65. Loo, J. A. (2000) Electrospray ionization mass spectrometry: a technology for studying noncovalent macromolecular complexes *Int. J. Mass Spectrom.* 200, 175-186.
 66. Loo, J. A. (2001) Probing protein-metal ion interactions by electrospray ionization mass spectrometry: enolase and nucleocapsid protein *Int. J. Mass Spectrometry* 204, 113-123.
 67. Lafitte, D., Capony, J. P., Grassy, G., Haiech, J., and Calas, B. (1995) Analysis of the ion binding sites of calmodulin by electrospray ionization mass spectrometry *Biochemistry* 34, 13825-13832.
 68. Veenstra, T. D., Johnson, K. L., Tomlinson, A. J., Craig, T. A., Kumar, R., and Naylor, S. (1998) Zinc-induced conformational changes in the DNA-binding domain of the vitamin D receptor determined by electrospray ionization mass spectrometry *J. Am. Soc. Mass Spectrom.* 9, 8-14.
 69. Veenstra, T. D., Johnson, K. L., Tomlinson, A. J., Naylor, S., and Kumar, R. (1997) Determination of calcium-binding sites in rat brain calbindin D28K by electrospray ionization mass spectrometry *Biochemistry* 36, 3535-42.
 70. Bredderman, P. J., and Wasserman, R. H. (1974) Chemical composition, affinity for calcium, and some related properties of the vitamin D dependent calcium-binding protein *Biochemistry* 13, 1687-1694.

71. Gross, M. D., Nelsestuen, G. L., and Kumar, R. (1987) Observations on the binding of lanthanides and calcium to vitamin D-dependent chick intestinal calcium-binding protein. Implications regarding calcium-binding protein function *J. Biol. Chem.* *262*, 6539-6545.
72. Veenstra, T. D., Gross, M. D., Hunziker, W., and Kumar, R. (1995) Identification of metal-binding sites in rat brain calcium-binding protein *J. Biol. Chem.* *270*, 30353-30358.
73. Huang, E. C., Pramanik, B. N., Tsarbopoulos, A., Reichert, P., Ganguly, A. K., Trotta, P. P., Nagabhushan, T. L., and Covey, T. R. (1993) Application of Electrospray Mass-Spectrometry in Probing Protein-Protein and Protein Ligand Noncovalent Interactions *J. Am. Soc. Mass Spectrom.* *4*, 624-630.
74. Ganguly, A. K., Pramanik, B. N., Tsarbopoulos, A., Covey, T. R., Huang, E., and Fuhrman, S. A. (1992) Mass-Spectrometric Detection of the Noncovalent Gdp-Bound Conformational State of the Human H-Ras Protein *J. Am. Chem. Soc.* *114*, 6559-6560.
75. Loo, J. A., Hu, P. F., McConnell, P., Mueller, W. T., Sawyer, T. K., and Thanabal, V. (1997) A study of Src SH2 domain protein-phosphopeptide binding interactions by electrospray ionization mass spectrometry *J. Am. Soc. Mass Spectrom.* *8*, 234-243.
76. Vollmerhaus, P. J., Breukink, E., and Heck, A. J. R. (2003) Getting closer to the real bacterial cell wall target: Biomolecular interactions of water-soluble lipid II with glycopeptide antibiotics *Chem.-Eur. J.* *9*, 1556-1565.
77. Jorgensen, T. J. D., Roepstorff, P., and Heck, A. J. R. (1998) Direct determination of solution binding constants for noncovalent complexes between bacterial cell wall peptide analogues and vancomycin group antibiotics by electrospray ionization mass spectrometry *Anal. Chem.* *70*, 4427-4432.
78. Grucza, R. A., Bradshaw, J. M., Futterer, K., and Waksman, G. (1999) SH2 domains: from structure to energetics, a dual approach to the study of structure-function relationships *Med. Res. Rev.* *19*, 273-293.
79. Chung, E. W., Henriques, D. A., Renzoni, D., Morton, C. J., Mulhern, T. D., Pitkeathly, M. C., Ladbury, J. E., and Robinson, C. V. (1999) Probing the nature of interactions in SH2 binding interfaces--evidence from electrospray ionization mass spectrometry *Protein Sci.* *8*, 1962-1970.
80. Rostom, A. A., Tame, J. R., Ladbury, J. E., and Robinson, C. V. (2000) Specificity and interactions of the protein OppA: partitioning solvent binding effects using mass spectrometry *J. Mol. Biol.* *296*, 269-279.
81. Cheng, X., Morin, P. E., Harms, A. C., Bruce, J. E., Ben-David, Y., and Smith, R. D. (1996) Mass Spectrometric Characterization of Sequence-Specific Complexes of DNA and Transcription Factor PU.1 DNA Binding Domain *Anal. Biochem.* *239*, 35-40.
82. Potier, N., Donald, L. J., Chernushevich, I., Ayed, A., Ens, W., Arrowsmith, C. H., Standing, K. G., and Duckworth, H. W. (1998) Study of a noncovalent trp repressor: DNA operator complex by electrospray ionization time-of-flight mass spectrometry *Protein Sci.* *7*, 1388-1395.
83. Bass, S., Sorrells, V., and Youderian, P. (1988) Mutant Trp repressors with new DNA-binding specificities *Science* *242*, 240-245.
84. Tahallah, N., Van Den Heuvel, R. H., Van Den Berg, W. A., Maier, C. S., Van Berkel, W. J., and Heck, A. J. (2002) Cofactor-dependent assembly of the flavoenzyme vanillyl-alcohol oxidase *J. Biol. Chem.* *277*, 36425-32.
85. Fabris, D., and Fenselau, C. (1999) Characterization of allosteric insulin hexamers by electrospray ionization mass spectrometry *Anal. Chem.* *71*, 384-387.
86. Fitzgerald, M. C., Chernushevich, I., Standing, K. G., Whitman, C. P., and Kent, S. B. (1996) Probing the oligomeric structure of an enzyme by electrospray ionization time-of-flight mass spectrometry *Proc. Natl. Acad. Sci. U S A.* *93*, 6851-6856.

87. Chen, L. H., Kenyon, G. L., Curtin, F., Harayama, S., Bembenek, M. E., Hajipour, G., and Whitman, C. P. (1992) 4-Oxalocrotonate Tautomerase, an Enzyme Composed of 62 Amino-Acid-Residues Per Monomer *J. Biol. Chem.* *267*, 17716-17721.
88. Roper, D. I., Subramanya, H. S., Shingler, V., and Wigley, D. B. (1994) Preliminary Crystallographic Analysis of 4-Oxalocrotonate Tautomerase Reveals the Oligomeric Structure of the Enzyme *J. Mol. Biol.* *243*, 799-801.
89. Yao, Y., Huang, L., Krutchinsky, A., Wong, M. L., Standing, K. G., Burlingame, A. L., and Wang, C. C. (1999) Structural and functional characterizations of the proteasome-activating protein PA26 from *Trypanosoma brucei* *J. Biol. Chem.* *274*, 33921-33930.
90. Zhang, Z. G., Krutchinsky, A., Endicott, S., Realini, C., Rechsteiner, M., and Standing, K. G. (1999) Proteasome activator 11S REG or PA28: Recombinant REG alpha/REG beta hetero-oligomers are heptamers *Biochemistry* *38*, 5651-5658.
91. Rostom, A. A., and Robinson, C. V. (1999) Disassembly of intact multiprotein complexes in the gas phase *Curr. Op. Struct. Biol.* *9*, 135-141.
92. Apostol, I. (1999) Assessing the relative stabilities of engineered hemoglobins using electrospray mass spectrometry *Anal. Biochem.* *272*, 8-18.
93. Lippincott, J., Fattor, T. J., Lemon, D. D., and Apostol, I. (2000) Application of native-state electrospray mass spectrometry to identify zinc-binding sites on engineered hemoglobin *Anal. Biochem.* *284*, 247-55.
94. Versluis, C., and Heck, A. J. R. (2001) On the gas-phase dissociation of hemoglobin *Int. J. mass spectrom.* *210*, 637-649.
95. Zal, F., Green, B. N., Lallier, F. H., and Toulmond, A. (1997) Investigation by electrospray ionization mass spectrometry of the extracellular hemoglobin from the polychaete annelid *Alvinella pompejana*: an unusual hexagonal bilayer hemoglobin *Biochemistry* *36*, 11777-11786.
96. Zal, F., Green, B. N., Martineu, P., Lallier, F. H., Toulmond, A., Vinogradov, S. N., and Childress, J. J. (2000) Polypeptide chain composition diversity of hexagonal-bilayer haemoglobins within a single family of annelids, the alvinellidae *Eur. J. Biochem.* *267*, 5227-5236.
97. Ashcroft, A. E., Brinker, A., Coyle, J. E., Weber, F., Kaiser, M., Moroder, L., Parsons, M. R., Jager, J., Hartl, U. F., Hayer-Hartl, M., and Radford, S. E. (2002) Structural Plasticity and Noncovalent Substrate Binding in the GroEL Apical Domain. A study using electrospray ionization mass spectrometry and fluorescence binding studies *J. Biol. Chem.* *277*, 33115-33126.
98. Ofori-Acquah, S. F., Green, B. N., Davies, S. C., Nicolaidis, K. H., Serjeant, G. R., and Layton, D. M. (2001) Mass spectral analysis of asymmetric hemoglobin hybrids: demonstration of Hb FS (alpha2gamma-beta5) in sickle cell disease *Anal. Biochem.* *298*, 76-82.
99. McCammon, M. G., Scott, D. J., Keetch, C. A., Greene, L. H., Purkey, H. E., Petrassi, H. M., Kelly, J. W., and Robinson, C. V. (2002) Screening transthyretin amyloid fibril inhibitors: characterization of novel multiprotein, multiligand complexes by mass spectrometry *Structure* *10*, 851-863.
100. Miroy, G. J., Lai, Z., Lashuel, H. A., Peterson, S. A., Strang, C., and Kelly, J. W. (1996) Inhibiting transthyretin amyloid fibril formation via protein stabilization *Proc. Natl. Acad. Sci. U S A* *93*, 15051-15056.
101. Pinkse, M. W., Maier, C. S., Kim, J. I., Oh, B. H., and Heck, A. J. (2003) Macromolecular assembly of *Helicobacter pylori* urease investigated by mass spectrometry *J. Mass Spectrom.* *38*, 315-20.
102. Covacci, A., Telford, J. L., Del Giudice, G., Parsonnet, J., and Rappuoli, R. (1999) *Helicobacter pylori* virulence and genetic geography *Science* *284*, 1328-1333.
103. Hu, L. T., and Mobley, H. L. (1990) Purification and N-terminal analysis of urease from *Helicobacter pylori* *Infect. Immun.* *58*, 992-998.

104. Evans, D. J., Jr., Evans, D. G., Kirkpatrick, S. S., and Graham, D. Y. (1991) Characterization of the *Helicobacter pylori* urease and purification of its subunits *Microb. Pathog.* 10, 15-26.
105. Ha, N. C., Oh, S. T., Sung, J. Y., Cha, K. A., Lee, M. H., and Oh, B. H. (2001) Supramolecular assembly and acid resistance of *Helicobacter pylori* urease *Nat. Struct. Biol.* 8, 505-9.

Chapter 3

Probing metal ion binding and conformational properties of the colicin E9 endonuclease by electrospray ionization time-of-flight mass spectrometry

Ewald T.J. van den Bremer, Claudia S. Maier, Albert J. R. Heck¹

Wim Jiskoot²

Colin Kleanthous³

Richard James⁴

Geoffrey R. Moore⁵

Protein Science 2002; (11) 1738-1752

¹Dept. of Biomolecular mass spectrometry, Utrecht University, Utrecht

²Dept. of Pharmaceutics, Utrecht University, Utrecht

³Dept. of Biology, University of York, York

⁴Division of Microbiology & Infectious Diseases, University of Nottingham, Nottingham

⁵School of Chemical Sciences, University of East Anglia, Norwich

Abstract

Nano-Electrospray ionization time-of-flight mass spectrometry (nano-ESI-MS) was used to study the conformational consequences of metal ion binding to the colicin E9 endonuclease (E9 DNase) by taking advantage of the unique capability of ESI-MS to allow simultaneous assessment of conformational heterogeneity and metal ion binding. Alterations of charge state distributions upon metal ion binding/release were correlated with spectral changes observed in far- and near-UV circular dichroism and intrinsic tryptophan fluorescence. In addition, hydrogen/deuterium exchange experiments were utilized to probe structural integrity. The present study demonstrates that ESI-MS is sensitive to changes of the thermodynamic stability of E9 DNase as a result of metal ion binding/release in a manner consistent with that deduced from proteolysis and calorimetric experiments. Interestingly, acid-induced release of the metal ion from the E9 DNase causes dramatic conformational instability associated with a loss of fixed tertiary structure but secondary structure is retained. Furthermore, ESI-MS enabled the direct observation of the non-covalent protein complex of E9 DNase bound to its cognate immunity protein Im9 in presence and absence of Zn^{2+} . Gas phase dissociation experiments of the deuterium-labeled binary and ternary complexes revealed that not Im9 but metal ion binding results in a dramatic exchange protection of E9 DNase in the complex. In addition, our metal ion binding studies and gas phase dissociation experiments of the ternary E9 DNase- Zn^{2+} -Im9 complex have provided further evidence that electrostatic interactions govern the gas phase ion stability.

Introduction

Colicins are bacterial protein antibiotics that are released in times of nutrient or environmental stress by *Escherichia coli* (1). The family of E-type colicins can be subdivided in two major groups, a) pore-forming colicins such as E1 (2) and b) nuclease colicins with either RNase activity (E3, E5 and E6) or DNase activity (E2, E7, E8, and E9) (3, 4). Colicin E9 is a 60 kDa endonuclease composed of three functional domains: the N-terminal translocation domain, the receptor binding domain and the C-terminal cytotoxic domain (5). Although the cell killing mechanism is still not completely understood, it apparently involves three steps. Initial binding of the colicin E9 to the BtuB extracellular receptor for vitamin B₁₂ is followed by translocation of the E9 DNase domain into the periplasm through the Tol system of proteins (a process that is possibly assisted by the porin OmpF) (1, 6). Upon entry of the DNase domain of colicin E9 into the cytoplasm, cell death is caused by cleavage of the chromosomal DNA (7-9). The E9 DNase domain has a high sequence homology with at least three other members of the DNase family (the colicins E2, E7, and E8) (5). All these colicins share sequence identity with a larger group of enzymes known as H-N-H endonucleases (10, 11). Under normal conditions colicin-producing bacteria protect themselves from suicide by co-expressing a cognate immunity protein (5). Colicin E9 forms a tight heterodimeric complex with its cognate 9.5 kDa immunity protein Im9 with a dissociation constant of approximately 10⁻¹⁶ M (12, 13). Immunity proteins specific for other colicins (Im2, Im7 and Im8) also bind to the E9 DNase but with affinities that are 6-8 orders of magnitude weaker than the cognate immunity protein Im9, highlighting that these complexes exhibit both high affinity and a high degree of specificity (14). Recent X-ray crystal structures of the E9 DNase domain-Im9 complex (Figure 1) indicate that the E9 DNase is a metalloprotein containing a single transition metal within the active site located more than 10 Å away from the protein-protein interface. The H-N-H motif located at the C terminus spans 33 amino acids and wraps around the bound metal ion to form the core of the E9 DNase active site. Noteworthy, the transition metal ion is not essential for cleavage of double-stranded DNA even so it is centrally located in the active site of the enzyme (15). The crystallography data also revealed that the immunity protein does not bind directly at the active site of the DNase, but at an adjacent exosite (16-18). It is believed that bound Im9 sterically and electrostatically repels the putative substrate DNA and, thus, blocks the DNase activity (16, 19). An interesting conformational feature of the E9 DNase has been revealed by NMR studies. The E9 DNase interchanges between two conformers with a forward and a backward rate constant of approximately 1.6 s⁻¹ and 1.1 s⁻¹ (at 15 °C), respectively (20, 21) and this conformational equilibrium seems largely to be unaffected by the presence of Zn²⁺. No extensive conformational changes were observed upon Zn²⁺-binding (22).

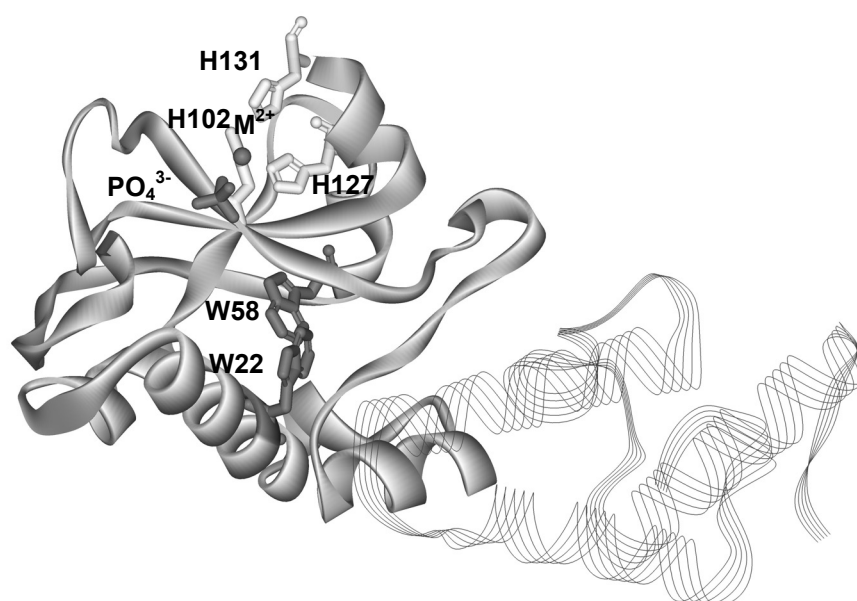


Figure 1. X-ray structure of the E9 DNase (solid ribbon) bound to Im9 (line ribbon) (PDB 1bxi). His residues H102, H127 and H131 coordinating the metal ion. The fourth metal ligand is a phosphate ion. Tryptophan residues W22 and W58 of the E9 DNase are highlighted.

In the present work, we report on the use of nano-electrospray ionization time-of-flight mass spectrometry (nano-ESI-MS) to probe the effect of metal ion binding/release and Im9-binding on the conformational properties of colicin E9 DNase. The determination of composition of metalloproteins and -peptides by ESI-MS is well documented (23-25). ESI-MS is also increasingly recognized as a technique capable to report on protein conformational changes (26-29). Here we take advantage of the unique capability of ESI-MS-based approaches to monitor conformational heterogeneity and metal ion binding simultaneously. In addition, hydrogen/deuterium (H/D) exchange monitored by mass spectrometry is utilized to obtain information regarding structural integrity, conformational heterogeneity and dynamics of the metal ion protein interaction. Circular dichroism and intrinsic fluorescence spectroscopy are used as complementary probes. We demonstrate that ESI-MS is capable to study in considerable detail the interaction of the colicin E9 DNase with metal ions as well as with its cognate immunity protein Im9. Furthermore, we provide evidence that ESI-MS is sensitive towards changes of the thermodynamic stability of E9 DNase. We also point out some limitations of our mass spectrometry-based approaches for studying conformational properties of proteins.

Experimental procedures

Protein samples - Colicin E9 DNase and its immunity protein Im9 were expressed in *Escherichia coli* and purified as previously described (13, 30). The concentrations for E9 DNase and Im9

were determined by measuring the UV absorption at 280 nm, using $\epsilon = 17,550 \text{ M}^{-1} \text{ cm}^{-1}$ and $11,400 \text{ M}^{-1} \text{ cm}^{-1}$, respectively (12). Confirmation of the expressed E9 DNase and Im9 by ESI-MS under denaturing conditions, i.e. 50 (v/v) % acetonitrile/water containing 0.1% formic acid, yielded average masses of $15,088.3 \pm 0.3 \text{ Da}$ and $9,582.0 \pm 0.8 \text{ Da}$, respectively. Both experimentally determined masses agreed well with the calculated masses (Table 1). The final protein concentrations used were $13 \mu\text{M}$ unless stated otherwise. Zinc acetate, nickel chloride and cobalt chloride (Merck, Darmstadt, Germany) were used without further purification. For the pH titration experiments the ammonium acetate solutions were adjusted by adding acetic acid or ammonia. The pH measurements were taken with a standard combi-electrode (Methrom Ltd, Herisau, Switzerland).

Table 1. Summary of the calculated and measured molecular masses of E9 DNase, E9 DNase bound to divalent transition metal ions, Im9 and the immunity complexes.

Protein	Calculated Mass (Da)	Measured Mass (Da)
apo-E9	15,088.0	$15,088.2 \pm 0.3$
E9-Zn ²⁺	15,515.4 ^{a)}	$15,151.2 \pm 0.3$
E9-Ni ²⁺	15,143.7 ^{a)}	$15,142.8 \pm 2.0$
E9-Co ²⁺	15,144.9 ^{a)}	$15,146.2 \pm 5.0$
Im9	9,582.5	$9,582.0 \pm 0.8$
E9Im9	24,670.5	$24,688.0 \pm 3.0$
E9-Zn ²⁺ -Im9	24,733.4 ^{a)}	$24,733.5 \pm 0.7$

^{a)} The average mass calculated for the holo-proteins based on the formula [apo-protein + $n \text{ Me}^m - n m \text{ H}^+$], where n is the number of metal ions and m their charge (23).

Preparation of deuterated proteins - The deuterium exchange experiments were proceeded by pre-diluting the samples in 100 mM ammonium acetate (1:1) followed by a 1:25 dilution in D₂O (> 99.9 % D Aldrich) containing 50 mM ammonium acetate (pD 7.2). The fully deuterated control samples were prepared by diluting the protein stock solutions (1:50) into D₂O at pD 2.4 containing 0.1% formic acid and incubated overnight at 37 °C.

Mass Spectrometry - Time-of-flight electrospray ionization mass spectra were recorded on a Micromass LC-T mass spectrometer (Manchester, U.K.) operating in the positive ion mode. Prior analysis a 600-3000 m/z scale was calibrated with CsI (2 mg/ml) in isopropanol/water (1:1). Samples for charge state distribution analysis were introduced via a nanoflow electrospray source. Nano-electrospray needles were made from borosilicate glass capillaries (Kwik-Fil, World Precision Instruments, Sarasota, FL) on a P-97 puller (Sutter Instruments, Novato, CA). The

needles were coated with a thin gold layer by using an Edwards Scancoat (Edwards Laboratories, Milpitas, CA) six Pirani 501 (at 40 mV, 1 kV, for 200 sec). In all experiments an aliquot (1-3 μ l) of protein sample at a concentration of 13 μ M was introduced into the electrospray needles. The nanospray needle potential was typically set to 1300 V and the cone voltage to 30 V. Source block temperature was set to 60 °C. The temperature at the location of capillary tip was measured with a thermocouple and was approximately 27 ± 2 °C. During individual titration experiments all parameters of the mass spectrometer were kept constant. For in source CID MSMS experiments the cone voltage was gradually increased up to 80 V.

Analysis of acid-induced conformational changes of bimodal charge state distributions were performed by assuming that the compact conformational state of the E9-DNase includes the charge-states 7+, 8+ and 9+ (termed F). For the more destabilized or loosely packed, states the charge-states 10+ to 24+ (termed U). The acid-induced folding curve as a function of pH was obtained by calculating the ion peak area ratio $A_F/(A_F+A_U)$ where A_F and A_U were obtained by summing the ion peak areas of charge states assigned to the compact conformational state (F) and the more destabilized or loosely packed, state (U) (31).

For the H/D exchange-in measurements "normal" ESI-MS was used to prevent the fast exchanging deuterium atoms from back exchanging. Nitrogen gas was used as desolvation gas with a flow rate of 250 l/h. The desolvation temperature was set 110 °C. The potential between the needle and the cone of the mass spectrometer was 3000 V; the cone voltage was set for 30 V. Samples were introduced into the ionization source at a flow rate of 5 μ l/min via a syringe pump. (kdScientific Inc., New Hope, PA). The syringe and transfer tubing were flushed prior sample introduction with the same solvent system to ensure that traces of previous samples were removed. The degree of deuterium incorporation was deduced from the protein's mass shift during the course of an experiment. The raw data were processed using the Masslynx software 3.5 with minimal smoothing.

Tryptophan fluorescence spectroscopy - Measurements of the intrinsic tryptophan fluorescence emission of E9 DNase, Im9 and the heterodimeric complex were performed on a Perkin Elmer LS50 luminescence spectrometer using an excitation wavelength of 295 nm. Emission spectra were recorded from 300-450 nm. The excitation bandwidth was set on 5 nm and the emission bandwidth on 10 nm. The protein concentrations were 6 μ M each in 50 mM ammonium acetate at various pH values. A quartz cell with a 5 mm path length was used at 25 °C. For the metal loaded protein experiment measurements were performed with a 6-fold excess (33 μ M) of zinc acetate.

Circular Dichroism Spectroscopy - A dual-beam DSM 1000 CD circular dichroism (CD) spectrophotometer (On-Line Instrument Systems, Bogart, GA) was used for CD measurements.

The subtractive double-grating monochromator was equipped with a fixed disk, holographic gratings (2400 lines/mm, blaze wavelength 230 nm), and 1.24-mm slits. Samples were measured in a 1 mm-path length cell. The E9 DNase concentration was 8 μM in 50 mM ammonium acetate. For the Zn^{2+} -containing experiments a 3-fold excess (24 μM) of zinc acetate was used. Denaturation was carried out by diluting the DNase in 6 M guanidine hydrochloride (Merck). Far-UV CD spectra were recorded from 260-200 nm at 25°C.

The E9 DNase concentration in the near-UV CD measurements was 50 μM and was measured in a cuvette with a path length of 10 mm. The subtractive double-grating monochromator was equipped with 0.6-mm slits. For the Zn^{2+} -containing E9 DNase measurements a 10-fold excess of zinc acetate (500 μM) was used. Near-UV CD spectra were recorded from 320-260 nm at 25°C. Each measurement was the average of at least six repeated scans (step resolution 1 nm, 1 s each step) from which the corresponding background spectrum was subtracted. The measured signals were converted to molar absorbance difference, based on mean residual weight of 112.6.

Results

Electrospray ionization mass spectrometry enables simultaneous observation of different conformational states for apo- and holo-E9 DNase in solution - Initial efforts were directed towards establishing experimental conditions that allow the observation of the metal protein complex. The ESI mass spectrum of apo-E9 DNase, acquired in 50 mM ammonium acetate adjusted to pH 7.2, displayed a bimodal charge state distribution encompassing a broad distribution of charge states (with a maximum at 18+) and a second narrow distribution of approximately 3 charge states (with a maximum at 8+) (Figure 2). The calculated masses of the protein, using the individual two charge distributions, were both identical to the expected mass of apo-E9 DNase (Table 1). Bimodal charge distributions of proteins in ESI mass spectra are not unprecedented and it is assumed that protein populations with different conformational properties attribute to the appearance of the ESI mass spectrum (28, 32, 33). In the present case we assume that the charge states 7+, 8+ and 9+ originate primarily from more compact conformational states (termed F, folded), whereas the ions with charge states between 11+ to 22+ are considered to originate from more unfolded, loosely packed conformational states (termed U, unfolded). By using the total ion peak areas of the ion peaks termed F and U, respectively, an acid-induced unfolding curve for apo-E9 DNase was deduced by plotting the peak area ratio $A_F/(A_U+A_F)$ as a function of the pH of the solution (Figure 3). Upon further acidification no significant changes in the ESI spectra of apo-E9 DNase were observed, although the intensity of the highly charged ion peaks increased slightly (Figure 2).

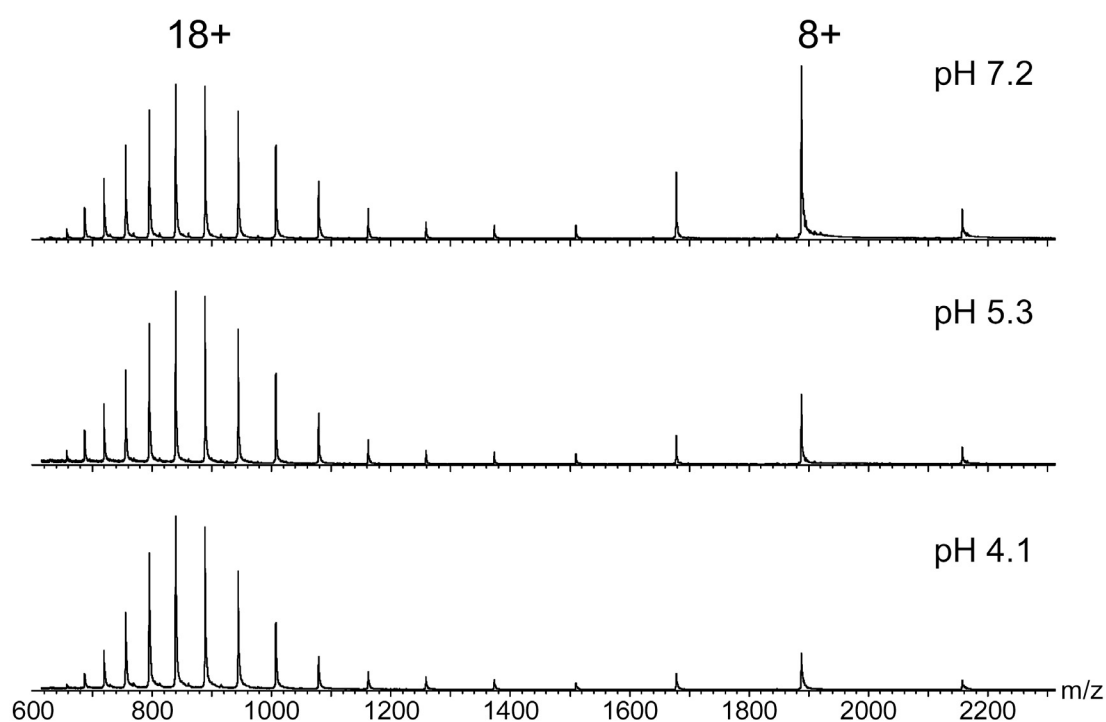


Figure 2. Nano-ESI mass spectra of the apo-E9 DNase recorded at different pH values: (a) 7.2, (b) 5.3, (c) 4.1.

A particularly interesting structural feature of the E9 DNase domain is the so-called H-N-H motif, an amino acid sequence stretch that is shared with homing endonucleases (10, 11). Two histidine residues within the H-N-H motif (His102 and His127) and one additional His located at the end of α helix 9 (His131) tetrahedrally coordinate the metal ion. A phosphate ion acts as a fourth ligand in the X-ray structure (16, 19). The transition metal ion Zn^{2+} binds with the highest affinity to the H-N-H motif of E9 DNase (15). Thus, metal binding studies were initiated by performing titration experiments with Zn^{2+} . Adding Zn^{2+} in stoichiometric amounts to a 13 μM apo-DNase E9 solution at pH 7.2 resulted in mass spectra that exhibited a dramatically different appearance compared to those observed for apo-E9 DNase under identical conditions. While for apo-E9 DNase a bimodal charge state distribution was observed (Figure 2), for Zn^{2+} -bound E9 DNase a narrow charge state distribution encompassing exclusively charge states between 7+ and 9+ (Figure 4) was observed. The measured mass of $15,151.2 \pm 0.3$ Da indicated that these ions originate from the E9 DNase protein bound to one single Zn^{2+} ion reflecting the expected 1:1 stoichiometry. In case of one equivalent of Zn^{2+} , binding appears to be completely saturated (Figure 4b). Even with a large excess of Zn^{2+} the protein with one metal ion bound was the predominantly observed species (Figure 4c). Less than stoichiometric amounts of Zn^{2+} resulted in mass spectra displaying concurrently the bimodal charge state distribution typically observed for the apo-protein and the narrow charge state envelope of the holo-protein (Figure 4a).

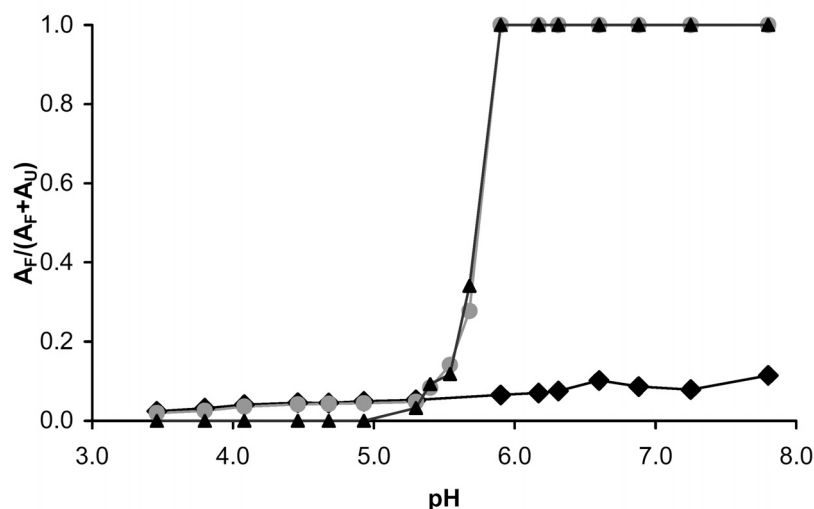


Figure 3. pH induced unfolding curves for the E9 DNase were deduced by plotting the peak area ratios $A_F/(A_U+A_F)$ as a function of pH. Unfolding curves of holo-E9 DNase and apo-E9 DNase are marked with (●) and (◆), respectively. Curve indicated with (▲) is deduced from $A_{F_{Zn}}/(A_{F_{Zn}}+A_{F_{apo}}+A_U)$. Whereby, (F) represents the folded conformer (from 9+ to 7+) and (U) the unfolded conformer (from 10+ to 22+) as illustrated in Figure 2. The data points for the unfolding curve of holo-E9 DNase were extracted from nano-ESI mass spectra of E9 DNase in the presence of an equimolar amount of Zn^{2+} in 50 mM ammonium acetate adjusted to different pH values. Some representative mass spectra are shown in Figure 6.

ESI-MS reports prevalence of E9 DNase for Zn^{2+} - Zn^{2+} is reported as the metal ion having the strongest affinity for the H-N-H motif of E9 DNase (K_d in the low nM range), whereas the affinity for Co^{2+} and Ni^{2+} is approximately 1000-fold lower (i.e. in the μM range) (15). Thus, we were interested if metal ion affinities for the E9 DNase derived from nano-ESI-MS would reflect the metal binding behavior in solution. Stoichiometric mixtures of the DNase and the two other transition metal ions, Co^{2+} and Ni^{2+} , respectively, were subjected to analysis. Mass spectrometric analysis of a stoichiometric mixture of apo-E9 DNase and Co^{2+} yielded ion species resulting in an average mass of $15,088.2 \pm 0.3$ Da (i.e., metal-free E9 DNase) and $15,146.2 \pm 5.0$ Da (i.e., Co^{2+} -bound E9 DNase), respectively, indicating the concomitant presence of the apo- and holo-protein. The Co^{2+} -bound holo-protein displayed again only a single, narrow charge state distribution encompassing the charge states 7+ to 9+. The mass spectrum reveals further that metal binding is not yet saturated when using one equivalent of Co^{2+} (data not shown). A similar experiment using a 1:1 molar mixture of E9 DNase and Ni^{2+} provided an ESI mass spectrum similar to the one observed for Co^{2+} , although the charge envelope for Ni^{2+} -bound holo-protein (giving an experimental mass of $15,142.8 \pm 2.0$ Da) was relatively more abundant than the one observed for the Co^{2+} -bound holo-protein (data not shown). Measured masses for the holo-proteins demonstrating 1:1 stoichiometry of transition metal ion binding are summarized in Table 1.

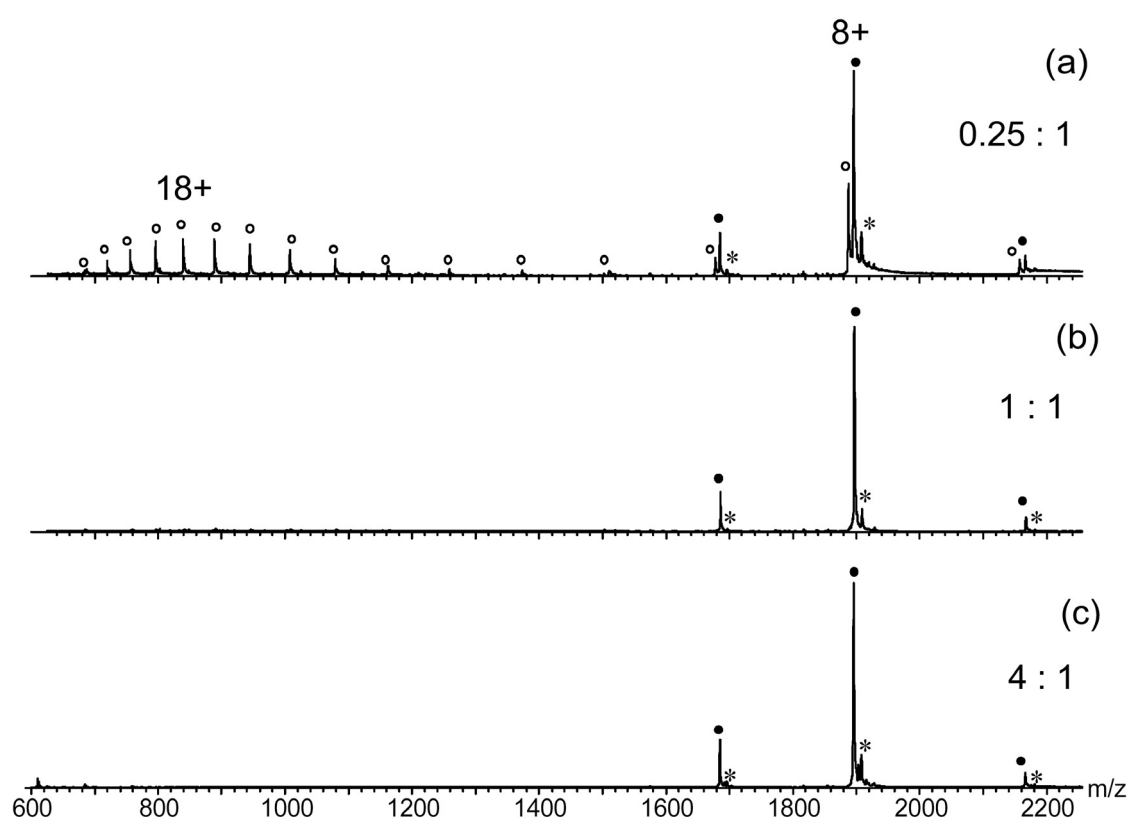


Figure 4. Nano-ESI mass spectra of E9 DNase in presence of increasing amounts of Zn^{2+} . Molar ratio of zinc acetate to apo-E9 DNase (a) 0.25:1, (b) 1:1, and (c) 4:1. Ion peaks of Zn^{2+} -bound and metal-free E9 DNase are marked with filled circles (●) and open circles (○), respectively. The ion series marked with * has an additional mass of 98 Da.

From the ESI mass spectra (at pH 7.2) obtained for the 1:1 mixtures of protein and different transition metal ions ratios of apo- to holo-ions were calculated by summing up the corresponding ion peak areas. These ratios are graphically presented in Figure 5. Assuming that the deduced apo- to holo-ion ratios reflect relative metal ion binding affinities it is found $\text{Zn}^{2+} > \text{Ni}^{2+} > \text{Co}^{2+}$, in qualitative agreement with literature data (15). Earlier work suggested that Mg^{2+} does not bind to the protein at least in the absence of DNA, but that it is essential for the non-specific endonuclease activity of E9 DNase, (15). Thus, Mg^{2+} was used as a probe to test the specificity of our mass spectrometry-based metal binding studies. Mass spectrometric analysis of an E9 DNase solution containing a 9-fold excess of Mg-acetate in ammonium acetate (pH 7.2) yielded exclusively the bimodal charge state distribution typically observed for the apo-protein. No charge states of Mg^{2+} -bound E9 DNase were observed (data not shown), thus stressing the specificity of the mass spectrometry-based metal binding study.

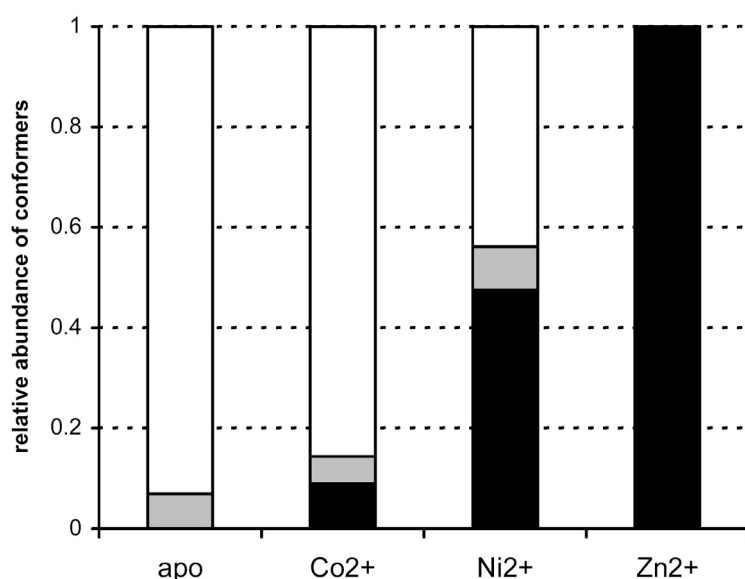


Figure 5. The relative binding affinities of the E9 DNase for different divalent metal ions. Bars shown in white represent the non-metal-containing unfolded conformer. Bars shown in grey represent the non-metal-containing folded conformer and in black, the folded metal-containing conformer.

Acid induced metal release causes conformational destabilization of E9 DNase - Pommer et al. (15) have suggested previously that association of colicin E9 with the outer membrane receptor BtuB and the periplasmic Tol proteins causes dissociation of both Im9 and the bound metal ion, in preparation for translocation of the cytotoxic DNase domain into the cell possibly via a destabilized state (15). Thus, we were interested to determine if the local acidic pH near the membrane surface of the target cell may trigger the release of the metal ion causing conformational destabilization of the DNase domain. ESI-MS is particularly well suited for this kind of conformational unfolding study because of its unique capability of monitoring simultaneously different conformational populations and metal ion binding. To study the pH-induced conformational transitions of the holo-E9 DNase, protein solutions with pH values between 3.5 and 7.8 were analyzed by nano-ESI-MS. Three illustrative ESI mass spectra are shown in Figure 6. The mass spectrum of the holo-E9 DNase at pH 7.2 was dominated by the less charged peaks with the 8+-ion peak as the predominant one. All the ions observed originate from the E9 DNase protein bound to one Zn^{2+} ion. Decreasing the pH to 5.3 caused metal ion release accompanied with the appearance of highly charged ion peaks in the lower m/z range. No Zn^{2+} binding was observed for these higher charge state ions that presumably originate from less compact conformational states. Upon further acidification, the abundance of the highly protonated charge states increased, but the maximum of the charge state envelopes remained at 18+ (Figure 6). As described for the apo-protein, the $A_F/(A_U+A_F)$ ratios were calculated from the ESI mass spectra acquired at different pH values, and gathered in Figure 3, illustrating a strong pH-dependent release of Zn^{2+} , which is apparently accompanied by major conformational destabilization.

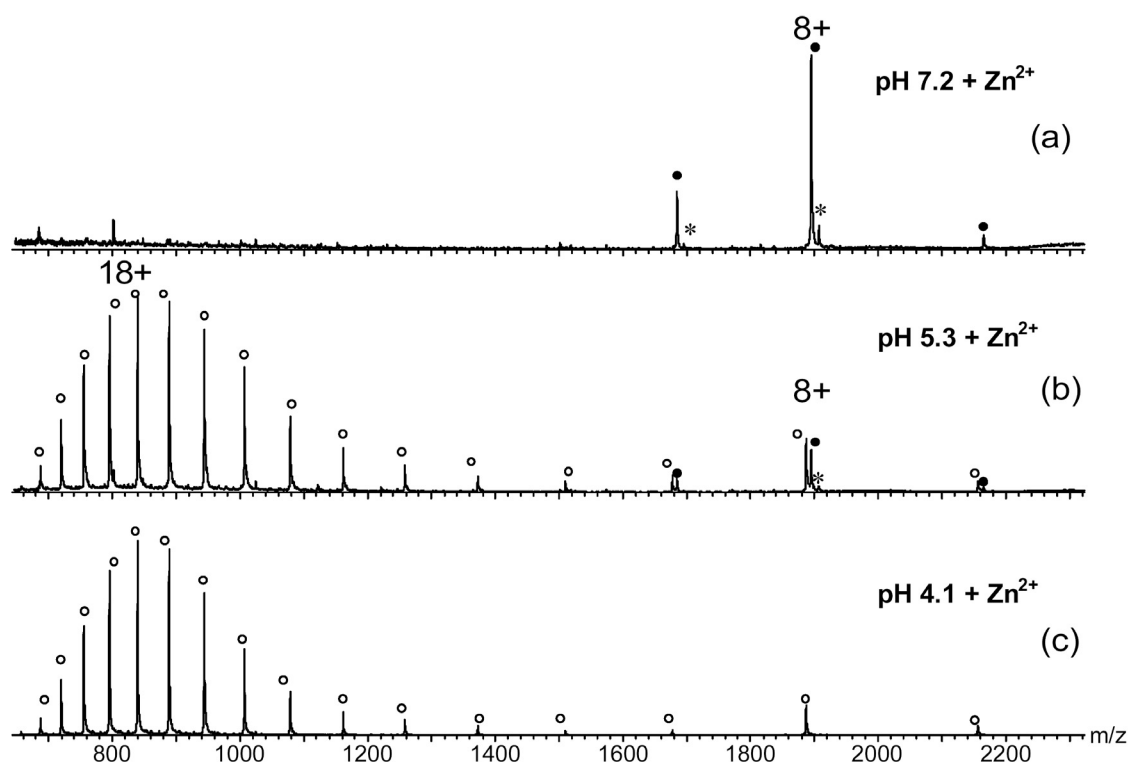


Figure 6. Nano-ESI mass spectra of E9 DNase in the presence of an equimolar amount of Zn^{2+} at pH 7.2 (a), 5.3 (b) and 4.1 (c) in 50 mM ammonium acetate. The filled circles (●) represent ion peaks of the Zn^{2+} bound and the open circles (○) ion peaks of the metal-free E9 DNase. The repeatedly observed ion series with an additional mass of 98 Da is marked with *.

Mass spectrometric characterization of E9 DNase in complex with its cognate immunity protein Im9 - To investigate E9 DNase in complex with Im9, an equimolar amount of Im9 was added to a solution of E9 DNase in ammonium acetate adjusted to pH 7.2. The nano-ESI spectrum of the E9 DNase-Im9 complex showed a very narrow charge state distribution dominated by two charge states, i.e. 9+ and 10+ at m/z 2743 and 2469, respectively (data not shown). The determined mass of $(24,668.0 \pm 3.0)$ Da agreed well with the expected mass of the E9 DNase-Im9 complex (Table 1). These narrow charge state distributions are frequently observed in studies of non-covalent complexes and are generally considered as an indication of compact structures that are preserved in the gas phase (34). Interestingly, at pH 7.2 the most abundant charge states observed in the ESI mass spectra of E9 DNase and Im9 are 8+ and 5+, respectively. The apparent reduction in the degree of protonation observed for the complex may to some extent be caused by salt bridges formed upon Im9 complexation linking Arg54 and Lys97 of E9 DNase with Glu30 and Glu41 of Im9, respectively (19).

Nano-ESI-MS of the ternary complex obtained by adding zinc acetate to the preformed E9 DNase-Im9 complex (at pH 7.2) revealed a charge state distribution comparable to the one

observed for the binary complex, encompassing the charge states 8+ to 10+ at m/z 2249, 2474 and 2749, respectively (Figure 7). The observed mass of $24,733.5 \pm 0.7$ Da is consistent with the expected mass of the Zn-bound E9 DNase-Im9 ternary complex (Table 1).

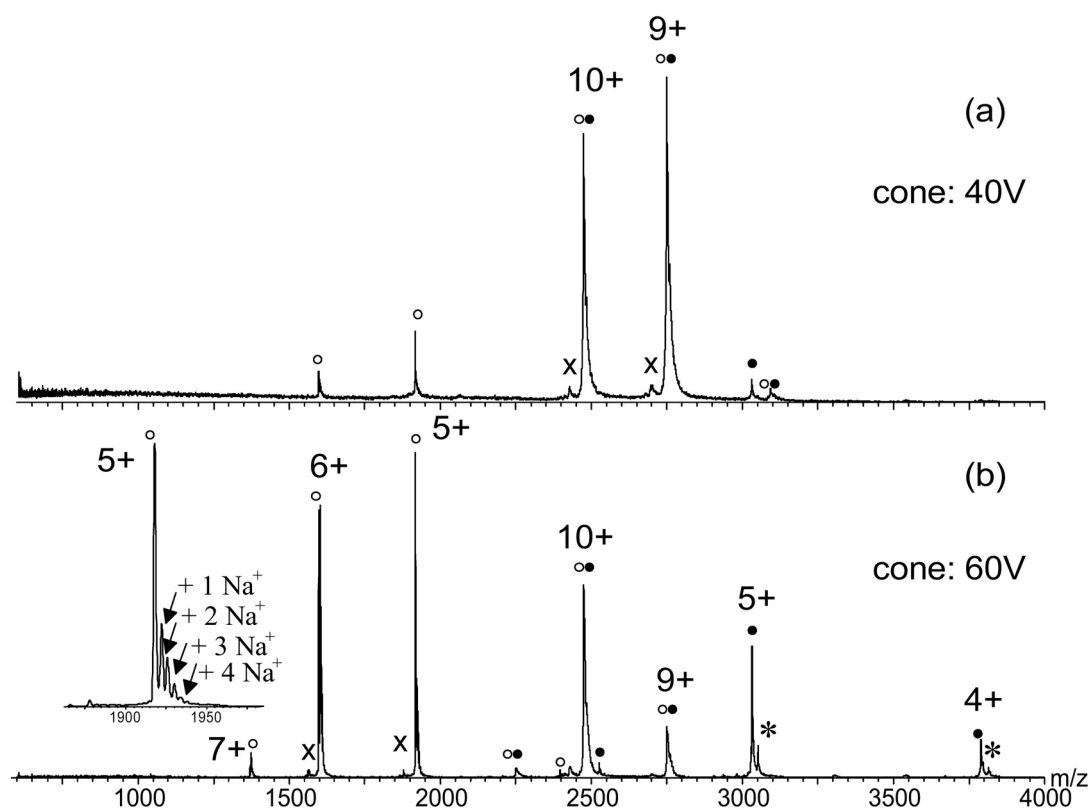


Figure 7. Nano-ESI-MS spectra of the E9 DNase-Im9-Zn complex in 50 mM ammonium acetate, pH 7.2 at a cone voltages of (a) 40 V and (b) 60 V. The filled circles (●) represent ion peaks of the E9 DNase containing the Zn^{2+} ion and open circles (○) correspond to ion peaks of Im9 after cone voltage dissociation. The filled and open circles combined (○●) denote ion peaks representing the E9 DNase-Im9-Zn complex. The insert shows the 5+-ion peak of Im9 after cone voltage dissociation with up to four Na^+ -ions remaining. The ion series marked with (x) is lacking a mass of 475 ± 3 Da, probably due to a truncated Im9 variant missing the C-terminal tetrapeptide FKQG.

The gas phase stability of non-covalent complexes can be evaluated by collision-induced dissociation (CID-MS) experiments (35, 36). Dissociation of non-covalent complexes is achieved by increasing the internal energy of the ions entering the mass spectrometer. In our instrumental setup, the cone voltage can be used to incrementally increase the internal energy of the multiply charged ions until dissociation of the complex is achieved. Increasing the cone voltage above 35 V causes dissociation of the E9 DNase-Im9 binary complex resulting in two additional charge state distributions besides the one of the binary complex. The charge state envelope below m/z 2400 encompassing the charge states 4+ to 7+ is assigned to Im9. A more detailed look at the individual charge states of Im9 reveals presence of some sodium adduction. The second

envelope with charges states +4, +5, and +6 at m/z 3774, 3019 and 2516 is attributed to apo-E9 DNase. Interestingly, apo-E9 DNase ion peaks do not show sodium adduction. We may speculate that the high number of acidic residues in Im9 (16 out of 86) promotes alkali metal ion binding. Similar persistent sodium adduction is encountered in ESI-MS studies of oligonucleotides (37) and DNA-binding proteins (36) and here it is assumed that the highly negatively charged phosphate backbone of the oligonucleotide causes very tight alkali metal ion binding (38). At higher cone voltages very minor additional peaks, subsidiary to the predominant charge envelope of Im9, appear which may indicate breakage of covalent bonds in Im9 (data not shown).

Likewise, gas phase dissociation experiments of the ternary Zn^{2+} -loaded E9 DNase-Im9 complex (Figure 7) yielded mass spectra with similar to those observed for the binary complex. However, a more detailed analysis revealed that the charge state distribution assigned to E9 DNase results in an average mass of $(15,151.1 \pm 0.4)$ Da consistent with one Zn^{2+} -ion bound to E9 DNase. Despite the very high affinity of the E9 DNase-Im9 complex observed in solution, in the gas phase disruption of the protein-protein interaction occurs prior to dissociation of the protein-metal ion interaction. This is in accordance with the emerging view that electrostatic interactions are enhanced while the hydrophobic effect becomes less significant in the gas phase (39, 40).

Assessing the conformational integrity of E9 DNase by hydrogen/deuterium (H/D) exchange -

The E9 DNase domain possesses a total of 261 exchangeable hydrogens (123 backbone amide hydrogens, 135 side-chain hydrogens and 3 hydrogens from both termini). For Im9, a total of 153 labile hydrogens were counted (82 backbone hydrogens, 68 side-chain hydrogens and 3 hydrogens from the termini). ESI-MS was used to monitor directly H/D exchange of peptide amide and side-chain hydrogens. Consequently, multiply deuterated molecular ions, i.e. $[M+D]^{n+}$, rather than multiply protonated protein ions, i.e. $[M+H]^{n+}$, were observed. It is important to point out that all H/D exchange experiments were monitored by "normal" ESI-MS and that the protein solutions were introduced into the ESI source via a syringe pump. With this setup, deuterium levels for fully deuterated E9 DNase and Im9 of $97 \pm 1\%$ and $96 \pm 1\%$, respectively, were observed.

H/D exchange data for the E9 DNase were obtained from three independent measurements in the presence and absence of a 6-fold excess of Zn^{2+} ions. An attempt was made to follow the H/D exchange kinetically. However, it was observed that deuterium incorporation had reached already a plateau-level approximately 2 minutes after diluting the protein solution into deuterating ammonium acetate solution. Since this time is about the earliest time point that was achieved with the current instrumental set-up, we decided instead to focus on the number of deuterons present in the protein under equilibrium conditions, i.e. an incubation period of 5 min.

More extended incubation periods (up to 1 hr) did not result in substantially higher deuterium incorporation. The results of the H/D experiments are summarized in Table 2.

Table 2. Levels of deuterium incorporation observed for E9 DNase, Im9 and the E9 DNase/Im9 complex in presence and absence of Zn^{2+} . Noted as well are the deuterium levels determined for E9 DNase and Im9 after collision-induced dissociation of the immunity complex.

complex	protein	Deuterium incorporation after 5 min. H/D exchange pD 7.2		Deuterium incorporation fully deuterated ^{a)}	
		Da	%	Da	%
	E9	246 ± 4	94 ± 2	253 ± 3	97 ± 1
	E9- Zn^{2+}	197 ± 2	75 ± 1	n.m. ^{c)}	n.m. ^{c)}
	Im9	115 ± 5	75 ± 3	147 ± 2	96 ± 1
E9-Im9	E9 ^{b)}	243 ± 6	93 ± 2	n.m. ^{c)}	n.m. ^{c)}
	Im9 ^{b)}	99 ± 6	65 ± 4	n.m. ^{c)}	n.m. ^{c)}
E9-Im9- Zn^{2+}	E9- Zn^{2+} ^{b)}	188 ± 3	72 ± 1	n.m. ^{c)}	n.m. ^{c)}
	Im9 ^{b)}	97 ± 6	63 ± 4	n.m. ^{c)}	n.m. ^{c)}

^{a)} after 12h at 37°C in pD 2.4; ^{b)} after cone voltage dissociation; ^{c)} no complex at pD 2.4

For the apo-E9 protein at pD 7.2, H/D exchange resulted after 5 min in an average mass increase of (246 ± 4) Da corresponding to an exchange of (94 ± 2) % of all labile hydrogens to deuterons (Table 2). No difference in mass increase was observed for any of the charge states assigned to the bimodal charge state distribution typically observed for apo-E9 DNase. In contrast, holo-E9 DNase domain showed a significantly lower deuterium uptake and the observed average mass increase was (197 ± 2) Da, indicating that approximately (75 ± 1) % of all labile hydrogens experienced exchange (Table 2). For the binary complex composed of apo-E9 DNase and Im9 a deuterium uptake of 342 ± 6 (83 ± 1 %) was determined, whereas the ternary complex, i.e. Zn^{2+} -bound E9 and Im9, showed a drastically lower deuterium incorporation (i.e. 285 ± 6; 68 ± 1 %) (Table 2). A somewhat lower deuterium uptake as a consequence of complex formation is anticipated because previous solvent accessible labile hydrogens will become buried within the protein-protein interface. However, to further be able to rationalize the drastically different exchange behaviour of the binary compared to the ternary complex, the labelled complexes were subjected to collision-induced dissociation experiments. Subsequently, the deuterium levels were determined from the mass shifts of the complex constituents observed. The deuterium level found for Im9 as a constituent of the binary complex was very similar to the one which was found for Im9 in the ternary complex, namely approximately (99 ± 6) in the binary complex and (97 ± 6) in the ternary complex (Table 2). In contrast, holo-E9 DNase when

a constituent of the ternary complex showed significantly less deuterium incorporation, i.e. (188 ± 3) versus the (243 ± 6) found for apo-E9 DNase in the binary complex (Table 2).

Conformational studies of E9 DNase by tryptophan fluorescence emission spectroscopy - To complement our mass spectrometric experiments we studied the consequence of metal binding/release on the conformational properties of E9 DNase by intrinsic tryptophan fluorescence emission spectroscopy. It has been shown previously that tryptophan fluorescence emission is a sensitive probe to study changes of the tertiary structure of the E9 DNase (15). The nuclease contains two Trp residues, W22 and W58 (Figure 1). Both Trp residues are part of helical regions and are buried in the protein core. The Trp residues are therefore sensitive probes to study the conformational transitions of E9 DNase upon acid-induced metal ion release and complementing the mass spectrometry-derived findings on changes in the tertiary structure of E9 DNase. The fluorescence spectrum of holo-E9 DNase at pH 7.4 in 50 mM ammonium acetate shows an emission maximum at 334 nm indicating that the Trp residues are buried in the non-polar protein core. The fluorescence spectrum of the apo-protein (under identical solution conditions) was similar to that recorded for the holo-protein, i.e. $\lambda_{\text{max}} = 334$ nm, but with a slight fluorescence enhancement. These data are in agreement with previously reported fluorescence data obtained in potassium phosphate buffer (15) indicating that the absence of phosphate ions seems not to substantially affect the tertiary structural properties of E9 DNase. This is important because all mass spectrometric experiments were performed in 50 mM ammonium acetate solutions (as preferred for the ESI process). Furthermore, the similarity of the fluorescence spectra for apo- and holo-protein is interesting because dramatically different ESI mass spectra were obtained for the holo- and apo-protein under corresponding solution conditions, i.e. for the holo-E9 DNase a unimodal charge state distribution was observed whereas the apo-protein exhibited a bimodal charge state distribution.

However, pH-induced unfolding experiments revealed differences in conformational stability of apo- and Zn^{2+} -bound E9 DNase. Illustrative fluorescence spectra of the apo- and holo-E9 DNase are shown in Figure 8. Fluorescence spectra of the holo-E9 DNase did not change significantly between pH 7.4 and 5.3, but further acidification caused red-shifting of the fluorescence maximum to about 353 nm marking unfolding. In contrast, the fluorescence spectra of the apo-E9 DNase revealed a gradual shift of the fluorescence maximum with decreasing pH values. At pH 3.9 the fluorescence spectra of the apo- and holo-E9 DNase proteins were very similar, exhibiting fluorescence maxima of 353 nm observed typically for unfolded states.

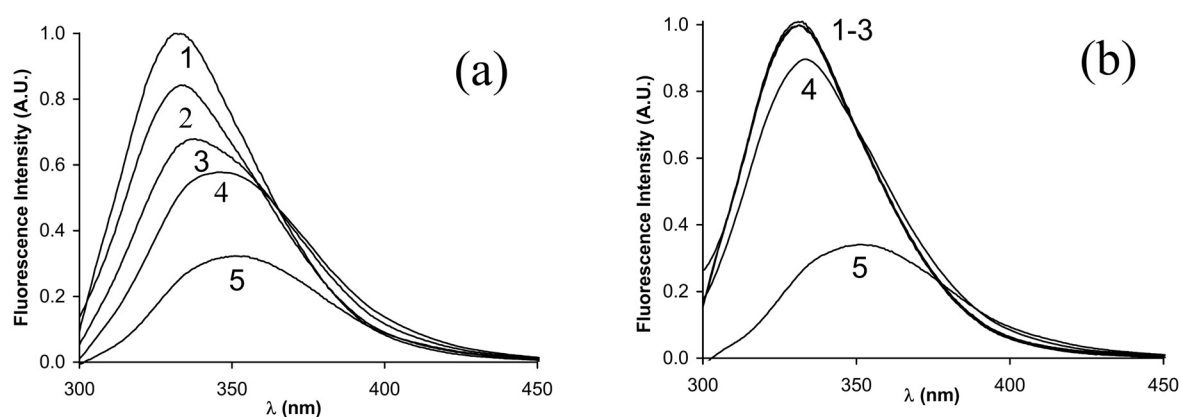


Figure 8. Changes in the tryptophan fluorescence emission spectra during acid-induced unfolding of E9 DNase (6 μM), Im9 (6 μM) and E9 DNase-Im9 complex (6 μM) in 50 mM ammonium acetate. (a) Curves 1-5 represent the apo-E9 DNase at pH 7.4; 5.9; 5.3; 4.9 and 3.9, and (b) curves 1-5 represent E9 DNase in the presence of a 6-fold molar excess of Zn^{2+} at pH 7.4; 5.9; 5.3; 4.9 and 3.9, respectively.

Acid-induced metal ion release probed by circular dichroism spectroscopy - In addition, CD spectroscopy was used to assess structural changes in E9 DNase on addition of acid in the presence and absence of Zn^{2+} . Far-UV CD spectra of apo- (Figure 9a) and holo-protein (Figure 9b) in 50 mM ammonium acetate at neutral pH were similar to those previously reported (15) confirming that apparently only minor changes in the secondary structure occur upon metal binding/release. Interestingly, upon acidification to pH 4 the negative ellipticity at 222 nm remained largely unaffected independent of the presence or absence of Zn^{2+} . In contrast, a conformational transition upon acid-induced metal release was observed in the ESI-MS as well as in the fluorescence spectroscopic experiments.

The near-UV CD spectrum of holo-E9 DNase at neutral pH shows a broad prominent positive band at 275 nm and a minor one at 295 nm (Figure 9c). Under identical solution conditions, the near-UV CD spectrum of the apo-protein has a very similar appearance (Figure 9c) stressing the fact that apo-E9 DNase has a defined tertiary structure even in the absence of the metal ions. However, at pH 4 apo- and holo-E9 preparations are devoid of the near-UV CD signal, thus, indicating loss of ordered structure (Figure 9c).

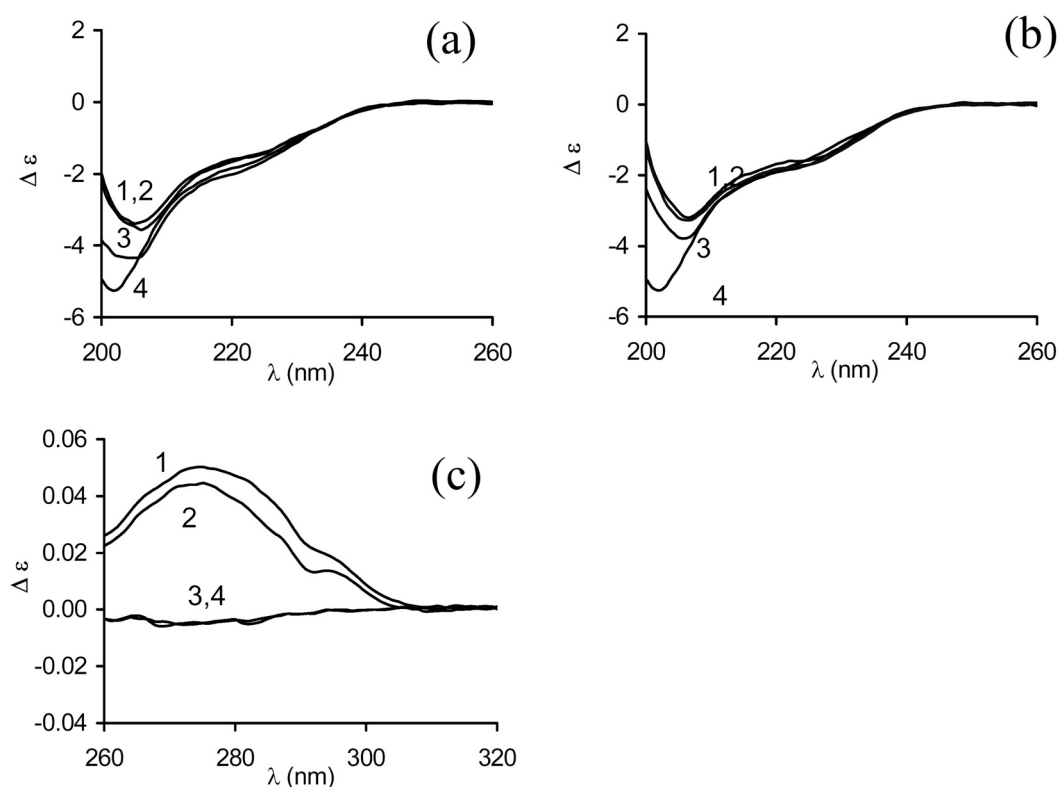


Figure 9. Far-UV (a, b) and near-UV (c) CD spectra of E9 DNase in 50 mM ammonium acetate. Curves 1-5 in (a) and (b) represent pH 7.4; 5.9; 5.3; and 3.9 of the apo- and holo E9 DNase (8 μ M), respectively. Curves 1 and 2 in (c) denote the E9 DNase (50 μ M) at pH 7.4 in the absence and presence of Zn^{2+} . Curves 3 and 4 represent the E9 DNase at pH 3.9 in the absence and presence of Zn^{2+} .

Discussion

ESI-MS is sensitive to metal induced changes in the thermodynamic stability of E9 DNase - In this work, we evaluate the use of nano-ESI-MS to probe the conformational properties of the metalloprotein colicin E9 DNase. In the ESI-MS process, multiple protonated protein ions (charge states) are generated and transferred intact into the gas phase of the mass spectrometer (41). It has been observed that ESI mass spectra of a protein analyzed from solutions causing protein unfolding experience a greater extent of charging in the ESI process, when compared to the same protein analyzed from solutions that favor the folded, "native" conformation (33, 42, 43). The metal binding stoichiometry is in ESI mass spectra reflected as corresponding mass shifts. Thus, these intrinsic properties of ESI-MS allow simultaneous assessment of the composition of the protein-ligand complex and the conformational heterogeneity. In contrast, the optical techniques commonly used to monitor conformational changes, such as circular dichroism (44), and fluorescence spectroscopy (45), measure the average properties of an ensemble but do not allow a direct observation of distinct conformational states.

The metal-free colicin E9 DNase domain showed bimodal charge state distributions in which the charge states centered around the 18-fold protonated ion peak were attributed to loosely packed, conformational states of metal-free E9 DNase and those centered around the 8-fold protonated ion peak to more compact, folded states. No intermediate charge states were observed. These results have been interpreted as showing that the apo-E9 DNase is significantly destabilized in solution with the ESI mass spectra able to reflect to the conformational states populated in solution, i.e. more loosely packed, unfolded conformational states, collectively termed "U"-states, in equilibrium with more compact, folded "F"-states. The thermodynamic stability of E9 DNase increases substantially upon metal ion binding (15), thus, shifting the thermodynamic equilibrium to the compact states. This shift of the conformational equilibrium is reflected in the ESI mass spectra by the absence of highly charged state ion peaks. Hence, ESI-MS seems to be very responsive to changes of protein conformational stability.

However, the present work also provides evidence that ESI-MS overestimates somewhat the contribution of the loosely packed conformational states to the conformational heterogeneity in solution. For instance, the ion peak ratio $A_F/(A_U+A_F)$ is close to 1/9 at neutral pH (Figure 3), but the fluorescence spectrum under identical solution condition is clearly dominated by a strong intrinsic fluorescence emission at 334 nm indicating that the two tryptophans in E9 DNase, W22 and W58, are in a non-polar environment (Figure 8). Likewise, apo-E9 DNase at neutral pH showed a strong near UV CD signal (Figure 9) indicating also dominance of folded conformational states with stable tertiary structure. To rationalize the pronounced bimodal charge state distribution observed for apo-E9 DNase, we have to recall some intrinsic features of ESI-MS. Firstly, the relative abundance of conformer-specific ions in ESI mass spectra cannot simply be related to their fractional contribution in solution. Recent work by Cech and Enke (46, 47) on tripeptides demonstrates that the ionization efficiency depends critically on the tripeptide's relative affinity for the droplet surface. Tripeptides with higher non-polar character, and, thus higher affinity for the droplet surface, gave a higher ESI response than more hydrophilic ones. It can be speculated that in highly destabilized conformational states the increased exposure of hydrophobic patches enhances the affinity for the droplet surface, leading to relatively increased ionization rates and ESI response. Dobo and Kaltashov also observed an apparent higher ionization efficiency for structurally disordered protein conformational states (48). Secondly, for highly charged ions the ion detection efficiency is somewhat increased. Both aspects of ESI-MS contribute that, ions originating from disordered conformational states show relatively increased signals in ESI-MS.

The intrinsic conformational heterogeneity of E9 DNase is not observed in ESI-MS experiments- NMR experiments have revealed that the E9 DNase slowly interconverts between two conformers. Two distinct regions exhibiting this conformational heterogeneity have been identified, namely the sequence stretches encompassing the residues 20-25 and 65-72 (49).

Hannan et al. reported that upon Zn^{2+} -binding the conformational equilibrium remains undisturbed and that Zn^{2+} -binding does not result in significant conformational changes in E9 DNase (22). However, in our present MS experiments at pH 7, holo-E9 DNase yielded mass spectra exhibiting a unimodal charge envelope with a charge maximum at 8+. Narrow charge envelopes are generally considered as indication of compact gas phase structures originating from compact conformational states. Hence, it has to be concluded that ESI-MS failed to report on the conformational heterogeneity described for the Zn^{2+} -bound E9 DNase. In the X-ray structure, the conformationally heterogeneous regions are in spatial proximity and located at or near the protein surface. Thus, we may speculate that the conformational switch between the two conformers has to be rather localized and apparently does not result in changes of the accessibility of protonation sites. At present, a full understanding of the conformational heterogeneity of E9 DNase is still lacking. Apparently, Trp 22 plays a central role in the conformational dynamics (49). However, to further elucidate if a possible reorientation of the Trp residue is involved in the multiple conformations observed in NMR we intend to apply time-resolved tryptophan fluorescence in combination with time-resolved anisotropy.

Acid-induced metal ion release studies underscore the role of the metal ion as a conformational clamp - ESI-mass spectra of colicin E9 DNase in the presence of Zn^{2+} at pH values ranging from 4 to 5.5 enabled the observation of distinctive charge state distributions for the apo- and holo-protein at the same time, i.e. the bimodal charge state distribution attributed to apo-E9 DNase and the narrow charge state distribution of the holo-E9 DNase are observed simultaneously. The lack of intermediate charge state distributions upon acid-induced metal release is interpreted as indication that partially folded conformational states are not significantly sampled. There was also no indication that partly unfolded holo-species were present as observed in the study of the N-lobe of transferrin upon acid-induced unfolding (50). In addition, our Zn^{2+} -titration experiments provide further evidence that metal ion binding is exclusively associated with the folded state.

Interestingly, apo-E9 DNase at low pH had negative ellipticity at 222 nm while the near UV-CD signal and the Trp fluorescence were lost. Thus, at least under acidic conditions, apo-E9 DNase seems to adopt features that are reminiscent of molten globule-like states, i.e. states that lack a fixed tertiary structure but where secondary structure is retained (51, 52). In this regard, it is intriguing to speculate that the local acidic pH at the membrane surface triggers metal ion release and concomitantly renders the DNase in a molten globule-like state competent for membrane translocation (53-55). Interestingly, Chak et al. have suggested that colicin E7 uptake into cells is aided by the acidic pH at the membrane surface and involves an unfolded intermediate (51). Furthermore, it is reported that insertion of the pore-forming domain of colicin A in the cytoplasmic membrane is preceded by a native to molten globule transition at acidic pH (56).

Gas phase stability and, thus, ESI-MS detectability is governed by electrostatic interactions -

E9 DNase is a metalloprotein that binds a single transition metal ion within the H-N-H motif. Isothermal titration calorimetry established that Zn^{2+} is by far the tightest binding metal ion compared to the other two tested transition metal ions, namely Co^{2+} and Ni^{2+} . Zn^{2+} possesses K_d values in the low nanomolar range, whereas the K_d values for Co^{2+} and Ni^{2+} are in the micromolar range (15). Although the presented metal ion binding studies qualitatively indicate the prevalence of E9 DNase for Zn^{2+} they do not accurately reflect the solution-derived binding parameters. We believe this deviation is a strong indication that the stabilization of gas phase complexes by electrostatic interactions, may have a dramatic influence on the ion species detected by ESI-MS. In the absence of an aqueous environment, van der Waals interactions become less important while ionic and hydrogen bonding interactions are enhanced. As a consequence the stability of metal ion-protein complexes derived from ESI-MS experiments do not reflect necessarily their solution stability.

Noticeably, our gas phase dissociation experiments of the ternary E9 DNase-Zn-Im9 complex highlight the dominance of electrostatic interactions in influencing the gas phase stability of noncovalent complexes. The protein-protein complex of E9 DNase and its cognate immunity protein Im9 is considered as having one of lowest equilibrium dissociation constants reported so far for a protein complex ($K_d \sim 10^{-16}$ M in the absence of salt) (12). In fact, the difference in binding affinity between Zn^{2+} and Im9 for the E9 DNase is 7 orders of magnitude. Nevertheless, in our gas phase dissociation experiments, dissociation of the protein constituents occurs prior to the release of the metal ion. A detailed analysis of the protein-protein interface of the E9 DNase-Im9 complex (16, 19) shows that 14 residues from the E9 DNase and 17 residues from Im9 are directly involved in forming the interfacial contact. Key contributions in defining stability and specificity of the complex are (a) a hydrophobic core, with in the center a stacking interaction between Phe86 of the E9 DNase and Tyr54 of Im9, (b) a hydrogen bonding network of 12 hydrogen bonds including two salt bridges, Arg54 and Lys97 from the E9 DNase and Glu30 and Glu41 from Im9, respectively, and (c) five interfacial water molecules, two of which are completely buried. The interfacial water molecules are involved in an extended network of inter-protein hydrogen bonds mediating stability and specificity of the interface. The mass spectra of the E9 DNase/Im9 complexes in presence and absence of Zn^{2+} showed no indication of the presence of bound water molecules. Recent surveys of structural data on protein-protein and protein-DNA interface indicate that water molecules play a crucial role in mediating polar interactions that stabilize complexes (57). Thus, we may speculate that the diminishing complex stabilization in the gas phase by van der Waals forces and water-mediated inter-protein hydrogen bonding interactions may contribute, at least to some extent, for the apparent weakening of the protein-protein interaction.

Another interesting feature is noticeable in ESI mass spectra of holo- and apo-E9 DNase under solution conditions favouring the folded species. Under these conditions, we repeatedly

observed that exclusively the charge states of the folded states showed a second minor charge state envelope with a mass difference of 98 Da (marked with * in Figure 2, 4 and 6). Interestingly, in the X-ray structures of the E9 DNase-Im9 complex in presence of Ni^{2+} a phosphate ion is seen within the active site cleft (16) which is retained in the absence of a bound metal ion (19). The phosphate is thought to represent the binding site for the product of DNA hydrolysis (58). We may speculate that the low abundant ion species observed may represent compact protein ions retaining a specifically bound phosphate ion in the gas phase. Non-specific ion adduction is less likely because the ion peaks assigned to the "U"-states do not show corresponding satellite peaks.

H/D exchange experiments highlight that metal ion binding and not Im9 binding induces the conformational stabilization of the colicin E9 DNase - Hydrogen /deuterium exchange is a sensitive method to probe protein structures and folding/unfolding mechanisms (59-62). In proteins, side chain and backbone amide hydrogens are exchangeable whereby the latter ones report on the protein structural properties. Before backbone amide hydrogen exchange in proteins can take place, hydrogen bonds have to be broken and exposed to solvent. In general, in H/D exchange experiments, more open protein conformational states with a weak hydrogen bonding network and/or increased solvent accessibility show more rapid exchange reaction than do stable, compact conformational states (63). The utility of MS for extracting exchange levels allows distinguishing of coexisting protein structural populations that experience different exchange rates. Our H/D exchange data obtained for apo-E9 DNase enabled us to conclude that (i) the interconversion between the population termed F and U has to be fast relative to the exchange rate because for both charge envelopes identical exchange-in rates were observed and (ii) the high deuterium incorporation indicated lack of persistent structure. In contrast, in Zn^{2+} -bound E9 DNase approximately 19 % of all labile hydrogen were found to be protected against exchange indicating the presence of compact structural elements associated with hydrogen bonding and reduced surface accessibility, consistent with the increased thermodynamic stability of holo-E9 DNase.

Interestingly, upon Im9-binding apo-E9 DNase apparently still lacks or, at best, possesses only to a minor extent persistent structural elements as indicated by the high deuterium uptake. Recently reported NMR studies demonstrate that the slow conformational dynamics of the E9 DNase seems to persist after binding to its cognate immunity protein Im9, although a general decrease in the extent of the heterogeneity was observed (49). However, Zn^{2+} -binding of Im9-bound E9 DNase apparently diminishes the conformational instability of E9 DNase, as evident from the reduced deuterium uptake (Table 2), and in line with the Zn^{2+} -induced increase of conformational stability. On the other side, one can argue that the H/D exchange of the complex constituents can be rationalized by taking into account that transient dissociation of the complex is a prerequisite for global exchange. In the absence of Zn^{2+} , the

dissociated E9 unfolds, resulting in high deuterium incorporation, while in the presence of Zn^{2+} it remains folded and less deuterium incorporation is observed. However, under the conditions used the K_d of the E9 DNase/Im9 complex is in the femtomolar range, thus the dissociation rate is very low. We therefore believe that the relatively elevated deuterium level for E9 DNase observed in the absence of Zn^{2+} rather relates to the intrinsic conformational mobility of apo-E9 DNase.

Acknowledgments

We thank Christine Moore, Ann Reilly, and Nick Cull (University of East Anglia) for technical assistance

References

1. James, R., Kleanthous, C., and Moore, G. R. (1996) The biology of E colicins: paradigms and paradoxes *Microbiology* **142**, 1569-1580.
2. Cramer, W. A., Cohen, F. S., Merrill, A. R., and Song, H. Y. (1990) Structure and dynamics of the colicin E1 channel *Mol. Microbiol.* **4**, 519-526.
3. Lau, P. C. K., Parsons, M., and Uchimura, T. (1992) in *Bacteriocins, Microcins and Lantibiotics* (James, R., Lazdunski, C., and Pattus, F., Eds.) pp 353-348, Springer-Verlag, Berlin.
4. Masaki, H., Yajima, S., Akutsu-Koide, A., Ohta, T., and Uozumi, T. (1992) in *Bacteriocins, Microcins and Lantibiotics* (James, R., Lazdunski, C., and Pattus, F., Eds.) pp 379-395, Springer-Verlag, Berlin.
5. Kleanthous, C., Hemmings, A. M., Moore, G. R., and James, R. (1998) Immunity proteins and their specificity for endonuclease colicins: telling right from wrong in protein-protein recognition *Mol. Microbiol.* **28**, 227-233.
6. Lazdunski, C. J., Bouveret, E., Rigal, A., Journet, L., Lloubes, R., and Benedetti, H. (1998) Colicin import into Escherichia coli cells *J. Bacteriol.* **180**, 4993-5002.
7. Chak, K. F., Kuo, W. S., Lu, F. M., and James, R. (1991) Cloning and characterization of the ColE7 plasmid *J. Gen. Microbiol.* **137**, 91-100.
8. Pommer, A. J., Wallis, R., Moore, G. R., James, R., and Kleanthous, C. (1998) Enzymological characterization of the nuclease domain from the bacterial toxin colicin E9 from Escherichia coli *Biochem. J.* **334**, 387-392.
9. Schaller, K., and Nomura, M. (1976) Colicin E2 is DNA endonuclease *Proc. Natl. Acad. Sci. U S A* **73**, 3989-3993.
10. Gorbalenya, A. E. (1994) Self-splicing group I and group II introns encode homologous (putative) DNA endonucleases of a new family *Prot. Sci.* **3**, 1117-1120.
11. Shub, D. A., Goodrich-Blair, H., and Eddy, S. R. (1994) Amino acid sequence motif of group I intron endonucleases is conserved in open reading frames of group II introns *Trends Biochem. Sci.* **19**, 402-404.
12. Wallis, R., Moore, G. R., James, R., and Kleanthous, C. (1995a) Protein-protein interactions in colicin E9 DNase-immunity protein complexes. 1. Diffusion-controlled association and femtomolar binding for the cognate complex *Biochemistry* **34**, 13743-13750.
13. Wallis, R., Moore, G. R., Kleanthous, C., and James, R. (1992) Molecular analysis of the protein-protein interaction between the E9 immunity protein and colicin E9 *Eur. J. Biochem.* **210**, 923-930.

14. Wallis, R., Leung, K. Y., Pommer, A. J., Videler, H., Moore, G. R., James, R., and Kleanthous, C. (1995b) Protein-protein interactions in colicin E9 DNase-immunity protein complexes. 2. Cognate and noncognate interactions that span the millimolar to femtomolar affinity range *Biochemistry* **34**, 13751-13759.
15. Pommer, A. J., Kuhlmann, U. C., Cooper, A., Hemmings, A. M., Moore, G. R., James, R., and Kleanthous, C. (1999) Homing in on the role of transition metals in the HNH motif of colicin endonucleases *J. Biol. Chem.* **274**, 27153-27160.
16. Kleanthous, C., Kuhlmann, U. C., Pommer, A. J., Ferguson, N., Radford, S. E., Moore, G. R., James, R., and Hemmings, A. M. (1999) Structural and mechanistic basis of immunity toward endonuclease colicins *Nat. Struct. Biol.* **6**, 243-252.
17. Kleanthous, C., and Walker, D. (2001) Immunity proteins: enzyme inhibitors that avoid the active site *Trends Biochem. Sci.* **26**, 624-631.
18. Ko, T. P., Liao, C. C., Ku, W. Y., Chak, K. F., and Yuan, H. S. (1999) The crystal structure of the DNase domain of colicin E7 in complex with its inhibitor Im7 protein *Structure Fold. Des.* **7**, 91-102.
19. Kuhlmann, U. C., Pommer, A. J., Moore, G. R., James, R., and Kleanthous, C. (2000) Specificity in protein-protein interactions: the structural basis for dual recognition in endonuclease colicin-immunity protein complexes *J. Mol. Biol.* **301**, 1163-1178.
20. Whittaker, S. B., Boetzel, R., MacDonald, C., Lian, L. Y., James, R., Kleanthous, C., and Moore, G. R. (1999) Assignment of ¹H, ¹³C and ¹⁵N signals of the DNase domain of colicin E9 *J. Biomol. NMR* **14**, 201-202.
21. Whittaker, S. B., Boetzel, R., MacDonald, C., Lian, L. Y., Pommer, A. J., Reilly, A., James, R., Kleanthous, C., and Moore, G. R. (1998) NMR detection of slow conformational dynamics in an endonuclease toxin *J. Biomol. NMR.* **12**, 145-159.
22. Hannan, J. P., Whittaker, S. B., Hemmings, A. M., James, R., Kleanthous, C., and Moore, G. R. (2000) NMR studies of metal ion binding to the Zn-finger-like HNH motif of colicin E9 *J. Inorg. Biochem.* **79**, 365-370.
23. Lei, Q. P., Cui, X., Kurtz, D. M., Jr., Amster, I. J., Chernushevich, I. V., and Standing, K. G. (1998) Electrospray mass spectrometry studies of non-heme iron-containing proteins *Anal. Chem.* **70**, 1838-1846.
24. Loo, J. A., Hu, P. F., McConnell, P., Mueller, W. T., Sawyer, T. K., and Thanabal, V. (1997) A study of Src SH2 domain protein-phosphopeptide binding interactions by electrospray ionization mass spectrometry *J. Am. Soc. Mass Spectrom.* **8**, 234-243.
25. Veenstra, T. D., Johnson, K. L., Tomlinson, A. J., Craig, T. A., Kumar, R., and Naylor, S. (1998) Zinc-induced conformational changes in the DNA-binding domain of the vitamin D receptor determined by electrospray ionization mass spectrometry *J. Am. Soc. Mass Spectrom.* **9**, 8-14.
26. Konermann, L., Rosell, F. I., Mauk, A. G., and Douglas, D. J. (1997) Acid-induced denaturation of myoglobin studied by time-resolved electrospray ionization mass spectrometry *Biochemistry* **36**, 6448-6454.
27. Krutchinsky, A. N., Ayed, A., Donald, L. J., Ens, W., Duckworth, H. W., and Standing, K. G. (2000) Studies of noncovalent complexes in an electrospray ionization/time-of-flight mass spectrometer *Methods Mol. Biol.* **146**, 239-249.
28. Maier, C. S., Schimerlik, M. I., and Deinzer, M. L. (1999) Thermal denaturation of Escherichia coli thioredoxin studied by hydrogen/deuterium exchange and electrospray ionization mass spectrometry: monitoring a two-state protein unfolding transition *Biochemistry* **38**, 1136-1143.
29. Vis, H., Heineman, H., Dobson, C. M., and Robinson, C. V. (1998) Detection of a monomeric intermediate associated with dimerization of protein HU by mass spectrometry *J. Am. Chem. Soc.* **120**, 6427-6428.

30. Wallis, R., Reilly, A., Barnes, K., Abell, C., Campbell, D. G., Moore, G. R., James, R., and Kleanthous, C. (1994) Tandem overproduction and characterisation of the nuclease domain of colicin E9 and its cognate inhibitor protein Im9 *Eur. J. Biochem.* *220*, 447-454.
31. Mirza, U. A., Cohen, S. L., and Chait, B. T. (1993) Heat-induced conformational changes in proteins studied by electrospray ionization mass spectrometry *Anal. Chem.* *65*, 1-6.
32. Konermann, L., and Douglas, D. J. (1998) Equilibrium unfolding of proteins monitored by electrospray ionization mass spectrometry: distinguishing two-state from multi-state transitions *Rapid Commun. Mass Spectrom.* *12*, 435-442.
33. Chowdhury, S. K., Katta, V., and Chait, B. T. (1990) Probing conformational changes in proteins by mass spectrometry *J. Am. Chem. Soc.* *112*, 9012-9013.
34. Loo, J. A. (2000) Electrospray ionization mass spectrometry: a technology for studying noncovalent macromolecular complexes *Int. J. Mass Spectrom.* *200*, 175-186.
35. Versluis, C., and Heck, A. J. R. (2001) On the gas-phase dissociation of hemoglobin *Int. J. mass spectrom.* *210*, 637-649.
36. Potier, N., Donald, L. J., Chernushevich, I., Ayed, A., Ens, W., Arrowsmith, C. H., Standing, K. G., and Duckworth, H. W. (1998) Study of a noncovalent trp repressor: DNA operator complex by electrospray ionization time-of-flight mass spectrometry *Protein Sci.* *7*, 1388-1395.
37. Liu, C., Wu, Q., Harms, A. C., and Smith, R. D. (1996) On-line microdialysis sample cleanup for electrospray ionization mass spectrometry of nucleic acid samples *Anal. Chem.* *68*, 3295-3299.
38. Donald, L. J., Hosfield, D. J., Cuvelier, S. L., Ens, W., Standing, K. G., and Duckworth, H. W. (2001) Mass spectrometric study of the Escherichia coli repressor proteins, IclR and GclR, and their complexes with DNA *Protein Sci.* *10*, 1370-1380.
39. Smith, R. D., Bruce, J. E., Wu, Q. Y., and Lei, Q. P. (1997) New mass spectrometric methods for the study of noncovalent associations of biopolymers *Chem. Soc. Rev.* *26*, 191-202.
40. Loo, J. A. (1997) Studying noncovalent protein complexes by electrospray ionization mass spectrometry *Mass Spectrom. Rev.* *16*, 1-23.
41. Smith, R. D., Loo, J. A., Edmonds, C. G., Barinaga, C. J., Udseth, H. R. (1990) New developments in biochemical mass spectrometry: Electrospray ionization *Anal. Chem.* *62*, 882-899.
42. Konermann, L., Collings, B. A., and Douglas, D. J. (1997) Cytochrome c folding kinetics studied by time-resolved electrospray ionization mass spectrometry *Biochemistry* *36*, 5554-5559.
43. Przybylski, M., Glocker, M. O. (1996) Electrospray mass spectroemtry of biomolecular complexes with noncovalent interactions - New analytical perspectives for supramolecular chemistry and molecular recognition processes *Angew. Chem. Int. Ed. Engl.* *35*, 806-826.
44. Swint, L., and Robertson, A. D. (1993) Thermodynamics of unfolding for turkey ovomucoid third domain: thermal and chemical denaturation *Protein Sci.* *2*, 2037-2049.
45. Eftink, M. R. (1994) The use of fluorescence methods to monitor unfolding transitions in proteins *Biophys. J.* *66*, 482-501.
46. Cech, N. B., and Enke, C. G. (2000) Relating electrospray ionization response to nonpolar character of small peptides *Anal. Chem.* *72*, 2717-2723.
47. Cech, N. B., and Enke, C. G. (2001) Effect of affinity for droplet surfaces on the fraction of analyte molecules charged during electrospray droplet fission *Anal. Chem.* *73*, 4632-4639.
48. Dobo, A., and Kaltashov, I. A. (2001) Detection of multiple protein conformational ensembles in solution via deconvolution of charge-state distributions in ESI MS *Anal. Chem.* *73*, 4763-4773.
49. Whittaker, S. B., Czisch, M., Wechselberger, R., Kaptein, R., Hemmings, A. M., James, R., Kleanthous, C., and Moore, G. R. (2000) Slow conformational dynamics of an endonuclease persist in its complex with its natural protein inhibitor *Protein Sci.* *9*, 713-720.

50. Gumerov, D. R., and Kaltashov, I. A. (2001) Dynamics of iron release from transferrin N-lobe studied by electrospray ionization mass spectrometry *Anal. Chem.* **73**, 2565-2570.
51. Chak, K.-F., Hsieh, S.-Y., Lao, C.-C., and Kan, L.-S. (1998) Change of thermal stability of colicin E7 triggered by acidic pH suggests the existence of unfolded intermediate during the membrane-translocation phase *Proteins* **32**, 17-25.
52. Le, W. P., Yan, S. X., Zhang, Y. X., and Zhou, H. M. (1996) Acid-induced folding of yeast alcohol dehydrogenase under low pH conditions *J. Biochem. (Tokyo)* **119**, 674-679.
53. Bychkova, V. E., Dujsekina, A. E., Klenin, S. I., Tiktopulo, E. I., Uversky, V. N., and Ptitsyn, O. B. (1996) Molten globule-like state of cytochrome c under conditions simulating those near the membrane surface *Biochemistry* **35**, 6058-6063.
54. McLaughlin, S. (1989) The electrostatic properties of membranes *Annu. Rev. Biophys. Biophys. Chem.* **18**, 113-136.
55. Prats, M., Teisié, J., and Tocanne, J.-F. (1986) Lateral proton conduction at lipid-water interfaces and its implications for the chemiosmotic-coupling hypothesis *Nature* **322**, 756-758.
56. Van der Goot, F. G., Gonzalez-Manas, J. M., Lakey, J. H., and Pattus, F. (1991) A 'molten-globule' membrane-insertion intermediate of the pore-forming domain of colicin A *Nature* **354**, 408-410.
57. Janin, J. (1999) Wet and dry interfaces: the role of solvent in protein-protein and protein-DNA recognition *Structure Fold. Des.* **7**, R277-279.
58. Pommer, A. J., Cal, S., Keeble, A. H., Walker, D., Evens, S. J., Kuhlman, U. C., Cooper, A., Connolly, B. A., Hemmings, A. M., Moore, G. R., James, R., and Kleantous, C. (2001) Mechanisms and cleavage specificity of the H-N-H endonuclease colicin E9 *J.Mol.Biol.* **314**, 735-749.
59. Engen, J. R., and Smith, D. L. (2001) Investigating protein structure and dynamics by hydrogen exchange MS *Anal. Chem.* **73**, 256A-265A.
60. Englander, S. E., Sosnick, T. R., Enlander, J. J., and Mayne, L. (1996) Mechanisms and uses of hydrogen exchange *Curr. Opin. Struc. Biol.* **6**, 18-23.
61. Miranker, A., Robinson, C. V., Radford, S. E., Aplin, R. T., and Dobson, C. M. (1993) Detection of transient protein folding populations by mass spectrometry *Science* **262**, 896-900.
62. Nemirovskiy, O., Giblin, D. E., and Gross, M. L. (1999) Electrospray ionization mass spectrometry and hydrogen/deuterium exchange for probing the interaction of calmodulin with calcium *J. Am. Soc. Mass. Spectrom.* **10**, 711-718.
63. Englander, S. W., and Kallenbach, N. R. (1983) Hydrogen exchange and structural dynamics of proteins and nucleic acids *Q. Rev. Biophys.* **16**, 521-655.

Chapter 4

Distinct conformational stability and functional activity of four highly homologous endonuclease colicins

Ewald T.J. van den Bremer, Robin E.J. Spelbrink, Claudia S. Maier, Albert J. R. Heck¹
Wim Jiskoot²
Anthony H. Keeble, Colin Kleanthous³
Arie van Hoek, Antonie J.W.G. Visser⁴
Richard James⁵
Geoffrey R. Moore⁶

Protein Science 2004; in press

¹Dept. of Biomolecular mass spectrometry, Utrecht University, Utrecht

²Dept. of Pharmaceutics, Utrecht University, Utrecht

³Dept. of Biology, University of York, York

⁴MicroSpectroscopy Centre, Wageningen University, Wageningen

⁵Division of Microbiology & Infectious Diseases, University of Nottingham, Nottingham

⁶School of Chemical Sciences, University of East Anglia, Norwich

Abstract

The family of conserved colicin DNases E2, E7, E8 and E9 are microbial toxins that kill bacteria through random degradation of the chromosomal DNA. In the present work we compare side-by-side the conformational stabilities of these four, highly homologous, colicin DNases. Our results indicate that the apo-forms of these colicins are at room temperature and neutral pH in a dynamic conformational equilibrium between at least two quite distinct conformers. We show that the thermal stabilities of the apo-proteins differ by up to 20 °C. The observed differences correlate with the observed conformational behavior, i.e., the tendency of the protein to form either an open, less stable, or closed, more stable, conformation in solution, as deduced by both tryptophan accessibility studies and electrospray ionization mass spectrometry. Given these surprising structural differences, we next probed the catalytic activity of the four DNases and also observed a significant variation in relative activities. However, no unequivocal link between the activity of the protein and its thermal and structural stability could easily be made. The observed differences in conformational and functional properties of the four colicin DNases are surprising given that they are a closely related ($\geq 65\%$ identity) family of enzymes containing a highly conserved ($\beta\beta\alpha$ -Me) active site motif. The different behavior of the apo-enzymes must therefore most likely depend on more subtle changes in aminoacid sequences, most likely in the exosite region (residues 72-98) that is required for specific high affinity binding of the cognate immunity protein.

Introduction

Colicins are a group of toxins produced by *Escherichia coli* to kill other *E. coli* strains and related bacteria in order to gain a competitive advantage under nutrient stress conditions (1). Colicins comprise a three domain organization with the role of two of the domains (the receptor binding and translocation domains) being to bind the target cell and allow the third domain (the cytotoxic domain) to translocate to its site of action, which can be either the periplasm, inner membrane, or cytoplasm depending on the colicin (1). A sub-group comprises colicins E2-E9, act within the cytoplasm and kill the target cell through a nuclease activity. They are further subdivided into three sequence groups: 1) E2 like (comprising E2, E7, E8, and E9) within which their cytotoxic domains show strong sequence homology ($\geq 65\%$), having a Mg^{2+} -dependent, T-base-specific activity aimed at the chromosomal DNA, although with a weak, metal ion independent, activity on RNA (2, 3); 2) E3 like (comprising E3, E4, and E6) cleaving the 16S rRNA at the ribosomal A site (between nucleotides 1493 and 1494) (4); and 3) E5, which cleaves a range of tRNA molecules (5).

The active DNase site of the E2, E7, E8, and E9 DNases comprises the last ~ 30 residues of the proteins (Figure 1A), and has a fold made up of two anti-parallel β -strands and an α -helix (Figure 1B) and resembles a distorted zinc-finger. Consequently, the active site fold has been called the $\beta\beta\alpha$ -Me finger (6). This motif is found within nucleases spanning all biological kingdoms that otherwise have structurally diverse and unrelated protein scaffolds. Examples includes apoptotic endonucleases (DNases), bacterial toxins and homing endonucleases (6-8). Biochemical analysis of colicin DNase function has previously focused on the E9 DNase (2, 3, 9, 10) and E7 DNase (11).

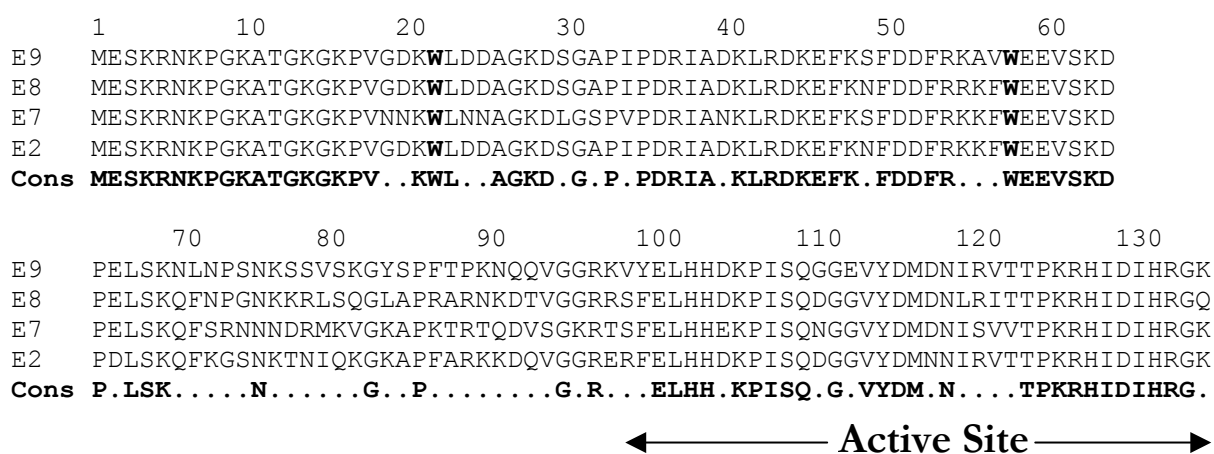


Figure 1 (A). Sequence alignments for the E colicin DNase domains E2, E7, E8 and E9.

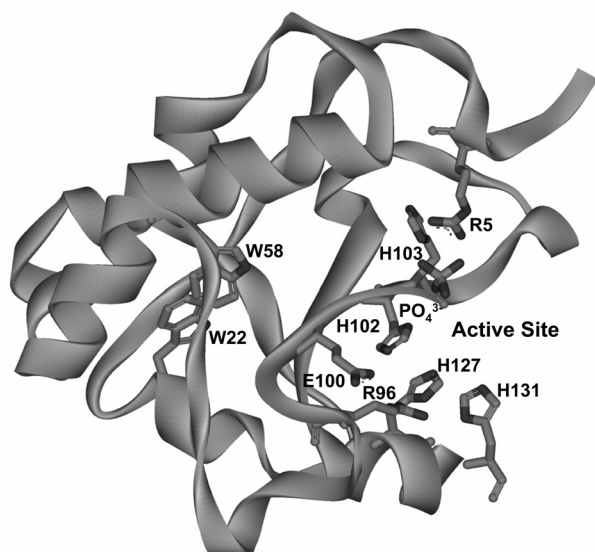


Figure 1 (B). The crystal structure of the apo-E9 DNase (12) showing the two buried tryptophans (W22 and W58), and the active site residues that are essential for the Mg^{2+} -dependent DNase activity (3).

The cytotoxic effect of colicins are prevented from killing their producing cell by the co-expression of an antidote called an immunity protein, which, in the case of the nuclease colicins, is a small (9-10 kDa) globular protein that binds with high affinity to the cytotoxic domain (13-15). The competitive influence of the colicins is based on the specific tight binding of the cognate immunity protein over the different non-cognate immunity proteins (15, 16). In order to achieve this, a region of the DNase domain (residues 72-98; Figure 1A) has a variable sequence, although the rest of the protein is highly conserved, allowing specific binding interactions to be achieved.

Given that the E2 group is the most numerous E colicin nuclease group and is the best characterized, both structurally, with crystal structures of E7 and E9 available (17, 18), and functionally (2, 3, 9-11), we presently focused on this group. Specifically, we investigated structural features of the four isolated related 15 kDa cytotoxic DNase domains by assessing their thermal stabilities and conformational properties in solution by differential scanning calorimetry, tryptophan accessibility studies and electrospray ionization mass spectrometry. Taken the remarkable outcome, which revealed strikingly different thermal and conformational stabilities of the four apo-DNases, we also compared their enzymatic activities and also observed a significant variation. Therefore, the present studies supplements colicin structural and functional biology since, in contrast to E7 and E9, comparatively little biophysical and biochemical characterization has been carried out for E2 and E8.

More generally, the present study reiterates that conformational dynamics, thermal stabilities and functional activities of proteins are impossible to predict purely from primary sequence information. In particular in this case, the four colicins have a high degree of sequence conservation within the active site, with all the residues as being critical for catalysis being absolutely conserved (3). The observed differences in stability and activity therefore most likely originate from differences in the variable region, which is involved in cognate immunity protein

recognition. A better understanding of the physicochemical characteristics of the cytotoxic domain of these enzymes is important as the structural flexibility has earlier been proposed to be of importance in the process translocation to its site of action (10).

Experimental procedures

Protein samples - Colicin DNase domains, E2, E7, E8 and E9 were expressed in *Escherichia coli* and purified as previously described (3). Confirmation of each expressed DNase (E2, E7, E8 and E9) by nano-electrospray ionization mass spectrometry (ESI-MS) under denaturing conditions (50 (v/v) % acetonitrile/water containing 0.1% formic acid) yielded average masses of (15329.9 ± 0.4) Da; (15374.7 ± 0.3) Da, (15322.6 ± 0.4) Da and (15088.2 ± 0.3) Da, respectively. These masses are all within 1 Da of those calculated from the amino acid sequence.

Nano Electrospray Ionization Mass Spectrometry - Time-of-flight electrospray ionization mass spectra were recorded on a Micromass LC-T mass spectrometer (Manchester, U.K.) operating in the positive ion mode. Prior to analysis a 600-3000 m/z scale was calibrated with CsI (2 mg/ml) in isopropanol/water (1:1). Samples for charge state distribution analysis were introduced via a nanoflow electrospray source. Nano-electrospray needles were prepared as described previously (19). Unless stated otherwise all samples were dissolved in 50 mM aqueous ammonium acetate solutions at pH 7.4. In all experiments an aliquot (1-3 µl) of protein sample at a concentration of 10 µM was introduced into the electrospray needles. The nanospray needle potential was typically set to 1200 V and the cone voltage to 30 V. The mass spectrometer was operated without source heating. During individual titration experiments all parameters of the mass spectrometer were kept constant (19).

Steady-State Fluorescence Spectroscopy - Quenching of tryptophan fluorescence by acrylamide in the range 0-0.33 M was performed by adding aliquots of acrylamide (1.4 M in 50 mM ammonium acetate) to a solution containing 6 µM DNase. For experiments on the holo-proteins 46 µM of zinc acetate was added. To avoid interference by acrylamide absorption, the excitation wavelength was set at 300 nm. The fluorescence intensity was monitored at 345 nm. Measurements were performed with an LS-50 Luminescence spectrophotometer (Perkin Elmer, Norwalk, CT) at 20°C. In all studies, excitation and emission bandwidths were set at 5.0 and 7.0 nm, respectively. Spectra were corrected for dilution and background. The data were analyzed by a modified form of the Stern-Volmer equation: $F_0/F = 1 + K_{SV} [Q] e^{V[Q]}$, where F_0 and F are the fluorescence intensities in the absence and presence, respectively, of quencher (acrylamide) at concentration $[Q]$, K_{SV} is the Stern-Volmer constant for dynamic quenching, and V is a constant representing static contributions to the quenching. In addition, K_{SV} is equal to $k_q \langle \tau \rangle$, where k_q is the apparent bimolecular rate constant for the collision of the quencher and the protein, and

$\langle\tau\rangle$ is the average excited-state lifetime of the tryptophan residues in the absence of quencher. We used the average lifetime $\langle\tau\rangle$ taken at 349 nm emission wavelength to calculate k_q (20).

Time-Resolved Fluorescence Spectroscopy - Time-resolved fluorescence decay times were measured in a home-built setup with mode-locked continuous wave laser excitation and time-correlated photon counting detection. The pump laser was a CW diode-pumped, frequency-doubled Nd:YVO₄. The mode-locked laser was a titanium: sapphire laser coupled with a pulse picker which decreased the repetition rate of the excitation pulses to 3.8×10^6 pulses per second. The maximum pulse energy was a few pJ, the wavelength 295 nm and the pulse duration 3 ps. The temperature was controlled and set on 20°C. Fused silica cuvettes of 10 mm light path were used. The fluorescence emission was collected at 348.8 nm at an angle of 90° with respect to the direction of the excitation light beam.

Experimental data consisted of repeating sequences of measurements of the polarized emission (parallel and perpendicular component) fluorescence decays of the reference compound (three cycles of 20 s), the protein sample (10 cycles of 20 s), the background (two cycles of 20 s), and again the reference compound. In that way an eventual temporal shift can be traced and corrected. All cuvettes were carefully cleaned and checked for background luminescence prior to the measurements. For obtaining a dynamic instrumental response of the setup, the single exponential fluorescence decay was measured of paraterphenyl in a mixture of cyclohexane and CCl₄ in a 50/50 % volume ratio. See for further details as described by Visser et al. (21) Data analysis was performed using a home-built computer program (22, 23).

Differential Scanning Calorimetry - Differential Scanning Calorimetry (DSC) was used to measure transition temperatures (T_m) of the DNases in the presence and absence of Zn²⁺. T_m is defined as the temperature at which the excess heat capacity is maximal. Lyophilized proteins were diluted in 50 mM ammonium acetate pH 7.4. Excess heat (C_p) *versus* temperature scans were obtained from 0.3 mg/ml (~20 μM) protein solutions using a high sensitivity differential scanning calorimeter MicroCal VP-DSC (MicroCal, Inc., North Hampton, Massachusetts). The sample and reference solutions were carefully degassed under vacuum for 15 min before loading the cells (0.514 ml). Prior to each analysis the system was equilibrated for 20 min at 15 °C. During measurements the temperature was increased from 15 °C to 80 °C at scan rates of 1 °C/min.

Kunitz assay - Calf thymus DNA (~50 μg DNA ml⁻¹ to give a final A₂₆₀ of 1) was made up in 50 mM triethanolamine buffer pH 7.4 containing 10 mM MgCl₂ to assay the DNase activity. 10 μg of DNase was used per 1.0 ml for each assay. Prior to the analysis of the enzymatic reaction the enzyme was preincubated at the temperature of interest. Reactions were initiated by addition

of the enzyme and the ΔA_{260} was observed over 600 seconds in a dual beam UV/Visible Cintra10 spectrophotometer (GBC Scientific Equipment Pty Ltd, Australia) thermostatted at different temperatures by using a Peltier-element. The reference cuvette contained identical amounts of calf thymus DNA and metal ion as the sample cuvette. Data were downloaded and processed with Microsoft Excel. Activities were calculated as $\Delta A_{260} \text{min}^{-1} \mu\text{g}^{-1}$ protein and converted to Kunitz units (KU) where $1 \text{ KU} = 0.001 \Delta A_{260} \text{min}^{-1} \mu\text{g}^{-1}$ protein.

Plasmid nicking assay - Assays were performed in 50 mM triethanolamine buffer pH 7.4 containing $\sim 1 \mu\text{g}$ of plasmid DNA (pUC18) and 20 mM MgCl_2 . Reactions were started by the addition of E2, E7, E8 or E9 DNase and incubated for 10 min at different temperatures. The reactions were stopped by adding 5 μl stop mix (containing EDTA) before electrophoresis in a 1.2 % (w/v) agarose gel. Gels were stained with ethidium bromide.

Results

Conformational variability monitored by tryptophan fluorescence quenching - To investigate and characterize structural features of the DNases in solution, we used two independent techniques, tryptophan fluorescence quenching (this section) and (nano) electrospray ionization mass spectrometry (ESI-MS) (following section) to address the conformation of the proteins. Colicin DNases contain two strictly conserved tryptophans that are buried within the interior of the protein. Consequently, as typical for tryptophans buried in the interior of folded proteins, the fluorescence emission wavelength maxima for the four DNases are in the range 333-336 nm. In such a case their accessibility to the non-charged collisional quencher acrylamide should be dependent upon the global conformational state of the protein, being high for more open conformational states but low for closed conformers. N-Acetyl-L-tryptophanamide (NATA) was used as a reference compound that is fully and easily accessible to the quencher and is characterized by a high Stern-Volmer quenching constant (K_{SV}). Results for the steady-state acrylamide quenching of apo- and holo- E2, E7, E8 and E9 are summarized in Figure 2 and Table 1, along with the NATA control.

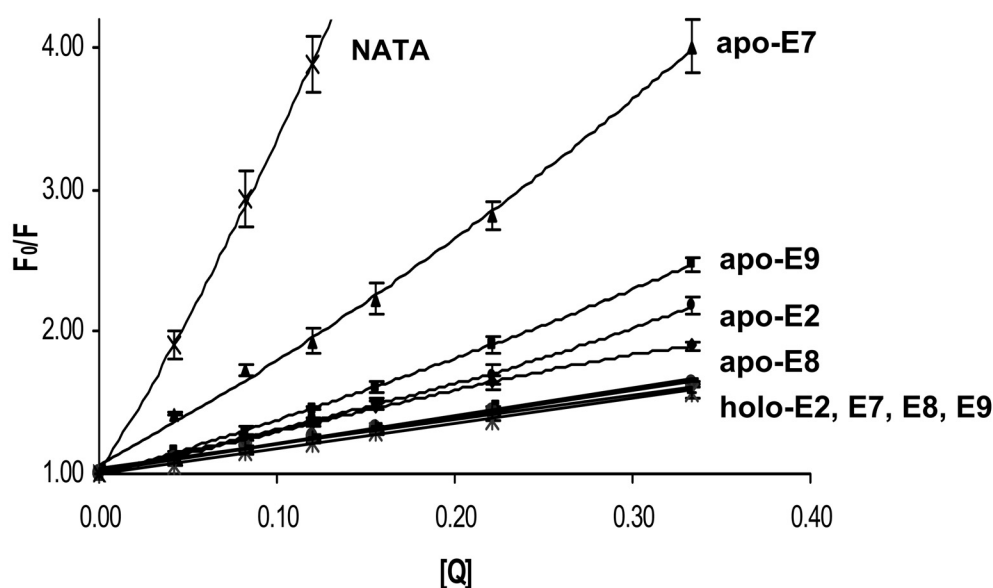


Figure 2. Stern-Volmer plots of the quenching of the fluorescence of NATA and DNases E2, E7, E8 and E9 in the presence (holo) and absence (apo) of Zn^{2+} ions by acrylamide. The data were fitted by non-linear regression of three sets of measurements using a modification of the Stern-Volmer equation: $F_0 / F = 1 + K_{sv} [Q] e^{V \cdot [Q]}$.

Table 1. Acrylamide quenching parameters for E colicin DNases ^a

protein	apo DNases			holo DNases		
	K_{sv} (M^{-1})	V (M^{-1})	r^2	K_{sv} (M^{-1})	V (M^{-1})	r^2
E2	2.79 ± 0.15	0.74 ± 0.19	0.993	2.41 ± 0.11	^b	0.993
E7	7.37 ± 0.48	0.62 ± 0.24	0.989	2.45 ± 0.09	^b	0.993
E8	3.13 ± 0.11	^b	0.995	1.84 ± 0.08	^b	0.994
E9	3.49 ± 0.13	0.75 ± 0.14	0.996	2.29 ± 0.11	^b	0.991
NATA	20.55 ± 0.91	1.34 ± 0.15	0.994			

^a Data were fitted according to $F_0/F = 1 + K_{sv} \cdot [Q] \cdot e^{V \cdot [Q]}$

^b Static quenching component not observed

To further extend this analysis we determined k_q , the bimolecular collisional rate constant, which essentially represents the average number of collisional encounters between the tryptophans and acrylamide and, thus, is a quantification of their accessibilities. In order to do this we determined the average lifetime fluorescence $\langle \tau \rangle$ for each wild-type DNase in the absence of quencher using time-resolved fluorescence since k_q equals $K_{sv} / \langle \tau \rangle$. The recovered parameters for intensity decay and the collisional quenching constants are shown in Table 2 with each apo-DNase exhibiting a heterogeneous decay, described by a sum of three exponential terms ($p_1, p_2, p_3 / \tau_1, \tau_2, \tau_3$). The four apo-DNases show marked differences in their sensitivity to

acrylamide quenching implying that their structures have different relative degrees of compactness. Based on the present assay, apo-E7 has a significantly more open structure than the other apo-DNases since the tryptophans are more accessible to the quencher (k_q is 1.8-fold greater than for E9 and ~ 3.5 -fold for E2 and E8). Summarizing, the combination of fluorescence quenching and lifetime measurements suggest that the conformational compactness of the four colicins is strikingly different and follow the order $E7 < E9 < E2 \approx E8$.

Table 2. Fluorescence lifetime data analysis

apo protein	p ₁ p ₂ p ₃ ^a	τ_1 τ_2 τ_3 (ns) ^b	χ^2	$\langle\tau\rangle$ (ns)	k_q ($10^9\text{M}^{-1}\text{s}^{-1}$) ^c
E2	0.069 0.160 0.771	0.91 ± 0.16 3.52 ± 0.46 7.78 ± 0.06	1.069	6.63 ± 0.09	0.42 ± 0.17
E7	0.131 0.309 0.560	0.87 ± 0.06 3.60 ± 0.18 6.50 ± 0.05	1.075	4.87 ± 0.06	1.51 ± 0.48
E8	0.059 0.102 0.839	0.53 ± 0.10 3.58 ± 0.49 7.82 ± 0.05	1.070	6.96 ± 0.07	0.45 ± 0.13
E9	0.159 0.397 0.450	0.78 ± 0.05 2.91 ± 0.07 6.53 ± 0.03	1.060	4.21 ± 0.03	0.83 ± 0.13

^a Normalized P-values representing fractional contributions.

^b The excited-state lifetimes, τ_1 τ_2 τ_3 , were determined from single-photon timing measurements (data not shown).

^c Biomolecular rate constant for acrylamide quenching was calculated using $\langle\tau\rangle$ and K_{SV} (see Table 1)

The χ^2 values are "reduced chi-squares" indicating goodness of fit.

Upon Zn^{2+} binding, all the colicin DNases show a significant decrease in K_{SV} values, to a more or less uniform value (Table 1), indicating that metal binding results in substantial protection of the tryptophans. Thus, the fluorescence quenching measurements suggest that all four holo-enzymes share a similar conformational compactness. We therefore measured only the lifetime of the Zn^{2+} -containing E9 DNase, which revealed an average lifetime of 3.7 nsec (data not shown) and a k_q value of $0.62 \times 10^9 \text{M}^{-1}\text{s}^{-1}$. This latter value indicates a $\sim 25\%$ decrease in tryptophan accessibility when compared to apo-E9 DNase. This change in accessibility for colicin E9 correlates well with the increased thermal stability induced by metal ion binding (10).

Conformational variability monitored by (nano) ESI-MS - In the previous section we related the accessibilities of the buried tryptophans to the global structure of the proteins. However, since local, in addition to global, structural features may affect the accessibility of the tryptophans, we next used ESI-MS to address the global structural conformation of the DNases. This technique provides some unique features for the investigation of conformational properties of proteins as it has the ability to simultaneously provide information about the conformation of the protein and ligand binding (24-26). Additionally, it has an advantage over techniques, such as circular dichroism (CD) and steady state fluorimetry, that sub-populations of protein conformers can be analyzed simultaneously instead of the ensemble of different sub-populations. The relevance to the present study is that, under certain conditions, ESI-MS can reveal the dynamic features of conformational stability. Importantly, despite being a gas-phase based technique, results from ESI-MS experiments can, when carefully evaluated, be informative about solution phase properties (27-29).

We have previously used ESI-MS to investigate the E9 DNase (19). In the present work we compare these previous results with those obtained for the E2, E7, and E8 DNases (Figure 3). As before, samples are being electrosprayed from solutions under conditions that are known to preserve “native” conformations (see also experimental procedures). In the ESI-MS process proteins become ionized through multiple protonations (30, 31) with the resulting mass spectrum typically displaying a single continuous (“Gaussian”) charge state envelope. However, for all of the colicin DNases, a bimodal charge distribution is observed comprising a broad distribution encompassing ion peaks from 10+ to 23+ (with a maximum located at 18+), and a second narrow distribution of three ion peaks (7+, 8+, 9+) with a maximum located at 8+ (Figure 3). In each case both of the charge distributions produce a calculated mass for the protein identical to the theoretical mass based on the amino acid sequence. However, the relative abundance of each distribution is different for the four colicin DNases with the high charge state distribution (around 18+) being dominant for the E7 DNase, the low charge state (around 8+) dominant for E8. The charge distributions observed for the DNases E2 and E9 are found to be somewhat intermediate. Several control experiments were carried out to exclude the possibility that the differences observed in the mass spectra were the result of unforeseen experimental artefacts such as variations in spray conditions. The results of one of those control experiments is given in Figure 4 where the mass spectrum of an equimolar mixture of the apo-E7 and E8 DNases is shown. The spectrum resembles a combination of the two spectra obtained for the isolated DNases (compare Figure 3), confirming the strikingly different behavior of apo-E7 and apo-E8 in ESI-MS.

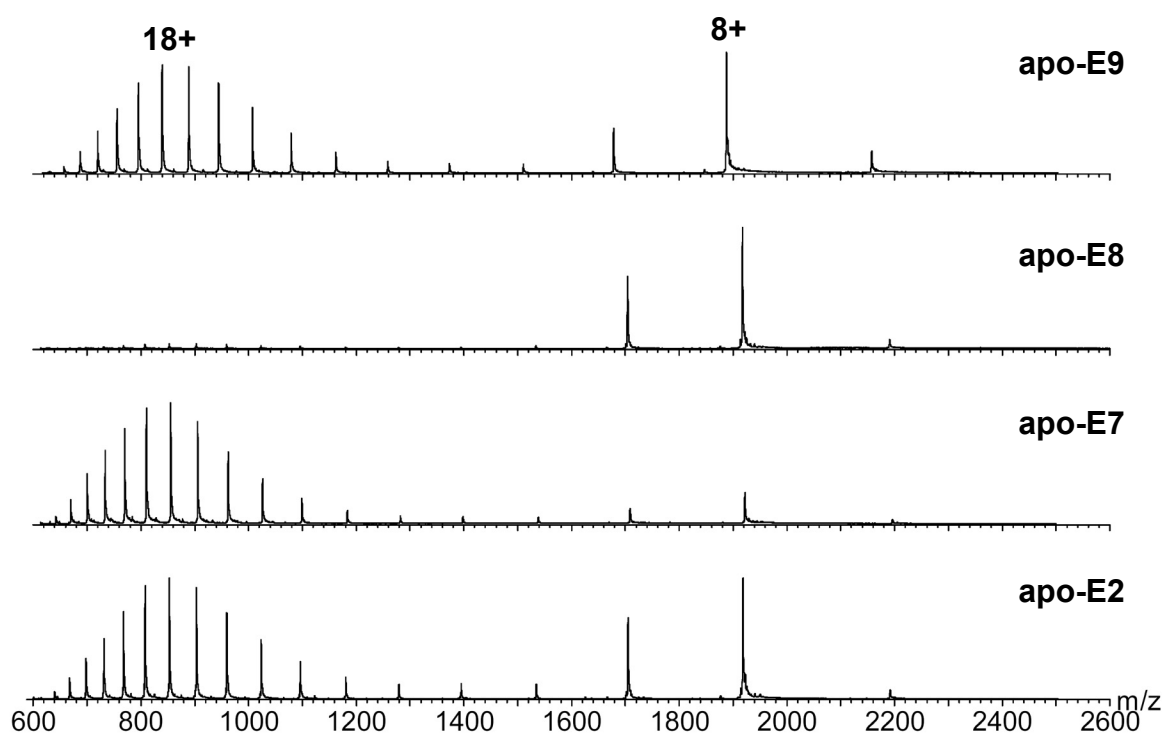


Figure 3. Nano-electrospray ionization (ESI) mass spectra of the apo-DNases E2, E7, E8 and E9 (10 μ M) sprayed from an aqueous 50 mM ammonium acetate solution at pH 7.4.

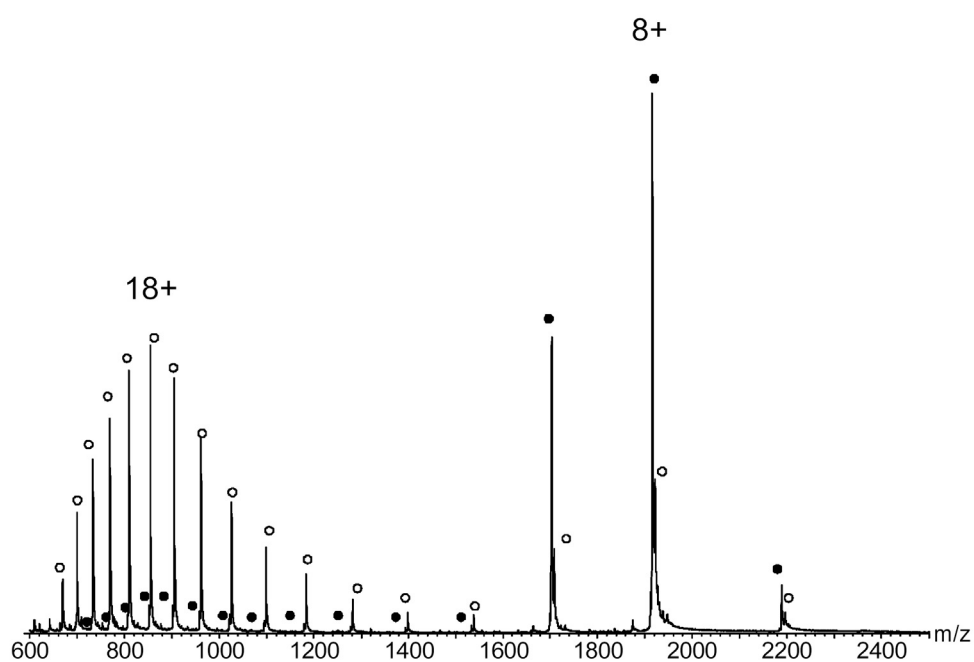


Figure 4. Nano-electrospray ionization (ESI) mass spectra of an equimolar mixture (10 μ M each) of apo-DNases E7 and E8 sprayed from an aqueous 50 mM ammonium acetate solution at pH 7.4. Ion peaks representing DNases apo-E7 and E8 are highlighted by open (o) and filled circles (●), respectively.

The extent of protonation of a protein during the ESI process is dependent upon the number of basic sites at the surface of the proteins and thus also on the conformation/structure of the protein (25). In general, proteins that exhibit unfolded, open, or flexible structures become more protonated than proteins with compact, highly folded structures (19, 32, 33). The observed 18 charges on a 15 kDa protein is atypical and very high for a protein sprayed from buffered neutral ammonium acetate solutions (34), which must indicate that the protein is in a solution-phase conformation that is likely very open. In our original ESI-MS study on the E9 DNase (19) we assigned the low charge distribution (states 7+, 8+, and 9+) as originating from compact, folded-like, conformational states (termed F). We assigned the high charge distribution (11+ to 22+) as originating from a population of open, more unfolded, conformational states (termed U). We showed by hydrogen-deuterium exchange mass spectrometry that these two conformers are in rapid equilibrium (on the seconds time-scale) (19). A semi-quantitative assessment of the relative contribution of the two distinct populations of conformers may be given by the ratio of their summed peak areas ($(A_F/(A_U+A_F))$) (19, 35). Such an approach provides values of 0.05, 0.29, 0.32, and 0.92 for the E7, E9, E2, and E8 DNases, respectively, indicating that E7 is, on average, predominantly in its highly unfolded conformational state, whereas E8 is in time on average more in its compact conformational state. Summarizing, the conformational equilibrium observed follows, when ranked from mostly unfolded to more folded, the order $E7 < E9 \approx E2 < E8$.

Some care must be taken when relating the relative sizes of the two populations in the mass spectra to the fractional contributions of the protein conformers in solution since unfolded/open like states are usually detected more readily (19, 36-38). Nevertheless, the values for the relative fractions of folded conformers correlate very well with the tryptophan accessibility experiments of the apo-DNases. Both tryptophan fluorescence quenching and mass spectrometric experiments indicate that the global structures show different relative levels of compactness. The ESI-MS results imply that the E2 DNase is more unfolded compared to the E8 DNase in contrast to the similarity in the degrees of solvent protection of the tryptophans (Table 1). However, E8 experiences only one type of fluorescence quenching whereas E2 experiences two types (i.e. dynamic and static) suggesting that the E2 structure is more open than E8, and thus follows the same order of our ESI-MS findings.

The E9 DNase, which has a nM affinity for Zn^{2+} , undergoes metal ion induced conformational changes that are localized near the active site of the protein (12, 39, 40) and result in increased stability (10). This is reflected in the ESI-MS spectra which show, besides the observed mass increase of 63 Da (65 Da minus $2H^+$) due to specific binding of one Zn^{2+} ion, a change in the charge distributions in the holo-E9 DNase, so that only the low-charge distribution was observed (19). In the present work, we sprayed the other colicin DNases in the presence of a 5-fold excess of Zn^{2+} and also observed only the low-charge distribution is

detected (data not shown). These results are also in agreement with the tryptophan fluorescence quenching results obtained for the holo-enzymes as described in the previous section. In contrast, when experiments were repeated with the apo-DNases sprayed in the presence of a large excess of Mg^{2+} , the natural co-factor, the ESI-MS spectra were identical to those of the apo-DNases alone. Thus, Mg^{2+} does not significantly bind nor does stabilize the apo-DNases. This absence of binding is in agreement with previous isothermal titration calorimetry experiments where no Mg^{2+} binding could be observed indicating that binding was very much weaker than mM (10). Therefore, specific Mg^{2+} binding to E9 DNase *in vivo* is unlikely.

Thermal stability probed by Differential Scanning Calorimetry - Given the observed differences in the conformational properties of the four colicin DNases we addressed their thermodynamic stabilities and therefore investigated the thermal unfolding of the colicin DNases in both the apo-(metal free) and holo-forms by differential scanning calorimetry (DSC). The results are summarized in Table 3.

Table 3. Calorimetric data of colicin DNases in the presence and absence of Zn^{2+}

DNase	apo	holo
	T_m (°C)	T_m (°C)
E2	37.3	61.2
E7	26.3	59.9
E8	45.5	63.7
E9	36.6	63.0

The midpoint melting temperatures (T_m) for the apo- (36.6 °C) and transition metal bound-E9 DNase (63 °C) determined in the present work are in good agreement with the values of Pommer *et al.* (10). In all cases the holo-DNases were found to be much more stable than the apo-DNases, and to have similar T_m values (60-64 °C). In contrast, the T_m values vary quite considerably between the apo-DNases, 26.3 °C for apo-E7 DNase to 45.5 °C for the apo-E8 DNase, with the T_m of E2 DNase being similar to that of E9 DNase (37 °C). Hence, despite their high sequence identities the apo-DNases have significantly different thermal stabilities, which may be of biological importance as they are observed to vary to both sides of the biologically important mammal-body temperature of 37 °C. It is interesting to note that the observed order of T_m values for the apo-DNases is $E7 < E9 \approx E2 < E8$, very similar to the extent of unfolding/folding observed in the electrospray mass spectra.

Comparison of the enzymatic activities of the colicin DNases - *A priori* we supposed that these four proteins have identical folding properties and thus similar enzymatic activities. Now that we observed these striking differences we decided to probe the DNase activities also as a function of temperature. We have previously used two different assays to monitor DNA cleavage each using a different type of DNA substrate - the spectrophotometric Kunitz assay to monitor double strand cleavage of linear calf thymus dsDNA, and a nicking assay using supercoiled pUC18 to monitor single strand cleavage. In the present work we have used the assays (Figure 5) as a semi-quantitative comparison of the relative catalytic activities, an approach we have previously used when comparing active site mutants of the E9 DNase (3).

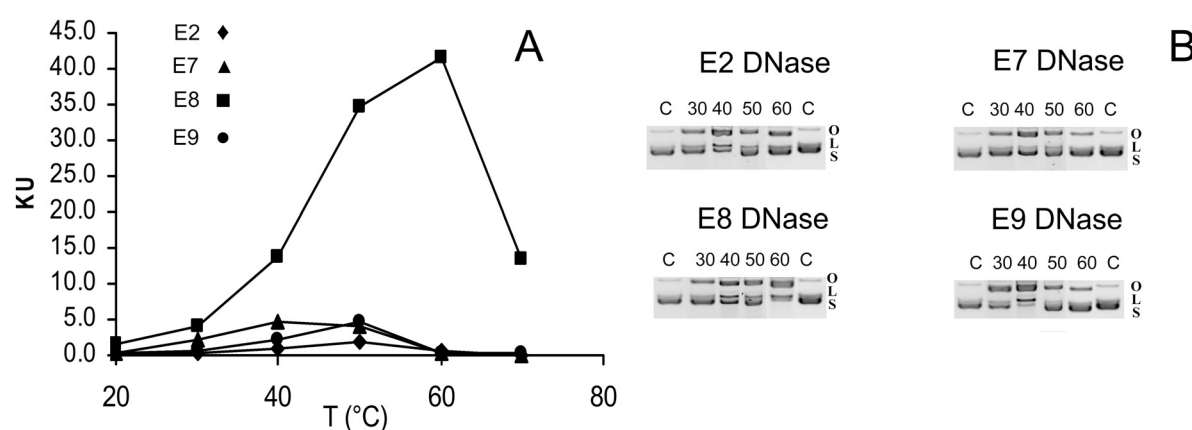


Figure 5. (A) Temperature dependent Kunitz activity assays in the presence of 20 mM Mg^{2+} in 50 mM triethanolamine buffer pH 7.4 (1 KU = 0.001 $\Delta A_{260} \text{min}^{-1} \mu\text{g}^{-1}$ protein) (B) Plasmid nicking assays: Each panel indicates the migration of supercoiled (S), open circular (O) and linear DNA (L) after 10 min incubation. Control (C) is an identical reaction in the absence of Mg^{2+} ions.

We carried out the assays on the four apo-colicin DNases in the presence of Mg^{2+} , the physiologically relevant divalent metal ion for DNA cleavage (3). As Mg^{2+} does not significantly bind, these assays provide data on the activity of the non-metal bound DNases. The assays were carried out over a range of temperatures from 20 to 70 °C. In the Kunitz assay the E2, E7, and E9 DNases show similar levels of activity although the E2 and E9 DNases have a higher optimal temperature (~50 °C) than the E7 DNase (~40 °C). In contrast, the E8 DNase shows both a higher activity (up to 10-fold) at all temperatures tested, and a higher optimal temperature (~60 °C). The temperature dependences of the activities from the plasmid-nicking assay essentially parallel these results. However, the DNases show different nicking profiles, with E8 DNase showing activity over the whole temperature range and being most active at 60 °C, where it ran out of supercoiled plasmid DNA substrate. DNases E2 and E9 have their optimum at 40 °C. At this temperature both DNases produce mostly linear products, however, E9 DNase ran out of supercoiled plasmid DNA substrate whereas the E2 DNase did not. This indicates that at 40 °C the E9 DNase is more active compared to E2. Linear cleavage products were not observed for

E7 at any assayed temperatures indicating a weaker activity. Summarizing, the catalytic properties and activities of the four apo-colicin DNases differ strikingly, not only in catalytic rates, but also in selectivity and temperature dependence. In contrast, no activity at any temperature was observed for any of the DNases in the presence of Zn^{2+} (data not shown). Although this metal ion binds with a high affinity to the active site, this observed inactivity is in line with our previous studies on the E9 DNase (10).

Discussion

In the present work we have probed the sequence-structure-function relationships within a group of highly similar proteins – the colicin DNases. The advantage of analyzing a group of proteins is that the conserved features of structure and function can be ascertained, as well as differences. Despite a high degree of sequence identity ($\geq 65\%$) and structural homology, we find that both the structural and functional properties of the proteins vary widely. The observed thermal stabilities of the colicin apo-proteins vary in a manner consistent with their conformational state as observed by fluorescence quenching and electrospray mass spectrometry. These differences were unexpected although differences have also been seen previously for mammalian apo-myoglobins while the holo-variants are structurally and functionally similar (41).

Some members of the E colicin nuclease group have been quite well characterized by X-ray crystallography with crystal structures of E7 and E9 available (17, 18). These structures are highly similar and show no striking differences. Therefore, the observed differences in structural and functional behavior described in the present work cannot be explained on the basis of these X-ray structures. We believe this is caused by the fact that in solution there is a dynamic conformational equilibrium, whereas in X-ray crystallography primarily only a static lowest energy structure is probed.

Given the fact that the other parts of the sequences are highly similar, the differences in behavior are most likely a result of the sequence variation within the exosite (residues 72-98) that is required for specific high affinity binding of the cognate immunity protein. The greater sequence variation in this area is a consequence of the evolution of highly specific binding of the cognate immunity protein over other, structurally similar, non-cognate immunity proteins. The hypothesis that this part of the sequence may be important in explaining the observed variation is supported by findings in the co-crystal structure of the E9 DNase with single-stranded DNA, which shows that residue Tyr83, which is non-conserved and a putative specificity determining residue for binding immunity proteins (42), intercalates with the DNA (43). The precise molecular origins of how the catalytic activities and thermal stabilities/conformational states are produced, is beyond the scope of the present study, but are the focus of ongoing investigations.

A remaining question is whether the observed differences in conformational stability and activity of the apo-DNase domains of the four wild-type colicins are correlated and whether they have biological implications. It has been shown that the ability to insert and pass through the inner membrane (as judged by an *in vitro* lipid bilayer experiment) are similar for all colicins, both in the apo- and holo-form (44) and thus likely independent of thermal and structural stability. This argues against the proposal by Pommer *et al.* (10) that a structurally destabilized DNase domain might be important for colicin DNase uptake into the target cell. Additionally, all colicin DNases have temperature optima at or above 40 °C (Figure 5), which fits with the expected temperature of their natural *in vivo* environment (37-40 °C). The conformationally most stable colicin DNase E8 shows by far the highest *in vitro* activity in the present Kunitz assay (Figure 5). However, the impact of this on the *in vivo* cytotoxicity is unknown and is subject for further analysis.

In summary, we have demonstrated that there are marked differences in the conformational properties and activities of the four apo-colicin DNases. These differences were *a priori* unexpected given the 1) high sequence identity of the colicin DNases in the active site region (Figure 1A) whereby all the residues identified as being essential for activity (3) are absolutely conserved and 2) the high similarities between the known X-ray crystal structures of the DNase domains. Therefore, an important observation of this study is that the correlation between (highly similar) sequence information on the one hand and dynamic structural features and activity on the other hand is not self-evident.

Acknowledgments

We acknowledge the European Molecular Biology Organization for their support. (EMBO ASTF No. 45.00-03 to ETJvdB). We thank Christine Moore, Ann Reilly and Nick Cull (UEA), and Nadine Kirkpatrick (York) for technical assistance. We also thank Rien de Ruiter at Organon for technical assistance and the use of the DSC equipment.

References

1. James, R., Penfold, C. N., Moore, G. R., and Kleanthous, C. (2002) Killing of *E. coli* cells by E group nuclease colicins *Biochimie* 84, 381-389.
2. Pommer, A. J., Cal, S., Keeble, A. H., Walker, D., Evens, S. J., Kuhlman, U. C., Cooper, A., Connolly, B. A., Hemmings, A. M., Moore, G. R., James, R., and Kleanthous, C. (2001) Mechanisms and cleavage specificity of the H-N-H endonuclease colicin E9 *J.Mol.Biol.* 314, 735-749.
3. Walker, D. C., Georgiou, T., Pommer, A. J., Walker, D., Moore, G. R., Kleanthous, C., and James, R. (2002) Mutagenic scan of the H-N-H motif of colicin E9: implications for the mechanistic enzymology of colicins, homing enzymes and apoptotic endonucleases *Nucleic Acids Res.* 30, 3225-3234.

4. Bowman, C. M., Sidikaro, J., and Nomura, M. (1971) Specific inactivation of ribosomes by colicin E3 in vitro and mechanism of immunity in colicinogenic cells *Nat. New Biol.* 234, 133-137.
5. Ogawa, T., Tomita, K., Ueda, T., Watanabe, K., Uozumi, T., and Masaki, H. (1999) A cytotoxic ribonuclease targeting specific transfer RNA anticodons *Science* 283, 2097-2100.
6. Kuhlmann, U. C., Moore, G. R., James, R., Kleanthous, C., and Hemmings, A. M. (1999) Structural parsimony in endonuclease active sites: should the number of homing endonuclease families be redefined? *FEBS Lett.* 463, 1-2.
7. Galburt, E. A., and Stoddard, B. L. (2002) Catalytic mechanisms of restriction and homing endonucleases *Biochemistry* 41, 13851-13860.
8. Scholz, S. R., Korn, C., Bujnicki, J. M., Gimadutdinow, O., Pingoud, A., and Meiss, G. (2003) Experimental Evidence for a betabetaalpha-Me-Finger Nuclease Motif To Represent the Active Site of the Caspase-Activated DNase *Biochemistry* 42, 9288-9294.
9. Pommer, A. J., Wallis, R., Moore, G. R., James, R., and Kleanthous, C. (1998) Enzymological characterization of the nuclease domain from the bacterial toxin colicin E9 from *Escherichia coli* *Biochem. J.* 334, 387-392.
10. Pommer, A. J., Kuhlmann, U. C., Cooper, A., Hemmings, A. M., Moore, G. R., James, R., and Kleanthous, C. (1999) Homing in on the role of transition metals in the HNH motif of colicin endonucleases *J. Biol. Chem.* 274, 27153-27160.
11. Cheng, Y. S., Hsia, K. C., Doudeva, L. G., Chak, K. F., and Yuan, H. S. (2002) The crystal structure of the nuclease domain of colicin E7 suggests a mechanism for binding to double-stranded DNA by the H-N-H endonucleases *J. Mol. Biol.* 324, 227-236.
12. Kuhlmann, U. C., Pommer, A. J., Moore, G. R., James, R., and Kleanthous, C. (2000) Specificity in protein-protein interactions: the structural basis for dual recognition in endonuclease colicin-immunity protein complexes *J. Mol. Biol.* 301, 1163-1178.
13. James, R., Kleanthous, C., and Moore, G. R. (1996) The biology of E colicins: paradigms and paradoxes *Microbiology* 142, 1569-1580.
14. Walker, D., Moore, G. R., James, R., and Kleanthous, C. (2003) Thermodynamic consequences of bipartite immunity protein binding to the ribosomal ribonuclease colicin E3 *Biochemistry* 42, 4161-4171.
15. Wallis, R., Moore, G. R., James, R., and Kleanthous, C. (1995a) Protein-protein interactions in colicin E9 DNase-immunity protein complexes. 1. Diffusion-controlled association and femtomolar binding for the cognate complex *Biochemistry* 34, 13743-13750.
16. Wallis, R., Leung, K. Y., Pommer, A. J., Videler, H., Moore, G. R., James, R., and Kleanthous, C. (1995b) Protein-protein interactions in colicin E9 DNase-immunity protein complexes. 2. Cognate and noncognate interactions that span the millimolar to femtomolar affinity range *Biochemistry* 34, 13751-13759.
17. Ko, T. P., Liao, C. C., Ku, W. Y., Chak, K. F., and Yuan, H. S. (1999) The crystal structure of the DNase domain of colicin E7 in complex with its inhibitor Im7 protein *Structure Fold. Des.* 7, 91-102.
18. Kleanthous, C., Kuhlmann, U. C., Pommer, A. J., Ferguson, N., Radford, S. E., Moore, G. R., James, R., and Hemmings, A. M. (1999) Structural and mechanistic basis of immunity toward endonuclease colicins *Nat. Struct. Biol.* 6, 243-252.
19. Van den Bremer, E. T. J., Jiskoot, W., James, R., Moore, G. R., Kleanthous, C., Heck, A. J. R., and Maier, C. S. (2002) Probing metal ion binding and conformational properties of the colicin E9 endonuclease by electrospray ionization time-of-flight mass spectrometry *Protein Sci.* 11, 1738-1752.
20. Lakowicz, J. R. (1999) *Principles of Fluorescence Spectroscopy*, Second ed., Kluwer Academic / Plenum Publishers, New York, Dordrecht, London, Moscow.

21. Visser, A. J. W. G., Vanengelen, J., Visser, N. V., Vanhoek, A., Hilhorst, R., and Freedman, R. B. (1994) Fluorescence Dynamics of Staphylococcal Nuclease in Aqueous- Solution and Reversed Micelles *Biochim. Biophys. Acta* 1204, 225-234.
22. Digris, A. V., Skakun, V. V., Novikov, E. G., Van Hoek, A., Claiborne, A., and Visser, A. J. W. G. (1999) Thermal stability of a flavoprotein assessed from associative analysis of polarized time-resolved fluorescence spectroscopy. *Eur. Biophys. J* 28., 526-531.
23. Novikov, E. G., Van Hoek, A., Visser, A. J. W. G., and Hofstraat, J. W. (1999) Linear algorithms for stretched exponential decay analysis. *Opt. Commun.* 166, 189-198.
24. Kaltashov, I. A., and Eyles, S. J. (2002) Studies of biomolecular conformations and conformational dynamics by mass spectrometry *Mass Spectrom. Rev.* 21, 37-71.
25. Konermann, L., and Simmons, D. A. (2003) Protein-folding kinetics and mechanisms studied by pulse-labeling and mass spectrometry *Mass Spectrom. Rev.* 22, 1-26.
26. Veenstra, T. D. (1999) Electrospray ionization mass spectrometry in the study of biomolecular non-covalent interactions *Biophys. Chem.* 79, 63-79.
27. Loo, J. A. (1997) Studying noncovalent protein complexes by electrospray ionization mass spectrometry *Mass Spectrom. Rev.* 16, 1-23.
28. Loo, J. A. (2001) Probing protein-metal ion interactions by electrospray ionization mass spectrometry: enolase and nucleocapsid protein *Int. J. Mass Spectrometry* 204, 113-123.
29. Hernandez, H., and Robinson, C. V. (2001) Dynamic protein complexes: insights from mass spectrometry *J. Biol. Chem.* 276, 46685-46688.
30. Fenn, J. B., Mann, M., Meng, C. K., Wong, S. F., and Whitehouse, C. M. (1989) Electrospray ionization for mass spectrometry of large biomolecules *Science* 246, 64-71.
31. Smith, R. D., Loo, J. A., Edmonds, C. G., Barinaga, C. J., Udseth, H. R. (1990) New developments in biochemical mass spectrometry: Electrospray ionization *Anal. Chem.* 62, 882-899.
32. Chowdhury, S. K., Katta, V., and Chait, B. T. (1990) Probing conformational changes in proteins by mass spectrometry *J. Am. Chem. Soc.* 112, 9012-9013.
33. Przybylski, M., Glocker, M. O. (1996) Electrospray mass spectroemtry of biomolecular complexes with noncovalent interactions - New analytical perspectives for supramolecular chemistry and molecular recognition processes *Angew. Chem. Int. Ed. Engl.* 35, 806-826.
34. Heck, A. J. R., and Van den Heuvel, R. H. H. Investigation of Intact Protein Complexes by Mass Spectrometry *Mass Spectrom. Rev.*, *in press*.
35. Mirza, U. A., Cohen, S. L., and Chait, B. T. (1993) Heat-induced conformational changes in proteins studied by electrospray ionization mass spectrometry *Anal. Chem.* 65, 1-6.
36. Cech, N. B., and Enke, C. G. (2000) Relating electrospray ionization response to nonpolar character of small peptides *Anal. Chem.* 72, 2717-2723.
37. Cech, N. B., and Enke, C. G. (2001) Effect of affinity for droplet surfaces on the fraction of analyte molecules charged during electrospray droplet fission *Anal. Chem.* 73, 4632-4639.
38. Dobo, A., and Kaltashov, I. A. (2001) Detection of multiple protein conformational ensembles in solution via deconvolution of charge-state distributions in ESI MS *Anal. Chem.* 73, 4763-4773.
39. Keeble, A. H., Hemmings, A. M., James, R., Moore, G. R., and Kleanthous, C. (2002) Multistep Binding of Transition Metals to the H-N-H Endonuclease Toxin Colicin E9 *Biochemistry* 41, 10234-10244.
40. Hannan, J. P., Whittaker, S. B., Hemmings, A. M., James, R., Kleanthous, C., and Moore, G. R. (2000) NMR studies of metal ion binding to the Zn-finger-like HNH motif of colicin E9 *J. Inorg. Biochem.* 79, 365-370.

41. Scott, E. E., Paster, E. V., and Olson, J. S. (2000) The stabilities of mammalian apomyoglobins vary over a 600-fold range and can be enhanced by comparative mutagenesis *J. Biol. Chem.* 275, 27129-27136.
42. Curtis, M. D., and James, R. (1991) Investigation of the specificity of the interaction between colicin E9 and its immunity protein by site-directed mutagenesis *Mol. Microbiol.* 5, 2727-33.
43. Kolade, O. O., Carr, S. B., Kuhlmann, U. C., Pommer, A., Kleanthous, C., Bouchcinsky, C. A., and Hemmings, A. M. (2002) Structural aspects of the inhibition of DNase and rRNase colicins by their immunity proteins *Biochimie* 84, 439-446.
44. Mosbahi, K., Lemaitre, C., Keeble, A. H., Mobasheri, H., Morel, B., James, R., Moore, G. R., Lea, E. J., and Kleanthous, C. (2002) The cytotoxic domain of colicin E9 is a channel-forming endonuclease *Nat. Struct. Biol.* 9, 476-484.

Chapter 5

Ligand induced changes in the conformational dynamics of a bacterial cytotoxic endonuclease

Ewald T.J. van den Bremer, Albert J. R. Heck¹

Wim Jiskoot²

Anthony H. Keeble, Colin Kleanthous³

Arie van Hoek, Antonie J.W.G. Visser⁴

Biochemistry 2004; in press

¹Dept. of Biomolecular mass spectrometry, Utrecht University, Utrecht

²Dept. of Pharmaceutics, Utrecht University, Utrecht

³Dept. of Biology, University of York, York

⁴MicroSpectroscopy Centre, Wageningen University, Wageningen

Abstract

Knowledge about the conformational dynamics of a protein is key to understanding its biochemical and biophysical properties. In the present work we investigated the dynamic properties of the enzymatic domain of DNase colicins, via time-resolved fluorescence and anisotropy decay analysis in combination with steady state acrylamide quenching experiments. The dynamic properties of the apo-enzyme were compared to those of the E9 DNase ligated to the transition metal ion Zn^{2+} and the natural inhibitor Im9. We further investigated the contributions of each of the two tryptophans within the E9 DNase (Trp22 and Trp58), using two single-tryptophan mutants (E9 W22F and E9 W58F). Wild-type E9 DNase, E9 W22F and E9 W58F, as well as Im9 showed multiple lifetime decays. The time-resolved and steady-state fluorescence results indicated that complexation of E9 DNase with Zn^{2+} induces compaction of the E9 DNase structure, accompanied by immobilization of Trp22 along with a reduced solvent accessibility for both tryptophans. Im9 binding resulted in immobilization of Trp22 along with a decrease in the longest lifetime component. In contrast, Trp58 experienced less restriction on complexation of E9 DNase with Im9 and showed an increase in the longest lifetime component. Furthermore, the results point out that the Im9 induced changes in the conformational dynamics of E9 DNase are predominant and occur independently of the Zn^{2+} induced conformational effects.

Introduction

Colicins are a group of plasmid-encoded toxins produced by *Escherichia coli* under times of nutrient stress and are used to kill related bacterial cells (1). Cell death is generally mediated by one of two types of cytotoxic activity – proton-motive force depolarization by formation of a pore within the inner-membrane or a nuclease activity acting within the cytoplasm (1). Members of the E-colicin DNase sub-group (E2, E7, E8, and E9) kill the target cell by degrading the chromosomal DNA using a Mg^{2+} -dependent and essentially non-specific DNase activity (2, 3). The cytotoxic activity is housed within a 134 residue C-terminal domain, with a central domain responsible for binding to the extracellular receptor for vitamin B12, BtuB, and an N-terminal domain required for translocation across the outer membrane of a sensitive bacterial cell (4, 5). An antidote protein, called an immunity protein, is co-expressed to protect the producing cell from the cytotoxic effect of the colicin. These 9-10 kDa proteins bind the DNase domain at an exosite adjacent to the active site (Figure 1).

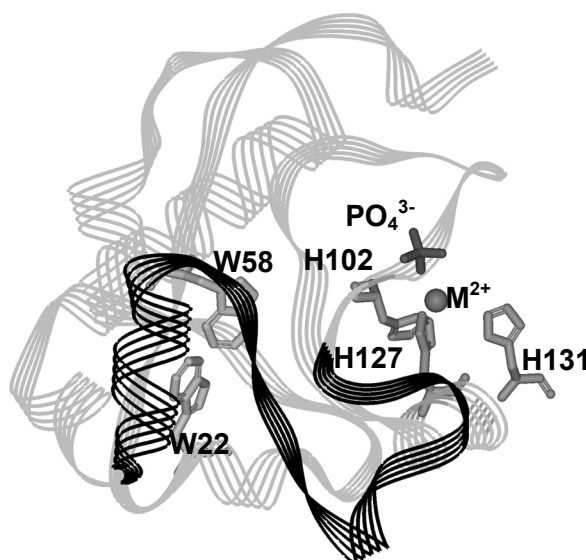


Figure 1. Ribbon diagram of the E9 DNase domain showing the Im9 binding site (labeled black), and the positions of the two tryptophans (W22 and W58) relative to the transition metal and the three coordinating histidine residues plus the ligating phosphate ion.

Modeling studies indicated that inhibition relies on the polymeric nature of the DNA and occurs through steric and electronic blocking of binding away from the cleavable bond (6). This mode of inhibition is distinctly different from the conventional mode of nuclease inhibitor binding e.g., barnase-barstar where the inhibitor directly ligates the active site residues (7). Exosite binding by immunity proteins is instead a reflection of the requirement for the DNase to be able to evolve novel immunity protein binding specificities to gain a competitive advantage, with the exosite being the most sequence divergent region amongst the four colicin DNase domains (8). The active site comprises the C-terminal ~30 residues and contains the consensus

sequence for the H-N-H group of homing endonucleases and has a fold conserved with the $\beta\beta\alpha$ -Me family of nucleases (9, 10) including the eukaryotic apoptotic DNase CAD (3, 11). The structure of the active site resembles that of a zinc finger. Indeed transition metals, including zinc, have previously been shown to bind to all colicin DNases (12). Ligation of the tetrahedrally coordinated metal ion (Figure 1) involves three histidine residues (His102, His127 and His131) and a non-covalently bound phosphate ion (6, 13).

The immunity protein and metal ions, such as Zn^{2+} , bind with high affinity (fM and nM, respectively) to the colicin DNases, particularly E9, and the binding properties have been extensively studied using a range of biochemical and biophysical techniques (12, 14-16). Moreover, ligand binding involves mechanisms that include conformational changes. Ligand-induced conformational changes may be reported by the two tryptophans (W22 and W58; Figure 1), although they are distant from either ligand binding site (12, 15). Furthermore, high-field NMR (17, 18), and (nano) ESI-MS (19) have shown that the native state of the E9 DNase is a dynamic population of open and closed conformations. We recently showed this to be true for E2, E7, and E8 colicin DNases as well (20). It has been suggested that many conformational changes may be occurring independently of one another (12, 19, 21). For example, although binding of the Zn^{2+} ion and immunity protein both affect the fluorescence of E9 DNase, the kinetics of immunity protein association (as well the observed fluorescence changes coupled to binding) and dissociation are unaltered by the presence of transition metals in the active site (12). This observation overturned a previous hypothesis by Pommer *et al.* (16) that loss of the transition metal is important for cellular uptake of E9 colicin. Specifically, the acceleration of immunity protein dissociation by loss of the bound transition metal was proposed to explain the large difference between the kinetics of immunity protein dissociation ($\sim 10^{-6} s^{-1}$) and colicin-mediated cell killing ($\sim 10^{-3} s^{-1}$) (16). These observations are congruent with the transition metal induced conformational changes being localized to the active site (21, 22). Nevertheless, it remained unclear how the tryptophan fluorescence was being affected, since both tryptophans are located at a distance from the ligand binding sites (for example, in the X-ray structure the tryptophans are 15 (W22) and 13 Å (W58) from the transition metal binding site), without involving long range, allosteric, conformational changes.

In order to gain a better understanding of the molecular origins and the complexity of the conformational changes that occur within colicin DNases, we investigated the interaction of the DNase protein with Zn^{2+} , and its cognate immunity protein, using time-resolved fluorescence spectroscopy and steady-state fluorescence quenching studies. The advantage over other techniques is that processes taking place on the fluorescence time scale (i.e. nanoseconds) can be probed, for example rotation of the entire protein or segments thereof, and interactions with other molecules. We have previously determined the lifetimes and anisotropies of wild-type DNases E2, E7, E8 and E9 without Zn^{2+} and immunity protein (20) (and E.T.J.v.d.B and

A.J.R.H, unpublished observations). In order to probe the effects of Zn^{2+} and immunity protein binding to colicin DNases, we concentrated on the E9 DNase since it is the best characterized colicin DNase. A complicating factor in the analysis of time-resolved fluorescence data of colicin DNases is that the two tryptophans (W22 and W58) are located at a distance $<5\text{\AA}$ from each other (in the E9 DNase X-ray structure), which is close enough for energy transfer to occur (12). Therefore, single tryptophan mutants were constructed for E9 DNase, i.e., W58F (W22+) and W22F (W58+), enabling us to study the local environment of the individual tryptophans in the absence of any complicating energy transfer processes.

Experimental procedures

Protein samples - Tryptophan-to-alanine mutants were generated as previously described by Keeble *et al.* (12). Wild-type and single-tryptophan mutants of the E9-DNases, W22+ (which contains the W58F mutation) and W58+ (which contains the W22F mutation) were purified as described previously (23). Im9 was purified as described by Wallis *et al.* (15). Protein concentrations were determined by measuring the UV absorption at 280 nm. Molar absorption coefficients of the E9 wild-type, E9 mutants and Im9 are $17,550\text{ M}^{-1}\text{cm}^{-1}$, $10,700\text{ M}^{-1}\text{cm}^{-1}$ (for both mutants) and $11,400\text{ M}^{-1}\text{cm}^{-1}$, respectively. For the metal loaded proteins, zinc acetate (Merck, Darmstadt, Germany) was used without further purification. Samples contained $10\text{ }\mu\text{M}$ E9 DNase in 50 mM ammonium acetate (pH 7.4) with and without equimolar concentrations of zinc acetate and/or Im9. For measurements of the E9- Zn^{2+} -Im9 complex, Zn^{2+} and Im9 were successively added. For studying the effect of phosphate on the fluorescence characteristics of E9 DNase, 50 mM sodium phosphate buffer pH 7.4 was used. The samples were prepared at least 24 h prior to analysis.

Picosecond polarized time-resolved fluorescence and anisotropy - Time-resolved fluorescence and anisotropy decay times were measured in a home-built setup with mode-locked continuous wave laser excitation and time-correlated photon counting detection. The pump laser was a CW diode-pumped, frequency-doubled Nd:YVO₄. The mode-locked laser was a titanium:sapphire laser coupled with a pulse picker, which decreased the repetition rate of the excitation pulses to 3.8×10^6 pulses per second. The maximum pulse energy was a few pJ, the wavelength 295 nm and the pulse duration 3 ps. The temperature was controlled and set at 20°C . Fused silica cuvettes of 10 mm light path were used. The fluorescence emission was collected at 348.8 nm at an angle of 90° with respect to the direction of the excitation light beam. Care was taken to avoid artefacts from depolarization effects. At the front of the sample housing a Glan-laser polarizer was mounted, optimizing the already vertical polarization of the input light beam. Between sample and photomultiplier a single fast lens, an interference filter, a computer controlled rotatable sheet type polarizer and a second single fast lens were placed focusing the

fluorescence on the photomultiplier cathode. All polarizers were carefully aligned and the setup was finally checked by measuring reference samples. Detection electronics were standard time-correlated single photon counting modules. With a small portion of the mode-locked light a fast PIN-photodiode was excited. The output pulses were fed to one channel of a quad constant fraction discriminator and then used as a stop signal for a time-to-amplitude converter. Subsequently, the output pulses were analyzed by an analogue-to-digital converter and were collected in 4096 channels of a multichannel analyzer. The channel time spacing was 11.1 ps. A microchannel plate photomultiplier was used for detection of the fluorescence photons. By reducing the energy of the excitation pulses with neutral density filters, the rate of fluorescence photons was decreased to 30,000 per second to prevent pile-up distortion (24). Other instrumental sources of data distortion were minimized to below the noise level of normal photon statistics (25).

Experimental data consisted of repeating sequences of measurements of the polarized emission (parallel and perpendicular component) fluorescence decays of the reference compound (three cycles of 20 s), the protein sample (10 cycles of 20 s), the background (two cycles of 20 s), and again the reference compound. In that way an eventual temporal shift can be traced and corrected. All cuvettes were carefully cleaned and checked for background luminescence prior to the measurements. For obtaining a dynamic instrumental response of the setup, the single exponential fluorescence decay was measured of paraterphenyl in a mixture of cyclohexane and CCl_4 in a 50/50 % volume ratio.

Time-resolved fluorescence data analysis - The time-resolved fluorescence emission $I(t)$ and anisotropy $r(t)$ decays were globally analyzed using a home-built computer program, which employs a reweighed iterative reconvolution method (26, 27). The parameters of the fluorescence decay were obtained from iterative convolution of the measured decay of the reference compound using a modified model function. The experimental data for the fluorescence decay were analysed assuming that it is multiexponential and, thus, can be described by,

$$I(t) = \sum_{i=1}^M \alpha_i \cdot e^{-t/\tau_i} \quad (1)$$

where the relative amplitudes, α_i , and the decay fluorescence lifetimes, τ_i , are the numerical parameters of the i^{th} component to be determined, and M is the number of fluorescent components. The weighted average fluorescence lifetime $\langle \tau \rangle$ was calculated according to the equation:

$$\langle \tau \rangle = \frac{\sum_{i=1}^M \alpha_i \tau_i}{\sum_{i=1}^M \alpha_i} \quad (2)$$

The anisotropy decay can also be described by a sum of M discrete exponential terms:

$$r(t) = \sum_{i=1}^M \beta_i \cdot e^{-t/\varphi_i} \quad (3)$$

where φ_i is the rotational correlation time of rotational component i and the pre-exponential terms β_i is the contribution of the correlation time of the i^{th} component to the total anisotropy decay.

Fitting sessions were performed by generated starting values of the parameters. The goodness-of-fit was judged by the value of parameter reduced χ^2 and inspection of the residual function graphs for each data set fitted. For all our tabulated data (Tables 1-5), reduced χ^2 values were close to unity, and the weighted residuals and autocorrelation function of the residuals were uniformly distributed around zero, indicating an optimal fit. In all cases the simplest model was chosen. Attempted fits of the experimental data to a model with less independent components showed a substantial increase in χ^2 value. On the other hand, an exponential fit using more components did not lead to a significant improvement in χ^2 value.

The angular displacement ψ (degrees) of the fluorophore was calculated from:

$$\frac{\beta_2}{\beta_1 + \beta_2} = \frac{1}{2} \cos \psi \cdot (\cos \psi + 1) \quad (4)$$

where β_1 and β_2 are the contributions of the correlation times (φ_1 and φ_2) to the total anisotropy decay (28).

Steady-State Fluorescence - Steady state fluorescence experiments were performed on a Fluorolog-3 spectrofluorometer (Jobin Yvon/Horiba, Longjumeau, France) using 1-cm quartz cuvettes. The temperature was controlled and set at 20°C. Excitation and emission bandwidths were set at 5 nm. For acrylamide quenching experiments, aliquots of acrylamide (1.4 M in ammonium acetate) were added to the protein solution in a range from 0 to 0.33 M. To avoid interference by acrylamide absorption, the excitation wavelength was set to 300 nm. The fluorescence intensity was monitored at 345 nm and corrected for dilution and buffer background.

Stern-Volmer quenching constants (K_{SV}) were obtained from the relationship (29):

$$F_0/F = 1 + K_{SV}[Q] = 1 + k_q \langle \tau \rangle [Q] \quad (5)$$

where F_0 and F are the fluorescence intensities in the absence and presence of quencher, respectively, Q is the acrylamide concentration, and K_{SV} is the Stern-Volmer quenching constant. In addition, K_{SV} is equal to $k_q \langle \tau \rangle$, where k_q is the apparent bimolecular rate constant for

collisional encounters and $\langle\tau\rangle$ is the average excited-state lifetime in the absence of quencher, as determined by time-resolved fluorescence measurements (see above, equation (2)).

Results

Fluorescence decays of colicin E9 DNase wild-type and Im9 - Typical fluorescence decay curves, with associated fits, are shown in Figure 2 for Im9 and apo-E9 DNase with further results summarized in Table 1. These results illustrate how different the environments of the tryptophans are within these two proteins. The decay for the free E9 DNase could be described as a sum of three single-exponential decays with an average lifetime of 4.2 ns. The addition of Zn^{2+} resulted in a decrease of the average lifetime to 3.7 ns. This indicates that at least one of the two tryptophans was quenched. X-ray structures have revealed that the Zn^{2+} ion is tetrahedrally coordinated (6). The fourth ligand (in addition to the three histidines) is a single phosphate ion. The phosphate ion binds specifically in the presence of Zn^{2+} with a K_d in the μM range (See chapter 6) but is not essential to stabilize the Zn^{2+} ion. Therefore, we were interested to measure the E9 DNase lifetimes with and without Zn^{2+} in the presence of phosphate ions. Table 1 shows that in both cases the lifetimes in phosphate buffer (50 mM sodium phosphate, pH 7.4) are identical to those measured in 50 mM ammonium acetate solutions at identical pH. This demonstrates that the presence phosphate ions and, most probably, phosphate ion ligation did not change the local environment of both tryptophans.

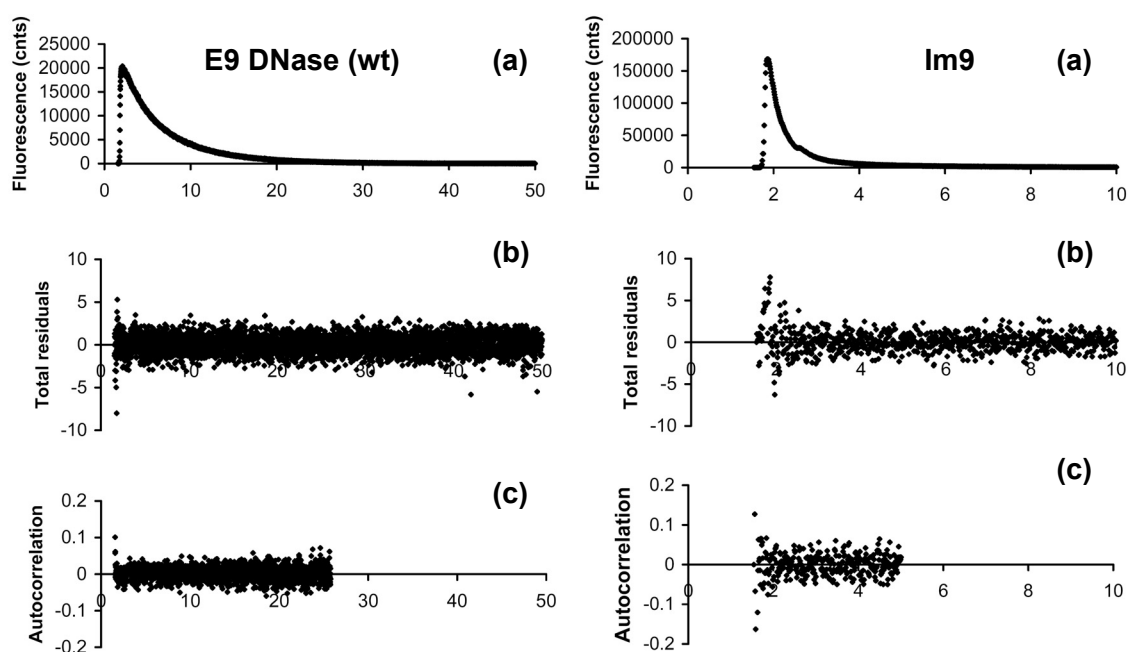


Figure 2. Experimental and fitted fluorescence decay of apo-E9 DNase wild-type and immunity protein Im9: (a) fluorescence decay, (b) residuals between measured and fitted data, and (c) autocorrelation of the residuals. Fitting parameters are shown in Table 1.

Table 1. Fluorescence decay parameters for the E9 DNase wild-type

Protein ^a	α_1^b	α_2	α_3	α_4	τ_1 (ns)	τ_2 (ns)	τ_3 (ns)	τ_4 (ns)	$\langle\tau\rangle$ (ns)	χ^2^c
E9		0.135	0.403	0.463		0.45±0.02	2.75±0.04	6.50±0.02	4.17	1.14
E9-Zn²⁺		0.134	0.438	0.428		0.40±0.02	2.59±0.03	5.89±0.01	3.71	1.16
E9-Im9	0.074	0.375	0.165	0.385	0.03±0.01	0.27±0.01	2.82±0.05	6.71±0.01	3.15	1.08
E9-Zn²⁺-Im9	0.414	0.057	0.224	0.305	0.28±0.01	1.52±0.46	3.90±0.40	6.78±0.09	3.13	1.39
E9-PO₄³⁻		0.134	0.394	0.473		0.43±0.02	2.75±0.03	6.35±0.01	4.14	1.09
E9-Zn²⁺-PO₄³⁻		0.122	0.441	0.436		0.48±0.03	2.61±0.03	5.88±0.01	3.78	1.18
Im9	0.604	0.355	0.033	0.086	0.11±0.01	0.39±0.01	2.33±0.03	6.53±0.05	0.34	1.77

^a E9 and Im9 represent the wild-type E9 DNase and immunity protein Im9, respectively, in the absence and presence of zinc (Zn²⁺) or phosphate (PO₄³⁻)

^b α_1 , α_2 , α_3 , and α_4 are the fractional preexponential factors corresponding to lifetimes τ_1 , τ_2 , τ_3 and τ_4 , respectively.

^c Reduced χ^2 values indicate goodness of fit.

Prior to lifetime analysis of the E9-Im9 binary complex, lifetimes of the free Im9 protein were determined, showing an ultra-short average lifetime of 0.34 ns. Im9 contains one tryptophan (Trp74), which showed a lifetime decay with four components (see Table 1). The lifetime analysis of the E9-Im9 complex resulted in the appearance of a fourth, ultra-short lifetime component and a reduction of the average lifetime, as compared to the free E9 DNase. Since the observed decay results are from contributions of three tryptophans, it seems impossible to correlate these findings with conformational changes in E9 resulting from interactions with Im9. However, by comparing the lifetime decays of E9-Im9 ($\langle\tau\rangle = 3.15$ ns) and in E9-Zn²⁺-Im9 ($\langle\tau\rangle = 3.13$ ns), we conclude that Zn²⁺ binding to the binary complex did not alter the average lifetime.

Table 2. Anisotropy decay parameters for the E9 DNase wild-type

Protein ^a	β_1^b	β_2	ϕ_1 (ns)	ϕ_2 (ns)	χ^2^c
E9	0.071	0.102	0.27±0.02	8.6±0.2	1.14
E9-Zn²⁺	0.058	0.106	0.26±0.02	8.1±0.1	1.09
E9-Im9	0.088	0.092	0.42±0.02	14.0±0.3	1.12
E9-Zn²⁺-Im9	0.111	0.102	0.28±0.01	13.4±0.3	1.34
E9-PO₄³⁻	0.073	0.101	0.24±0.02	9.10±0.20	1.04
E9-Zn²⁺-PO₄³⁻	0.066	0.107	0.25±0.16	9.06±0.02	1.09
Im9		0.219		2.69±0.03	3.51

^a E9 and Im9 represent the wild-type E9 DNase and immunity protein Im9, respectively, in the absence and presence of zinc (Zn²⁺) or phosphate (PO₄³⁻)

^b β_1 and β_2 are the amplitudes corresponding to the rotational correlation times ϕ_1 and ϕ_2 , respectively.

^c Reduced χ^2 values indicate goodness of fit.

Time-resolved fluorescence anisotropy of colicin E9 DNase wild-type - Time-resolved fluorescence anisotropy measurements were done to gain insight into the conformational dynamics of E9 DNase. Rotational correlation times were recovered from the obtained polarized decays (Table 2). The anisotropy decay curve for free E9 DNase revealed two rotational correlation times (ϕ). The slow motion ($\phi = 8.6$ ns) reflects the tumbling of the entire protein while the fast motion ($\phi = 0.27$ ns) reflects local mobility of the tryptophans and possibly contributions from energy transfer. Upon Zn^{2+} binding both motions were mostly unaffected. The presence of phosphate ions had no significant influence on the correlation times (Table 2) and was therefore not further investigated. Ligation of Im9 resulted in a significant increase of the long rotational correlation time from ~ 8 ns to ~ 14 ns. Since the mass of the E9-Im9 complex is significantly larger than that of E9 by its self (24.6 kDa vs 15 kDa) this was expected. The individual Im9 protein showed one rotational correlation time (2.7 ns), reflecting the global motion of the Im9 molecule and indicating that the sole Trp74 is immobile.

Fluorescence decays of colicin E9 DNase mutants W22+ and W58+ - The above experiments on the E9-Im9 and E9- Zn^{2+} -Im9 complexes are complicated by the presence of three tryptophans with two less than 5 Å apart. The use of mutant proteins containing less tryptophans than wild-type (by mutation to phenylalanine) has previously been shown to be a useful tool to perform fluorescence based conformational analysis of proteins (30-32). Two single-tryptophan mutants (W22+ and W58+) were produced (12) to probe the effects of ligand binding on the individual tryptophans of the E9 DNase. We have previously demonstrated that electrospray ionization mass spectrometry (ESI-MS) is a sensitive method to measure the conformational state of E9 DNase (19, 20). When such experiments were repeated on the two single-tryptophan mutants, W22+ and W58+, they yielded results similar to that of the wild-type E9 DNase, indicating that the mutations had a negligible effect on the structure and stability of the proteins (data not shown).

The results of the fluorescence lifetime analysis of these mutants are summarized in Table 3. The fluorescence decay of the W22+ mutant was adequately described by a sum of three exponential terms (Table 3). The average lifetime of the E9 DNase W22+ mutant decreased after addition of Zn^{2+} (from 3.8 to 2.9 ns). This indicates an increase in collisional quenching of Trp22 by neighboring amino acid residues upon Zn^{2+} binding. Ligating Im9 to the W22+ mutant also resulted in a decrease in the average lifetime, as seen for the E9 DNase wild type. A slight further quench was achieved for the E9- Zn^{2+} -Im9 ternary complex. The free W58+ mutant showed a multi-exponential fluorescence decay that could be best described as a sum of four individual components (Table 3). In the absence of Zn^{2+} an ultra-short lifetime of 23 ps with a significant fractional contribution was observed. Upon Zn^{2+} binding the ultra-short component disappeared. Consequently, and also because of an increased contribution (α_4) of the

longest individual lifetime (τ_4), the average lifetime was substantially prolonged from 3.6 to 6.5 ns. Remarkably, binding Im9 to apo-W58+ mutant did not result in a significant change in the average lifetime. This is most likely due to the occurrence of changes that largely counteracted one another – the second lifetime (τ_2) *shortened* whilst the fourth lifetime (τ_4) *lengthened*; furthermore, the corresponding fractional contributions (α_2 and α_4) increased at the expense of α_3 .

Table 3. Fluorescence decay parameters for the E9 DNase mutants W22+ and W58+

Protein ^a	α_1^b	α_2	α_3	α_4	τ_1 (ns)	τ_2 (ns)	τ_3 (ns)	τ_4 (ns)	$\langle\tau\rangle$ (ns)	χ^2^c
W22+		0.156	0.493	0.351		0.96±0.05	3.43±0.12	5.49±0.08	3.77	1.10
W22+-Zn ²⁺		0.280	0.261	0.459		0.87±0.04	2.14±0.11	4.63±0.02	2.93	1.14
W22+-Im9	0.263	0.294	0.181	0.263	0.17±0.01	0.69±0.05	1.71±0.09	4.84±0.01	1.83	1.15
W22+-Zn ²⁺ -Im9	0.269	0.365	0.196	0.170	0.14±0.01	0.71±0.03	1.83±0.06	4.71±0.02	1.45	1.20
W58+	0.213	0.156	0.298	0.333	0.02±0.01	0.67±0.03	3.08±0.06	7.71±0.03	3.60	1.06
W58+-Zn ²⁺		0.063	0.161	0.776		0.53±0.08	3.19±0.18	7.67±0.03	6.50	1.01
W58+-Im9	0.234	0.287	0.050	0.429	0.05±0.01	0.33±0.01	2.56±0.20	8.20±0.02	3.75	1.03
W58+-Zn ²⁺ -Im9	0.245	0.286	0.052	0.418	0.03±0.01	0.31±0.01	2.31±0.16	8.30±0.01	3.69	1.00

^a W22+ and W58+ represent the protein E9 DNase containing solely Trp22 or Trp58, respectively, in the absence or presence of zinc (Zn²⁺). Im9 represent the immunity protein Im9.

^b α_1 , α_2 , α_3 , and α_4 are the fractional preexponential factors corresponding to lifetimes τ_1, τ_2, τ_3 and τ_4 , respectively.

^c Reduced χ^2 values indicate goodness of fit.

Comparison of the two binary complexes (DNase-Zn²⁺ and DNase-Im9) with the ternary complex, both for W22+ and the W58+ mutant, demonstrates that the effects induced by Im9 binding overwhelmed those caused by Zn²⁺ binding (Table 3). Nevertheless, the data shown in Table 3 suggest that the fluorescence decays of W22+-Im9 and W22+-Zn²⁺-Im9 are significantly different. This was confirmed by global analysis of both data sets: when the individual lifetimes of W22+-Im9 and W22+-Zn²⁺-Im9 were forced to be the same, the overall χ^2 increased to 10.5. When lifetimes were not linked, a χ^2 of 1.17 was observed. Hence, binding of Zn²⁺ to the E9 DNase-Im9 complex does affect the local environment of Trp22, whereas Trp58 is not measurably affected.

Anisotropy decay analysis of the W22+ and W58+ mutant E9 DNases - Both tryptophans have two distinct rotational correlation times (see Table 4). For both mutants, the long rotational correlation time (ϕ_2), which reflects the motion of the entire molecule, was predominant. Furthermore, the amplitude of the local motion of Trp58 was significantly larger than that of Trp22 ($\beta_1^{W58+} > \beta_1^{W22+}$), indicating that local motions of Trp22 are more restricted as compared to Trp58. This is reflected by differences in angular displacements (see eqn 4 in the Experimental

procedures) of the two tryptophans within the apo-proteins being 16 and 40 degrees for Trp22 and Trp58, respectively. The lower value for the short rotational time (ϕ_1) for W58+ indicates that, in addition to a larger angular freedom, Trp58 moves faster than Trp22.

Binding of Zn^{2+} to either W22+ or W58+ (Table 4) resulted in a reduction of the long rotational correlation time (ϕ_2) in both the Im9 free and bound forms, consistent with the effects on the wild-type protein (Table 2). Moreover, Zn^{2+} binding as well as Im9 binding had a marked effect on the local mobility (ϕ_1) of both Trp22 and Trp58. Binding of either Zn^{2+} or Im9 (or both) to W22+ eliminated (ϕ_1), indicating that Trp22 was immobilized within the protein. Whilst binding either ligand did not eliminate the shorter correlation time in W58+ (Table 4), it did reduce its contribution (β_1) substantially. Hence, whilst the rate of rotation had not decreased, the angular displacement of Trp58 was reduced from 40° to 16° and 22° upon Zn^{2+} and Im9 binding, respectively. As compared with the binary W58+-Im9 complex, the angular displacement of Trp58 was the same for W58+- Zn^{2+} -Im9. Moreover, the differences in the short correlation time (ϕ_1) are not significantly distinct (binary complex 0.8 ± 0.2 ns *vs* ternary complex 0.6 ± 0.1 ns). This was confirmed by global analysis of both data sets: when the individual anisotropy decays of W58+-Im9 and W58+- Zn^{2+} -Im9 were forced to be the same, the overall χ^2 remained small (1.13).

Table 4. Anisotropy decay parameters for the E9 DNase mutants W22+ and W58+

Protein ^a	β_1 ^b	β_2	ϕ_1 (ns)	ϕ_2 (ns)	χ^2 ^c	ψ ^d
W22+	0.011	0.183	1.39±0.72	11.6±0.3	1.11	16
W22+-Zn^{2+}		0.201		9.4±0.1	1.12	0
W22+-Im9		0.209		18.6±0.2	1.13	0
W22+-Zn^{2+}-Im9		0.203		18.3±0.3	1.22	0
W58+	0.061	0.132	0.68±0.05	11.5±0.2	1.05	40
W58+-Zn^{2+}	0.013	0.208	0.69±0.26	9.7±0.1	1.01	16
W58+-Im9	0.022	0.192	0.83±0.16	17.0±0.2	1.02	22
W58+-Zn^{2+}-Im9	0.024	0.192	0.64±0.12	16.6±0.2	1.03	22

^a W22+ and W58+ represent the protein E9 DNase containing solely Trp22 or Trp58, respectively, in the absence or presence of zinc (Zn^{2+}). Im9 represent the immunity protein Im9.

^b β_1 and β_2 are the amplitudes corresponding to the rotational correlation times ϕ_1 and ϕ_2 , respectively.

^c Reduced χ^2 values indicate goodness of fit.

^d ψ is the angular displacement in degrees ($^\circ$) of the fluorophore.

Steady-state fluorescence quenching studies of the E9 DNase mutants - The solvent accessibility of the tryptophans in the E9 DNase variants was probed by acrylamide quenching experiments. The resulting Stern-Volmer plots and constants are shown in Figure 3 and listed in

Table 5, respectively. Upon Zn^{2+} binding (Table 5), both the W22+ mutant and the W58+ mutant showed a clear decrease in collisional encounters between the fluorophore and acrylamide. This indicates that both tryptophans experience solvent protection. However, the protection provided by Zn^{2+} was more pronounced for Trp58 than for Trp22. In contrast, Im9 affected the two protein differently – Im9 binding to W22+ did not significantly affect the rate of collisional encounters, whereas it reduced it by ~ 7 -fold for W58+ (see Table 5 and Figure 3). This indicates that the solvent accessibility of Trp22 was largely unaffected by Im9 binding, whereas for Trp58 it decreased dramatically. The presence of Zn^{2+} in the ternary E9- Zn^{2+} -Im9 complexes had no substantial effect, in agreement with the dominant effect of Im9 binding described above.

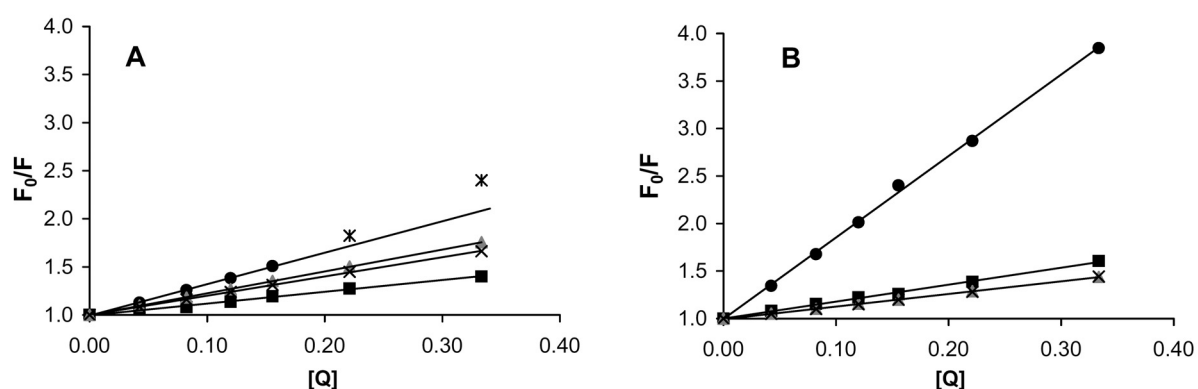


Figure 3. Acrylamide quenching of the fluorescence of single-Trp mutants. Stern-Volmer plots were obtained from the steady-state fluorescence quenching experiments of E9 DNase mutants W22+ and W58+ shown in panel A en B, respectively. Lines representing the free E9 DNase are shown by (●); in the presence of Zn^{2+} (■); in the presence of immunity protein Im9 (▲) and in the presence of Zn^{2+} and Im9 (x). Before fitting two final data points (✱) (indicative of a static component) were omitted.

Table 5. Summary of fluorescence quenching studies with acrylamide.

Protein ^a	K_{SV} (M^{-1}) ^b	k_q ($nsec^{-1} M^{-1}$)
W22+	3.28 ± 0.26 ^c	1.11
W22+- Zn^{2+}	1.22 ± 0.03	0.42
W22+-Im9	2.26 ± 0.03	1.23
W22+- Zn^{2+} -Im9	2.01 ± 0.02	1.38
W58+	8.63 ± 0.07	2.40
W58+- Zn^{2+}	1.80 ± 0.06	0.28
W58+-Im9	1.33 ± 0.02	0.35
W58+- Zn^{2+} -Im9	1.33 ± 0.02	0.36

^a W22+ and W58+ represent the protein E9 DNase containing Trp22 and Trp58, respectively, in the absence or presence of zinc (Zn^{2+}). Im9 represent the immunity protein Im9.

^b K_{SV} values were determined via Stern-Volmer analysis (See experimental procedures eq. (5)).

^c Before fitting, the two final data points (indicative of a static component) were omitted. (See also Figure 3A)

Discussion

In the present work we have used time-resolved fluorescence and anisotropy to analyze how binding of two inhibitors of DNase activity affected the conformational dynamics of colicin E9 DNase on the nanosecond timescale. We focused on the E9 DNase, as it is the best characterized of the four colicin DNases (E2, E7, E8 and E9). The two inhibitors were chosen because they bind at different sites on the protein (the active site and an exosite, respectively) and inhibit the enzyme by different mechanisms (chelation of catalytic residues, and steric electronic exclusion, respectively).

Ligand-induced conformational changes: Zinc - Whilst the average fluorescence lifetime for both W22+ and W58+ DNases is affected upon Zn^{2+} binding, the manner by which it occurs differs markedly. The decrease in average lifetime for W22+ implies that upon Zn^{2+} binding the indole side-chain of Trp22 (located in the short helix II, length $\sim 9\text{\AA}$) interacts to a greater extent with neighboring groups within E9 DNase. This effect is accompanied by a decrease in its solvent exposure (Figure 3A) and the disappearance of its rotational freedom (Table 4), all pointing to an increased compactness of the E9 DNase in the Zn^{2+} bound form, an effect that we have previously observed by ESI-MS (19). This increased compactness of the E9 DNase also affects Trp58 (located in helix IV, length $\sim 21\text{\AA}$), resulting in a decreased solvent accessibility (Figure 3B) and rotational freedom ψ drops (from 40° to 16° , Table 4). This increased compactness is likely to be the origin of the increased average lifetime for Trp58 that occurs due to the disappearance of the subnanosecond lifetime component τ_1 (0.21 ns) and a decrease in the contribution of τ_2 (~ 0.50 ns). Subnanosecond lifetimes are interpreted as the result of excited-state quenching of tryptophan emission by the protein backbone (33). Apparently, in the Zn^{2+} -ligated compact state the E9 DNase adopts a conformation that prohibits interaction between Trp58 and the protein backbone. The remaining lifetime components τ_3 (3.1 ns) and τ_4 (7.7 ns) are typical decay times for the tryptophan's indole moiety in environments of different polarity and these were unaffected upon Zn^{2+} binding.

Crystal structures of the E9 DNase in different metal ion occupancies demonstrate that, in the crystal state Zn^{2+} binding to E9 DNase induces conformational changes that involve rearrangements of hydrogen bonding patterns as well as movement of the C-terminal α -helix to produce a closure of the active site and a more compact structure (22, 34, 35). Recently, we showed by ESI-MS that compaction of colicin DNase on Zn^{2+} binding also occurs in the solution state (19, 20). The decrease in the long rotational correlation time (Table 4) confirms these observations.

Although the two tryptophans of the E9 DNase are 13-15 \AA from the position of the metal ion, Trp58 is at the base of the active site cleft and is significantly more solvent exposed, as

indicated by the fluorescence emission maximum of 338 nm for W58+ compared to 333 nm for W22+ (12). Accordingly, Zn^{2+} binding closes the active site protecting Trp58, sitting at its base, from acrylamide. Whereas both NMR and crystallography indicate that closure of the E9 DNase structure is structurally localized to the active site (21, 22), our ESI-MS experiments (19, 20) demonstrate that binding of Zn^{2+} does have a greater impact on the global structure of the protein in solution. These findings correlate with the present results where the environment of Trp22 is affected in addition to that of Trp58. To account for this ‘globally transmitted’ effect we suggest that closure of the active site upon Zn^{2+} binding occurs like a clasp closing with the pivot point located near to Trp22. This would explain why relatively small structural changes close to Trp22 have a disproportionately large effect on its mobility at the nanosecond timescale, which are not detected by NMR (21). Moreover, such a clasp closure mechanism is in good agreement with our ESI-MS experiments (19, 20).

Ligand induced conformational changes: Im9 - The ultra-short lifetime of Im9 alone is most likely due to hydrogen bonding between Trp74 and His46, which covers most of the indole side-chain. This interaction is likely the reason why Im9 is immobile on the (sub)nanosecond time scale. No additional rotational correlation times appear on Im9 binding to E9 DNase. These observations are consistent with previous structural data, which shows only very minor conformational changes for Im9 on complexation with E9 DNase (36). Since both the single tryptophan of Im9 and the tryptophans within E9 DNase have multiple lifetime components, caution must be taken when analyzing the effects of Im9 binding on the lifetimes of Trp22 and Trp58. Hence, based on fluorescence lifetime analysis firm conclusions are not easy to draw about the effect of Im9 binding on the conformational dynamics of E9. Efforts were made to construct a Trp-free Im9 protein, however, this resulted in a destabilization of the entire protein likely caused by removal of the hydrogen bond between Trp74 and His46 (A.H.K. and C.K. unpublished observations). Still, the amplitudes (α values) of the longer fluorescence lifetimes for Trp22 and Trp58 in the free E9 DNase are much greater than that of free Im9, they should dominate within the E9-Im9 complex if no structural changes would occur on complexation. Of particular interest is the effect of Im9 binding on the longest lifetime component (τ_4) of Trp22 and Trp58, which shows a small decrease (from 5.5 to 4.8 ns, Table 3) or increase (from 7.7 to 8.2 ns), respectively. The decrease for Trp22 indicates an increase in the interaction with neighboring groups within E9 DNase, which results in the loss of the short rotational correlation time (ϕ_i) and a decreased solvent accessibility. Furthermore, the observed decrease in angular displacement of Trp58 (Table 4) indicates restricted mobility on Im9 binding.

Analogous to Zn^{2+} binding, complexation of E9 DNase with Im9 leads to structural changes that are transmitted through the protein from the binding site for the immunity protein to the tryptophans, which are both away from the binding site. One of the regions of the E9

DNase affected by the mobility of Trp22 on the seconds timescale spans residues 67-72, with the immunity protein binding site extending from residues 72-99 (6, 18). Boetzel et al. (36) proposed that ligation of Asn72 of the E9 DNase to Im9 could explain the effects of Im9 binding on Trp22. However, the fluorescence changes accompanying Im9 binding to the wild-type E9 DNase have also been observed for the E9 DNase N72A mutant (A.H.K and C.K., unpublished observations). Instead, interactions of Im9 with the main-chain of the DNase within the immunity protein binding site are the likely origin of the alteration in Trp22 as transmitted by the 67-72 region of the DNase. For Trp58, binding effects are possibly transmitted through Pro85 which is the neighboring residue of Phe86 that is critical for the interaction with Im9, with the ring of Pro85 coming within Van der Waals distance (3.55-3.76 Å) from the indole ring of Trp58 (6, 22). However, comparison of the crystal structures of the immunity protein bound form and free DNase does not help since the positions of the side-chains within the DNase in both structures are essentially identical (35). The present work demonstrates that the structural changes induced by Im9 binding clearly affects both tryptophans, rather than only Trp22 as is implied by the proposed immunity protein binding mechanisms (17, 18).

Im9 induced conformational changes occur independently of Zn²⁺ induced conformational effects - Although Zn²⁺ binding affects the DNase tryptophan environment within the E9-Im9 binary complex (solely for Trp22), the extent of the effect is much less than for binding to the free E9 DNase, indicating that Im9 induced conformational changes have primacy over those induced by Zn²⁺ binding. This observation agrees well with stopped-flow fluorescence experiments of Keeble et al. (12), which demonstrated that kinetics of immunity protein binding to E9 DNase are essentially identical with or without bound metal ion, indicating that the bound metal ion does not affect the kinetics of Im9 binding. The present work also has important consequences for the mechanism of cell entry by colicin E9 proposed by Pommer et al. (16). They suggested that removal of the bound metal ion destabilizes the high affinity colicin DNase-immunity protein complex (K_d , $\sim 10^{-14}$ M (15)), thereby accelerating the dissociation rate so that it is not rate-limiting for toxin induced cell death. The present experiments discount this possibility and therefore, some other factor must be involved in enhancing the dissociation rate of the E9-Im9 complex at the cell surface.

Colicin DNases highlight distinct conformational equilibria - In the present work we have used a combination of time-resolved anisotropy and time-resolved fluorescence decays to investigate the conformational dynamics within colicin DNase domains. This represents the first analysis of the conformational dynamics of colicin DNases on the nanosecond timescale. The demonstration that both tryptophans are rotationally mobile relative to the protein is a feature that is not observed by either crystallography or NMR and illustrates the usefulness of the present techniques in fully understanding the conformational dynamics of the colicin DNases.

Moreover, time-resolved fluorescence decay experiments demonstrated that the presence of multiple fluorescence lifetimes in the wild-type E9 DNase is due to both Trp22 and Trp58. Many proteins containing only a single tryptophan exhibit multiple fluorescence lifetimes (29). This is due to the tryptophans experiencing different microenvironments within the protein and is thus a response to the presence of conformational dynamics within the protein. We have previously characterized two ‘forms’ of conformational dynamics that are present within colicin DNases. The first one represents an equilibrium between an open and closed conformation, as detected by ESI-MS, that is biased towards the open form for the E7 DNase and towards the closed form for the E8 DNase, and intermediate for E2 and E9 DNase (19, 20). The second form represents a type of conformational heterogeneity centered around Trp22, as detected by high-field NMR experiments, and affects residues within a 9 Å radius (17). However, the present time-resolved fluorescence and anisotropy results are inconsistent with these equilibria being the origin of the dynamics probed by tryptophan fluorescence measurements. Two examples illustrate this point. Firstly, the fluorescence lifetime and rotational correlation times are rather similar for the different wild-type colicin DNases (20) (E.T.J.v.d.B. and A.J.R.H., unpublished results), despite the observed differences between the open-closed equilibria. Secondly, the fluorescence decays are markedly affected upon Zn^{2+} binding, whereas NMR experiments showed no changes in the dynamics of the tryptophans occurring upon Zn^{2+} binding (21). Kinetic investigations of ligand binding to the colicin DNases (12) have also provided evidence for the independence of these processes from those that affect the tryptophans upon ligand binding. Furthermore, we have previously demonstrated that the conformational equilibria detected by ESI-MS are independent of those probed by NMR (19). However, a more fundamental reason underpins why the conformational dynamics detected in the present study are not a result of the dynamic processes monitored by NMR and ESI-MS that occur over much longer timescales. Whereas the processes probed by the present time-resolved experiments occur on the nanosecond timescale, the open-closed equilibrium detected by ESI-MS is likely to take place over microseconds to seconds (typical timescales for folding/unfolding events), whilst the NMR detects conformational heterogeneity occurring on the second timescale. Furthermore, the relative commonality of multiple fluorescence decays in single tryptophan-containing proteins itself argues that it is a fundamental dynamic property of the tryptophans rather than a side-effect of another process. However, it remains possible that these other conformational equilibria may influence the magnitudes of the fluorescence decay lifetimes if the microenvironments of the tryptophans are different between the conformers with the observed values being determined by the equilibrium contribution of each conformer.

In conclusion, using time-resolved tryptophan fluorescence and anisotropy, we have shown how binding of two inhibitors of DNase activity, Zn^{2+} and Im9, influence in a distinct manner the conformational dynamics of the DNase colicin E9. One feature both inhibitors share

is that these conformational differences are transmitted throughout the DNase protein from the metal binding site or from the immunity protein exosite to both tryptophans, which in this respect has not been detected with other techniques for colicin DNases so far. Moreover, the results of this study indicate that Im9 induced conformational effects predominate over Zn^{2+} induced effects.

References

1. James, R., Penfold, C. N., Moore, G. R., and Kleanthous, C. (2002) Killing of *E. coli* cells by E group nuclease colicins *Biochimie* 84, 381-389.
2. Pommer, A. J., Cal, S., Keeble, A. H., Walker, D., Evens, S. J., Kuhlman, U. C., Cooper, A., Connolly, B. A., Hemmings, A. M., Moore, G. R., James, R., and Kleanthous, C. (2001) Mechanisms and cleavage specificity of the H-N-H endonuclease colicin E9 *J. Mol. Biol.* 314, 735-749.
3. Walker, D. C., Georgiou, T., Pommer, A. J., Walker, D., Moore, G. R., Kleanthous, C., and James, R. (2002) Mutagenic scan of the H-N-H motif of colicin E9: implications for the mechanistic enzymology of colicins, homing enzymes and apoptotic endonucleases *Nucleic Acids Res.* 30, 3225-3234.
4. Taylor, R., Burgner, J. W., Clifton, J., and Cramer, W. A. (1998) Purification and characterization of monomeric *Escherichia coli* vitamin B12 receptor with high affinity for colicin E3 *J. Biol. Chem.* 273, 31113-31118.
5. Di Masi, D. R., White, J. C., Schnaitman, C. A., and Bradbeer, C. (1973) Transport of vitamin B12 in *Escherichia coli*: common receptor sites for vitamin B12 and the E colicins on the outer membrane of the cell envelope *J. Bacteriol.* 115, 506-513.
6. Kleanthous, C., Kuhlmann, U. C., Pommer, A. J., Ferguson, N., Radford, S. E., Moore, G. R., James, R., and Hemmings, A. M. (1999) Structural and mechanistic basis of immunity toward endonuclease colicins *Nat. Struct. Biol.* 6, 243-252.
7. Buckle, A. M., and Fersht, A. R. (1994) Subsite binding in an RNase: structure of a barnase-tetranucleotide complex at 1.76-Å resolution *Biochemistry* 33, 1644-1653.
8. Kleanthous, C., and Walker, D. (2001) Immunity proteins: enzyme inhibitors that avoid the active site *Trends Biochem. Sci.* 26, 624-631.
9. Galburt, E. A., and Stoddard, B. L. (2002) Catalytic mechanisms of restriction and homing endonucleases *Biochemistry* 41, 13851-13860.
10. Kuhlmann, U. C., Moore, G. R., James, R., Kleanthous, C., and Hemmings, A. M. (1999) Structural parsimony in endonuclease active sites: should the number of homing endonuclease families be redefined? *FEBS Lett.* 463, 1-2.
11. Scholz, S. R., Korn, C., Bujnicki, J. M., Gimadutdinow, O., Pingoud, A., and Meiss, G. (2003) Experimental Evidence for a bba-Me-Finger Nuclease Motif To Represent the Active Site of the Caspase-Activated DNase *Biochemistry* 42, 9288-9294.
12. Keeble, A. H., Hemmings, A. M., James, R., Moore, G. R., and Kleanthous, C. (2002) Multistep Binding of Transition Metals to the H-N-H Endonuclease Toxin Colicin E9 *Biochemistry* 41, 10234-10244.
13. Sui, M. J., Tsai, L. C., Hsia, K. C., Doudeva, L. G., Ku, W. Y., Han, G. W., and Yuan, H. S. (2002) Metal ions and phosphate binding in the H-N-H motif: crystal structures of the nuclease domain of ColE7/Im7 in complex with a phosphate ion and different divalent metal ions *Protein Sci.* 11, 2947-2957.

14. Wallis, R., Leung, K. Y., Pommer, A. J., Videler, H., Moore, G. R., James, R., and Kleanthous, C. (1995b) Protein-protein interactions in colicin E9 DNase-immunity protein complexes. 2. Cognate and noncognate interactions that span the millimolar to femtomolar affinity range *Biochemistry* **34**, 13751-13759.
15. Wallis, R., Moore, G. R., James, R., and Kleanthous, C. (1995a) Protein-protein interactions in colicin E9 DNase-immunity protein complexes. 1. Diffusion-controlled association and femtomolar binding for the cognate complex *Biochemistry* **34**, 13743-13750.
16. Pommer, A. J., Kuhlmann, U. C., Cooper, A., Hemmings, A. M., Moore, G. R., James, R., and Kleanthous, C. (1999) Homing in on the role of transition metals in the HNH motif of colicin endonucleases *J. Biol. Chem.* **274**, 27153-27160.
17. Whittaker, S. B., Boetzel, R., MacDonald, C., Lian, L. Y., Pommer, A. J., Reilly, A., James, R., Kleanthous, C., and Moore, G. R. (1998) NMR detection of slow conformational dynamics in an endonuclease toxin *J. Biomol. NMR.* **12**, 145-159.
18. Whittaker, S. B., Czisch, M., Wechselberger, R., Kaptein, R., Hemmings, A. M., James, R., Kleanthous, C., and Moore, G. R. (2000) Slow conformational dynamics of an endonuclease persist in its complex with its natural protein inhibitor *Protein Sci.* **9**, 713-720.
19. Van den Bremer, E. T. J., Jiskoot, W., James, R., Moore, G. R., Kleanthous, C., Heck, A. J. R., and Maier, C. S. (2002) Probing metal ion binding and conformational properties of the colicin E9 endonuclease by electrospray ionization time-of-flight mass spectrometry *Protein Sci.* **11**, 1738-1752.
20. Van den Bremer, E. T. J., Keeble, A., H., Jiskoot, W., Spelbrink, R. E. J., Maier, C. S., Van Hoek, A., Visser, A. J. W. G., James, R., Moore, G. R., Kleanthous, C., and Heck, A. J. R. (2004) Distinct conformational stability and functional activity of four highly homologous endonuclease colicins *Protein Sci (in press)*.
21. Hannan, J. P., Whittaker, S. B., Hemmings, A. M., James, R., Kleanthous, C., and Moore, G. R. (2000) NMR studies of metal ion binding to the Zn-finger-like HNH motif of colicin E9 *J. Inorg. Biochem.* **79**, 365-370.
22. Kuhlmann, U. C., Pommer, A. J., Moore, G. R., James, R., and Kleanthous, C. (2000) Specificity in protein-protein interactions: the structural basis for dual recognition in endonuclease colicin-immunity protein complexes *J. Mol. Biol.* **301**, 1163-1178.
23. GarinotSchneider, C., Pommer, A. J., Moore, G. R., Kleanthous, C., and James, R. (1996) Identification of putative active-site residues in the DNase domain of colicin E9 by random mutagenesis *J. Mol. Biol* **260**, 731-742.
24. Vos, K., Van Hoek, A., and Visser, A. J. W. G. (1987) Application of a reference convolution method to tryptophan fluorescence in proteins. A refined description of rotational dynamics. *Eur. J. Biochem.* **165**, 55-63.
25. Van Hoek, A., and Visser, A. J. W. G. (1985) Artefact and distortion sources in time correlated single photon counting. *Anal. Instrument.* **14**, 359-378.
26. Digris, A. V., Skakun, V. V., Novikov, E. G., Van Hoek, A., Claiborne, A., and Visser, A. J. W. G. (1999) Thermal stability of a flavoprotein assessed from associative analysis of polarized time-resolved fluorescence spectroscopy. *Eur. Biophys. J.* **28**, 526-531.
27. Novikov, E. G., Van Hoek, A., Visser, A. J. W. G., and Hofstraat, J. W. (1999) Linear algorithms for stretched exponential decay analysis. *Opt. Commun.* **166**, 189-198.
28. Szabo, A. (1984) Theory of fluorescence depolarization in macromolecules and membranes. *J. Chem. Phys.* **81**, 150-167.
29. Lakowicz, J. R. (1999) *Principles of Fluorescence Spectroscopy*, Second ed., Kluwer Academic / Plenum Publishers, New York, Dordrecht, London, Moscow.

30. Malnasi-Csizmadia, A., Woolley, R. J., and Bagshaw, C. R. (2000) Resolution of conformational states of Dictyostelium myosin II motor domain using tryptophan (W501) mutants: implications for the open-closed transition identified by crystallography *Biochemistry* 39, 16135-16146.
31. Moncrieffe, M. C., Venyaminov, S. Y., Miller, T. E., Guzman, G., Potter, J. D., and Prendergast, F. G. (1999) Optical spectroscopic characterization of single tryptophan mutants of chicken skeletal troponin C: evidence for interdomain interaction *Biochemistry* 38, 11973-11983.
32. Azuaga, A. I., Canet, D., Smeenk, G., Berends, R., Titgemeijer, F., Duurkens, R., Mateo, P. L., Scheek, R. M., Robillard, G. T., Dobson, C. M., and van Nuland, N. A. (2003) Characterization of single-tryptophan mutants of histidine-containing phosphocarrier protein: evidence for local rearrangements during folding from high concentrations of denaturant *Biochemistry* 42, 4883-4895.
33. Kungl, A. J., Visser, N. V., van Hoek, A., Visser, A. J. W. G., Billich, A., Schilk, A., Gstach, H., and Auer, M. (1998) Time-resolved fluorescence anisotropy of HIV-1 protease inhibitor complexes correlates with inhibitory activity *Biochemistry* 37, 2778-2786.
34. Ko, T. P., Liao, C. C., Ku, W. Y., Chak, K. F., and Yuan, H. S. (1999) The crystal structure of the DNase domain of colicin E7 in complex with its inhibitor Im7 protein *Structure Fold. Des.* 7, 91-102.
35. Kolade, O. O., Carr, S. B., Kuhlmann, U. C., Pommer, A., Kleanthous, C., Bouchcinsky, C. A., and Hemmings, A. M. (2002) Structural aspects of the inhibition of DNase and rRNase colicins by their immunity proteins *Biochimie* 84, 439-446.
36. Boetzel, R., Czisch, M., Kaptein, R., Hemmings, A. M., James, R., Kleanthous, C., and Moore, G. R. (2000) NMR investigation of the interaction of the inhibitor protein Im9 with its partner DNase *Protein Sci.* 9, 1709-1718.

Chapter 6

Metal induced selectivity in phosphate ion binding in colicin E9 DNase

Ewald T.J. van den Bremer, Albert J. R. Heck¹
Anthony H. Keeble, Colin Kleanthous²

Submitted for publication

¹Dept. of Biomolecular mass spectrometry, Utrecht University, Utrecht

²Dept. of Biology, University of York, York

Abstract

In nature the functioning of proteins often depends on subtle, multiple, specific non-covalent interactions with other molecules, such as other proteins, metals, DNA/RNA, co-factors etc. Therefore, means to monitor and validate such interactions are important. In this study we use electrospray ionization mass spectrometry (ESI-MS) for the measurement of the ligation of a single phosphate ion to the enzyme colicin E9. In contrast to what was expected from extensive X-ray structural data this single phosphate ion ligation turned out to be specifically regulated by preceding Zn^{2+} ligation to the enzyme. Our ESI-MS data were validated by isothermal titration calorimetry (ITC). As DNA is the natural substrate of the enzyme we hypothesize that the findings reported here may have impact on the detailed functional mechanism of the enzyme and the role of the metal ion co-factors therein.

Introduction

Colicin E9 is a member of a family of bacterial endonuclease colicins that are protein antibiotics released by *Escherichia coli* into the extracellular medium during times of nutrient or environmental stress. On entrance into target cells the 15-kDa C-terminal DNase domain is translocated into the cytoplasm. In the target cell the lethal effect is accomplished by the hydrolysis of chromosomal DNA. Four highly homologous DNase colicins that use this mechanism have been identified E2, E7, E8 and E9. The intact ~60 kDa proteins consists of three domains: a translocation domain, a receptor binding domain and the aforementioned DNase domain. The DNase domain can be isolated as an active enzyme. A large number of biochemical and structural studies have been carried out previously on these homologous DNase colicins (1, 2). For instance, X-ray structures of the DNases E7 and E9 are available and confirmed that the DNase proteins are able to coordinate a single transition metal ion within their active site. Zn^{2+} was observed in the reported E7 DNase structure (3), whilst Ni^{2+} was observed ligated to E9 DNase (4). The affinity of E9 DNase metal complexes have been probed by ITC and revealed that both Ni^{2+} and Zn^{2+} bind strongly, with dissociation constants of 0.7 μ M and 1-4 nM, respectively (5). Additionally, a single phosphate molecule has been observed in most of the reported X-ray structures, in close proximity to the active site of the DNase (see Figure 1). These phosphate ions likely originate from the phosphate buffer solutions that are used in the preparation of the samples. This single phosphate ion was observed in the same location in X-ray structures of metal free E9 DNase (6), Ni^{2+} ligated E9 DNase (6), Zn^{2+} ligated E9 DNase (1FSJ PDB, unpublished), and Zn^{2+} ligated E7 DNase (3) and seems thus to be independent of the metal ion. As shown in Figure 1 the phosphate ion is bridged between the Ni^{2+} ion and a histidine and arginine residue of the DNase active site. This phosphate ion binding likely denotes the position either of the scissile bond or even the product 5'-phosphate.

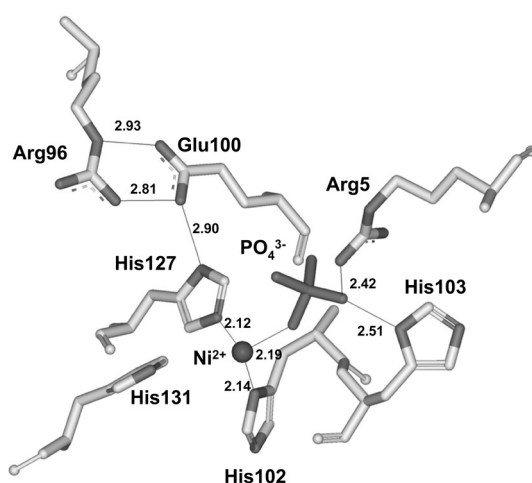


Figure 1. X-ray structure of the E9 DNase active site (4), whereby the location of the Ni^{2+} and phosphate ion and their interactions with the enzyme are highlighted. Values indicate distances in angstroms (\AA).

Since its introduction electrospray ionization (7) has evolved into a method that may be used to investigate non-covalent interactions (8). Recently, we have shown that specific immunity protein binding and metal ion binding can be monitored by ESI-MS. More specifically, we revealed that the conformation of E9 DNase in solution dramatically alters upon metal ion binding (for both Ni^{2+} and Zn^{2+}). The metal free DNase domain is in solution in an equilibrium between a highly flexible open conformer and a more rigid compact folded conformer, whereas metal binding induces the protein to adopt solely its compact folded structure (9, 10). In these ESI-MS experiments we did not use the commonly used phosphate containing buffers but the for electrospray more amendable, volatile ammonium acetate buffers. Therefore, we were initially unable to observe specific phosphate ion binding. In this work we set out to investigate whether we could use ESI-MS to observe any specific phosphate ion binding.

Experimental procedures

Protein samples - Colicin E9 DNase was expressed in *Escherichia coli* and purified as previously described (11, 12). Confirmation of the expressed proteins by nano electrospray ionization mass spectrometry (ESI-MS) under denaturing conditions, i.e. 50 (v/v) % acetonitrile/water containing 0.1% formic acid, yielded average masses that agreed well within 0.5 Da error with the calculated masses obtained from the primary amino acid sequence.

Electrospray ionization mass spectrometry - Time-of-flight electrospray ionization mass spectra were recorded on a Micromass LC-T mass spectrometer (Manchester, U.K.) operating in the positive ion mode. Prior to analysis a 600-3000 m/z scale was calibrated with CsI (2 mg/ml) in isopropanol/water (1:1). Nano-electrospray needles were prepared as described previously (9). In all experiments an aliquot (1-3 μl) of protein sample at a concentration of 10 μM was introduced into the electrospray needles. All samples were dissolved in 50 mM aqueous ammonium acetate solutions at pH 7.4. The nanospray needle potential was typically set to 1200 V and the cone voltage to 30 V. During the individual ESI-MS experiments all parameters of the mass spectrometer were kept constant (9)

Isothermal Titration Calorimetry - Isothermal titration calorimetry measurements were performed using a MicroCal Omega high-sensitivity titration calorimeter (MicroCal, Norhampton, MA). All solutions were thoroughly degassed before use by stirring under vacuum. The sample cell was loaded with 40 μM E9 DNase in 50 mM triethanol amine at pH 7.4. Zinc chloride and nickel chloride were used in a 5-fold, dependent on the experiment, to saturate the E9 DNase with metal ions. Titrations were carried out using a 250 μl syringe filled with sodium phosphate buffer (510 μM) of pH 7.4 at 25 °C. Injections were started after baseline stability was achieved. A titration experiment consisted of 25 consecutive injections of 10 μl volume.

Calorimetric data were analyzed using MicroCal ORIGIN software provided with the instrument. Heats obtained from blanc titrations of ligand into buffer were subtracted from each binding titration to obtain net binding heats which were normalized to molar amounts ligand added per injection.

Results

In Figure 2 ESI mass spectra are shown for 10 μM colicin E9 DNase in aqueous 50 mM ammonium acetate at pH 7.4, in the presence of low concentrations of metal and phosphate ions. We observed primarily the charge states from 7+ to 9+. The spectra were recorded from solutions containing less than stoichiometric amounts of metal and ammonium phosphate ions, so that metal free E9 DNase was always detectable. From the charge states the molecular mass of the metal free E9 DNase protein could be measured i.e. 15088.3 ± 0.3 Da, which is in excellent agreement with the calculated mass (15088.7 Da). The bottom mass spectrum (Figure 2a) shows ion signals of both the metal-free and Ni^{2+} -ligated E9 DNase, which are differentiated by a mass increase of approximately 56 Da ($58 - 2\text{H}$). Upon addition of ammonium phosphate to the solution used in Figure 2a, the resulting spectrum in Figure 2b revealed clearly no phosphate ion ligation (+98 Da) to either the metal free E9 DNase and the Ni^{2+} -ligated E9 DNase. Performing similar experiments now with Zn^{2+} , instead of Ni^{2+} , provided a very different picture, as shown in Figure 2c. The ESI spectrum of the solution containing a less than stoichiometric amount of Zn^{2+} resulted in a spectrum very similar as shown in Figure 2a, with ion signals of both the metal-free and Zn^{2+} -ligated E9 DNase, which could be differentiated by a mass increase of approximately 63 Da ($65 - 2\text{H}$). Surprisingly, when a small amount of ammonium phosphate was added the Zn^{2+} -ligated E9 DNase ligated additionally a single phosphate ion (as indicated by the mass increase of $63 + 98$ Da), however, no ligation was observed for the metal-free E9 DNase. It should be noted that these observations are monitored from a single solution, in the same ESI spectrum, thus sprayed under identical conditions, undoubtedly indicating that phosphate ion binding is Zn^{2+} dependent. Increasing the concentrations for both Zn^{2+} and ammonium phosphate resulted finally in a fully saturated 1:1:1 E9- Zn^{2+} - PO_4^{3-} ternary complex. In contrast, increasing concentrations further for both Ni^{2+} and ammonium phosphate merely resulted in a fully saturated 1:1 E9- Ni^{2+} binary complex. The formation of the ternary complex for the Zn^{2+} -bound state was unexpected, since from the reported X-ray structures it was suggested that phosphate binding is not Zn^{2+} specific, and not even metal ion dependent (3, 6).

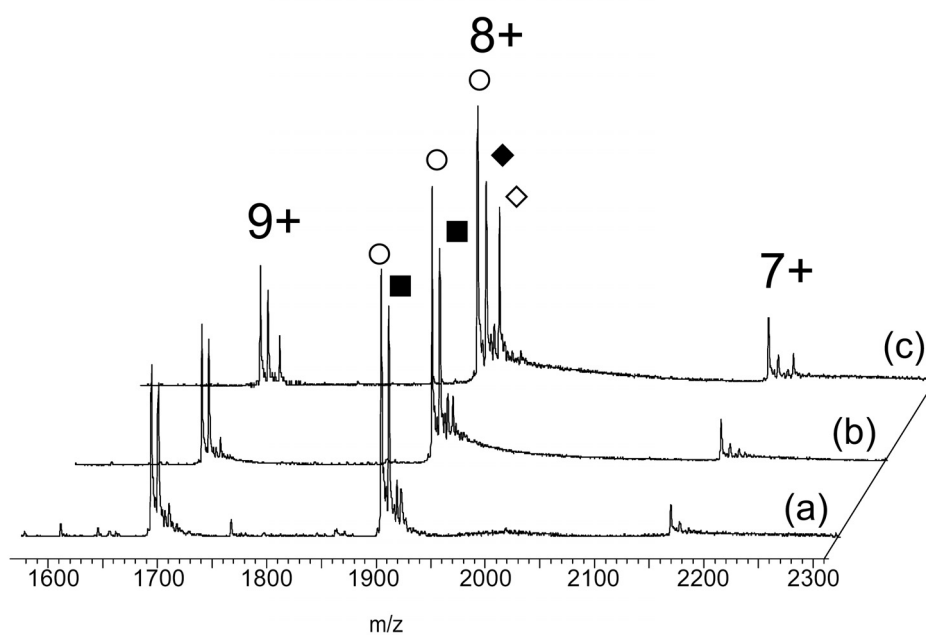


Figure 2. ESI-MS spectra of E9 DNase (10 μM) in the presence of (a) Ni^{2+} , (b) Ni^{2+} and PO_4^{3-} , and (c) Zn^{2+} and PO_4^{3-} . Ligand concentrations are $\sim 6 \mu\text{M}$. Signals indicated by (○) represent the metal-free; (■) Ni^{2+} -ligated; (◆) Zn^{2+} -ligated and (◇) Zn^{2+} - PO_4^{3-} -ligated DNase.

Although a vast amount of data exist nowadays validating the use of ESI-MS for the investigation of non-covalent interactions in solution, we further addressed this unexpected phenomenon by a more direct solution-phase based complementary method. We therefore performed isothermal titration calorimetry (ITC) experiments to monitor the role of Zn^{2+} in phosphate binding. As in the ESI-MS experiments we first made sure no spurious phosphate ions were present in the used solutions by thorough dialysis. We titrated aqueous sodium phosphate solutions into aqueous 50 mM triethanolamine solutions containing respectively metal-free E9 DNase, Ni^{2+} saturated and Zn^{2+} saturated E9 DNase (pH 7.4, 25 °C). The resulting data are shown in Figure 3. These ITC results show that no phosphate ion ligation could be observed in the solutions containing either metal-free E9 DNase and Ni^{2+} saturated E9 DNase. Performing identical titrations in the presence of Zn^{2+} resulted in a complete single phosphate ion binding isotherm. The dissociation constant for phosphate ion binding to the Zn^{2+} saturated E9 DNase was 15 μM . The ITC measurements therefore confirm the ESI-MS findings.

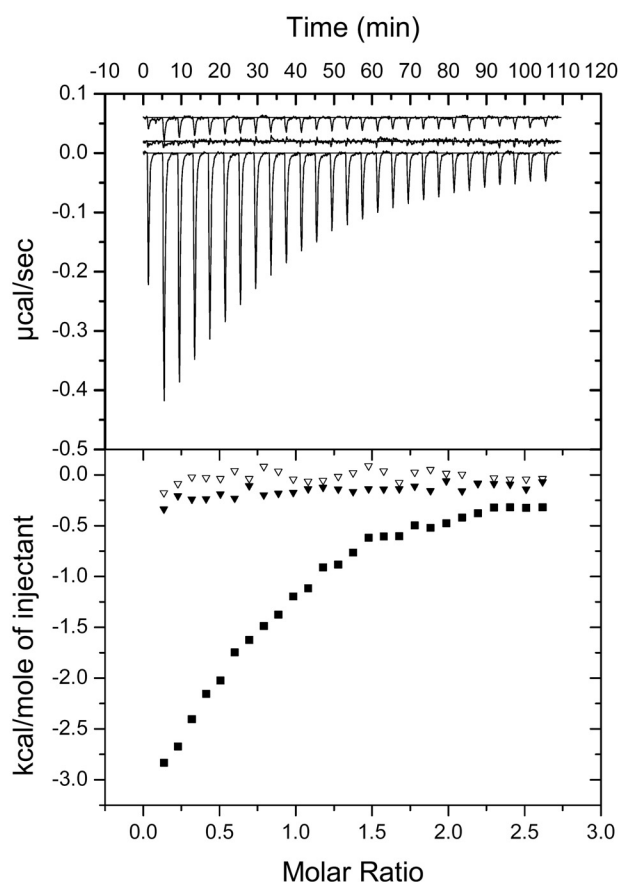


Figure 3. ITC data showing the binding of a single phosphate ion to E9 DNase. Top panel shows the calorimetric response of 25 10- μ l injections of 510 μ M phosphate to 40 μ M E9 DNase in 50 mM triethanolamine buffer, pH 7.4 and 25 $^{\circ}$ C. Bottom panel shows integrated injections heats for the above data. The produced injection heats indicated by (\blacktriangledown), (∇) and (\blacksquare) are from metal-free, E9-Ni $^{2+}$ and E9-Zn $^{2+}$, respectively.

Conclusion

Our combined findings indicate that metal ion binding and phosphate ion binding (and possibly DNA substrate binding) are intriguingly regulated in the E9 colicin DNase system. This is even more remarkable as the high-resolution X-ray structures available provide no clue for the observed behavior as both the position of the metal ion as well as the interactions with the amino acids in the catalytic site of the E9 DNase seem to be very similar. At present we are pursuing our studies by investigating the effects of specific single amino acid mutants in the catalytic site, which potentially are involved in metal ion binding and/or phosphate ion binding. Additionally, we hope to further elucidate the functional role of the specific metals on the biological activity of the DNase enzymes.

References

1. James, R., Penfold, C. N., Moore, G. R., and Kleanthous, C. (2002) Killing of *E. coli* cells by E9 group nuclease colicins *Biochimie* 84, 381-389.
2. Pommer, A. J., Cal, S., Keeble, A. H., Walker, D., Evens, S. J., Kuhlman, U. C., Cooper, A., Connolly, B. A., Hemmings, A. M., Moore, G. R., James, R., and Kleanthous, C. (2001)

- Mechanisms and cleavage specificity of the H-N-H endonuclease colicin E9 *J.Mol.Biol.* 314, 735-749.
3. Sui, M. J., Tsai, L. C., Hsia, K. C., Doudeva, L. G., Ku, W. Y., Han, G. W., and Yuan, H. S. (2002) Metal ions and phosphate binding in the H-N-H motif: crystal structures of the nuclease domain of ColE7/Im7 in complex with a phosphate ion and different divalent metal ions *Protein Sci* 11, 2947-2957.
 4. Kleanthous, C., Kuhlmann, U. C., Pommer, A. J., Ferguson, N., Radford, S. E., Moore, G. R., James, R., and Hemmings, A. M. (1999) Structural and mechanistic basis of immunity toward endonuclease colicins *Nat. Struct. Biol.* 6, 243-252.
 5. Pommer, A. J., Kuhlmann, U. C., Cooper, A., Hemmings, A. M., Moore, G. R., James, R., and Kleanthous, C. (1999) Homing in on the role of transition metals in the HNH motif of colicin endonucleases *J. Biol. Chem.* 274, 27153-27160.
 6. Kuhlmann, U. C., Pommer, A. J., Moore, G. R., James, R., and Kleanthous, C. (2000) Specificity in protein-protein interactions: the structural basis for dual recognition in endonuclease colicin-immunity protein complexes *J. Mol. Biol.* 301, 1163-1178.
 7. Fenn, J. B., Mann, M., Meng, C. K., Wong, S. F., and Whitehouse, C. M. (1989) Electrospray ionization for mass spectrometry of large biomolecules *Science* 246, 64-71.
 8. Ganem, B., Li, Y. T., and Henion, J. D. (1991) Observation of Noncovalent Enzyme Substrate and Enzyme Product Complexes by Ion-Spray Mass-Spectrometry *J. Am. Chem. Soc.* 113, 7818-7819.
 9. Van den Bremer, E. T. J., Jiskoot, W., James, R., Moore, G. R., Kleanthous, C., Heck, A. J. R., and Maier, C. S. (2002) Probing metal ion binding and conformational properties of the colicin E9 endonuclease by electrospray ionization time-of-flight mass spectrometry *Protein Sci.* 11, 1738-1752.
 10. Van den Bremer, E. T. J., Keeble, A., H., Jiskoot, W., Spelbrink, R. E. J., Maier, C. S., Van Hoek, A., Visser, A. J. W. G., James, R., Moore, G. R., Kleanthous, C., and Heck, A. J. R. (2004) Distinct conformational stability and functional activity of four highly homologous endonuclease colicins *Protein Sci.* (in press).
 11. Wallis, R., Moore, G. R., Kleanthous, C., and James, R. (1992) Molecular analysis of the protein-protein interaction between the E9 immunity protein and colicin E9 *Eur. J. Biochem.* 210, 923-930.
 12. Wallis, R., Reilly, A., Barnes, K., Abell, C., Campbell, D. G., Moore, G. R., James, R., and Kleanthous, C. (1994) Tandem overproduction and characterisation of the nuclease domain of colicin E9 and its cognate inhibitor protein Im9 *Eur. J. Biochem.* 220, 447-454.

Chapter 7

**Probing the H-N-H active site
in colicin E9 for metal
and phosphate-ligand binding**

Abstract

Colicin E9 is a microbial toxin that kills bacteria through random degradation of chromosomal DNA via a highly conserved ($\beta\beta\alpha$ -Me) active site motif. This motif of colicin DNases is structurally homologous to the active sites of other endonucleases, including those of the homing endonuclease I-P ϕ I, a His-Cys box enzyme, and the non-specific nuclease from *Serratia*. Metal ions Zn^{2+} and Ni^{2+} are found in several E colicin DNase X-ray structures and bind and stabilize colicin DNases significantly but display very distinct metal co-factor properties. Zn^{2+} inhibits the DNase system while Ni^{2+} enhances DNA hydrolysis. In the present work we have used electrospray ionization mass spectrometry (ESI-MS) and isothermal titration calorimetry (ITC) in combination with site-directed mutagenesis to probe metal and phosphate ion ligation to the active site of colicin E9. Our results show that H131 is involved in metal ion ligation for both metal ions Ni^{2+} and Zn^{2+} . The similar role of H131 in E9- Ni^{2+} and E9- Zn^{2+} does not explain the mode of Zn^{2+} inhibition. H103 seems to selectively bind one 5'-rAMP molecule in the presence of Zn^{2+} and not in the presence of Ni^{2+} . This may have consequences for the Zn^{2+} inhibition mechanism and we speculate on the role of H103 therein. However, 5'-dAMP binding seems not to be specifically regulated by preceding Zn^{2+} ion ligation. This was unexpected and more experiments are needed to elucidate further the role of Zn^{2+} in the inhibition mechanism.

Introduction

Colicins are a large and varied family of plasmid-encoded bacterial toxins that are produced to respond to signals of stress by strains of *Escherichia coli* (1). This study is focused on colicin E9 that belongs to the family of the H-N-H homing endonucleases, which kill target cells by non-specific degradation of the chromosomal DNA. The DNase domain being responsible for the cytotoxic effect comprises 134 amino acid residues and binds a cognate immunity protein, which is an *in vivo* inhibitor, thereby preventing suicide of the producing cell (2, 3). These 9-10 kDa immunity proteins bind the DNase domain at an exosite adjacent to the active site with K_d 's in femtomolar range (4). Modeling studies have indicated that inhibition relies on the polymeric nature of the DNA and occurs through steric and electronic blocking of binding away from the cleavable bond (2). The active site comprises the C-terminal ~30 residues and contains the consensus sequence for the H-N-H group of homing endonucleases and has a fold conserved with the $\beta\beta\alpha$ -Me family of nucleases (5, 6) The structure of the active site resembles that of a zinc finger and transition metals ions such as Zn^{2+} , Co^{2+} and Ni^{2+} bind indeed to all colicin DNases (7, 8) (Figure 1).

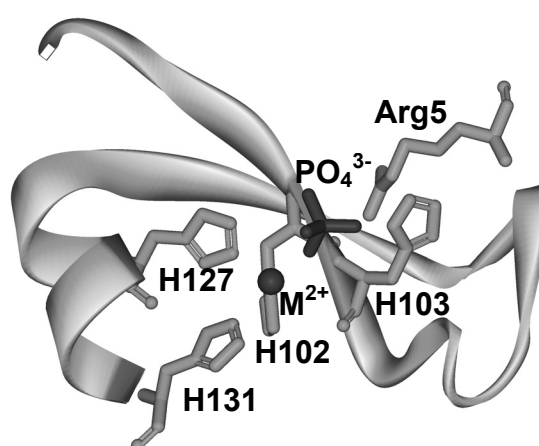


Figure 1. X-ray structure of the E9 DNase $\beta\beta\alpha$ active site motif. Key residues supposed to be involved in metal ion and phosphate ion binding are highlighted (2, 9).

Ligation of the tetrahedrally coordinated Zn^{2+} ion occurs via three histidine residues (H102, H127 and H131) and a non-covalently bound phosphate ion (2, 10). The three histidines are clearly well defined ligands in the Zn^{2+} -ligated structures found in colicin E7 (10, 11), however, X-ray structures showing Ni^{2+} in the active-site of colicin E9 highlight that only H102 and H127 bind to the metal ion (2). The role of His131 is somewhat uncertain since NMR studies revealed that Ni^{2+} is ligated via His131 (12) but is not essential for DNase activity (9). The final coordination site for the Ni^{2+} and Zn^{2+} in the E9 DNase X-ray structure seemed to be

a phosphate molecule ((13) and 1FSJ PDB unpublished). The presence of phosphate in the active site of E9 DNase may denote the position either of the scissile bond or, more likely the product 5' phosphate generated by the enzyme (14). In the previous chapter we demonstrated that, in contrast to what was expected from the extensive X-ray structural data, this single phosphate ion ligation is specifically regulated by preceding Zn^{2+} ligation (15). The single phosphate ion is in close proximity of Arg5 and His103. Arg5 is likely involved in stabilization of the DNA backbone and His103 in coordination of a water molecule needed for nucleophilic attack (H103) (14). The H-N-H motif mediates the function of DNA hydrolysis (9) but the role of the Zn^{2+} is still elusive (14, 16). Both ions Ni^{2+} and Zn^{2+} stabilize the DNase significantly, however, enzymatic activity is not observed in the presence of Zn^{2+} , while Ni^{2+} can be used as an excellent co-factor (17). To date, transition metal ion binding and co-factor dependent nuclease activity is reasonably well studied for colicin E9 (9, 14, 17). However, the intriguing question why Zn^{2+} is such a poor co-factor in contrast to Ni^{2+} remains unresolved. (18).

In this work, we first characterize the role of the three histidines (H102, H127 and H131) in transition metal ion binding by electrospray ionization mass spectrometry (ESI-MS). To elucidate further the role in the phosphate ion binding, as shown previously in chapter 6, we here studied metal ion depended nucleotide binding characteristics. We used single nucleotides i.e. ribose- and deoxyribose adenine monophosphate (rAMP and dAMP, respectively) along with site directed mutagenesis. Isothermal titration calorimetry (ITC) experiments were performed to validate our ESI-MS findings.

Experimental procedures

Protein samples - Colicin E9 DNase site-directed mutants and wild-type were expressed in *Escherichia coli* and purified as previously described (19, 20). Confirmation of the expressed proteins by nano electrospray ionization mass spectrometry (ESI-MS) under denaturing conditions, i.e. 50 (v/v) % acetonitrile/water containing 0.1% formic acid, yielded average masses that agreed well (within 0.5 Da) with the calculated masses obtained from the primary amino acid sequence.

Electrospray ionization mass spectrometry - Time-of-flight electrospray ionization mass spectra were recorded on a Micromass LC-T mass spectrometer (Manchester, U.K.) operating in the positive ion mode. Prior to analysis a 600-3000 m/z scale was calibrated with CsI (2 mg/ml) in isopropanol/water (1:1). Nano-electrospray needles were prepared as described previously (18). In all experiments an aliquot (1-3 μ l) of protein sample at a concentration of 10 μ M was introduced into the electrospray needles. All samples were dissolved in 50 mM aqueous ammonium acetate solutions at pH 7.4. The nanospray needle potential was typically set to

1200V and the cone voltage to 30 V. During the individual ESI-MS experiments all parameters of the mass spectrometer were kept constant (18)

Isothermal Titration Calorimetry - Isothermal titration calorimetry measurements were performed using a MicroCal Omega high-sensitivity titration calorimeter (MicroCal, Norhampton, MA). All solutions were thoroughly degassed before use by stirring under vacuum. The sample cell was loaded with 40 μ M E9 DNase in 50 mM ammonium acetate at pH 7.4 or in 50 mM triethanol amine (TEA) buffer pH 7.4. Zinc acetate and Nickel acetate were used in a 5-fold, dependent on the experiment, to saturate the E9 DNase with metal ions. Titrations were carried out using a 250 μ l syringe filled with ribose adenine monophosphate (5'-rAMP) in 50 mM ammonium acetate (pH 7.4). Also ITC titrations were carried out using a 250 μ l syringe filled with 5'-rAMP or 5'-dAMP in 50 mM triethanol amine (TEA) (pH 7.4) with identical protein concentrations. Injections were started after baseline stability was achieved. A titration experiment consisted of 25 consecutive injections of 10 μ l volume. Calorimetric data were analyzed using MicroCal ORIGIN software provided with the instrument. Heats obtained from blank titrations of ligand into buffer were subtracted from each binding titration to obtain net binding heats which were normalized to molar amounts ligand added per injection.

Results

H131 is involved in Ni²⁺ ligation - The X-ray structure of E9 DNase has revealed that only two clearly identifiable amino acid residues bind the Ni²⁺ ion (His102 and His127) and a third (His131) that is in a poor position to bind the metal ion. In contrast, solution NMR experiments have revealed three histidine ligands for the Ni²⁺ ion in E9 DNase. In addition, the E7 DNase-Zn²⁺ crystal structure showed clearly an additional H131 ligation. Hence, Pommer et al. postulated that these differences in coordination chemistry are the origin of the different affinities of the metal ions for the E9 DNase. (21). The K_d's for Zn²⁺ and Ni²⁺ are in the nM and μ M range, respectively (21).

In accordance, enzymatic assays and ANS fluorescence experiments on H102A and H127A mutants have previously shown to eliminate completely enzymatic activity and metal ion binding capability. Still, the E9 DNase H131A mutant exhibit 27% DNase activity in the Ni²⁺ mediated catalysis and thus H131 has been stated not to be essential for metal ion ligation and enzymatic activity (9). To date, the role of H131 is still somewhat controversial. Hence, ESI-MS was used to observe the Ni²⁺ and Zn²⁺ binding capabilities for each histidine-to-alanine mutant (i.e. H102A, H127A and H131A).

We have previously used ESI-MS to investigate the conformational properties of E9 DNase and used it also to probe metal ion binding (see chapters 3, 4 and 6). We showed this technique can be used to characterize non-covalent protein-metal interactions.

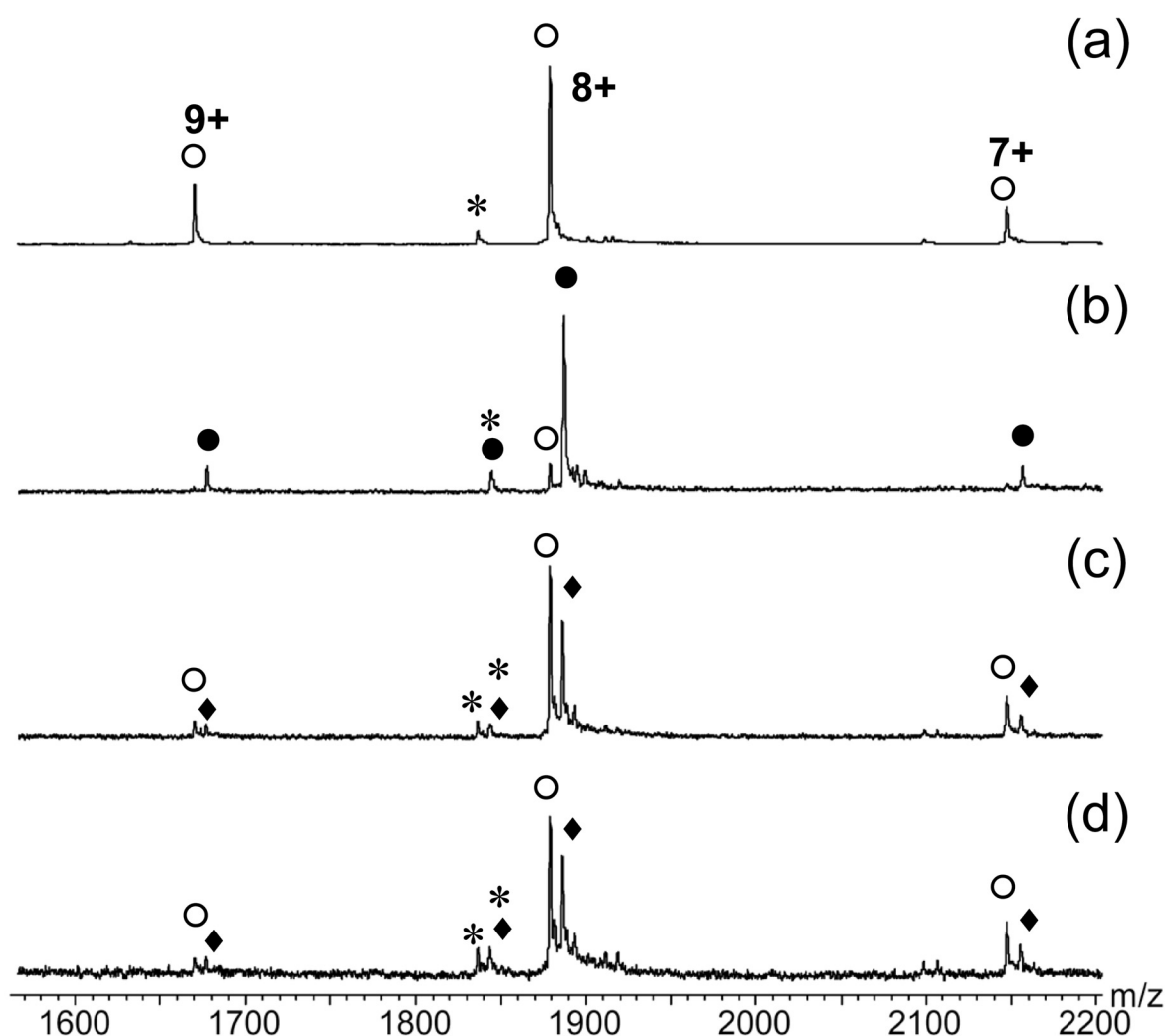


Figure 2. Nano ESI mass spectra of colicin E9 DNase H131A mutant (10 μM). Protein ion signals are indicated for metal-free (\circ), Zn^{2+} ligated (\bullet) and Ni^{2+} ligated (\blacklozenge) E9 DNase. Spectrum (a) is recorded in the absence of metal ions. Spectrum (b) is recorded in the presence of 50 μM ZnAc_2 . Spectrum (c) and (d) are recorded in the presence of 50 and 100 μM NiAc_2 , respectively. Ion signals highlighted by (*) are lacking the N-terminal peptide sequence MES (-365 Da).

For both Ni^{2+} and Zn^{2+} bound E9 DNase wild-type a single narrow charge state distribution is observed encompassing three ion peaks (7+, 8+, 9+) with a maximum located at 8+ (see also chapter 3 Figures 4 and 6). H131A shows similar Zn^{2+} binding capabilities as seen for the wild-type protein. Although Zn^{2+} binding seems not significantly affected, the 8+ ion signal is not completely saturated ($\sim 96\%$) indicating somewhat weaker binding (Figure 2b). Ni^{2+} binding is more affected. H131A is capable to bind Ni^{2+} only to a small extent in the presence of 5-fold excess Ni^{2+} (Figure 2c). Increasing the Ni^{2+} concentration further up to a 10-fold resulted in no saturation of the enzyme (Figure 2d). The results show that H131 plays an important role in Ni^{2+} binding. The remaining DNase activity (27%) (9) could originate from the fact that Ni^{2+}

binding is not completely abolished. H127A and H102A mutants showed no metal binding capabilities for both Ni^{2+} and Zn^{2+} in our ESI-MS experiments (data not shown), which is in good agreement with ANS fluorescence quenching experiments on Zn^{2+} binding (9). Our results clearly show that both Ni^{2+} and Zn^{2+} use all three histidine residues. Thus, the E9- Zn^{2+} inhibition mechanism proposed by Pommer et al. that is due to an additional H131 ligation selectively by Zn^{2+} is unlikely (14).

rAMP binding is transition metal dependent - X-ray structures of E9 DNase (and E7 DNase) show a fourth ligand bound to metal ion; a single phosphate ion located in the H-N-H motif (2, 11). A structural comparison between the H-N-H motif and active sites of other H-N-H family members such as *I-PpoI* and *Serratia* nuclease, reveals via superposition that the single phosphate ion is at the center where DNA hydrolysis occurs (5). Also, Walker et al. showed via site directed mutagenesis that the H-N-H motif is the site where DNA hydrolysis is taking place (9). The presence of phosphate in the active site of the E9 DNase in the X-ray structures likely denotes the position either of the scissile bond or, more likely, the product 5' phosphate generated by the enzyme. Single phosphate ion ligation turned out to be specifically regulated by preceding Zn^{2+} ligation to the enzyme (see Chapter 6). As DNA is the natural substrate of the enzyme we postulated that it may have impact on the detailed functional mechanism of the enzyme and the role of metal ion co-factors therein.

To find the molecular origin of E9 DNase- Zn^{2+} inhibition, we were interested to study single phosphate ion binding in further detail. Pommer et al. have previously demonstrated that in the absence of metal ions small oligonucleotides (<5 bases) bind poorly to E9 DNase, whereas single-stranded DNA substrates > 10 bases are optimal for binding (14). In this work single nucleotides were used to extend the single phosphate binding studies described in the previous chapter into the direction of the natural substrate. Initially, ligation experiments for 5'-rAMP and 3'-rAMP to E9 DNase were addressed. Although, 5'-rAMP is more a model compound representing RNA instead of DNA, we used it as also RNA cleavage has been observed for E9 DNase, albeit solely in the presence of Ni^{2+} and not with Zn^{2+} (14).

The recorded ESI spectra show no significant ligation of 5'-rAMP to E9 DNase wild-type (Figure 3a) in the absence of metal ions. This is in agreement with previous ANS fluorescence experiments by Pommer et al. (14), who observed that small oligonucleotides < 5 bases do not bind in the absence of metal ions. E9 DNase saturated with Ni^{2+} also showed no considerable 5'-rAMP binding (Figure 3b). For the Zn^{2+} ligated protein, on the other hand, significant 5'-rAMP ligation is observed (Figure 3c). ESI-spectra of E9 DNase wild-type at 6-fold 5'-rAMP concentrations (60 μM) show that Zn^{2+} -bound E9 DNase is almost fully saturated with 5'-rAMP by showing a mass increase of 347 Da. This remarkable difference in 5'-rAMP binding,

dependent of preceding Zn^{2+} ion ligation, is in agreement with our previous studies on phosphate ion binding as described in chapter 6.

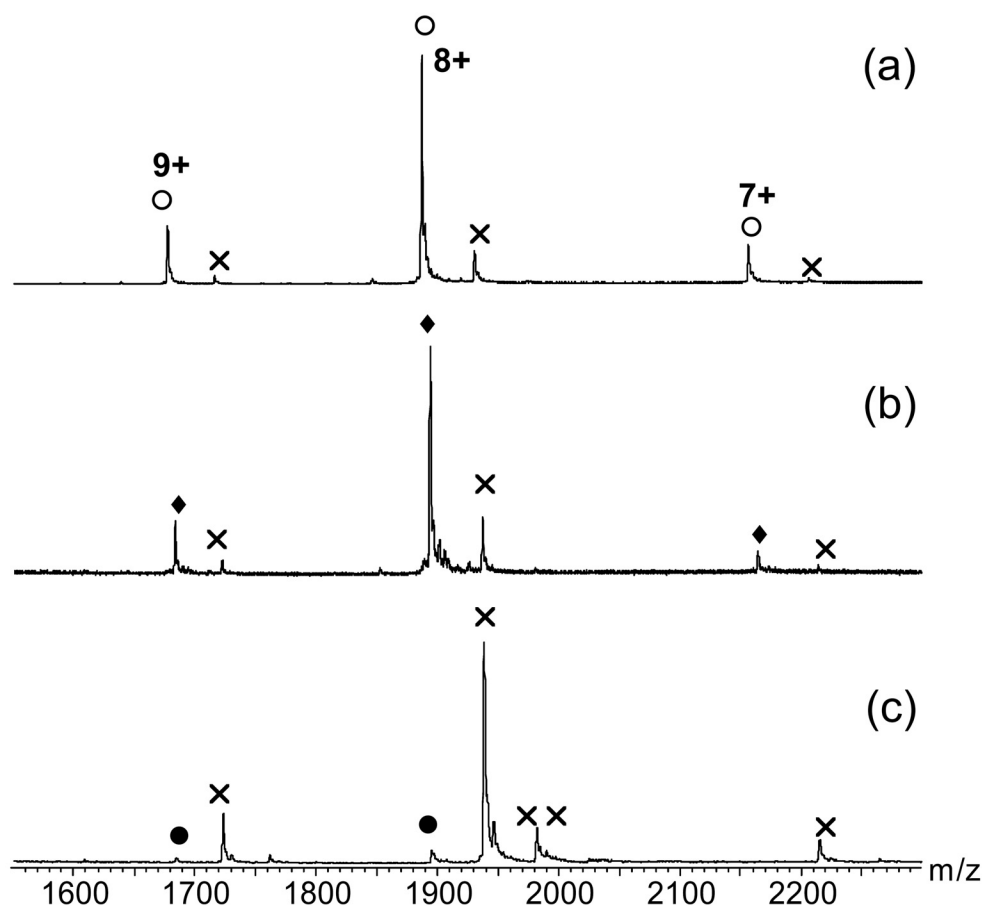


Figure 3. Nano ESI mass spectra of colicin E9 DNase wild-type (10 μM). Protein ion signals are indicated for metal-free (\circ), Ni^{2+} ligated (\blacklozenge) and Zn^{2+} ligated (\bullet) E9 DNase. Spectrum (a) is recorded in the absence of metal ions. Spectrum (b) is recorded in the presence of 50 μM NiAc_2 . Spectrum (c) is recorded in the presence of 50 μM ZnAc_2 . Protein ion signals showing 5'-rAMP ligation (+347 Da) are marked by (x).

The phosphate ion found in the X-ray could denote the product 5' phosphate generated by the enzyme (14). Therefore, we were interested to perform identical ligation experiments in the presence of 3'-rAMP. These experiments yielded spectra for the E9 DNase that are similar to those obtained for 5'-rAMP, however, interestingly, 3'-AMP binds slightly weaker (see Figure 4).

Ligand binding curves were obtained for E9 DNase wild-type (10 μM) recorded from solutions containing different concentrations of 5'-rAMP and 3'-rAMP (from 0 to 60 μM). Curves were deduced by plotting peak ratios of ligand bound *versus* the total ion peak area (bound + unbound) of ion peaks 7+, 8+ and 9+. These binding curves are presented in figure 4. These curves summarize our findings and show that the metal-free E9 DNase has overall poor ligand binding properties comparable to those obtained for the Ni^{2+} ligated protein. Thus, Ni^{2+}

does not enhance rAMP binding at all. Surprisingly, however, the presence of Zn^{2+} in the H-N-H active site of colicin E9 DNase shows a remarkable difference in rAMP binding. Ligand binding curves of E9- Zn^{2+} show an estimated K_d in the ~ 20 - $30 \mu M$ range. This remarkable fact may have consequences for the Zn^{2+} inhibition mechanism.

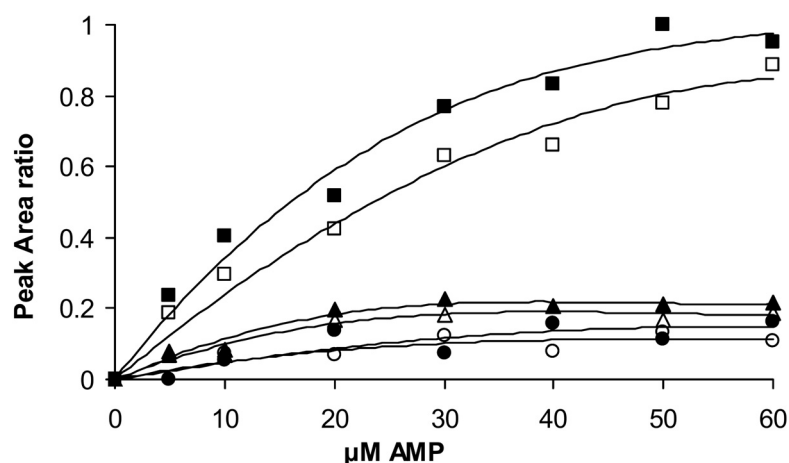


Figure 4. Metal ion dependent rAMP binding curves at increasing concentrations of rAMP to E9 DNase wild-type ($10 \mu M$). Showing ESI-MS ion peak area ratios of E9 DNase-rAMP bound. (●)(5'-rAMP) and (○)(3'-rAMP) in the absence of metal ions; (▲)(5'-AMP) and (△)(3'-rAMP) in the presence of Ni^{2+} ($50 \mu M$); (■)(5'-rAMP) and (□)(3'-rAMP).in the presence of Zn^{2+} ($50 \mu M$).

His103 is required for E9 DNase- Zn^{2+} 5'-rAMP ligation – Two amino acids appear to be absolutely conserved over all H-N-H enzymes and are in close proximity of the non-covalently bound phosphate ion. These residues are identified, by structural superposition, as His103 and Arg5 (see Figure 1). The latter contacts the bound phosphate in the E9 DNase X-ray structure and is equivalent to Arg61 in *I-PpoI* (and Arg57 of *Serratia*) where its role is in stabilizing the product 5'-phosphate. His98 in *I-PpoI* serves as a general base to activate a water molecule, which functions as a nucleophile to attack the scissile phosphate group (14). Hence, we decided to study the effect of the mutants R5A and H103A on the rAMP binding properties of the Zn^{2+} -bound enzyme.

ESI-MS analysis revealed that both H103A and R5A have similar metal ion affinities as the wild-type (data not shown). ESI-MS data for the Zn^{2+} ligated H103A mutant showed in the presence of 8-fold 5'-rAMP no significant ligand binding. Still, at $160 \mu M$ 5'-rAMP (16-fold excess) only weak binding (possibly non-specific) was observed (Figure 5). Strikingly, the spectrum obtained for E9 DNase R5A- Zn^{2+} shows an increase of 347 Da indicating one 5'-rAMP molecule binds specifically to the protein (Figure 6). Thus, R5A mutation seems not to affect 5'-rAMP binding. From our ESI-MS experiments it seems that H103 play an important role in stabilization of the phosphate group of rAMP that binds solely in the presence of Zn^{2+} .

As the findings by ESI-MS are quite intriguing we decided to validate our ESI-MS data by isothermal titration calorimetry (ITC). First the binding of 5'-rAMP was investigated.

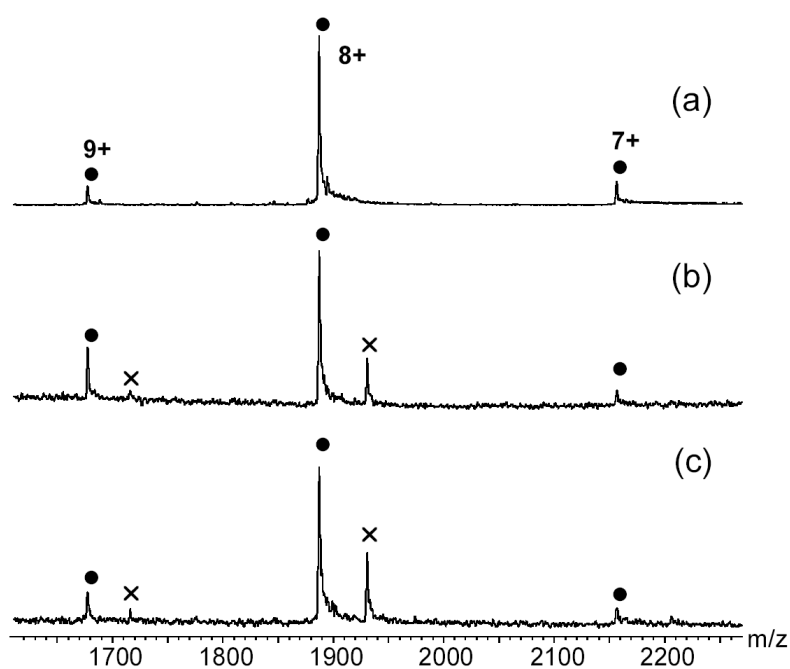


Figure 5. Nano ESI mass spectra of E9 DNase H103A (10 μ M) in the presence of 50 μ M ZnAc₂. Ion peaks highlighted as (●) represent the Zn²⁺ ligated protein. Spectra (a,b and c) were recorded in the presence of 0, 80 and 160 μ M 5'-rAMP, respectively. Protein ion signals showing 5'-rAMP ligation (+347 Da) are marked (x).

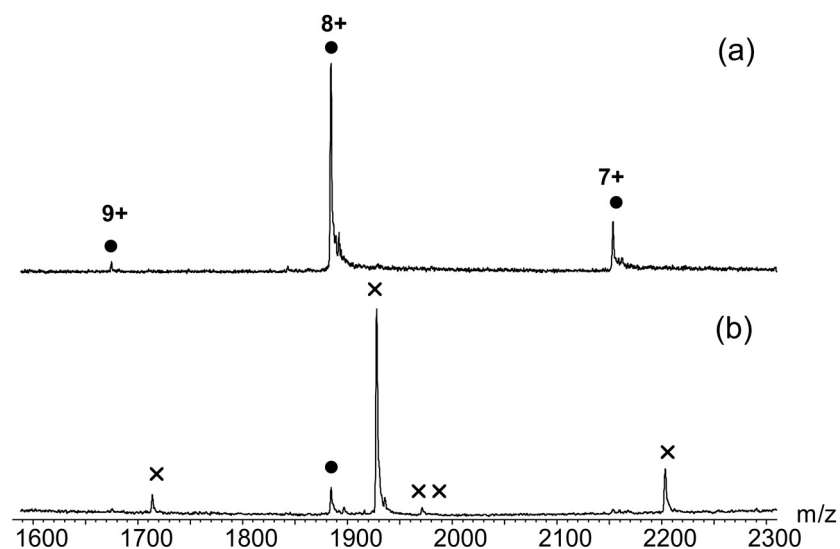


Figure 6. Nano ESI mass spectra of E9 DNase R5A (10 μ M) in the presence of 50 μ M ZnAc₂. Ion peaks highlighted as (●) represent the Zn²⁺ ligated protein. Spectra (a and b) were recorded in the presence of 0 and 80 μ M 5'-rAMP, respectively. Protein ion signals showing 5'-rAMP ligation (+347 Da) are marked (x).

A complete single binding isotherm for 5'-rAMP was obtained in the presence of Zn^{2+} , from which a dissociation constant could be derived of $\sim 30 \mu M$ (Figure 7B). For the Ni^{2+} ligated E9 DNase no 5'-rAMP binding could be observed (Figure 7A). These findings correlate well with our ESI-MS data. To further investigate the cooperative effect of Zn^{2+} and AMP ligation, ITC experiments were performed for 5'-dAMP and 5'-rAMP in TEA buffers. To our surprise 5'-dAMP, which is one building block of the natural DNA substrate, does not bind to E9- Zn^{2+} . If at all 5'-dAMP binds much weaker than rAMP in identical buffer solutions (data not shown).

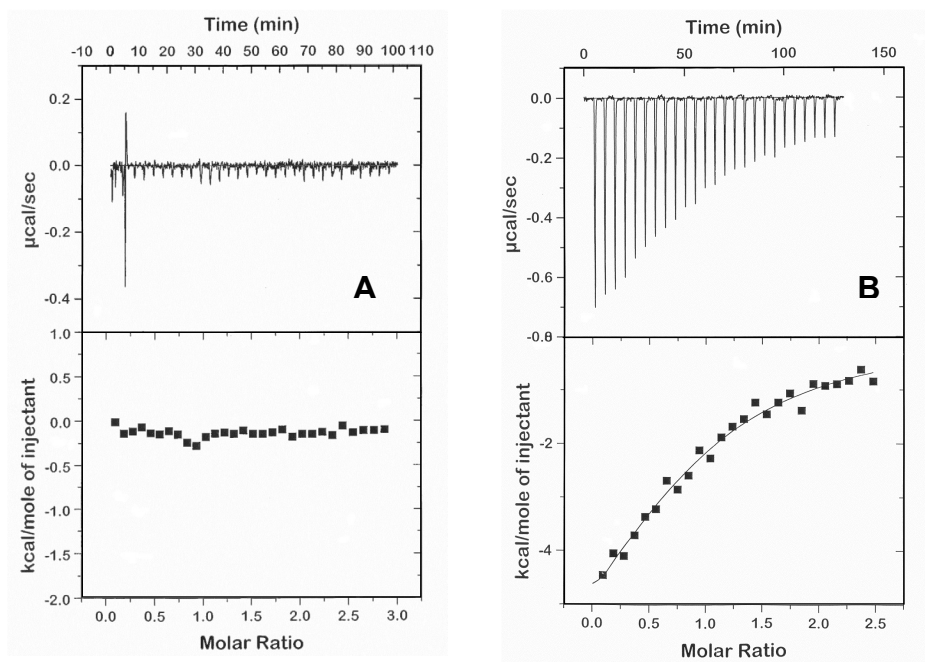


Figure 7. Isothermal titration calorimetry data showing the binding of 5'-rAMP to (A) E9- Ni^{2+} and (B) E9- Zn^{2+} . Top panel shows the calorimetric response of 25 10- μl injection of 5'-rAMP to 40 μM E9-DNase wild-type in 50 mM ammonium acetate pH 7.4. Bottom panel shows integrated injection heats for the above data fitted to a simple, non-cooperative binding model.

Discussion

We have shown in chapter 6 that phosphate ion binding (and possibly DNA substrate binding) is intriguingly regulated in the E9 DNase system. That is phosphate binding selectively occurs by preceding Zn^{2+} binding. In this chapter we further evaluated the metal (Ni^{2+} and Zn^{2+}) and phosphate-ligand (rAMP and dAMP) binding properties to the colicin E9 DNase. Therefore, we used ESI-MS and ITC in combination with site directed mutagenesis. The metal and phosphate-ligand binding capabilities have been put into context of the E9 DNase Zn^{2+} inhibition mechanism.

Hydrolysis of a phosphodiester bond requires three general entities in the active site: a general base to activate a nucleophile; a Lewis acid to stabilize the phospho-pentacoordinate

transition state; and a general acid to protonate the leaving group (22). As a result, some endonucleases share no sequence homology or overall structural resemblance, but have a similar active site. One example is the similarity observed in a small region between H-N-H homing endonucleases I-*PpoI*, *Serratia* nuclease, phage T4 endonuclease VII and nuclease colicin DNases E9 and E7. I-*PpoI* is a His-Cys box homing endonuclease that cleaves site specifically. *Serratia* nuclease is similar to E9 DNase that is both cleave rather non-specifically single-stranded and double stranded DNA and RNA (14). X-ray structures of I-*PpoI* and *Serratia* nuclease contain detailed information about their DNA hydrolysis mechanisms. A detailed comparison of the X-ray structures of I-*PpoI* and *Serratia* nuclease with that of E9 DNase let Pommer et al. postulate a mechanism for DNA hydrolysis in E colicin endonucleases (14) making the assumption that the activation of the hydrolytic water remains the role of H103. Subsequently, the Ni²⁺-coordinated water molecule fulfills the role as putative general acid, taking one of the four coordination sites of the metal ion. Pommer et al. stated that this would explain why Zn²⁺ does not support catalysis in colicin DNases since the bound transition metal ion would need to have two free metal coordination sites for catalysis to proceed, whereas only one is available in the E9-Zn²⁺ X-ray structure (14). In this work we have shown that H131 is involved in Ni²⁺ ligation and therefore Ni²⁺ does not have any longer two free coordination sites. This is only true, of course, when the maximum available coordination sites for Ni²⁺ in E9 DNase is indeed four (additional water molecules ligated to Ni²⁺, are not present in the available X-ray structures). Hence, it seems unlikely that E9 DNase is inactivated upon Zn²⁺ binding due to additional ligation of H131. The residue that fulfills the role as general acid is without further (structural) information still unclear.

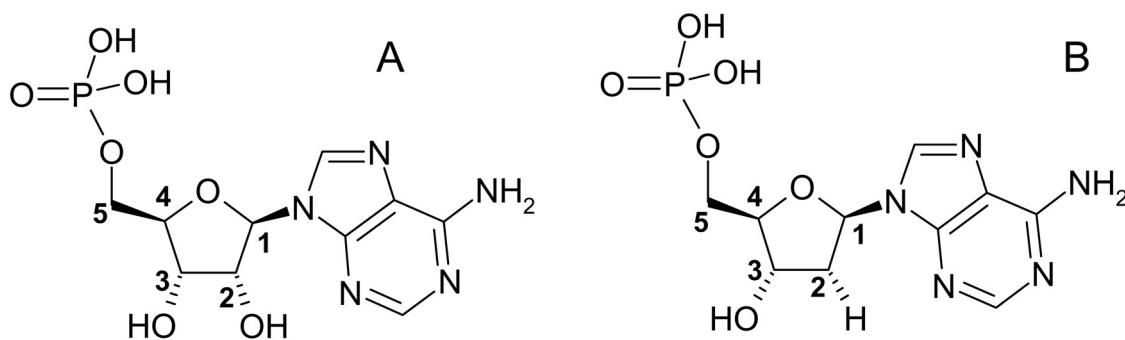


Figure 8. Structures of 5'-ribose AMP (A) and 5'-deoxyribose AMP (B).

From our data it is intriguing to speculate that due to H103-rAMP ligation, H103 cannot any longer coordinate a water molecule needed as general base. As a consequence, the water molecule cannot perform a nucleophilic attack at the phosphodiester bond to start hydrolysis. This residue is of high importance since it is conserved over all H-N-H homing endonucleases. However, our preliminary experiments on 5'-dAMP show no binding to E9-Zn²⁺ at all in striking

contrast to 5'-rAMP. Pommer et al. showed that the E9 DNase cleaves ssDNA, ssRNA and dsDNA, thereby demonstrating a lack of specificity for the sugar moiety of the nucleic acid (14). Our preliminary experiments suggest that 2'-OH of the ribose present in rAMP (lacking in dAMP) (Figure 8) must be involved in binding. Therefore, we conclude that more experiments are needed to further elucidate substrate and the role Zn^{2+} in the inhibition mechanism. For that reason, we intent to extend our ESI-MS, ITC and site directed mutagenesis experiments in combination with different single- and oligonucleotides in the near future.

Acknowledgments

I would like to thank Richard James and Chris Penfold for providing the colicin E9 DNase R5A, H103A and H131A mutants. Colin Kleanthous and Anthony Keeble for the H127A and H102A E9 DNase variants. Further I would like to acknowledge Eefjan Breukink for assistance with the ITC equipment at Utrecht University.

References

1. James, R., Penfold, C. N., Moore, G. R., and Kleanthous, C. (2002) Killing of *E. coli* cells by E group nuclease colicins *Biochimie* 84, 381-389.
2. Kleanthous, C., Kuhlmann, U. C., Pommer, A. J., Ferguson, N., Radford, S. E., Moore, G. R., James, R., and Hemmings, A. M. (1999) Structural and mechanistic basis of immunity toward endonuclease colicins *Nat. Struct. Biol.* 6, 243-252.
3. Kleanthous, C., Hemmings, A. M., Moore, G. R., and James, R. (1998) Immunity proteins and their specificity for endonuclease colicins: telling right from wrong in protein-protein recognition *Mol. Microbiol.* 28, 227-233.
4. Wallis, R., Moore, G. R., James, R., and Kleanthous, C. (1995a) Protein-protein interactions in colicin E9 DNase-immunity protein complexes. 1. Diffusion-controlled association and femtomolar binding for the cognate complex *Biochemistry* 34, 13743-13750.
5. Kuhlmann, U. C., Moore, G. R., James, R., Kleanthous, C., and Hemmings, A. M. (1999) Structural parsimony in endonuclease active sites: should the number of homing endonuclease families be redefined? *FEBS Lett.* 463, 1-2.
6. Galburt, E. A., and Stoddard, B. L. (2002) Catalytic mechanisms of restriction and homing endonucleases *Biochemistry* 41, 13851-13860.
7. Keeble, A. H., Hemmings, A. M., James, R., Moore, G. R., and Kleanthous, C. (2002) Multistep Binding of Transition Metals to the H-N-H Endonuclease Toxin Colicin E9 *Biochemistry* 41, 10234-10244.
8. Van den Bremer, E. T. J., Keeble, A., H., Jiskoot, W., Spelbrink, R. E. J., Maier, C. S., Van Hoek, A., Visser, A. J. W. G., James, R., Moore, G. R., Kleanthous, C., and Heck, A. J. R. (2004) Distinct conformational stability and functional activity of four highly homologous endonuclease colicins *Protein Sci.* (in press).
9. Walker, D. C., Georgiou, T., Pommer, A. J., Walker, D., Moore, G. R., Kleanthous, C., and James, R. (2002) Mutagenic scan of the H-N-H motif of colicin E9: implications for the mechanistic enzymology of colicins, homing enzymes and apoptotic endonucleases *Nucleic Acids Res.* 30, 3225-3234.

10. Sui, M. J., Tsai, L. C., Hsia, K. C., Doudeva, L. G., Ku, W. Y., Han, G. W., and Yuan, H. S. (2002) Metal ions and phosphate binding in the H-N-H motif: crystal structures of the nuclease domain of ColE7/Im7 in complex with a phosphate ion and different divalent metal ions *Protein Sci* 11, 2947-2957.
11. Ko, T. P., Liao, C. C., Ku, W. Y., Chak, K. F., and Yuan, H. S. (1999) The crystal structure of the DNase domain of colicin E7 in complex with its inhibitor Im7 protein *Structure Fold. Des.* 7, 91-102.
12. Hannan, J. P., Whittaker, S. B. M., Davy, S. L., Kuhlmann, U. C., Pommer, A. J., Hemmings, A. M., James, R., Kleanthous, C., and Moore, G. R. (1999) NMR study of Ni²⁺ binding to the H-N-H endonuclease domain of colicin E9 *Protein Sci.* 8, 1711-1713.
13. Kuhlmann, U. C., Pommer, A. J., Moore, G. R., James, R., and Kleanthous, C. (2000) Specificity in protein-protein interactions: the structural basis for dual recognition in endonuclease colicin-immunity protein complexes *J. Mol. Biol.* 301, 1163-1178.
14. Pommer, A. J., Cal, S., Keeble, A. H., Walker, D., Evens, S. J., Kuhlman, U. C., Cooper, A., Connolly, B. A., Hemmings, A. M., Moore, G. R., James, R., and Kleanthous, C. (2001) Mechanisms and cleavage specificity of the H-N-H endonuclease colicin E9 *J.Mol.Biol.* 314, 735-749.
15. Van den Bremer, E. T. J., Keeble, A., H., Kleanthous, C., and Heck, A. J. (submitted) Metal induced selectivity in phosphate ion binding in colicin E9 DNase.
16. Ku, W. Y., Liu, Y. W., Hsu, Y. C., Liao, C. C., Liang, P. H., Yuan, H. S., and Chak, K. F. (2002) The zinc ion in the HNH motif of the endonuclease domain of colicin E7 is not required for DNA binding but is essential for DNA hydrolysis *Nucleic Acids Res.* 30, 1670-1678.
17. Pommer, A. J., Wallis, R., Moore, G. R., James, R., and Kleanthous, C. (1998) Enzymological characterization of the nuclease domain from the bacterial toxin colicin E9 from *Escherichia coli* *Biochem. J.* 334, 387-392.
18. Van den Bremer, E. T. J., Jiskoot, W., James, R., Moore, G. R., Kleanthous, C., Heck, A. J. R., and Maier, C. S. (2002) Probing metal ion binding and conformational properties of the colicin E9 endonuclease by electrospray ionization time-of-flight mass spectrometry *Protein Sci.* 11, 1738-1752.
19. Wallis, R., Moore, G. R., Kleanthous, C., and James, R. (1992) Molecular analysis of the protein-protein interaction between the E9 immunity protein and colicin E9 *Eur. J. Biochem.* 210, 923-930.
20. Wallis, R., Reilly, A., Barnes, K., Abell, C., Campbell, D. G., Moore, G. R., James, R., and Kleanthous, C. (1994) Tandem overproduction and characterisation of the nuclease domain of colicin E9 and its cognate inhibitor protein Im9 *Eur. J. Biochem.* 220, 447-454.
21. Pommer, A. J., Kuhlmann, U. C., Cooper, A., Hemmings, A. M., Moore, G. R., James, R., and Kleanthous, C. (1999) Homing in on the role of transition metals in the HNH motif of colicin endonucleases *J. Biol. Chem.* 274, 27153-27160.
22. Pingoud, A., and Jeltsch, A. (1997) Recognition and cleavage of DNA by type-II restriction endonucleases *Eur. J. Biochem.* 246, 1-22.

Chapter 8

**Summarizing
discussion**

Colicins are bacterial protein antibiotics that are released in times of nutrient or environmental stress by *Escherichia coli* (1). The family of E-type colicins can be subdivided in two major groups, a) pore-forming colicins such as E1 (2) and b) nuclease colicins with either RNase activity (E3, E5 and E6) or DNase activity (E2, E7, E8, and E9) (3, 4). Colicins E2, E7, E8 and E9 are ~60 kDa endonucleases composed of three functional domains: the N-terminal translocation domain, the receptor binding domain and the C-terminal cytotoxic domain (5). Although the cell killing mechanism is still not completely understood, it apparently involves three steps. Initial binding of the endonuclease colicin to the BtuB extracellular receptor for vitamin B₁₂ is followed by translocation of the C-terminal cytotoxic DNase domain into the periplasm through the Tol system of proteins (see Chapter 1). As a result, cell death is caused by cleavage of the chromosomal DNA (6). Colicin endonucleases are very efficient bacterial killers that engage in a variety of molecular associations with target cells into which they transfer their C-terminal cytotoxic DNase domain. These DNase domains are therefore remarkable multifunctional proteins capable of binding co-factor metal ions, immunity proteins, DNA and even lipids (e.g. (7)). To gain further understanding in the cytotoxic mechanism of the DNase domain, investigation of molecular interactions and dynamics are important.

In this thesis I studied the C-terminal cytotoxic DNase domain of colicins E2, E7, E8 and E9.

The work described in **Chapter 3** shows that the cytotoxic domain of endonuclease colicin E9 exist at neutral pH in a dynamic equilibrium between a compact ‘closed’ and a loosely packed ‘open’ conformation. This is different to the heterogeneity observed in NMR (8, 9), i.e. the MS-based findings highlight protein heterogeneity on a globally level whilst heterogeneity observed by NMR is more localized. Binding of a transition metal ion (e.g. Zn²⁺) induces the protein to adopt an entirely closed conformation while, in this state the NMR observed heterogeneity is unaffected (8, 9). These ESI-MS findings are also confirmed with hydrogen/deuterium exchange experiments in which the closed conformation is shown to exchange ~20% less hydrogens than the open state.

The conformational equilibrium of E9 DNase is shifted gradually further to the loosely packed open state upon acidification, whereas the metal containing protein is stabilized till ~pH 5.5. Subsequently, at pH values < 5.5, the metal ion is released likely due to protonation of the three Zn²⁺ coordinating histidine residues, resulting into a completely destabilized E9 DNase. These findings are confirmed with steady-state fluorescence. Moreover, far-UV circular dichroism (CD) experiments show no significant changes upon acidification in secondary structure elements while near-UV CD experiments have indicated that the tertiary structure is lost upon acidification. Therefore, I have postulated that at least under acidic conditions the metal-free E9 DNase seems to adopt features that are reminiscent of molten-globule like states, that is, states that lack a fixed tertiary structure, but in which the secondary structure is retained.

(10, 11). In this regard it is intriguing to speculate that the local acidic pH at the membrane surface of the target cell triggers metal ion release, thereby, altering the DNase to adopt a molten-globule like state that may be required to translocate the DNase over the membrane of the target cell. (12-14).

The observed conformational equilibrium for E9 DNase was surprising. Therefore, I have extended this work to other colicin DNases i.e. E2, E7, and E8 as described in **Chapter 4**. This work demonstrates that there are marked differences in the conformational properties of the four apo-colicin DNases. These differences were *a priori* unexpected given the high sequence identities ($\geq 65\%$) and the known X-ray crystal structures of the DNase domains (15, 16).

The equilibrium found between a loosely packed open and a compact closed conformation is present in all four colicin DNases. However, the E7 DNase is biased towards the open form while E8 is more closed. E2 and E9 DNase behave intermediate. In summary, the conformational equilibrium observed follows, when ranked from mostly unfolded to more folded, the order $E7 < E9 \approx E2 < E8$.

However, care must be taken when relating the relative sizes of the two populations in the mass spectra to the fractional contributions of the protein conformers in solution since unfolded/open like states are usually detected more readily (17-20). To complement these MS-based findings solution phase experiments are conducted to determine the intrinsic tryptophan accessibility and the thermal stability. The results indicates that the two conserved (buried) tryptophans are accessible (on average) in the following order $E7 > E9 > E2 \approx E8$. For the thermal stability a similar result is obtained, i.e. $E7 < E9 \approx E2 < E8$.

Since it was supposed that these four proteins have identical folding properties and thus similar enzymatic activities, it was interesting to probe the DNase activities also as a function of temperature. The DNase activity assays on the four metal-free colicin DNases are performed in the presence of Mg^{2+} , the physiologically relevant divalent metal ion for DNA cleavage (21). The work described in Chapter 3 shows that Mg^{2+} does not significantly bind and/or stabilize the apo-DNases. However, the catalytic properties and activities of the four apo-colicin DNases show to differ strikingly, not only in catalytic rates, but also in selectivity and temperature dependence.

The observed differences in structural and functional behavior described in the present work cannot be explained on the basis of available X-ray structures. This may be caused by the fact that in solution there is a dynamic conformational equilibrium, whereas in X-ray crystallography primarily only a static lowest energy structure is probed.

Given the fact that the other parts of the sequences are highly similar, the differences in behavior are most likely a result of the sequence variation within the exosite (residues 72-98) that is required for specific high affinity binding of the cognate immunity protein. The greater sequence variation in this area is a consequence of the evolution of highly specific binding of the

cognate immunity protein over other, structurally similar, non-cognate immunity proteins. The hypothesis that this part of the sequence may be important in explaining the observed variation is supported by findings in the co-crystal structure of the E9 DNase with single-stranded DNA, which shows that residue Tyr83, which is non-conserved and a putative specificity determining residue for binding immunity proteins (22), intercalates with the DNA (23). The precise molecular origins of how the catalytic activities and thermal stabilities/conformational states are produced, are beyond the scope of the present study, but may have the focus of ongoing investigations.

A remaining question is whether the observed differences in conformational stability and activity of the apo-DNase domains of the four wild-type colicins have biological implications. It has been shown that the ability to insert and pass through the inner membrane (as judged by an *in vitro* lipid bilayer experiment) are similar for all colicins, both in the apo- and holo-form (7) and, thus, likely independent of thermal and structural stability. This argues against the proposal by Pommer *et al.* (24) that a structurally destabilized DNase domain might be important for colicin DNase uptake into the target cell. Additionally, all colicin DNases have temperature optima at or above 40 °C, which fits with the expected temperature of their natural *in vivo* environment (37-40 °C). The conformationally most stable colicin DNase E8 shows by far the highest *in vitro* activity in the present Kunitz assay. However, the impact of this on the *in vivo* cytotoxicity is unknown and may be subject for further analysis.

In order to gain a better understanding of the molecular origins and the complexity of the conformational changes that occur within colicin DNases, the interaction of the DNase protein with Zn^{2+} , and its cognate immunity protein, are investigated by using time-resolved fluorescence spectroscopy and steady-state fluorescence quenching studies. This work is described in **Chapter 5** and represents the first analysis of the conformational dynamics within colicin DNase domains on the nanosecond timescale. In order to probe the effects of Zn^{2+} and immunity protein binding to colicin DNases, we concentrate on the E9 DNase since it is the best characterized colicin DNase. A complicating factor in the analysis of time-resolved fluorescence data of colicin DNases is that the two tryptophans (W22 and W58) are located at a distance $<5\text{\AA}$ from each other (in the E9 DNase X-ray structure), which is close enough for energy transfer to occur (25). Therefore, single tryptophan mutants are constructed for E9 DNase, i.e., W58F (W22+) and W22F (W58+), enabling us to study the local environment of the individual tryptophans in the absence of any complicating energy transfer processes.

Wild-type E9 DNase, E9 W22F and E9 W58F, as well as Im9 showed multiple lifetime decays. The time-resolved and steady-state fluorescence results indicate that complexation of E9 DNase with Zn^{2+} induces compaction of the E9 DNase structure, accompanied by immobilization of Trp22 along with a reduction in solvent accessibility for both tryptophans. Im9 binding results in an immobilization of Trp22 along with a decrease in the longest lifetime

component. In contrast, Trp58 experiences less restriction on complexation of E9 DNase with Im9 and shows an increase in the longest lifetime component. The work described in this chapter shows via time-resolved tryptophan fluorescence and anisotropy how binding of Zn^{2+} and Im9, influences in a distinct manner the conformational dynamics of the DNase colicin E9. One feature both share is that these conformational differences are transmitted throughout the DNase protein from the metal binding site or from the immunity protein exosite to both tryptophans, which in this respect has not been detected with other techniques for colicin DNases so far. Moreover, the results of this study indicate that Im9 induced conformational effects predominate over Zn^{2+} induced effects.

The research described in **Chapter 6** shift the focus from conformational dynamics to non-covalent interactions. Although I have described these interactions in previous chapters, these were discussed more in terms of induced conformational effects. The functioning of proteins depends often on subtle, multiple, specific non-covalent interactions with other molecules, such as other proteins, metals, DNA/RNA, co-factors etc. Therefore, means to monitor and validate such interactions are important.

Several X-ray structures are available for the DNases E7 and E9. These structures confirm that the DNase proteins are able to coordinate a single transition metal ion within their active site. Zn^{2+} was observed in the reported E7 DNase structure (15), whilst Ni^{2+} was observed ligated to E9 DNase (16). Additionally, a single phosphate molecule has been observed in most of the reported X-ray structures, in close proximity to the active site of the DNase. These phosphate ions likely originate from the phosphate buffer solutions that are used in the preparation of the samples. This single phosphate ion is observed in the same location in X-ray structures of metal free E9 DNase (16), Ni^{2+} ligated E9 DNase (16), Zn^{2+} ligated E9 DNase (1FSJ PDB, unpublished), and Zn^{2+} ligated E7 DNase (15) and seems thus to be independent of the metal ion.

The work described in Chapter 6 shows the use of electrospray ionization mass spectrometry (ESI-MS) for the measurement of the ligation of a single phosphate ion for the enzyme colicin E9. To validate the ESI-MS based findings isothermal titration calorimetry experiments (ITC) were complementary conducted. These combined findings indicate that metal ion binding and phosphate ion binding (and possibly DNA substrate interactions) are intriguingly regulated in the E9 colicin DNase system. This is remarkable as the high-resolution X-ray structures available provided no clue for the observed behavior as both the position of the metal ion as well as the interactions with the amino acids in the catalytic site of the E9 DNase seem to be very similar.

In **chapter 7** we further evaluate the metal (Ni^{2+} and Zn^{2+}) and phosphate-ligand (rAMP and dAMP) binding properties to the colicin E9 DNase. Therefore, we used ESI-MS and ITC in

combination with site directed mutagenesis. The metal and phosphate-ligand binding capabilities have been put into context of the E9 DNase Zn^{2+} inhibition mechanism.

From our data it is intriguing to speculate that due to H103-rAMP ligation, H103 cannot any longer coordinate a water molecule needed as general base. As a consequence, the water molecule cannot perform a nucleophilic attack at the phosphodiester bond to start hydrolysis. This residue is of high importance since it is conserved over all H-N-H homing endonucleases. However, our preliminary experiments on 5'-dAMP show no binding to E9- Zn^{2+} at all, in striking contrast to 5'-rAMP. Pommer et al. showed that the E9 DNase cleaves ssDNA, ssRNA and dsDNA, thereby demonstrating a lack of specificity for the sugar moiety of the nucleic acid (26). Our preliminary experiments suggest that 2'-OH of the ribose present in rAMP (lacking in dAMP) (Figure 8) must be involved in binding. Therefore, we conclude that more experiments are needed to further elucidate substrate and the role Zn^{2+} in the inhibition mechanism. For that reason, we intent to extend our ESI-MS, ITC and site directed mutagenesis experiments in combination with different single- and oligonucleotides in the near future.

References

1. James, R., Penfold, C. N., Moore, G. R., and Kleanthous, C. (2002) Killing of *E. coli* cells by E group nuclease colicins *Biochimie* 84, 381-389.
2. Cramer, W. A., Cohen, F. S., Merrill, A. R., and Song, H. Y. (1990) Structure and dynamics of the colicin E1 channel *Mol. Microbiol.* 4, 519-526.
3. Lau, P. C. K., Parsons, M., and Uchimura, T. (1992) in *Bacteriocins, Microcins and Lantibiotics* (James, R., Lazdunski, C., and Pattus, F., Eds.) pp 353-348, Springer-Verlag, Berlin.
4. Masaki, H., Yajima, S., Akutsu-Koide, A., Ohta, T., and Uozumi, T. (1992) in *Bacteriocins, Microcins and Lantibiotics* (James, R., Lazdunski, C., and Pattus, F., Eds.) pp 379-395, Springer-Verlag, Berlin.
5. Kleanthous, C., Hemmings, A. M., Moore, G. R., and James, R. (1998) Immunity proteins and their specificity for endonuclease colicins: telling right from wrong in protein-protein recognition *Mol. Microbiol.* 28, 227-233.
6. Pommer, A. J., Wallis, R., Moore, G. R., James, R., and Kleanthous, C. (1998) Enzymological characterization of the nuclease domain from the bacterial toxin colicin E9 from *Escherichia coli* *Biochem. J.* 334, 387-392.
7. Mosbahi, K., Lemaitre, C., Keeble, A. H., Mobasher, H., Morel, B., James, R., Moore, G. R., Lea, E. J., and Kleanthous, C. (2002) The cytotoxic domain of colicin E9 is a channel-forming endonuclease *Nat. Struct. Biol.* 9, 476-484.
8. Whittaker, S. B., Boetzel, R., MacDonald, C., Lian, L. Y., Pommer, A. J., Reilly, A., James, R., Kleanthous, C., and Moore, G. R. (1998) NMR detection of slow conformational dynamics in an endonuclease toxin *J. Biomol. NMR.* 12, 145-159.
9. Whittaker, S. B., Czisch, M., Wechselberger, R., Kaptein, R., Hemmings, A. M., James, R., Kleanthous, C., and Moore, G. R. (2000) Slow conformational dynamics of an endonuclease persist in its complex with its natural protein inhibitor *Protein Sci.* 9, 713-720.
10. Le, W. P., Yan, S. X., Zhang, Y. X., and Zhou, H. M. (1996) Acid-induced folding of yeast alcohol dehydrogenase under low pH conditions *J. Biochem. (Tokyo)* 119, 674-679.

11. Chak, K.-F., Hsieh, S.-Y., Lao, C.-C., and Kan, L.-S. (1998) Change of thermal stability of colicin E7 triggered by acidic pH suggests the existence of unfolded intermediate during the membrane-translocation phase *Proteins* 32, 17-25.
12. Prats, M., Teisić, J., and Tocanne, J.-F. (1986) Lateral proton conduction at lipid-water interfaces and its implications for the chemiosmotic-coupling hypothesis *Nature* 322, 756-758.
13. Bychkova, V. E., Dujsekina, A. E., Klenin, S. I., Tiktopulo, E. I., Uversky, V. N., and Ptitsyn, O. B. (1996) Molten globule-like state of cytochrome c under conditions simulating those near the membrane surface *Biochemistry* 35, 6058-6063.
14. McLaughlin, S. (1989) The electrostatic properties of membranes *Annu. Rev. Biophys. Biophys. Chem.* 18, 113-136.
15. Ko, T. P., Liao, C. C., Ku, W. Y., Chak, K. F., and Yuan, H. S. (1999) The crystal structure of the DNase domain of colicin E7 in complex with its inhibitor Im7 protein *Structure Fold. Des.* 7, 91-102.
16. Kleanthous, C., Kuhlmann, U. C., Pommer, A. J., Ferguson, N., Radford, S. E., Moore, G. R., James, R., and Hemmings, A. M. (1999) Structural and mechanistic basis of immunity toward endonuclease colicins *Nat. Struct. Biol.* 6, 243-252.
17. Van den Bremer, E. T. J., Jiskoot, W., James, R., Moore, G. R., Kleanthous, C., Heck, A. J. R., and Maier, C. S. (2002) Probing metal ion binding and conformational properties of the colicin E9 endonuclease by electrospray ionization time-of-flight mass spectrometry *Protein Sci.* 11, 1738-1752.
18. Cech, N. B., and Enke, C. G. (2000) Relating electrospray ionization response to nonpolar character of small peptides *Anal. Chem.* 72, 2717-2723.
19. Cech, N. B., and Enke, C. G. (2001) Effect of affinity for droplet surfaces on the fraction of analyte molecules charged during electrospray droplet fission *Anal. Chem.* 73, 4632-4639.
20. Dobo, A., and Kaltashov, I. A. (2001) Detection of multiple protein conformational ensembles in solution via deconvolution of charge-state distributions in ESI MS *Anal. Chem.* 73, 4763-4773.
21. Walker, D. C., Georgiou, T., Pommer, A. J., Walker, D., Moore, G. R., Kleanthous, C., and James, R. (2002) Mutagenic scan of the H-N-H motif of colicin E9: implications for the mechanistic enzymology of colicins, homing enzymes and apoptotic endonucleases *Nucleic Acids Res.* 30, 3225-3234.
22. Curtis, M. D., and James, R. (1991) Investigation of the specificity of the interaction between colicin E9 and its immunity protein by site-directed mutagenesis *Mol. Microbiol.* 5, 2727-33.
23. Kolade, O. O., Carr, S. B., Kuhlmann, U. C., Pommer, A., Kleanthous, C., Bouchcinsky, C. A., and Hemmings, A. M. (2002) Structural aspects of the inhibition of DNase and rRNase colicins by their immunity proteins *Biochimie* 84, 439-446.
24. Pommer, A. J., Kuhlmann, U. C., Cooper, A., Hemmings, A. M., Moore, G. R., James, R., and Kleanthous, C. (1999) Homing in on the role of transition metals in the HNH motif of colicin endonucleases *J. Biol. Chem.* 274, 27153-27160.
25. Keeble, A. H., Hemmings, A. M., James, R., Moore, G. R., and Kleanthous, C. (2002) Multistep Binding of Transition Metals to the H-N-H Endonuclease Toxin Colicin E9 *Biochemistry* 41, 10234-10244.
26. Pommer, A. J., Cal, S., Keeble, A. H., Walker, D., Evens, S. J., Kuhlman, U. C., Cooper, A., Connolly, B. A., Hemmings, A. M., Moore, G. R., James, R., and Kleanthous, C. (2001) Mechanisms and cleavage specificity of the H-N-H endonuclease colicin E9 *J. Mol. Biol.* 314, 735-749.

List of abbreviations

CD	circular dichroism
CsI	cesium iodide
Da	dalton
DSC	differential scanning calorimetry
E9 DNase	C-terminal cytotoxic domain of endonuclease colicin E9
H102A	E9 DNase mutant in which histidine 102 is substituted to alanine
H103A	E9 DNase mutant in which histidine 103 is substituted to alanine
H127A	E9 DNase mutant in which histidine 127 is substituted to alanine
H131A	E9 DNase mutant in which histidine 131 is substituted to alanine
H/D	hydrogen/deuterium
Im	immunity protein
ITC	isothermal titration calorimetry
K_d	dissociation constant
MALDI	matrix-assisted laser desorption/ionization
m/z	mass-to-charge ratio
nano-ESI-MS	nano-flow electrospray ionization mass spectrometry
NMR	nuclear magnetic resonance
R5A	E9 DNase mutant in which arginine 5 is substituted to alanine
TOF	time-of-flight
W58+	E9 DNase mutant that contains only Trp58
W22+	E9 DNase mutant that contains only Trp22

Nederlandse samenvatting

Voor allen die altijd met veel belangstelling (of geduld) luisterden naar de verhalen over mijn avonturen op het lab, maar wie ik in veel gevallen een goede uitleg over wat ik daar uitvoerde schuldig bleef:

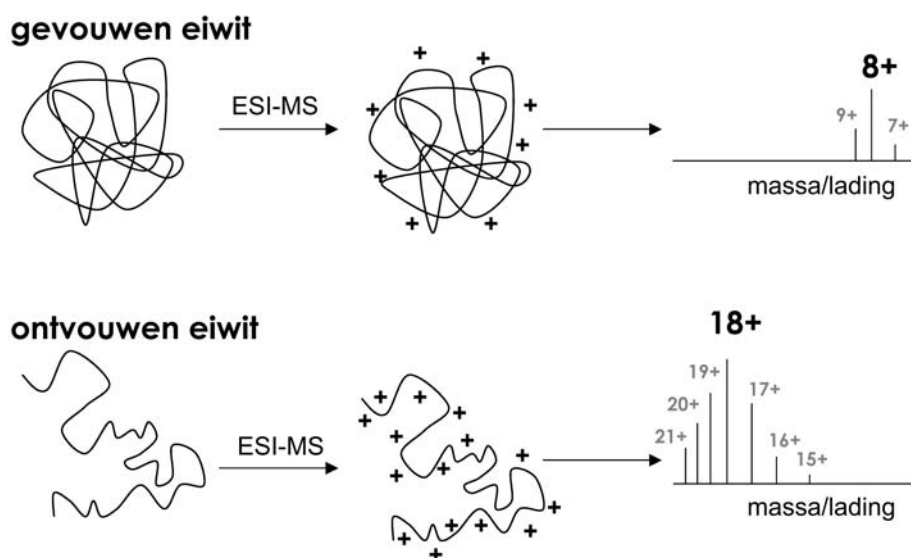
Elk levend organisme bestaat uit één (bijvoorbeeld een bacterie) of meerdere cellen (bijvoorbeeld de mens). In elke cel spelen zich allemaal ingewikkelde processen zich af om de cel in leven te houden en om de cel een specifieke taak te geven. Bijvoorbeeld een zenuwcel, spiercel, of een gistcel, ze doen totaal verschillende dingen. De processen die hierin plaatsvinden worden uitgevoerd door eiwitten, deze zijn als het ware de werkpaarden van het leven. Elk eiwit heeft zijn specifieke functie en met zoveel verschillende type cellen is het niet moeilijk om je voor te stellen dat er zeer veel verschillende eiwitten nodig zijn. Hoe kan je daarin dan zoveel diversiteit krijgen? Eiwitten bestaan uit ketens van soms wel honderden aminozuren lang. Zoals woorden in onze taal opgebouwd worden uit 26 letters, worden eiwitten opgebouwd uit 20 verschillende aminozuren welke uiteindelijk de structuur en de eigenschappen van het eiwit bepalen. De aminozuurvolgorde en -samenstelling zijn kenmerkend voor het betreffende eiwit. Je kunt je dus voorstellen dat er op deze manier een enorme variatie aan eiwitten mogelijk is. Hoe ziet zo'n structuur er dan uit? Kijk bijvoorbeeld in Hoofdstuk 4 naar Figuur 1B. Dit is een weergave van een eiwit dat ik bestudeerd heb. Wat doet dit eiwit eigenlijk? Dit eiwit (colicin E9) wordt aangemaakt door een bacterie (*Escherichia coli*) als het stress heeft bijvoorbeeld bij de aanwezigheid van te weinig voedsel. Vervolgens wordt dit eiwit buiten de cel gebracht en dringt het door een ingewikkeld proces (translocatie) bij een ander type maar wel soort gelijke bacterie naar binnen. Uiteindelijk wordt het DNA van deze bacterie aan stukjes geknipt en kan bacterie niet meer functioneren en komt te overlijden waardoor er meer kans op overleven bestaat voor de colicin E9 producerende bacterie. Wat Figuur 1B van Hoofdstuk 4 laat zien is alleen dat deel van het eiwit wat naar binnen dringt en verantwoordelijk is voor het bacteriedodende effect (het DNase- domein). De afgelopen vier jaar heb ik alleen aan dit deel van het colicin E9 eiwit onderzoek gedaan. Verder laat het figuur maar één structuur (kristalstructuur) zien alsof het in een bevroren toestand is. In werkelijkheid zwemmen ze in een oplossing (bijv. in waterige vloeistof binnen in de cel) en is hun structuur flexibel. Bijvoorbeeld ze vouwen zich op en ontvouwen zich weer, telkens weer opnieuw en kunnen dus tijdelijk verschillende vormen aannemen. Deze vormen zijn dan in, wat we noemen, dynamisch evenwicht. Voor een eiwit kan dit heel belangrijk zijn om zijn functie goed te kunnen uitvoeren. Verder werken eiwitten zelden alleen en werken ze samen met bijvoorbeeld andere eiwitten, metaaldeeltjes (bijv. koper, zink, mangaan) of andere verbindingen (bijv. vitaminen, kleine hormonen of zelfs DNA). Colicin E9 werkt ook niet alleen. Zoals je ziet in Figuur 1 van Hoofdstuk 3 “plakt” er nog een ander eiwit aan het E9 DNase-domein vast. Dit eiwit noemen we het immuniteitseiwit (Im9). Dit “plakken” noemen we een niet-covalente interactie. Het Im9 eiwit is belangrijk, omdat het indirect de plek

blokkeert van het E9 DNase-domein waar het DNA knippen plaats vindt. Als het Im9 eiwit er niet zou zijn, dan zou het E9 eiwit al te vroeg van start gaan en het DNA van zijn eigen cel in stukjes knippen en wordt het zelfmoord, hetgeen nooit de bedoeling kan zijn. Zoals je ziet in hetzelfde figuur plakt er ook nog wat anders aan het E9 eiwit. Dit is een metaalion (deeltje) dat als extra handje kan fungeren. Metaaldeeltjes kunnen verschillende functies hebben bijv. het op zijn plek houden van een watermolecuul dat nodig is om een enzymatische reactie te kunnen starten. Maar deze handjes kunnen ook een eiwit stabiliseren door bijvoorbeeld het instandhouden van de gevouwen vorm.

Door meer inzicht te krijgen in het dynamisch gedrag van een eiwit en in de samenwerking met bijv. andere eiwitten en metaalionen, kunnen we vaak beter begrijpen hoe deze ingewikkelde machine te werk gaat. Zoals ik al eerder schreef, zijn colicins antibacteriële eiwitten. Ik zie je al denken: waarom is dit belangrijk voor ons en geef ik daar al mijn belastingcenten aan uit? Dit is een veel gestelde vraag. Vandaag de dag worden vele type bacteriën resistent voor de antibiotica die we van de huisarts kennen. Het ontwikkelen van resistentie gaat in een erg snel tempo en over een aantal decennia kunnen we de huidige antibiotica nog maar moeilijk gebruiken. Daarom is het belangrijk om nu meer inzicht te krijgen in de werking van andere antibacteriële systemen, zodat men misschien tegen die tijd een alternatief op de plank heeft liggen om bacteriële infecties tegen te gaan.

Eiwitten kunnen bestudeerd worden met verschillende (biofysische) technieken, die allemaal hun voor- en nadelen hebben. Ik heb voor een nieuwe techniek gekozen om eiwitten te bestuderen, namelijk electrospray ionisatie massaspectrometrie (ESI-MS). Deze techniek wordt voornamelijk gebruikt om de moleculaire massa van eiwitten en peptiden (stukjes eiwit) heel nauwkeurig te bepalen. Het belang van deze techniek voor het onderzoek werd in 2002 onderstreept met het uitreiken van de Nobelprijs voor scheikunde aan de uitvinder van electrospray massaspectrometrie. Deze techniek wordt dan ook in heel veel laboratoria toegepast als algemene analytische techniek. Het gebruiken van deze techniek om eiwitconformaties (of eiwitvouwing) te bestuderen is nog zeker geen standaard methode die in elk lab gebruikt wordt. Nu vraag je je natuurlijk af hoe we met een apparaat dat massa's meet ook eiwit conformaties kunnen bestuderen. Hiervoor moet ik eerst wat uitleggen over de massaspectrometer (zie hoofdstuk 2, Figuur 1). Hier zie je dat eerst de eiwit oplossing wordt verstoven onder elektrische spanning (1200 V) tot kleine geladen druppeltjes (bijv. positief geladen). Vervolgens verdampen de vluchtige stoffen en houden we niet-vluchtige positief geladen deeltjes (bijv. eiwitten) over die vervolgens de massaspectrometer ingaan. In het apparaat leggen deze deeltjes allemaal een vaste afstand af en elk type deeltje neemt zijn eigen tijd ervoor om naar de detector toe te vliegen. De vliegtijd van het molecuul hangt van twee dingen af. Dat zijn de massa en de lading van het eiwit. Het resultaat dat we meten is het quotiënt van massa en lading (massa/lading). De hoeveelheid lading die we mee kunnen geven aan een eiwit tijdens het vernevelingsproces is afhankelijk van

de hoeveelheid plekken waarop zo'n positieve lading kan zitten en de toegankelijkheid van die plekken. Als een eiwit gevouwen en compact is wordt het binnenste van het eiwit afgeschermd van de vloeistof dat zich om het eiwit bevindt en kunnen de aminozuren die graag een positieve lading willen die niet krijgen. Als het eiwit ontvouwen is zijn diezelfde aminozuren beter toegankelijk en kan er aan het eiwit meer lading meegegeven worden tijdens het vernevelingsproces. Dus een oplossing van eiwit moleculen bij lage pH (meer ontvouwen) geeft een ander massaspectrum (piekenpatroon) dan een oplossing van hetzelfde eiwit bij neutrale pH, als gevolg van het verschil in lading (bij gelijke massa). Bijvoorbeeld voor het colicin E8 DNase-domein bij pH 4 krijgen de meeste van deze een 18+ lading, terwijl bij neutrale pH de meeste van deze eiwit moleculen een lading van 8+ krijgen (zie Figuur 1). De hoeveelheid ladingen die een eiwit kan krijgen, gevouwen of ontvouwen, is voor elk eiwit weer anders.



Figuur 1. ESI-MS karakteristieken voor gevouwen en ontvouwen eiwitten.

Verder kan je met massaspectrometrie in combinatie met deze vernevelingstechniek uiteraard massa's meten van het gehele eiwit. Maar het mooie van deze spraymethode is dat het veelal de zwakke niet-covalente interacties intact laat. Dus zo kan je ook conformatieveranderingen bestuderen als het bijvoorbeeld een metaalion, of een ander eiwit bindt.

Zoals ik al eerder aangaf, is het bestuderen van eiwitconformaties via deze techniek relatief nieuw. Verder meet je ook nog eens in de gasfase en niet in de vloeistoffase waar het echte leven zich afspeelt. Dus je moet je afvragen over wat er gemeten wordt in de gas fase klopt met wat er in werkelijkheid, de vloeistoffase, gebeurt. Daarom heb ik naast ESI-MS, technieken gebruikt die al veel langer bestaan en waarvan duidelijk is wat voor resultaten je krijgt als je conformatieveranderingen waarneemt terwijl het eiwit in oplossing is (i.p.v. als het aan het

vliegen is). De belangrijkste techniek die ik daarvoor heb gebruikt is fluorescentie. Deze probeer ik daarom in het kort uit te leggen.

Fluorescentiemetingen vinden plaats in het donker. Het apparaat schijnt met een speciaal licht door een glazen buisje die een waterige eiwitoplossing bevat. Een deel van dit licht wordt door de eiwitmoleculen opgenomen. Vervolgens wordt er onder een hoek van 90° gemeten (zodat je niet tegen lichtbron in meet) en wordt er gekeken wat voor licht er weer uit komt. Het licht wordt dus eerst opgenomen door het eiwit molecuul en zendt het zeer snel daarna zeer snel weer uit. Het verschil tussen de hoeveelheid en het type licht dat er ingaat en er uit komt wordt geeft informatie over de conformatie van het eiwit. Om licht op te kunnen nemen en uit te kunnen stralen heeft het eiwit een soort vlaggetje nodig (label). De meeste eiwitten hebben van nature één of meerdere aminozuren die als vlaggetje kunnen fungeren, bijv. het aminozuur tryptofaan. Als dit aminozuur helemaal in het binnenste van het eiwitmolecuul zit straalt het ander licht uit dan wanneer het meer aan de buitenkant van het eiwit zit. Dus mocht een tryptofaan residu in het binnenste van een compact gevouwen eiwit molecuul zitten, straalt het ander licht uit dan wanneer diezelfde tryptofaan in een ongevouwen eiwitconformatie zit. Fluorescentiemetingen kunnen op vele verschillende manieren worden uitgevoerd, afhankelijk van welke informatie je nodig hebt. Bij hele specialistische metingen kan zelfs worden gekeken naar hoe het vlaggetje ronddraait maar ook naar de omwentelingen van het hele eiwit. Is een eiwit compact opgevouwen dan heeft het een kleinere draaiings-as en zal de tijd die het erover doet om één omwenteling te maken korter zijn dan hetzelfde eiwit dat meer ontvouwen is. Deze experimenten vergen zeer specialistische apparatuur omdat een eiwit molecuul al volledig ronddraait in slechts enkele nanoseconden (1 nanoseconde is 0,000.000.001 seconde), Daarvoor zijn weer hele snelle pulserende lasers nodig (om door de eiwitoplossing te schijnen) en snelle en gevoelige detectiesystemen.

Dit proefschrift

In dit proefschrift beschrijf ik een studie naar de structuur-functierelaties van E-type colicin DNase eiwitten. In **Hoofdstuk 1** heb ik een inleiding gegeven over de colicin biologie. Daarin heb ik beschreven welke studies al aan colicins zijn gedaan en waar colicins vandaan komen en uitgelegd waarvoor ze gemaakt zijn.

In **Hoofdstuk 2** heb ik beschreven wat er zoal gepubliceerd is op het gebied van massaspectrometrie in het kader van eiwitconformatiestudies en niet-covalente interacties tussen eiwitten en andere moleculen of ionen.

In **Hoofdstuk 3** heb ik aangetoond dat het E9 DNase domein twee conformaties heeft bij een neutrale pH (zuurgraad). De ene vorm is open en losjes gepakt terwijl de andere meer compact en gesloten is. Dit was nog niet eerder gezien met andere technieken voor E9 DNase en daarom was deze uitkomst erg verrassend. Als het E9 DNase een zinkion bindt verandert de

open, losjes gepakte vorm volledig in de compacte gesloten vorm. Vervolgens heb ik beide situaties met en zonder zink bij verschillende pH waarden gemeten. Het blijkt dat het zink ion losgelaten wordt onder een pH waarde van 5.5 en als resultaat is het eiwit weer gedestabiliseerd. Dit heb ik ook direct in oplossing kunnen meten m.b.v. fluorescentie.

In **Hoofdstuk 4** heb ik ook naar andere DNase-domeinen uit diezelfde familie gekeken (E2, E7, E8), omdat de resultaten die beschreven zijn in Hoofdstuk 3 erg verrassend waren. Deze andere drie eiwitten E2, E7 en E8 lijken erg veel op E9 en ze hebben allemaal dezelfde functie. Zoals we al eerder bij E9 DNase hebben gezien bij afwezigheid van zink (een open en een gesloten conformatie), zien we na een ESI-MS analyse vrijwel hetzelfde voor E2 DNase. De resultaten voor E7 en E8 waren echter onverwacht anders. E8 DNase laat voornamelijk een gevouwen compacte vorm zien terwijl E7 meer dan E2 en E9 ontvouwen is. Dus samengevat van ontvouwen naar meest gevouwen: $E7 < E9 \approx E2 < E8$. In aanwezigheid van zink krijgen alle vier DNase domeinen een gevouwen compacte vorm. Dit heb ik ook met fluorescentie kunnen aantonen door te kijken hoe toegankelijk de tryptofaangroepen (vlaggetjes) zijn. Uit deze analyse blijkt weer dat tryptofaangroepen het meest toegankelijk zijn voor E7 en minst voor E8, wat er op duidt dat E7 wat meer losjes ontvouwen is dan E8. De aanwezigheid van zink maakt in alle vier de DNase-domeinen de tryptofanen behoorlijk ontoegankelijk, wat er weer op duidt dat door metaalbinding deze eiwitten compact opgevouwen zijn. Als laatste heb ik differentiële scanning calorimetrie (DSC) gebruikt om de thermische stabiliteit van deze vier eiwitten in oplossing te meten en weer blijkt dat E7 het minst stabiel is en E8 het meest stabiel met E2 en E9 ertussenin.

In **Hoofdstuk 5** heb ik een wat meer gespecialiseerde fluorescentietechniek gebruikt om de beweeglijkheid het E9 DNase-domein wat meer in detail te bestuderen. Maar om deze techniek goed te kunnen gebruiken moest eerst aan het E9 DNase-domein wat gesleuteld worden. Het E9 DNase-domein bevat van nature twee tryptofaan aminozuren (de vlaggetjes, W22 en W58) maar deze zitten in de driedimensionale structuur erg dichtbij elkaar. Als je in detail wilt kijken naar de eigenschappen het vlaggetje kan het erg storend werken dat ze vlak naast elkaar zitten. Daarom zijn er twee varianten van dit eiwit gemaakt met elk één vlaggetje (W22+ en W58+).

Ik heb het gedrag van deze vlaggetjes bestudeerd in aan- en afwezigheid van zink, met en zonder het immuniteits-eiwit (Im9) en in een combinatie met beide (E9-Zn-Im9). De resultaten laten zien dat het W22 vlaggetje na zink binding niet meer ronddraait en dat het gehele eiwitmolecuul sneller gaat omwentelen, wat er op duidt dat het E9 DNase-domein een compactere vorm heeft gekregen. Het W58 vlaggetje blijft nog wel ronddraaien, maar heeft beduidend minder de ruimte gekregen. Als het E9 DNase-domein (zowel W22+ als W58+) Im9 bindt, dan worden alle door zink geïnduceerde effecten tenietgedaan en zijn de effecten die door Im9-binding worden veroorzaakt dominant.

In **Hoofdstuk 6** heb ik gekeken naar de niet-covalente interacties van het fosfaatmolecuul dat gevonden is in verschillende E9 en E7 DNase kristalstructuren. Het functioneren van eiwitten hangt vaak af van vele kleine subtiele niet-covalente interacties met andere moleculen, zoals andere eiwitten, metalen, DNA/RNA en co-factoren. Het is daarom belangrijk om meer zicht te krijgen in zulke interacties.

Het werk beschreven in dit hoofdstuk laat zien dat je met ESI-MS specifiek één niet-covalent gebonden fosfaatmolecuul kan aantonen. Dit heb ik bevestigd met isotherme titratie calorimetrie (ITC), een techniek waarmee je interacties in oplossing kunt volgen door het meten van vrijgekomen warmte. Deze bevindingen laten zien dat metaalbinding en fosfaation-binding (een misschien DNA binding, omdat DNA veel fosfaatgroepen heeft) nauwkeurig gereguleerd zijn. Dit omdat fosfaat alleen maar bindt in aanwezigheid van zink, terwijl de hoge-resolutie kristalstructuren suggereren dat dit niet zo is.

In **Hoofdstuk 7** ben ik verder gegaan met de bevindingen uit hoofdstuk 6. Nu is het zo dat in de aanwezigheid van zink het E9 DNase-domein inactief is, terwijl nikkel uitstekend kan helpen om knippen van DNA op gang te brengen. Het E9 DNase-domein is in combinatie met een nikkalion niet in staat om een enkel fosfaation specifiek te laten binden. Dus misschien kan dit betrekking hebben op de inactivatie van het DNase-domein in aanwezigheid van zink. In dit hoofdstuk hebben we gekeken naar enkele bouwstenen van het DNA en RNA. Eén bouwsteen DNA/RNA bevat ook één fosfaatgroep. (zie Hoofdstuk 7 figuur 8). Verder hebben we verschillende E9 DNase-mutanten (varianten) gemaakt, zodat we kunnen kijken welke aminozuren verantwoordelijk zijn voor fosfaatbinding. De eerste resultaten laten zien dat het fosfaatgedeelte van een bouwsteen van RNA (rAMP) interactie heeft met het aminozuur His103 (histidine) alleen in de aanwezigheid van zink. Van dit aminozuur wordt verondersteld dat het een belangrijke functie heeft in het DNA knipproces. In eerste instantie leek het logisch dat het voor een enkele bouwsteen van DNA (dAMP) hetzelfde moest gelden, maar nu blijkt uit eerste metingen dat het toch niet zo is. Dit was verrassend omdat de literatuur vermeldde dat alleen het fosfaatgedeelte betrokken zou zijn bij binding aan het E9 DNase-domein. Het enige verschil tussen rAMP en dAMP is een $-OH$ groep (zie Hst 7 figuur 8). Dus zeer waarschijnlijk is deze extra $-OH$ groep in rAMP betrokken bij E9-Zn-rAMP binding. Om dit beter te kunnen begrijpen moeten er meer experimenten gedaan worden.

In **Hoofdstuk 8** heb ik de in dit proefschrift verkregen resultaten en de betekenis ervan nog eens op een rijtje gezet.

Dankwoord

Mijn boekje is af! Het (schrijf)werk zit er op. Ik moet zeggen dat het een erg goed gevoel geeft. De afgelopen vier jaren heb ik een leuke tijd gehad en ze zijn omgevlogen. Zonder de hulp van vele mensen om mij heen had ik dit onderzoek nooit tot een goed einde kunnen brengen. Daarom wil ik van deze gelegenheid gebruik maken om een aantal mensen te bedanken.

Allereerst wil ik mijn begeleider en promotor Albert bedanken die zich in de afgelopen vier jaren heeft ingezet voor mijn onderzoek. Albert, jouw enthousiasme en betrokkenheid bij mijn onderzoek heb ik altijd erg gewaardeerd. Aanvankelijk zou ik aan het vancomycineproject gaan werken, maar je vertelde dat je een interessant eiwit had gekegen, het colicin E9 DNase eiwit, en of ik daar eerst een maandje aan wilde gaan meten. Je ziet het resultaat, het maandje is uiteindelijk toch wat langer geworden met een heel boekje vol aan resultaten. Verder waardeer ik het zeer dat je me de mogelijkheid hebt gegeven om naast massaspectrometrie ook andere analyse technieken erbij te mogen betrekken. Het maakte het werk erg leuk en afwisselend met daarbij een aantal leuke samenwerkingen.

Colin, I would like to thank you for the great and productive collaboration we had over the past four years. Thank you and your people in the lab for providing me with all the colicin and immunity proteins. I had a great time during the colicin mini-symposia and I enjoyed working in your lab and maybe some day I will stop by. Anthony, our communication could not be better. Swapping e-mails from Utrecht to York and *vice versa*, sometimes three times within five minutes with remarks, suggestions, results, manuscripts, etc. etc., it was like I was permanently in the colicin lab. Thanks for your interest and critical view on my work. I had a great time working with you.

Wim, op zoek naar een fluorimeter in het Went-gebouw en na wat rondvragen hier en daar kwam ik al snel bij jou terecht. Je was al gauw erg enthousiast over mijn onderzoek en tot de dag van vandaag is dat zo gebleven. Je bent er steeds meer bij betrokken geraakt en uiteindelijk ben je mijn copromotor geworden. Bedankt voor het nakijken van de manuscripten en zo. Ik ben nog niemand tegengekomen die dat zo snel en gedetailleerd doet. Je hebt me in contact gebracht met fluorescentiespecialist prof. Ton Visser in Wageningen wat ook weer tot een leuke samenwerking en een publicatie heeft geleid. Claudia, ik wil je bedanken dat je voor mij in de eerste twee jaar van het AIO'ën het aanspreekpunt was. Ik heb veel van je kunnen leren en je kennis van de literatuur was altijd erg up-to-date. Hopelijk heb het erg naar je zin aan de Oregon State University.

Hier in de vakgroep heb ik de afgelopen vier jaar een enorme keur aan collega's gehad. De uitdaging om ze allemaal op te noemen wil ik niet aangaan, dus bij deze wil ik iedereen bedanken. Ik heb een hele leuke tijd gehad! Bij een aantal wil ik echter wel eventjes stilstaan. Edwin en kamergenote Annemieke, leuk dat jullie mijn paranimfen zijn. Ik zal nog vaak aan de vele Catan-avondjes terugdenken. Edwin, veel succes in San Diego. Jeroen als je weer terug bent

uit New York moeten we maar weer eens partijtje gaan squashen. Ik heb niet stilgezeten misschien kan ik nu dus wel wat vaker van je winnen. Kees, bedankt voor je nooit aflatende technische bijstand. Ik heb veel van je kunnen leren. Verder wil ik mijn student Robin bedanken voor zijn verrichte werk.

Buiten het werk heb heel veel gehad aan mijn vrienden, kennissen en familie. Ze zorgden voor de nodige afleiding en ontspanning. Bedankt voor jullie geduld en interesse! Ik hoop dat jullie na het lezen van de Nederlandse samenvatting een beetje een idee hebben van datgene waar ik me de afgelopen vier jaren mee bezig heb gehouden.

Stephan en Suzanne, Marco en Nicola, bedankt dat jullie altijd naar mijn verhalen hebben willen luisteren. Pa en ma, bedankt dat jullie me altijd hebben gesteund in mijn keuzes; jullie stonden altijd voor mij klaar.

Ewald

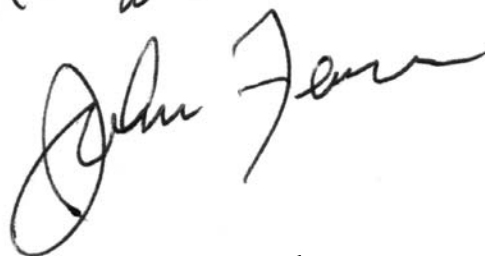
Gordon Research Conferences, Connecticut College,
July 20-25, 2003

Dear Ewald

Beautiful work!

Keep it up!

Best wishes

A handwritten signature in cursive script that reads "John Fenn". The signature is written in dark ink and is positioned below the words "Best wishes".

John Fenn

John Fenn received the Nobel Prize in Chemistry 2002
for the invention of Electrospray Ionization (ESI).

Curriculum Vitae

Ewald van den Bremer werd geboren op 17 september 1973 te Leusden. Na het behalen van zijn MAVO-diploma in 1990 aan de I.V.O. school (Individualiserend Voortgezet Onderwijs) te Amersfoort werd in datzelfde jaar begonnen met de Middelbare Laboratorium Opleiding (MLO) aan het MBO College Eemvoorde in diezelfde gemeente met als richting analytische chemie. Deze werd afgerond in juni 1994 na een stage van tien maanden bij het Regionaal Laboratorium van Nestlé Nederland B.V. te Nunspeet. In datzelfde jaar werd begonnen met de Hogere Laboratorium Opleiding (HLO) aan de Hogeschool van Utrecht met als afstudeerrichting Biochemie. Als onderdeel van zijn afstuderen deed hij 10 maanden onderzoek aan de Portland State University (Portland, Oregon) onder leiding van Dr. Bryant A. Gilbert. Na het behalen van het diploma in februari 1998 werkte hij twee jaar bij Numico Research B.V. in Wageningen. In mei 2000 is hij begonnen als onderzoeker in opleiding bij de sectie Biomoleculaire Massaspectrometrie op een door NWO gefinancierd project. In deze functie werd het in dit proefschrift beschreven onderzoek verricht onder leiding van Prof. Dr. Albert J.R. Heck. In deze periode heeft hij twee maanden onderzoek gedaan aan de University of York in de groep van Prof. Dr. Colin Kleanthous op een “EMBO short-term fellowship”. Onderzoekresultaten werden onder meer gepresenteerd tijdens lezingen op colicin mini-symposia in Norwich en York, als mede door middel van posterpresentaties op conferenties in onder meer Orlando, Florence en New London.

List of publications

Van den Bremer, E. T. J., Jiskoot, W., James, R., Moore, G. R., Kleanthous, C., Heck, A. J. R., and Maier, C. S. 2002. Probing metal ion binding and conformational properties of the colicin E9 endonuclease by electrospray ionization time-of-flight mass spectrometry, *Protein Sci.* 11, 1738-1752.

Van den Bremer, E. T. J., Keeble, A., H., Jiskoot, W., Spelbrink, R. E. J., Maier, C. S., Van Hoek, A., Visser, A. J. W. G., James, R., Moore, G. R., Kleanthous, C., and Heck, A. J. R. 2004. Distinct conformational stability and functional activity of four highly homologous endonuclease colicins, *Protein Sci.*, *in press*.

Van den Bremer, E. T. J., Keeble, A., H., Visser, A. J. W. G., Van Hoek, A., Kleanthous, C., Heck, A. J. R., and Jiskoot, W. 2004. Ligand induced changes in the conformational dynamics of a bacterial cytotoxic endonuclease, *Biochemistry*, *in press*.

Van den Bremer, E. T. J., Keeble, A., H., Kleanthous, C., and Heck, A. J. R.. 2004. Metal induced selectivity in phosphate ion binding in colicin E9 DNase, *submitted*.

Van den Bremer, E. T. J., and Heck, A.J.R. 2004. In: *Biotechnology pharmaceutical aspects*. Vol.3 Methods for Structural Analysis of Protein Pharmaceuticals, Arlington, VA: AAPS Press, *in press*.